

ISSN 1881-7815 Online ISSN 1881-7823

BST

BioScience Trends

Volume 18, Number 3
June, 2024



www.biosciencetrends.com

BST

BioScience Trends



ISSN: 1881-7815
Online ISSN: 1881-7823
CODEN: BTIRCZ
Issues/Year: 6
Language: English
Publisher: IACMHR Co., Ltd.

BioScience Trends is one of a series of peer-reviewed journals of the International Research and Cooperation Association for Bio & Socio-Sciences Advancement (IRCA-BSSA) Group. It is published bimonthly by the International Advancement Center for Medicine & Health Research Co., Ltd. (IACMHR Co., Ltd.) and supported by the IRCA-BSSA.

BioScience Trends devotes to publishing the latest and most exciting advances in scientific research. Articles cover fields of life science such as biochemistry, molecular biology, clinical research, public health, medical care system, and social science in order to encourage cooperation and exchange among scientists and clinical researchers.

BioScience Trends publishes Original Articles, Brief Reports, Reviews, Policy Forum articles, Communications, Editorials, News, and Letters on all aspects of the field of life science. All contributions should seek to promote international collaboration.

Editorial Board

Editor-in-Chief:

Norihiro KOKUDO
National Center for Global Health and Medicine, Tokyo, Japan

Co-Editors-in-Chief:

Xishan HAO
Tianjin Medical University, Tianjin, China
Takashi KARAKO
National Center for Global Health and Medicine, Tokyo, Japan
John J. ROSSI
Beckman Research Institute of City of Hope, Duarte, CA, USA

Hongen LIAO
Tsinghua University, Beijing, China
Misao MATSUSHITA
Tokai University, Hiratsuka, Japan
Fanghua QI
Shandong Provincial Hospital, Ji'nan, China
Ri SHO
Yamagata University, Yamagata, Japan
Yasuhiko SUGAWARA
Kumamoto University, Kumamoto, Japan
Ling WANG
Fudan University, Shanghai, China

Senior Editors:

Tetsuya ASAKAWA
The Third People's Hospital of Shenzhen, Shenzhen, China
Yu CHEN
The University of Tokyo, Tokyo, Japan
Xunjia CHENG
Fudan University, Shanghai, China
Yoko FUJITA-YAMAGUCHI
Beckman Research Institute of the City of Hope, Duarte, CA, USA
Jianjun GAO
Qingdao University, Qingdao, China
Na HE
Fudan University, Shanghai, China

Proofreaders:

Curtis BENTLEY
Roswell, GA, USA
Thomas R. LEBON
Los Angeles, CA, USA

Editorial and Head Office

Pearl City Koishikawa 603,
2-4-5 Kasuga, Bunkyo-ku, Tokyo 112-0003, Japan
E-mail: office@biosciencetrends.com

BioScience Trends

Editorial and Head Office

Pearl City Koishikawa 603, 2-4-5 Kasuga, Bunkyo-ku,
Tokyo 112-0003, Japan

E-mail: office@biosciencetrends.com
URL: www.biosciencetrends.com

Editorial Board Members

Girdhar G. AGARWAL
(Lucknow, India)

Hirotsugu AIGA
(Geneva, Switzerland)

Hidechika AKASHI
(Tokyo, Japan)

Moazzam ALI
(Geneva, Switzerland)

Ping AO
(Shanghai, China)

Hisao ASAMURA
(Tokyo, Japan)

Michael E. BARISH
(Duarte, CA, USA)

Boon-Huat BAY
(Singapore, Singapore)

Yasumasa BESSHO
(Nara, Japan)

Generoso BEVILACQUA
(Pisa, Italy)

Shiuan CHEN
(Duarte, CA, USA)

Yi-Li CHEN
(Yiwu, China)

Yue CHEN
(Ottawa, Ontario, Canada)

Naoshi DOHMAE
(Wako, Japan)

Zhen FAN
(Houston, TX, USA)

Ding-Zhi FANG
(Chengdu, China)

Xiao-Bin FENG
(Beijing, China)

Yoshiharu FUKUDA
(Ube, Japan)

Rajiv GARG
(Lucknow, India)

Ravindra K. GARG
(Lucknow, India)

Makoto GOTO
(Tokyo, Japan)

Demin HAN
(Beijing, China)

David M. HELFMAN
(Daejeon, Korea)

Takahiro HIGASHI
(Tokyo, Japan)

De-Fei HONG
(Hangzhou, China)

De-Xing HOU
(Kagoshima, Japan)

Sheng-Tao HOU
(Guanzhou, China)

Xiaoyang HU
(Southampton, UK)

Yong HUANG
(Ji'ning, China)

Hirofumi INAGAKI
(Tokyo, Japan)

Masamine JIMBA
(Tokyo, Japan)

Chun-Lin JIN
(Shanghai, China)

Kimataka KAGA
(Tokyo, Japan)

Michael Kahn
(Duarte, CA, USA)

Kazuhiro KAKIMOTO
(Osaka, Japan)

Kiyoko KAMIBEPPU
(Tokyo, Japan)

Haidong KAN
(Shanghai, China)

Kenji KARAKO
(Tokyo, Japan)

Bok-Luel LEE
(Busan, Korea)

Mingjie LI
(St. Louis, MO, USA)

Shixue LI
(Ji'nan, China)

Ren-Jang LIN
(Duarte, CA, USA)

Chuan-Ju LIU
(New York, NY, USA)

Lianxin LIU
(Hefei, China)

Xinqi LIU
(Tianjin, China)

Daru LU
(Shanghai, China)

Hongzhou LU
(Guanzhou, China)

Duan MA
(Shanghai, China)

Masatoshi MAKUUCHI
(Tokyo, Japan)

Francesco MAROTTA
(Milano, Italy)

Yutaka MATSUYAMA
(Tokyo, Japan)

Qingyue MENG
(Beijing, China)

Mark MEUTH
(Sheffield, UK)

Michihiro Nakamura
(Yamaguchi, Japan)

Munehiro NAKATA
(Hiratsuka, Japan)

Satoko NAGATA
(Tokyo, Japan)

Miho OBA
(Odawara, Japan)

Xianjun QU
(Beijing, China)

Carlos SAINZ-FERNANDEZ
(Santander, Spain)

Yoshihiro SAKAMOTO
(Tokyo, Japan)

Erin SATO
(Shizuoka, Japan)

Takehito SATO
(Isehara, Japan)

Akihito SHIMAZU
(Tokyo, Japan)

Zhifeng SHAO
(Shanghai, China)

Xiao-Ou SHU
(Nashville, TN, USA)

Sarah Shuck
(Duarte, CA, USA)

Judith SINGER-SAM
(Duarte, CA, USA)

Raj K. SINGH
(Dehradun, India)

Peipei SONG
(Tokyo, Japan)

Junko SUGAMA
(Kanazawa, Japan)

Zhipeng SUN
(Beijing, China)

Hiroshi TACHIBANA
(Isehara, Japan)

Tomoko TAKAMURA
(Tokyo, Japan)

Tadatoshi TAKAYAMA
(Tokyo, Japan)

Shin'ichi TAKEDA
(Tokyo, Japan)

Sumihito TAMURA
(Tokyo, Japan)

Puay Hoon TAN
(Singapore, Singapore)

Koji TANAKA
(Tsu, Japan)

John TERMINI
(Duarte, CA, USA)

Usa C. THISYAKORN
(Bangkok, Thailand)

Toshifumi TSUKAHARA
(Nomi, Japan)

Mudit Tyagi
(Philadelphia, PA, USA)

Kohjiro UEKI
(Tokyo, Japan)

Masahiro UMEZAKI
(Tokyo, Japan)

Junming WANG
(Jackson, MS, USA)

Qing Kenneth WANG
(Wuhan, China)

Xiang-Dong WANG
(Boston, MA, USA)

Hisashi WATANABE
(Tokyo, Japan)

Jufeng XIA
(Tokyo, Japan)

Feng XIE
(Hamilton, Ontario, Canada)

Jinfu XU
(Shanghai, China)

Lingzhong XU
(Ji'nan, China)

Masatake YAMAUCHI
(Chiba, Japan)

Aitian YIN
(Ji'nan, China)

George W-C. YIP
(Singapore, Singapore)

Xue-Jie YU
(Galveston, TX, USA)

Rongfa YUAN
(Nanchang, China)

Benny C-Y ZEE
(Hong Kong, China)

Yong ZENG
(Chengdu, China)

Wei ZHANG
(Shanghai, China)

Wei ZHANG
(Tianjin, China)

Chengchao ZHOU
(Ji'nan, China)

Xiaomei ZHU
(Seattle, WA, USA)

(as of June 2024)

Editorial

- 201-205 **Integration of wearable devices and deep learning: New possibilities for health management and disease prevention.**
Kenji Karako
- 206-211 **Recent trends and new developments in liver transplantation.**
Yasuhiko Sugawara, Taizo Hibi

Policy Forum

- 212-218 **Addressing healthy aging in China: Practices and prospects.**
Haiyin Wang, Dan Qin, Liang Fang, Hui Liu, Peipei Song
- 219-223 **The latest policies, practices, and hotspots in research in conjunction with the aging of Japan's population.**
Yuan Liu, Susumu Kobayashi, Kenji Karako, Peipei Song, Wei Tang

Review

- 224-232 **Trends in the treatment of advanced pancreatic cancer.**
Hirokazu Momose, Shohei Kudo, Tomoyuki Yoshida, Nobuhiro Hasui, Ryota Matsuki, Masaharu Kogure, Yoshihiro Sakamoto

Original Article

- 233-249 **Revealing the gut microbiome mystery: A meta-analysis revealing differences between individuals with autism spectrum disorder and neurotypical children.**
Changjiang Yang, Hongli Xiao, Han Zhu, Yijie Du, Ling Wang
- 250-262 **Revealing the enhancement effect of social capital on the individual performance of core members in elderly caring organizations: A study from Anhui, China.**
Shuo Ding, Fuqin Xu, Guoqing Liu, Xin Zheng, Lanlan Zhao, Otsen Benjamin, Ziwen Xu, Jiajie Zhao, Sanyuan Hao, Ren Chen
- 263-276 **A predictive radiotranscriptomics model based on DCEMRI for tumor immune landscape and immunotherapy in cholangiocarcinoma.**
Lu Chen, Guotao Yin, Ziyang Wang, Zifan Liu, Chunxiao Sui, Kun Chen, Tianqiang Song, Wengui Xu, Lisha Qi, Xiaofeng Li
- 277-288 **Establishment of nomogram prediction model of contrast-enhanced ultrasound and Gd-EOB-DTPA-enhanced MRI for vessels encapsulating tumor clusters pattern of hepatocellular carcinoma.**
Feiqian Wang, Kazushi Numata, Akihiro Funaoka, Xi Liu, Takafumi Kumamoto, Kazuhisa Takeda, Makoto Chuma, Akito Nozaki, Litao Ruan, Shin Maeda

- 289-302** **Suppression of STK39 weakens the MASLD/MASH process by protecting the intestinal barrier.**
Qing Xu, Fei Liu, Zhenru Wu, Menglin Chen, Yongjie Zhou, Yujun Shi

Integration of wearable devices and deep learning: New possibilities for health management and disease prevention

Kenji Karako*

Department of Surgery, Graduate School of Medicine, The University of Tokyo, Tokyo, Japan.

SUMMARY In recent years, the market for wearable devices has been rapidly growing, with much of the demand for health management. These devices are equipped with numerous sensors that detect inertial measurements, electrocardiograms, photoplethysmography signals, and more. Utilizing the collected data enables the monitoring and analysis of the user's health status in real time. With the proliferation of wearable devices, research on applications such as human activity recognition, anomaly detection, and disease prediction has advanced by combining these devices with deep learning technology. Analyzing heart rate variability and activity data, for example, enables the early detection of an abnormal health status and prompt, appropriate medical interventions. Much of the current research focuses on short-term predictions, but adopting a long-term perspective is essential for further development of wearable devices and deep learning. Continuously recording user behavior, anomalies, and physical information and collecting and analyzing data over an extended period will enable more accurate disease predictions and lifestyle guidance based on individual habits and physical conditions. Achieving this requires the integration of wearable devices with medical records. A system needs to be created to integrate data collected by wearable devices with medical records such as electronic health records in collaboration with medical facilities like hospitals and clinics. Overcoming this challenge will enable optimal health management and disease prediction for each user, leading to a higher quality of life.

Keywords wearable device, deep learning, healthcare

1. Introduction

In recent years, the demand for health management has been increasing, leading to rapid growth in the market for wearable devices such as smartwatches and fitness trackers. These devices, equipped with sensors that measure heart rate, sleep patterns, and physical activity, serve as tools to help users record their activity levels and manage their health. The wearable technology market size is projected to grow from \$157.94 billion in 2024 to \$1.41526 trillion by 2032, with an average annual growth rate of 31.5% (1).

The applications of wearable devices are not limited to health management and fitness; they also extend to gaming, entertainment, fashion, and education, among others. The health and fitness sector has the largest market share of these devices. The use of wearable devices has made people increasingly aware of the importance of fitness and health. In particular, wearable devices are expected to encourage users to take an active approach to their health by providing critical

health indicators in real time. Moreover, these devices are increasingly being used to share information with medical facilities and monitor patients' health remotely. This allows patients to check their condition and progress without visiting a medical facility, which is beneficial for those with chronic diseases.

As the wearable device market grows, research using deep learning to effectively utilize the information obtained from these devices is garnering attention. A type of machine learning, deep learning has seen significant advances in fields like image recognition and natural language processing with methods such as convolutional neural networks (CNN) (2-4) and Transformers (5). Deep learning can also be applied to time-series data obtained from sensors. When estimating a user's level of activity (such as walking or running) from measured sensor information, for example, deep learning requires actual sensor data and corresponding information on the level of activity. By collecting accurate data on sensor information and the level of activity and training deep learning models with this data,

the models themselves acquire methods with which to extract the necessary information for task estimation from sensor data. The sensors equipped on wearable devices are diverse, including inertial measurement unit (IMU) that measure acceleration, gyroscope, and magnetic force, electrocardiograms (ECG), heart rate sensors, photoplethysmography (PPG) sensors that can measure blood oxygen saturation, electromyography (EMG) sensors, and mechanomyography (MMG) sensors (6-8). There are a wide range of research applications for these sensor data, including activity estimation, anomaly detection, and disease prediction.

enables the recording of daily activities and is expected to lead to the early detection and prevention of diseases.

2. Predictions using deep learning

Research utilizing deep learning is advancing to support healthcare in areas such as health management, anomaly detection, and early disease detection, as shown in Table 1. Wearable devices can continuously record dynamic information from users through inertial sensors, but they cannot identify user activities directly. User activities need to be estimated based on sensor information.

Table 1. Overview of studies related to wearable devices and deep learning

Task/Research	Sensors/Signals used	Dataset
Human activity recognition		
Wang K, <i>et al.</i> (9)	• Inertial measurement unit (IMU)	• Human Activity Recognition Using Smartphones (35)
Jiang W, <i>et al.</i> (10)	• IMU	• Human Activity Recognition Using Smartphones (35), USC-HAD (36,37)
Chen Y, <i>et al.</i> (11)	• IMU	• Dataset containing 31688 samples with 8 activities
Zeng M, <i>et al.</i> (12)	• IMU	• OPPORTUNITY (16), Skoda (38), Actitracker (39)
Yen CT, <i>et al.</i> (13)	• IMU	• Human Activity Recognition Using Smartphones (35)
Stress detection		
Patlar Akbulut F, <i>et al.</i> (17)	• Electrocardiogram (ECG), electrical conductivity of the skin, oxygen saturation, and blood pressure	• Dataset of 312 records from 30 participants
Arrhythmias detection		
Lee KS, <i>et al.</i> (18)	• ECG	• Dataset of 28,308 unique patients (15,412 normal and 12,896 with arrhythmia)
Shashikumar SP, <i>et al.</i> (19)	• ECG, photoplethysmography (PPG), IMU	• Dataset of 98 patients (45 with atrial fibrillation and 53 with other rhythms)
Seizures detection		
Meisel C, <i>et al.</i> (20)	• Electrodermal activity, body temperature, blood volume pulse, and actigraphy	• Dataset of 69 patients with epilepsy (total duration > 2,311 hours, 452 seizures)
Stirling RE, <i>et al.</i> (21)	• Heart rate, sleep, and step counts	• Dataset of 11 epilepsy patients followed for more than 6 months
Parkinson's disease detection		
Camps J, <i>et al.</i> (23)	• IMU	• Dataset of 21 Parkinson's disease patients who manifested freezing of gait episodes
Zia J, <i>et al.</i> (24)	• IMU	• Daphnet Freezing of Gait (40)
Assessment of sleep state		
Cho T, <i>et al.</i> (25)	• IMU	• Dataset of 10 subjects sleeping for 8 hours
Sleep disorders detection		
Wang T, <i>et al.</i> (26)	• ECG	• PhysioNet Apnea-ECG dataset (34), University College Dublin Sleep Apnea Database (41)
Ye G, <i>et al.</i> (27)	• PPG	• PhysioNet Apnea-ECG dataset (34), University College Dublin Sleep Apnea Database (41), Apnea Interventions for Research (42)
Dementia detection		
Lim J, <i>et al.</i> (30)	• Electrical conductivity of the skin, body temperature, and IMU	• Dataset of 18 elderly subjects (5 males, 13 females) age 65 years or older
Saif N, <i>et al.</i> (31)	• Sleep cycle, heart rate variability, and IMU	• Dataset of 33 subjects recruited at the Alzheimer's Prevention Clinic
Lee H, <i>et al.</i> (32)	• IMU	• Dataset of 60 subjects (30 cognitively normal and 30 with mild cognitive impairment)
Jeon Y, <i>et al.</i> (33)	• IMU	• Gait data from 145 subjects

The combination of wearable devices and deep learning

This task is called human activity recognition (HAR),

which can predict and record activities such as sitting, walking, lying down, climbing stairs, jogging, running, and falling. HAR research is important as it allows users to reflect on their actions and habits and consider their lifestyle. Various deep learning models have been proposed to achieve HAR (9-13). These studies mainly use deep learning models based on CNNs. Commonly used in image recognition, CNNs are also suitable for signal processing. CNNs excel in extracting features from short-term signal information and are well-suited for regular human activities of a brief duration. One reason why HAR is actively researched is the availability of abundant datasets. Large amounts of quality data are required to make estimates using deep learning. There are extensive datasets for HAR, such as the University of California Riverside-Time Series Classification (UCR-TSC) archive (14), the University of East Anglia multivariate time series classification (UEA-MTSC) archive (15), and the OPPORTUNITY dataset (16). Each dataset includes time-series signals measured by various sensors: UCR-TSC has 128 datasets, UEA-MTSC has 30 datasets, and the OPPORTUNITY dataset includes data collected from 12 subjects that consists of 18 types of activity information and measurements from 7 IMU and 12 3D accelerometers.

In addition to HAR, anomaly detection is also being researched. For instance, detecting stress states (17), arrhythmias (18,19), and seizures (20,21) are some of the approaches being researched to detect abnormal states in users. In stress detection research, for example, models evaluating stress levels using ECG, skin conductance, oxygen saturation, and blood pressure measurements have been developed for patients with metabolic syndrome. Early intervention is crucial because chronic symptoms worsen when these patients are exposed to stress. In arrhythmia detection, techniques utilizing CNN-based deep learning models to detect arrhythmias in PPG and ECG data with a high level of accuracy have been proposed. For example, atrial fibrillation is asymptomatic in about 10% of cases (22) and it increases the risk of stroke and myocardial infarction, so early detection is important. Arrhythmia detection research has proposed CNN-based deep learning models using PPG and ECG data collected from wearable devices to detect arrhythmias with an accuracy of over 95%. Epilepsy is a neurological disorder affecting the central nervous system, causing seizures, limb spasms, and loss of consciousness. Research predicts high-risk states of seizures using information such as skin conductance, body temperature, heart rate, sleep, and steps. Predicting seizures allows patients to avoid high-risk periods and prepare a safe environment. These studies showcase significant technological advances in the early detection and rapid response to abnormal states, ensuring user safety and health.

Constantly worn in daily life, wearable devices are suitable for monitoring signs of disease. Diagnostic

models are being developed for various diseases (e.g., Parkinson's disease, sleep disorders, and dementia). Parkinson's disease is a neurodegenerative disorder affecting movement and speech, with symptoms such as uncontrollable tremors, muscle rigidity, and slowed movements. As an example, studies have proposed deep learning models that predict freezing of gait and tremors using acceleration and rotational motion information measured by IMU (23,24). Sleep quality is crucial for health, but identifying problems on one's own is difficult. Wearable devices help monitor, measure, and provide feedback on sleep states. For example, studies on sleep stage identification enable the detection of sleep and wake states and quality assessment (25). Sleep apnea syndrome, a common breathing disorder, is also detected using wearable devices by analyzing ECG and PPG signals (26,27). In an aging society, early detection of dementia is a crucial issue. Indirect methods are effective for early detection and intervention in signs of dementia. Research is underway to estimate cognitive decline using blood, gait patterns, and voice as indirect information to allow inference (28,29). Studies using wearable devices have similarly attempted to predict cognitive decline using a combination of information from IMU, skin conductance, and body temperature to ascertain the indirect effects of cognitive decline on the body (30-33).

Obtaining datasets for predictions related to such diseases is a significant challenge. Unlike HAR, the difficulty of data collection results in limited available data. An open dataset that is beneficial for prediction tasks involving clinical data and wearable device measurement data is PhysioNet (34). PhysioNet has helped to develop wearable devices and deep learning by providing physiological and clinical data in many areas, including arrhythmias, Parkinson's disease, and cognitive decline.

3. Possible applications of wearable devices and deep learning from a long-term perspective

Thus far, we have described various areas of predictive research using deep learning with information obtained from wearable devices. Many studies focus on estimating the user's state at a specific time from short-term signal information, primarily using CNN-based algorithms. While CNNs excel at extracting local patterns and features from input signals, they may not be suitable for long-term predictions.

From a long-term perspective, the information recorded by wearable devices may contain abnormal data with features and patterns related to the user's behavior, lifestyle, and disease predictions. Utilizing this information can enable predictions of diseases related to future lifestyle habits, allowing recommendations to improve those habits. Models based on Transformers are effective for long-term predictions. Initially proposed for natural language processing, Transformers divide

text into meaningful chunks called tokens and learn the relationships between these tokens. When Transformers is applied to long-term predictions from sensor data, meaningful token information needs to be extracted from the signals. CNN models built for HAR or anomaly detection are effective at extracting these tokens. HAR estimation converts signal information into user activity data, giving meaning to the signals. Converting sensor information into event data for individuals through existing HAR and anomaly detection will enable the early detection of diseases and the provision of personalized lifestyle guidance based on long-term event histories. For long-term prediction models to become a reality, long-term wearable device data and clinical data are necessary, making data collection a significant challenge. With the growth of the wearable device market, the hope is that new mechanisms will be created to collect and record sensor information linked to medical and health data. In addition, wearable devices will presumably be increasingly used in research that guides users' lives from a long-term perspective.

4. Conclusion

The combination of wearable devices and deep learning holds great potential for health management and disease prevention. These technologies are useful for health monitoring, anomaly detection, and even early disease detection. As a long-term perspective on data collection and analysis is adopted, providing personalized health management tailored to individual users will become possible. In addition, the accuracy and applicability of deep learning models will increase as datasets become more comprehensive. Wearable devices will continue to increase in predictive value as specific applications such as HAR, anomaly detection, and disease prediction progress. In the future, balancing efficient data collection with privacy protection will be a crucial challenge. Overcoming this challenge will allow wearable devices to further integrate into daily life, where they will serve as essential tools to encourage the health of more people.

Ultimately, the fusion of wearable devices and deep learning provides innovative means to more accurately understand individual health conditions and promote preventive medicine. This will enable us to lead healthier and more fulfilling lives, and it is expected to significantly change the nature of healthcare.

Funding: None.

Conflict of Interest: The author has no conflicts of interest to disclose.

References

1. Wearable Technology Market Size, Share, Value | Growth, 2032. <https://www.fortunebusinessinsights.com/wearable-technology-market-106000> (accessed June 15, 2024).
2. LeCun Y, Bottou L, Bengio Y, Haffner P. Gradient-based learning applied to document recognition. *Proceedings of the IEEE*. 1998;86:2278-2324.
3. Simonyan K, Zisserman A. Very deep convolutional networks for large-scale image recognition. In: *CoRR*. Vol abs/1409.1556.
4. Krizhevsky A, Sutskever I, Hinton GE. ImageNet classification with deep convolutional neural networks. *Commun ACM*. 2017; 60:84-90.
5. Vaswani A, Shazeer N, Parmar N, Uszkoreit J, Jones L, Gomez AN, Kaiser Ł, Polosukhin I. Attention is all you need. *Advances in neural information processing systems*. 2017; 30.
6. Zhang S, Li Y, Zhang S, Shahabi F, Xia S, Deng Y, Alshurafa N. Deep learning in human activity recognition with wearable sensors: A review on advances. *Sensors*. 2022; 22:1476.
7. Sabry F, Eltaras T, Labda W, Alzoubi K, Malluhi Q. Machine learning for healthcare wearable devices: The big picture. *J Healthc Eng*. 2022; 2022:4653923.
8. Jiang Z, Van Zoest V, Deng W, Ngai ECH, Liu J. Leveraging machine learning for disease diagnoses based on wearable devices: A Survey. *IEEE Internet Things J*. 2023; 10: 21959-21981.
9. Wang K, He J, Zhang L. Attention-based convolutional neural network for weakly labeled human activities' recognition with wearable sensors. *IEEE Sens J*. 2019; 19: 7598-7604.
10. Jiang W, Yin Z. Human activity recognition using wearable sensors by deep convolutional neural networks. In: *Proceedings of the 2015 ACM Multimedia Conference*. 2015; 1307-1310.
11. Chen Y, Xue Y. A deep learning approach to human activity recognition based on single accelerometer. In: *Proceedings of 2015 IEEE International Conference on Systems, Man, and Cybernetics*. 2015; 1488-1492.
12. Zeng M, Nguyen LT, Yu B, Mengshoel OJ, Zhu J, Wu P, Zhang J. Convolutional Neural Networks for human activity recognition using mobile sensors. In: *Proceedings of the 2014 6th International Conference on Mobile Computing, Applications and Services*. 2014; 197-205.
13. Yen CT, Liao JX, Huang YK. Human daily activity recognition performed using wearable inertial sensors combined with deep learning algorithms. *IEEE Access*. 2020; 8:174105-174114.
14. Dau HA, Bagnall A, Kamgar K, Yeh CM, Zhu Y, Gharghabi S, Ratanamahatana CA, Keogh E. The UCR time series archive. *IEEE/CAA Journal of Automatica Sinica*. 2019; 6:1293-1305.
15. Bagnall A, Dau HA, Lines J, Flynn M, Large J, Bostrom A, Southam, Keogh, E. The UEA multivariate time series classification archive, 2018. In: *CoRR*. Vol abs/1811.00075.
16. Chavarriaga R, Sagha H, Calatroni A, Digumarti ST, Tröster G, Millán JR, Roggen D. The Opportunity challenge: A benchmark database for on-body sensor-based activity recognition. *Pattern Recognit Lett*. 2013; 34:2033-2042.
17. Patlar Akbulut F, Ikitimur B, Akan A. Wearable sensor-based evaluation of psychosocial stress in patients with metabolic syndrome. *Artif Intell Med*. 2020; 104: 101824.
18. Lee KS, Park HJ, Kim JE, Kim HJ, Chon S, Kim S, Jang J, Kim JK, Jang S, Gil Y, Son HS. Compressed deep learning to classify arrhythmia in an embedded wearable

- device. *Sensors*. 2022; 22:1776.
19. Shashikumar SP, Shah AJ, Li Q, Clifford GD, Nemati S. A deep learning approach to monitoring and detecting atrial fibrillation using wearable technology. In: 2017 IEEE EMBS International Conference on Biomedical and Health Informatics. 2017; 141-144.
 20. Meisel C, El Atrache R, Jackson M, Schubach S, Ufongene C, Loddenkemper T. Machine learning from wristband sensor data for wearable, noninvasive seizure forecasting. *Epilepsia*. 2020; 61:2653-2666.
 21. Stirling RE, Grayden DB, D'Souza W, Cook MJ, Nurse E, Freestone DR, Payne DE, Brinkmann BH, Attia TP, Viana PF, Richardson MP, Karoly PJ. Forecasting seizure likelihood with wearable technology. *Front Neurol*. 2021; 12:704060.
 22. Flaker GC, Belew K, Beckman K, Vidaillet H, Kron J, Safford R, Mickel M, Barrell P, the AFFIRM Investigators. Asymptomatic atrial fibrillation: Demographic features and prognostic information from the Atrial Fibrillation Follow-up Investigation of Rhythm Management (AFFIRM) study. *Am Heart J*. 2005; 149:657-663.
 23. Camps J, Samà A, Martín M, *et al*. Deep learning for freezing of gait detection in Parkinson's disease patients in their homes using a waist-worn inertial measurement unit. *Knowl Based Syst*. 2018; 139: 119-131.
 24. Zia J, Tadayon A, McDaniel T, Panchanathan S. Utilizing neural networks to predict freezing of gait in Parkinson's patients. In: Proceedings of the 18th International ACM SIGACCESS Conference on Computers and Accessibility. 2016; 333-334.
 25. Cho T, Sunarya U, Yeo M, Hwang B, Koo YS, Park C. Deep-ACTINet: End-to-end deep learning architecture for automatic sleep-wake detection using wrist actigraphy. *Electronics*. 2019; 8:1461.
 26. Wang T, Lu C, Shen G, Hong F. Sleep apnea detection from a single-lead ECG signal with automatic feature-extraction through a modified LeNet-5 convolutional neural network. *PeerJ*. 2019; e7731.
 27. Ye G, Yin H, Chen T, Chen H, Cui L, Zhang X. FENet: A frequency extraction network for obstructive sleep apnea detection. *IEEE J Biomed Health Inform*. 2021; 25:2848-2856.
 28. Karako K, Song P, Chen Y. Recent deep learning models for dementia as point-of-care testing: Potential for early detection. *Intractable Rare Dis Res*. 2023; 12:1-4.
 29. Karako K. Predictive deep learning models for cognitive risk using accessible data. *Biosci Trends*. 2024; 18:66-72.
 30. Lim J. A smart healthcare-based system for classification of dementia using deep learning. *Digit Health*. 2022; 8:20552076221131667.
 31. Saif N, Yan P, Niotis K, Scheyer O, Rahman A, Berkowitz M, Krikorian R, Hristov H, Sadek G, Bellara S, Isaacson RS. Feasibility of using a wearable biosensor device in patients at risk for Alzheimer's disease dementia. *J Prev Alzheimers Dis*. 2020; 7:104-111.
 32. Lee H, Shahzad A, Kim K. Automated prescreening of MCI through deep learning models based on wearable inertial sensors data. *Alzheimer's & Dementia*. 2021; 17:e052744.
 33. Jeon Y, Kang J, Kim BC, Lee KH, Song JI, Gwak J. Early Alzheimer's disease diagnosis using wearable sensors and multilevel gait assessment: A machine learning ensemble approach. *IEEE Sens J*. 2023; 23:10041-10053.
 34. Goldberger AL, Amaral LAN, Glass L, Hausdorff JM, Ivanov PC, Mark RG, Mietus JE, Moody GB, Peng C, Stanley HE. PhysioBank, PhysioToolkit, and PhysioNet. *Circulation*. 2000; 101:e215-e220.
 35. Anguita D, Ghio A, Oneto L, Parra X, Reyes-Ortiz JL. A public domain dataset for human activity recognition using smartphones. In: Proceedings of 21st European Symposium on Artificial Neural Networks, Computational Intelligence and Machine Learning. 2013; 3.
 36. Zhang M, Sawchuk AA. USC-HAD: A daily activity dataset for ubiquitous activity recognition using wearable sensors. In Proceedings of the 2012 ACM Conference on Ubiquitous Computing. 2012; 1036-1043.
 37. Shoaib M, Bosch S, Durmaz Incel O, Scholten H, Havinga PJM. Fusion of smartphone motion sensors for physical activity recognition. *Sensors*. 2014; 14:10146-10176.
 38. Chennuru S, Chen PW, Zhu J, Zhang JY. Mobile lifelogger – Recording, indexing, and understanding a mobile user's life. In: Lecture Notes of the Institute for Computer Sciences, Social-Informatics and Telecommunications Engineering. 2012; 263-281.
 39. Zappi P, Lombriser C, Stiefmeier T, Farella E, Roggen D, Benini L, Tröster G. Activity recognition from on-body sensors: Accuracy-power trade-off by dynamic sensor selection. *Wireless Sensor Networks, Lecture Notes in Computer Science*. 2008; 4913:17-33.
 40. Daphnet Freezing of Gait - UCI Machine Learning Repository. <https://archive.ics.uci.edu/dataset/245/daphnet+freezing+of+gait> (accessed June 15, 2024).
 41. St. Vincent's University Hospital / University College Dublin Sleep Apnea Database v1.0.0. <https://physionet.org/content/ucddb/1.0.0/> (accessed June 15, 2024).
 42. Gleason K, Shin D, Rueschman M, Weinstock T, Wang R, Ware JH, Mittleman MA, Redline S. Challenges in recruitment to a randomized controlled study of cardiovascular disease reduction in sleep apnea: An analysis of alternative strategies. *Sleep*. 2014; 37:2035-2038.

Received May 21, 2024; Revised June 24, 2024; Accepted June 26, 2024.

*Address correspondence to:

Kenji Karako, Department of Surgery, Graduate School of Medicine, The University of Tokyo, 7-3-1 Hongo, Bunkyo, Tokyo 113-8655, Japan.
E-mail: tri.leafs@gmail.com

Released online in J-STAGE as advance publication June 27, 2024.

Recent trends and new developments in liver transplantation

Yasuhiko Sugawara*, Taizo Hibi

Department of Transplantation/Pediatric Surgery, Postgraduate School of Life Science, Kumamoto University, Kumamoto, Japan.

SUMMARY Liver transplantation (LT) has been an established treatment for end-staged liver disease for acute, chronic, metabolic diseases and liver cancer. Advanced surgical techniques, refined indications and contraindications for LT, improvements of donor selection, prognostic scorings system and immunosuppressive regimens have contributed to the improved outcomes of liver transplantation. The etiologies of cirrhosis have been shifting from viral hepatitis to metabolic associated fatty liver disease. New indications include peripheral or mass forming bile duct cancer, metastases from bowel cancers or neuroendocrine tumors. Resection and partial liver segments 2-3 transplantation with delayed total hepatectomy has been performed to the limited cases, which was the explored technique of auxiliary partial orthotopic LT. Minimally invasive donor hepatectomy (laparoscopic or robotic) has been increasingly done. In this review are described the recent pressing topics in LT.

Keywords liver transplantation, living donor, hepatocellular carcinoma, metabolic associated steatohepatitis, bariatric surgery

Liver transplantation (LT) is the only recognized effective treatment for end-stage liver disease and acute fulminant liver failure. Nowadays, a good survival (of > 90% and > 75% at one year and five years) can be achieved. However, despite recent improvements in donor and recipient selection, perioperative management and organ preservation techniques, there are still several challenges that the transplant community has to face.

1. Metabolic associates steatohepatitis (MASH) for liver transplantation

1.1. Epidemiology

Metabolic syndrome manifest itself in the liver with metabolic dysfunction-associated fatty liver disease. It has affected approximately 25% of the population in the world. And 25% of them will suffer from the progressive inflammatory metabolic dysfunction-associated steatohepatitis (MASH) subtype (1). MASH increases to 17–42 million depending on a linear or exponential trendline (2). The growing prevalence has led MASH as one of the most common indications for LT (3). According to the United Network for Organ Sharing and Organ Procurement and Transplantation Network registry, the number of the patients listing for MASH have approximately three times in ten years (4).

A study disclosed that the F0–1 developed in 22–26 years in, F2 in 9 years, F3 in 2 years and F4 in 1 year

(4). The epidemic of MASH will decrease potential donor pools. It will increase the high-risk recipients. More than 50% of liver transplant patients are obese or morbidly obese (5). Obesity will necessitate challenges in the transplantation. The procedure will be technically more demanding with increased operation times and the complications will be expected.

1.2. Bariatric surgery relationship with LT

Bariatric surgery (BS) is a feasible treatment for obesity adjunct in the LT algorithm. BS plus LT will be more reliable procedure for weight loss than LT alone. However, the ideal timing of BS (before, after or simultaneous with LT) remains established (5).

The BS procedures include balloon insertion in the stomach, gastric banding, sleeve gastrectomy and gastric/small bowel bypass (5). Gastric banding is a less invasive, easy and safe procedure. It will not affect endoscopic access to the biliary tree. The complications will include poor efficacy, foreign body infection and migration of the band (1). Sleeve gastrectomy is effective for weight loss and accompanies with a balance between efficacy and safety (5). It does not cause malabsorption, affect immunosuppressive drug pharmacokinetics nor prevent access to the bile ducts by the endoscopy. The complication includes bleeding and leakage from the staple-line. Roux-en-Y bypass of small bowel has the largest efficacy for weight loss. However, it is

invasive and takes the longest duration for weight loss. Endoscopic access to the biliary tree is bothered and the immunosuppressive drug pharmacokinetics. The complications include malabsorption and sarcopenia (5).

BS before LT is safe and associated with zero-mortality and the reoperation rates ranged 5-17% (6). The limitations of the approach included that obesity of LT candidates is less prevalent than that in the general (7). One third of transplant recipients develop postoperative metabolic syndrome and/or a de novo obesity. Therefore, it has remained unclear if BS before LT has really had an effect on the obesity natural history of the liver recipients.

BS simultaneous with LT is an attractive idea. It will reduce the number of surgeries (8,9). In the selected patients, sleeve gastrectomy and gastric banding will be effective for weight loss. However the rates of the surgical complications are higher than those in the general population. A staple line leak rate is 14% and a reoperation rate is 13%. It can be explained by poor nutritional status of these patients and immunosuppressive drugs.

BS after LT will be the last possibility (10-12). The advantage of the strategy included that it could select the patients who survived LT and developed obesity after LT. The procedure is technically demanding. An open approach is 45% (11). Morbidity remains higher than that in the general. A reoperation rate is 33% (11). Totally 14% of the patients died within one year after BS (11).

2. LT for cancer except for hepatocellular carcinoma (HCC)

2.1. Peri-hilar cholangiocarcinoma (CCA)

Outcomes of the LT for peri-hilar CCA has been reported. The patients undergo neoadjuvant chemoradiotherapy (with which protocol from Mayo, Toronto, University of Michigan) (13). The outcome of the patients who underwent neoadjuvant chemoradiotherapy with Mayo protocol and subsequent LT in 17 centers was analyzed (14). The 5-year disease-free survival was 62%.

The United Network of Organ Sharing (UNOS) has now offered a model for end stage liver diseases score exception for peri-hilar CCA. Data from 12 the United States (US) transplantation centers ($n = 287$) showed post-transplant, recurrence-free survival rates at 5 years being 65% (15). Poor prognostic factors included outside the UNOS criteria (the maximum diameter of the tumor more than 3 cm, transperitoneal tumor biopsy or metastatic lesions) or a prior malignancy. The dropout rates from the waiting list is higher than that of HCC; the cumulative incidence rates at 6 and 12 months are 13% and 24% for peri-hilar CCA and 7% and 13% for HCC (16).

2.2. Intrahepatic CCA

Another primary liver malignant diseases indicated for

LT has included early stage intrahepatic CCA (single, less than 2 cm in diameter), which is unresectable due to the location or the poor liver functional reserve. According to a multicenter study of the 48 patients (17) were found to have intrahepatic CCA on explant pathology, 31% had "early" intrahepatic CCA (single, less than 2 cm in diameter) and 69% had "advanced" intrahepatic CCA (single tumor, more than 2 cm in diameter or multiple). The 1-, 3-, and 5-year recurrence rates in the very early cohort (7%, 18%, and 18%, respectively) were significantly lower than those in the advanced cohort (30%, 47%, and 61%). A median follow-up period was 35 months. The 5-year survival rate was 65% in the very early cohort, which was higher than that in the advanced cohort (45%, $p = 0.02$).

A more recent multi-center French study (18) reported outcomes of the patients with intrahepatic CCA < 5 cm who underwent LT ($n = 49$) or liver resection ($n = 26$). It showed that the patients who underwent LT had a higher 5-year recurrent-free survival (75% vs. 36%; $p = 0.004$). Data were shown from a single US center (19). The criteria include that unresectable intrahepatic CCA in normal function liver, without the vascular involvement of the tumors, no extrahepatic lesions, treated with gemcitabine-based chemotherapy with a minimum of 6 months and the radiographic response. Six of the 12 patients satisfied the criteria and underwent LT. The overall survival rates were 100% and 83% at 1 and 3 years, respectively and the recurrence-free survival was 50% at 3 years.

A follow up report from the group (20) revealed that the 18 patients with locally advanced intrahepatic CCA underwent neoadjuvant therapy and LT. The overall survival rates at 1-, 3-, and 5-years were 100%, 71%, and 57%, respectively. Seven of the them (39%) developed the recurrence of CCA.

2.3. Neuro-endocrine tumor (NET)

There are some established selection criteria of LT for NET. Mazzaferro *et al.* (21) proposed the Milan NET criteria (Table 1). They reported that a 5-year overall and disease-free survival rates were 97% and 89%, respectively. The 280 patients were referred for LT. Of them 88 patients (31%) were considered to be indicated for LT. And 42 patients (15%) actually underwent LT. The UNOS guidelines for NET (22) include no NET recurrence for 3 months and lymph node metastatic lesions, which will turn negative (examined by positron emission tomography scan) at least 6 months before re-enlisting.

According to the European liver transplant registry (ELTR) included the 213 patients who received LT for NET in 27 years. The tumors were synchronous in 119 patients. Prior to LT, 83% patients underwent resection of the tumors. The 76% patients underwent nonoperative treatment (trans-arterial chemoembolization and

Table 1. LT criteria for neuro-endocrine tumor

Milan criteria	
Absolute	
	G1 or G2 grade
	Primary tumor with portal drainage
	Extrahepatic lesions are curatively resected before transplantation
	Tumor involvement < 50% of liver
	Stable disease > 6 months
Relative	
	Age ≤ 60
UNOS guidelines (common with Milan and additionally needed)	
	Unresectable
	Radiographic characteristics of neuro-endocrine tumor
	Metastatic tumors are negative by positron emission tomography scan
	No extrahepatic lesions > 3 months
	If lymph node metastases are detected by positron emission tomography scan, they should become negative < 6 months before re-listing.

LT, liver transplantation; G, graft.

somatostatin analogues). The 1-, 3-, and 5-year overall survival and disease-free survival rates were 81%, 65% and 52%, and 65%, 40% and 30%, respectively.

A UNOS data-based study (23) disclosed that the overall survival rates of the patients who underwent LT for NET ($n = 184$) at 1-, 3-, and 5-years were 80%, 61% and 49%, respectively. Of them 39% occurred prior to model for end staged liver diseases (MELD) score introduction. The outcome of the was worse than those underwent LT after MELD adaptation. After MELD adaptation, the overall survival rates improve to be 85%, 65%, and 58%, respectively, at 1-,3-, and 5-years.

The study of University of Göteborg (24) showed that the 15 patients undergoing LT ($n = 10$) or multi-visceral transplantation ($n = 5$). The 5-year overall survival rate was of 90%. The recurrence-free survival rate was 70% at 1-year. The age, hepatic involvement, or Ki-67 was not associated with the outcome. The tumors of the 12 patients were greater than 50% of the total liver. The tumor proliferation rates were less than 10%.

Lim *et al.* (25) reported that the 5-year overall survival rate of the LT patients with NET and liver metastasis ranged from 41% to 71% which was comparable with that for the other indications. However the recurrence rate was higher (31-57%).

2.4. Colorectal liver metastasis (CRLM)

2.4.1. SECA study

The experience of LT for CRLM is still limited. The SECA-I study (26) was undertaken in Norway. The surgical outcome of the 21 patients who underwent LT was compared with that of the 47 patients treated with chemotherapy. The 5- year survival was higher in the LT recipients than that of the patients who were treated only by chemotherapy (56% vs. 9%; $p < 0.001$). There was no significant difference between the groups in

median disease-free survival (10 months and 8 months). In the LT patients, better prognostic factors included the small tumor (diameter less than 5.5 cm), time interval between the diagnosis of the primary therapy and the LT was more than 2 years, serum carcinoembryonic antigen level less than 80 mg/L and regression or stability of the CRLM lesions to neoadjuvant therapy.

2.4.2. Living donor liver transplantation (LDLT) for CRLM

A multi-center series (27) in North America included the 10 patients who underwent LDLT for CRLM. Of these, the 9 had synchronous lesions and the other developed metachronous disease. Three patients with poor differentiation were included. The median period from the diagnosis and LDLT was 2 years. Proceeding treatments to LDLT included liver resection ($n = 4$), trans hepatic arterial chemotherapy ($n = 3$) and tumor ablation ($n = 3$). The overall and recurrence-free survival was 100% and 62%, respectively.

Rajendran *et al.* (28) disclosed a LDLT experience for CRLM ($n = 7$). The prior treatment included chemotherapy (a median of 20–60 cycles) ($n = 6$) and partial liver resection ($n = 2$). The period between the assessment to LDLT was 15 months. The Oslo score was 0–2. Two patients developed recurrence 3 months after LDLT. The duration of the assessment to follow-up was 30 months (median). The overall 3-year survival rate from time of initial assessment was 100%. The 1- and 3-year recurrence-free survival rates were 86% and 69%, respectively.

To maximize the successful rates, a good timing of LT is mandatory. From the point of the view, LDLT will be advantageous. So far, the recurrence rates with LT for CRLM are higher than those of the other malignancies. Larger studies comparing LT with chemotherapy or locoregional therapy may be necessitated.

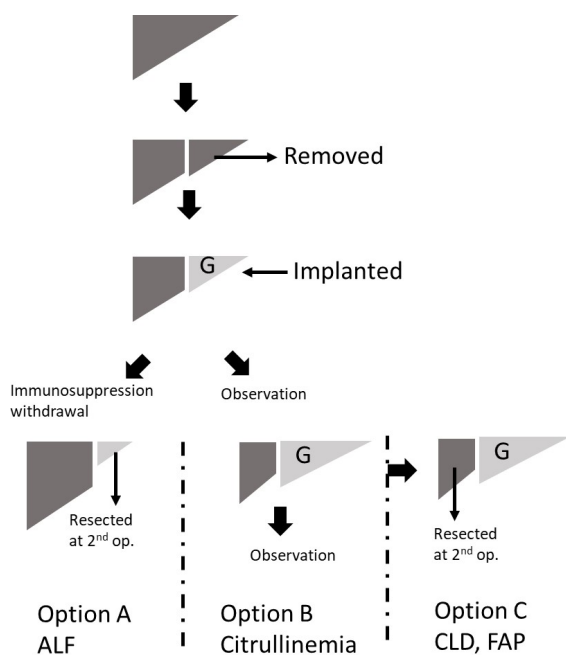


Figure 1. Schematic view of APOLT and RAPID. When indicated for acute liver failure patients, waiting recovering of the native liver, immunosuppressive drugs will be stopped. The graft will be atrophy, which will and be removed (A). Indicated for metabolic diseases which will cause an enzyme deficiency, the graft will be regenerated and observed (B). Indicated for chronic liver disease, HCC in the left liver, or familial amyloid polyneuropathy, the resection of native liver (usually left liver) is resected and a left liver graft is implanted. After the graft regeneration, the remained diseased liver will be removed (C). *Abbreviations:* APOLT, auxiliary partial orthotopic liver transplantation; RAPID, Resection and partial liver segments 2-3 transplantation with delayed total hepatectomy; ALF, acute liver failure, CLD, chronic liver diseases, FAP, familial amyloid polyneuropathy; G, graft.

2.5. Resection and partial liver segments 2-3 transplantation with delayed total hepatectomy (RAPID) procedure or auxiliary partial orthotopic liver transplantation (APOLT)

RAPID is a newly advocated concept, which is an extrapolation of auxiliary partial orthotopic liver transplantation (APOLT), which has been a long-used procedure. APOLT is a heterotopic implantation of a partial liver graft. When indicated for acute liver failure patients, the graft supports the liver function until the functional recovery of the native liver. Recovering of the native liver, immunosuppressive drugs will be stopped. The graft will be atrophy, which will be surgically removed (Figure 1A). When indicated for metabolic diseases which will cause an enzyme deficiency for example citrullinemia, the graft will be regenerated and observed (Figure 1B).

On the other hand, indicated for chronic liver disease, HCC in the left liver, the resection of native liver (usually left liver) with the transplantation of a left liver graft as a first step to secure a space for a graft. After the graft being regenerated, the diseased native liver will be removed in a second stage operation (Figure 1C). Familial amyloid polyneuropathy is a good indication.

This procedure is now called RAPID (29). A recent report (30) indicated that patients with a MELD score ≤ 27 and moderate portal hypertension (31) can be indicated for RAPID.

3. Minimum invasive procedures for donor hepatectomy

3.1. Laparoscopic donor hepatectomy (right liver) (32)

The donor is placed in the reverse Trendelenburg and lithotomy position. The 5 trocars are used: the 12-mm trocar in the umbilicus for a flexible laparoscope, another 12-mm trocar below the right costal margin and at the mid-clavicular line, both the 5-mm port and the 10-mm trocar below the xiphoid process for retraction of the liver and the 5-mm trocar in the left costal margin of the mid-clavicular line. Intra-operative cholangiography is not performed.

Liver dissection was done with a Cavitron ultrasonic surgical aspirator and a laparoscopic bipolar coagulator without inflow occlusion. The parenchymal transection line was determined by the branching pattern of middle hepatic vein (MHV) under ultrasound observation. The hepatic artery and portal vein were divided using Hem-o-lok. The right hepatic vein is closed with vascular stapler. The graft is resected, put in a retrieval bag and extracted through a 10-cm sized supra-pubic transverse incision.

3.2. Robotic Procedure (33)

The donors is in a 20-30 degrees reverse Trendelenburg position. The right shoulder will be upward (34). The 12-mm port is placed in the umbilicus. Four 8-mm trocars are placed on the right and left flank.

First, the inferior vena cava (IVC) ligaments are mobilized and the window between the right hepatic vein (RHV) and IVC was exposed. The liver is rotated to the left using the third arm. The short and right inferior hepatic veins are divided and ligated. The right liver was caudally to cranially mobilized until the root of the RHV is clearly identified.

Next, with the S4b segment lifted, the right hepatic artery and right portal vein are dissected and taped with a vascular loop. The right hepatic duct along Glisson's sheath were dissected. The fluorescent cholangiography was done for identifying the bile duct anatomy.

To expose the parenchyma 4-directional retraction is performed without inflow control. The hanging procedure is done using a Nelaton tube for lateral retraction. Liver parenchyma is transected with a Harmonic scalpel. Hemostasis was achieved with bipolar coagulation. V5 and V8 branches were clipped with Hemo-lok. Hepatic hilum and hepatic vein are divided.

3.3. Comparison between Minimum invasive and open for donor hepatectomy

The meta-analysis (35) showed the postoperative outcome of the donors who underwent right liver resection by a robotic or laparoscopic liver resection and conventional open approach. There were no statistical difference between the two groups in the complications \geq Dindo-Clavien classification IIIa, the estimated blood loss, or the length of postoperative hospital stay.

In 6 centers, totally 1194 donors underwent a right liver resection by a robotic ($n = 92$), laparoscopic ($n = 306$) and open approach ($n = 796$) (36). Conversions to open approach were in 1 (1%) robotic and 2 (2%) laparoscopic approach, respectively. Robotic approach had a longer operative time but reduced volume of donor blood loss ($p < 0.001$). There was no significant difference between the two arms in overall and Dindo-Clavien classification \geq IIIa complications. The donors by robotic hepatectomy had significantly less pain ($p < 0.001$).

4. Conclusions

The perioperative care and surgical techniques advancement have allowed the surgeons to use grafts with extended criteria. In the new era of transplant oncology (37) and constant innovation of surgical techniques, the field of LT may have continued to evolve progress also from now on.

Funding: None.

Conflict of Interest: The authors have no conflicts of interest to disclose.

References

- Battistella S, D'Arcangelo F, Grasso M, Zanetto A, Gambato M, Germani G, Senzolo M, Russo FP, Burra P. Liver transplantation for non-alcoholic fatty liver disease: Indications and post-transplant management. *Clin Mol Hepatol.* 2023; 29:S286-S301.
- Ahmed O, Liu L, Gayed A, Baadh A, Patel M, Tasse J, Turba U, Arslan B. The changing face of hepatocellular carcinoma: Forecasting prevalence of nonalcoholic steatohepatitis and hepatitis C cirrhosis. *J Clin Exp Hepatol.* 2019; 9:50-55.
- Zarrinpar A, Busuttil RW. Liver transplantation: past, present and future. *Nat Rev Gastroenterol Hepatol.* 2013; 10:434-440.
- Wong RJ, Aguilar M, Cheung R, Perumpail RB, Harrison SA, Younossi ZM, Ahmed A. Nonalcoholic steatohepatitis is the second leading etiology of liver disease among adults awaiting liver transplantation in the United States. *Gastroenterology.* 2015;148:547-555.
- Moctezuma-Velazquez C, Márquez-Guillén E, Torre A. Obesity in the liver transplant setting. *Nutrients.* 2019; 11:2552.
- Lin MY, Tavakol MM, Sarin A, Amirkiai SM, Rogers SJ, Carter JT, Posselt AM. Safety and feasibility of sleeve gastrectomy in morbidly obese patients following liver transplantation. *Surg Endosc.* 2013;27:81-85.
- Richards J, Gunson B, Johnson J, Neuberger J. Weight gain and obesity after liver transplantation. *Transpl Int.* 2005; 18:461-466.
- Campsen J, Zimmerman M, Shoen J, Wachs M, Bak T, Mandell MS, Kam I. Adjustable gastric banding in a morbidly obese patient during liver transplantation. *Obes Surg.* 2008; 18:1625-1627.
- Heimbach JK, Watt KD, Poterucha JJ, Ziller NF, Cecco SD, Charlton MR, Hay JE, Wiesner RH, Sanchez W, Rosen CB, Swain JM. Combined liver transplantation and gastric sleeve resection for patients with medically complicated obesity and end-stage liver disease. *Am J Transplant.* 2013; 13:363-368.
- Al-Nowaylati AR, Al-Haddad BJ, Dorman RB, Alsaied OA, Lake JR, Chinnakotla S, Slusarek BM, Sampson BK, Ikramuddin S, Buchwald H, Leslie DB. Gastric bypass after liver transplantation. *Liver Transpl.* 2013; 19:1324-1329.
- Lin MY, Tavakol MM, Sarin A, Amirkiai SM, Rogers SJ, Carter JT, Posselt AM. Safety and feasibility of sleeve gastrectomy in morbidly obese patients following liver transplantation. *Surg Endosc.* 2013; 27:81-85.
- Gentileschi P, Venza M, Benavoli D, Liroso F, Camperchioli I, D'Eletto M, Lazzaro A, Stolfi VM, Anselmo A, Di Lorenzo N, Tisone G, Gaspari AL. Intrahepatic balloon followed by biliopancreatic diversion in a liver transplant recipient: a case report. *Obes Surg.* 2009; 19:1460-1463.
- Giovinazzo F, Pascale MM, Cardella F, Picarelli M, Molica S, Zotta F, Martullo A, Clarke G, Frongillo F, Grieco A, Agnes S. Current Perspectives in Liver Transplantation for Perihilar Cholangiocarcinoma. *Curr Oncol.* 2023; 30:2942-2953.
- Breuer E, Mueller M, Doyle MB, *et al.* Liver Transplantation as a New Standard of Care in Patients With Perihilar Cholangiocarcinoma? Results From an International Benchmark Study. *Ann Surg.* 2022; 276:846-853.
- Darwish Murad S, Kim WR, Therneau T, Gores GJ, Rosen CB, Martenson JA, Alberts SR, Heimbach JK. Predictors of pretransplant dropout and posttransplant recurrence in patients with perihilar cholangiocarcinoma. *Hepatology.* 2012; 56:972-981.
- Ziogas IA, Hickman LA, Matsuoka LK, Izzy M, Montenovio MI, Rega SA, Feurer ID, Alexopoulos SP. Comparison of Wait-List Mortality Between Cholangiocarcinoma and Hepatocellular Carcinoma Liver Transplant Candidates. *Liver Transpl.* 2020; 26:1112-1120.
- Sapisochin G, Facciuto M, Rubbia-Brandt L, *et al.* Liver transplantation for "very early" intrahepatic cholangiocarcinoma: International retrospective study supporting a prospective assessment. *Hepatology.* 2016; 64:1178-1188.
- De Martin E, Rayar M, Golse N, *et al.* Analysis of Liver Resection Versus Liver Transplantation on Outcome of Small Intrahepatic Cholangiocarcinoma and Combined Hepatocellular-Cholangiocarcinoma in the Setting of Cirrhosis. *Liver Transpl.* 2020; 26:785-798.
- Lunsford KE, Javle M, Gaber AO, Vauthey JN, Ghobrial RM. Liver transplantation for locally advanced intrahepatic cholangiocarcinoma – Authors' reply. *Lancet Gastroenterol Hepatol.* 2018; 3:529-530.
- Terrault NA, Francoz C, Berenguer M, Charlton M,

- Heimbach J. Liver Transplantation 2023: Status Report, Current and Future Challenges. *Clin Gastroenterol Hepatol.* 2023; 21:2150-2166.
21. Mazzaferro V, Sposito C, Coppa J, Miceli R, Bhoori S, Bongini M, Camerini T, Milione M, Regalia E, Spreafico C, Gangeri L, Buzzoni R, de Braud FG, De Feo T, Mariani L. The Long-Term Benefit of Liver Transplantation for Hepatic Metastases From Neuroendocrine Tumors. *Am J Transplant.* 2016; 16:2892-2902.
 22. Maspero M, Rossi RE, Sposito C, Coppa J, Citterio D, Mazzaferro V. Long-term outcomes of resection versus transplantation for neuroendocrine liver metastases meeting the Milan criteria. *Am J Transplant.* 2022; 22:2598-2607.
 23. Nguyen NT, Harring TR, Goss JA, O'Mahony CA. Neuroendocrine Liver Metastases and Orthotopic Liver Transplantation: The US Experience. *Int J Hepatol.* 2011; 2011:742890.
 24. Olausson M, Friman S, Herlenius G, Cahlin C, Nilsson O, Jansson S, Wängberg B, Ahlman H. Orthotopic liver or multivisceral transplantation as treatment of metastatic neuroendocrine tumors. *Liver Transpl.* 2007; 13:327-333.
 25. Lim C, Lahat E, Osseis M, Sotirov D, Salloum C, Azoulay D. Liver Transplantation for Neuroendocrine Tumors: What Have We Learned? *Semin Liver Dis.* 2018; 38:351-356.
 26. Dueland S, Guren TK, Hagness M, Glimelius B, Line PD, Pfeiffer P, Foss A, Tveit KM. Chemotherapy or liver transplantation for nonresectable liver metastases from colorectal cancer? *Ann Surg.* 2015; 261:956-960.
 27. Hernandez-Alejandro R, Ruffolo LI, Sasaki K, *et al.* Recipient and Donor Outcomes After Living-Donor Liver Transplant for Unresectable Colorectal Liver Metastases. *JAMA Surg.* 2022; 157:524-530.
 28. Rajendran L, Claasen MP, McGilvray ID, Cattral MS, Ghanekar A, Selzner N, Burkes R, Winter E, Gallinger S, Sapisochin G. Toronto Management of Initially Unresectable Liver Metastasis from Colorectal Cancer in a Living Donor Liver Transplant Program. *J Am Coll Surg.* 2023; 237:231-242.
 29. Nadalin S, Settmacher U, Rauchfuß F, Balci D, Königsrainer A, Line PD. RAPID procedure for colorectal cancer liver metastasis. *Int J Surg.* 2020; 82s:93-96.
 30. Balci D, Kirimker EO, Bingol Kologlu M, Ustuner E, Goktug UU, Karadag Erkoc S, Yilmaz AA, Bayar MK, Azap A, Er RE, Dokmeci A, Karayalcin K. A New Approach for Increasing Availability of Liver Grafts and Donor Safety in Living Donor Liver Transplantation: LD-RAPID Procedure in the Cirrhotic Setting With Hepatocellular Carcinoma. *Liver Transpl.* 2021; 27:590-594.
 31. Deuffic-Burban S, Mathurin P, Rosa I, Bouvier AM, Cannesson A, Mourad A, Canva V, Louvet A, Deltenre P, Boleslawski E, Truant S, Pruvot FR, Dharancy S. Impact of emerging hepatitis C virus treatments on future needs for liver transplantation in France: a modelling approach. *Dig Liver Dis.* 2014; 46:157-163.
 32. Lee B, Choi Y, Han HS, Yoon YS, Cho JY, Kim S, Kim KH, Hyun IG. Comparison of pure laparoscopic and open living donor right hepatectomy after a learning curve. *Clin Transplant.* 2019; 33:e13683.
 33. Chen PD, Wu CY, Hu RH, Ho CM, Lee PH, Lai HS, Lin MT, Wu YM. Robotic liver donor right hepatectomy: A pure, minimally invasive approach. *Liver Transpl.* 2016; 22:1509-1518.
 34. Broering DC, Elsheikh Y, Alnemary Y, Zidan A, Elsarawy A, Saleh Y, Alabbad S, Sturdevant M, Wu YM, Troisi RI. Robotic Versus Open Right Lobe Donor Hepatectomy for Adult Living Donor Liver Transplantation: A Propensity Score-Matched Analysis. *Liver Transpl.* 2020; 26:1455-1464.
 35. Lai Q, Giovanardi F, Mennini G, Berardi G, Rossi M. The impact of mini-invasive right hepatectomy in the setting of living donation: A meta-analysis. *Updates Surg.* 2022; 74:23-34.
 36. Troisi RI, Cho HD, Giglio MC, Rhu J, Cho JY, Sasaki K, Han DH, Kwon CHD, Han HS, Chen PD, Wu YM, Choi GH, Choi GS, Kim KH. Robotic and laparoscopic right lobe living donation compared to the open approach: A multicenter study on 1194 donor hepatectomies. *Liver Transpl.* 2024; 30:484-492.
 37. Sapisochin G, Hibi T, Toso C, Man K, Berenguer M, Heimbach J, Greten TF, Pugh TJ, Dawson LA, Mazzaferro V. Transplant oncology in primary and metastatic liver tumors: principles, evidence, and opportunities. *Ann Surg.* 2021; 273:483-493.

Received June 15, 2024; Accepted June 27, 2024.

*Address correspondence to:

Yasuhiko Sugawara, Transplantation/Pediatric Surgery, Postgraduate School of Life Science, Kumamoto University, 1-1-1 Honjo, Chuo-Ku, Kumamoto 8603-8556, Japan.
E-mail: yasusuga-ky@umin.ac.jp

Released online in J-STAGE as advance publication June 29, 2024.

Addressing healthy aging in China: Practices and prospects

Haiyin Wang^{1,*}, Dan Qin², Liang Fang¹, Hui Liu³, Peipei Song⁴

¹ Shanghai Health Development Research Center (Shanghai Medical Information Center), Shanghai, China;

² School of Pharmaceutical Sciences and Yunnan Provincial Key Laboratory of Pharmacology for Natural Products, Kunming Medical University, Kunming, Yunnan, China;

³ Songjiang Hospital Affiliated to Shanghai Jiao Tong University School of Medicine, Shanghai, China;

⁴ National Center for Global Health and Medicine, Tokyo, Japan.

SUMMARY One important challenge for global development is aging. China is one of the world's countries with the highest elderly population and the most rapid aging; in 2022, the percentage of the population over 65 was 14.9%; by 2050, it is expected to rise to 26.1%. China's health security, elderly care, and healthcare services are facing serious challenges as a result of this aging trend. With 80% of provinces including medical and elderly care in national basic public health care programs, China has adopted a proactive national plan to combat population aging. Moreover, geriatric departments have been established at 69.3% of public general hospitals at secondary and higher tiers, 48% of provinces have devised preventive interventions for disability and dementia in the elderly, 48 percent of provinces are serving as test regions for medical care related to rehabilitation, and 49 cities are involved in long-term care insurance (LTCI) trials that encompass 170 million people. There are 4,259 medical and health care facilities that provide hospice care services, 152 hospice care pilot regions, and 87,000 pairs of contracts between medical and health care facilities and elderly care providers. These developments provide a strong basis, but there are still major obstacles to overcome. The Chinese Government is urged to adopt early preventive measures, offer more ongoing, practical, and cost-effective diagnostic and treatment services, allocate resources equitably, and use intelligent technologies to enhance elderly care. The ultimate goals are to lessen the financial burden, enhance the health of the elderly, and offer a vital global resource.

Keywords aging, China, health policy, long-term care insurance, prospects

1. Introduction

The world's population is about to begin aging, and this will significantly affect every nation. China has one of the highest aging rates in the world as well as the largest elderly population worldwide. China's population was moderately aged in 2022, when the number of people 65 and older climbed from 64 million in 1990 to 210 million and the population share rose from 5.57% to 14.9%. These figures are from the National Bureau of Statistics of China (1). The severity of the aging crisis is shown by the projection that 366 million Chinese people will be 65 years of age or older by 2050 (Figure 1), accounting for 26.1% of the country's total population (2).

Life expectancy in China has increased during population aging, rising from 68.55 years in 1990 to 77.7 years in 2019. By 2035, it is predicted to reach 81.3 years in mainland China (3). However, growing older

also presents a number of difficulties. According to one study, for example, the number of people in China who are 65 years of age or older and who have a disability will climb by 205% from 2010 to 2025. In the 65-79 age group, the number of patients with dementia or suffering from a stroke is expected to rise by 297.9% and 167.8% (4), respectively. China's health care system, which includes medical care, long-term care, rehabilitation, and mental health care, will face significant problems as a result of these changes. Moreover, healthcare spending per capita for those 65 and older is 1.61 times higher than for those 25 to 59 and 7.25 times higher than for those 25 to 25, placing a significant burden on China's medical insurance funds (5). In addition, a study has shown that the mortality risk for dementia patients over 60 in rural areas is three times higher than in urban areas, and the risk for depression is 4.15 times higher. These findings suggest that unequal resource allocation may contribute to health inequalities (6).

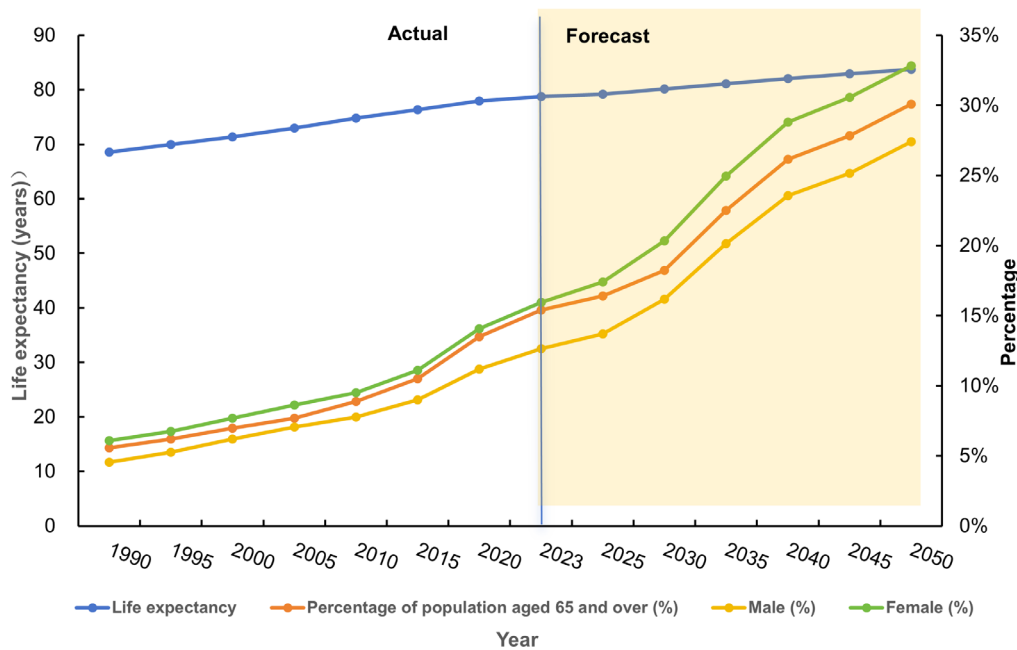


Figure 1. Trends in and Challenges from Aging in China.

2. Progress in China's healthy aging practices (Table 1)

2.1. Prevention and intervention

The "Healthy China 2030" Planning Outline was released by the Chinese Government in 2016 in order to reduce premature mortality from major chronic diseases by 30% by 2030 in comparison to 2015 (7). The Healthy China Initiative, which aims to improve the active health capacities of the elderly, was introduced in 2019 and includes a plan for older health promotion. According to one study, the illness burden climbed from 27th to 15th (8), and China's ranking for Alzheimer's disease mortality jumped from 10th in 1990 to 5th in 2019. An action plan (2023–2025) for the prevention of Alzheimer's disease and promotion of its care was formulated by the National Health Commission in 2023. It included sharing relevant information, guiding cognitive function screening and classified interventions in eligible regions, and investigating the creation of a service network for Alzheimer's disease prevention and treatment. By 2022, four provinces and one city had started initiatives to prevent falls among the elderly, and 25 provinces had incorporated medical and elderly care as well as health in old age into national basic public health care projects. Organized preventative interventions for dementia and older disabilities had been implemented in 15 provinces (9). One hundred and twenty-seven million senior citizens 65 years of age and older had their health managed at primary healthcare facilities in 2022.

2.2. Disease diagnosis and treatment

A notice on comprehensively enhancing elderly health care and guidelines for the design and administration

of geriatric departments were issued in 2021 by the National Health Commission and other agencies. These documents also promoted multidisciplinary models of diagnosis and treatment in healthcare facilities, improved the handling of geriatric syndromes, and changed the focus of elderly medical care from single-disease management to multi-morbidity management. Another requirement was standardizing the design and administration of geriatric departments. In 2023, the State Council published a report outlining its recommendations for expanding the medical and health care system. These included promoting urban medical alliances, county-level medical groups, joint clinics for chronic illness between medical facilities at the primary and higher tiers and improved management and capabilities for elderly medical care. In 2022, China surpassed the 2025 target of 60% (10) by having 5,909 secondary and above comprehensive hospitals with geriatric departments — representing 69.3% of such hospitals nationwide — and one national geriatric medical center in addition to six national clinical research centers for geriatric disorders.

2.3. Rehabilitation and nursing

The Implementation Plan to Enhance the Rehabilitation Capabilities of Traditional Chinese Medicine (2021–2025), published in 2020 by the National Health Commission and other departments, aims to increase the percentage of traditional Chinese medicine hospitals at the secondary and tertiary tiers with rehabilitation departments to 85% and 70%, respectively, by 2025. The National Health Commission designated 15 provinces as pilot regions in a notice on pilot work for rehabilitation care that was published in 2021. The pilot program's objectives included guiding the transformation of some

Table 1. Crucial occasions in China's reaction to healthy aging

Area	Year	Policy	Key Issues
Prevention	2019	Healthy China: Health Promotion Activities for the Elderly	Decreasing the prevalence of impairment in the 65–74 age group, moderating the rate at which dementia develops in the 65+ age group, and improving the design of geriatric medicine and rehabilitation units.
	2023	Action for the Prevention and Promotion of Alzheimer's Disease (2023–2025)	Reducing and avoiding the development of Alzheimer's disease.
	2024	Initiative for Health Promotion and Elderly Hearing (2024–2027)	Preventing and mitigating the development of hearing loss in the elderly.
Diagnosis and Treatment	2021	Comprehensive Enhancement of Elderly Health Care	Enhancing the medical and health care system's amenability, creating a comprehensive elderly health care system, and improving the elder's capacity to receive treatment of several diseases.
	2023	Further Improvement of the Medical and Health Care System	Enhancing the fairness, accessibility, and capacity to deliver quality medical and health care; further developing integrated medical and health care systems.
Rehabilitation and Nursing	2020	Implementation Plan for the Promotion of Chinese Medicine Rehabilitation Service Capabilities (2021–2025)	Capitalizing on the vital role of traditional Chinese medicine in disease rehabilitation, encouraging the integration of traditional Chinese medicine, traditional Chinese sports, and modern rehabilitation techniques, and producing rehabilitation medicine with Chinese characteristics.
	2021	Pilot Work on Rehabilitation Care	Investigating, developing, and implementing a variety of rehabilitation medical service models and a comparatively comprehensive rehabilitation medical service system.
	2022	National Nursing Career Development Plan (2021–2025)	Bolstering the development of nursing personnel, optimizing the distribution of nursing resources, and expand the availability of home-based, community-based, traditional Chinese medicine, and geriatric nursing.
Long-Term Care	2016	Guidance on a Pilot Project for a Long-Term Care Insurance System	Enhancing the standard of living and humanitarian care provided to people with disabilities by addressing challenges to long-term care.
	2020	Guidance on Expanding the Pilot Project for the Long-term Care Insurance System	Improving benefit payout, fund-raising, insurance participation and coverage, and institutional framework optimization.
Integrated Medical and Elderly Care	2016	Integrated Medical and Elderly Care Pilot Program	Investigating various local integrated medical and elderly care models and creating a medical service network that provides sufficient scale coverage for both rural and urban locations.
	2024	National Integrated Medical and Elderly Care Regions and Institutions	Providing a comprehensive policy framework for integrated medical and elderly care, take the lead, supporting and mentoring different localities to further advance integrated medical and elderly care, and summarizing and promoting successful experiences and practices.
Smart Elderly Care	2017	Action Plan for the Development of Smart Health and the Elderly Care Industry (2017–2020)	Encouraging the formation of a consortium of businesses, townships, or neighborhoods and trial sites that can offer developed smart health and elderly care services, solutions, platforms, or products; in addition, facilitating the growth and implementation of the smart health and elderly care sector.
	2020	Implementation Plan to Address Difficulties in the Use of Smart Technology by the Elderly	Promoting solutions to difficulties the elderly have using smart technology.
	2021	The Second Batch of Pilot Institutions for Remote Collaborative Services in Integrated Medical and Elderly Health Care	Using the Internet to enhance the quality, efficiency, and level of integrated medical and elderly care services.
	2023	Directorate to Promote Smart Health and Elderly Care Products and Services (2022 Edition)	Promoting the use and spread of typical smart health and elderly care products and services, and encouraging the development of the smart health and elderly care industry.
Palliative Care	2017	Palliative Care Practice Guidelines (Trial) and the First Batch of Palliative Care Pilot Programs	Advising local areas to further construct and manage palliative care centers, and standardizing palliative care practices.
	2019	The Second Batch of Palliative Care Pilot Programs	Devising working procedures, developing service systems, defining services, conducting pilot surveys, investigating institutional protections, fostering teamwork, creating standards and norms, and improving publicity and educational campaigns.
	2023	The Third Batch of Palliative Care Pilot Programs	Creating service teams, enhancing support policies, building service systems, and conducting publicity and educational campaigns.

primary and secondary hospitals into rehabilitation hospitals and expanding the number of beds and medical facilities offering rehabilitation services. The National Health Commission published the National Nursing Career Development Plan (2021–2025) in 2022. It aims to increase the number of registered nurses in the country to 5.5 million by 2025, or 3.8 nurses per 1,000 people. This will greatly boost the availability of home, community, and traditional Chinese medicine nursing, as well as care for the elderly. In order to hasten the growth of geriatric nursing, the strategy included suggested improvements. The percentage of nursing beds in primary healthcare facilities increased to 30% by 2022.

2.4. Long-term care insurance (LTCI)

Shanghai, Guangzhou, and Suzhou were among the 15 cities chosen by the Ministry of Human Resources and Social Security to participate in the LTCI system trial program, which was announced in 2016. Guidelines for expanding the LTCI pilot program were announced in 2020 by the Ministry of Finance and the National Medical Insurance Administration, bringing the total number of pilot cities and regions to 49 (11). LTCI prioritizes eligible senior citizens while addressing the fundamental care needs of people with severe disabilities. In 49 pilot cities, 169.902 million people took part in LTCI by 2022, with 1.208 million beneficiaries. Fund expenditures in 2022 totaled 10.44 billion Chinese yuan, while fund revenue came to 24.08 billion yuan. There were 331,000 carers and 7,679 certified LTCI facilities. From the perspective of implementation, the use of LTCI dramatically decreased the yearly frequency and cost of hospitalization (12) while also prolonging the survival time of those over 65 by 33.74 days (13) and reducing their mortality rate by 5.10%. Another analysis revealed that the LTCI pilot programs had a positive impact overall, although there were significant geographical differences. The majority of pilot city programs sought to lessen the financial burden on patients' families (14).

2.5. Smart homes and elderly care

The Action Plan for the Development of the Smart Healthy Aging Industry (2017–2020) was jointly issued in 2017 by the Ministry of Industry and Information Technology and other departments. Its objectives include encouraging businesses and healthy aging facilities to fully utilize smart healthy aging products and to develop innovative solutions for chronic disease management, home-based healthy aging, personalized health management, online health consultation, life care, and information services for elderly care facilities (15). The General Office of the State Council issued an implementation plan in 2020 with the goal of bridging the "digital gap" in healthcare and other

industries by addressing the challenges older people have when utilizing smart technologies. The National Health Commission, which identified 346 facilities, announced the second round of trial facilities for remote collaboration in integrated medical and geriatric care in 2021. The Catalog to Promote Smart Healthy Aging Products and Services (2022 Edition) was jointly published in 2023 by the Ministry of Industry and Information Technology and other agencies. It includes a list of 25 service providers and 54 product manufacturers. According to one study, China is progressively developing a community-based smart aging system that includes medical and elderly care interaction, home safety, institutional elderly care, community-based elderly care, and at-home elderly care (16).

2.6. Integrated medical and elderly care

Two batches of ninety national pilot projects for integrated medical and elder care were authorized by the Chinese Government in 2016 (17). The National Health Commission designated 100 counties (cities, districts) as national trial areas, 100 facilities as national trial sites, and Shandong Province as the national trial province for integrated medical and elderly care in 2024. In terms of integrated medical and elderly care, China has created four well-developed service models: collaboration between medical and health care facilities and facilities that provide elderly care services; medical and health care facilities offering integrated medical and elderly care; elderly care facilities offering medical care; and expanding medical care to homes and communities. By 2024, China will have 2 million beds, 7,800 integrated medical and elderly care facilities qualifying as medical facilities and registered as elderly care facilities, 87,000 signed contracts between medical and health care facilities and elderly care facilities, and an increase in the number of beds available. Studies have revealed that government agencies, like the Ministry of Industry and Information Technology (MIIT) and the National Health Commission (NHC), have worked closely together to improve interdepartmental cooperation over time. Research has indicated that integrated medical and elderly care significantly improves medication adherence, dietary habits, exercise routines, regular follow-ups, medical compliance behaviors, and reduces negative emotions (16). This is evident from studies on the Hospital-Community Integrated Service Model (HCISM) in the home rehabilitation of elderly stroke patients (18).

2.7. Hospice care

In addition to launching the first round of hospice care pilot projects in five locations, the National Health Commission published practice guidelines (draft) for hospice care in 2017. The Law of the People's Republic

of China on Basic Medical and Health Care and Health Promotion was passed by the Standing Committee of the National People's Congress in 2019. It stated that "all types of medical and health care facilities at all levels should provide citizens with comprehensive and life-cycle medical and health care, including hospice care." The National Health Commission announced the second batch of 71 city (district) pilot programs and in 2019 the third batch of 64 city (district) pilot programs in 2023. By 2023, 4,259 medical and healthcare facilities across the country had departments dedicated to hospice care, and there were 152 hospice care trial sites. China has investigated and developed a number of hospice care models (19), including home-based, hospital-based, community-based, integrated medical and geriatric care, remote hospice care, and hospice care directed by traditional Chinese medicine. By the end of 2020, hospice care at community health care centers was fully covered in Shanghai (20).

3. Prospects as aging proceeds in China

China still faces many obstacles, but it has made headway in handling its aging population. China will prioritize earlier preventive interventions, more continuous, convenient, and cost-effective diagnostic and treatment services, more balanced resource allocation, smarter products, and a friendlier social environment during the period of the "14th Five-Year Plan" and beyond due to its economic growth, the development of highly qualified public hospitals, and extensive research on and use of AI technologies. This will lessen the financial burden, enhance health outcomes, and more effectively address the healthcare needs of the elderly. The following describes the structural, process, and outcome aspects as aging proceeds in China based on its existing reality (Figure 2).

3.1. Improving resource allocation and interdepartmental policy coordination

China should improve interdepartmental policy coordination under the Healthy China agenda. To improve policy consistency, departments and organizations like the State Administration for Market Regulation, the China Disabled Persons' Federation, the National Health Commission, the Ministry of Science and Technology, and the Ministry of Industry and Information Technology should enhance their collaboration during the policy-making process. Second, the integration of traditional and modern medicine, integrated medical and elderly care facilities, and sports and health promotion should be enhanced. Third, to guarantee equitable and accessible elderly health care, balanced resource distribution among regions should be heavily encouraged, with central government transfers toward the west and rural areas.

3.2. Enhancing the management of integrated health and medical insurance

First, China should consider incorporating nursing homes, rehabilitation centers, and hospice care facilities into an integrated, continuing medical care system that includes prevention, diagnosis, treatment, and care for disease. This builds on the ongoing support of medical alliances and communities. Second, China should continue to encourage the formation of specialized geriatric alliances to improve coordinated geriatric medical care capabilities and efficiency. Third, China should sustainably advance LTCI pilot programs and protective measures to increase the security level for senior citizens.

3.3. Improving the use of digital products and technologies

First, China should concentrate on transitional applications and actively encourage the use of evaluation, diagnosis, and monitoring technologies appropriate for home and community applications to improve

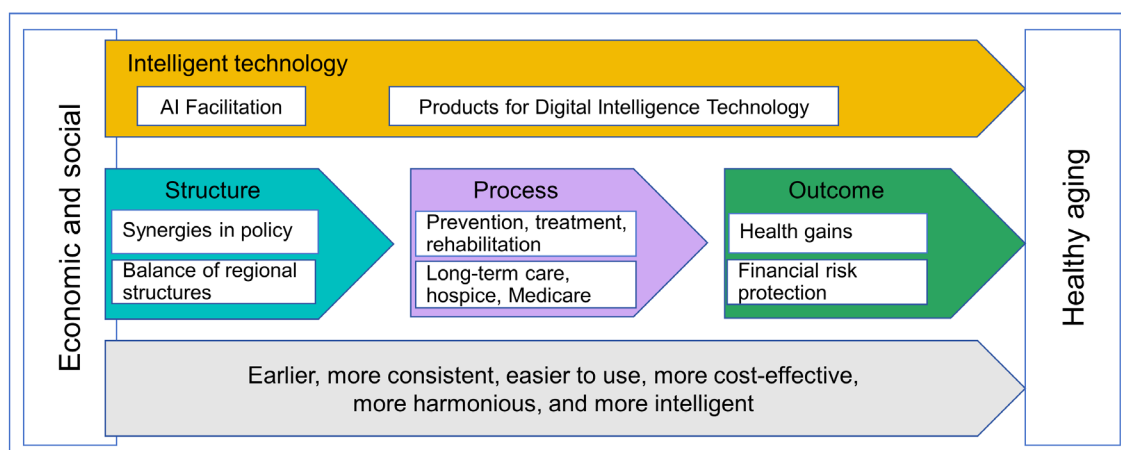


Figure 2. China's Active Aging Development Strategies

amenability to the elderly. This builds on the ongoing promotion of smart elderly care. Second, China should improve the cutting-edge "Internet +" elderly and elderly care models to raise the level and efficiency of intelligent elderly health care.

3.4. Improving the tracking and evaluation of health outcomes and financial risks for the elderly

China should create a results-driven monitoring and assessment system to track and analyze financial and health risks for the elderly on a regular basis, pinpoint successful and unsuccessful models, and compile insights and lessons learned. In order to increase the accessibility and integration of multi-source data on health outcomes and individual burdens, China first needs to further create pertinent database systems. Second, China needs to improve data-driven decision-making, promptly evaluate health technologies, choose safe, efficient, cost-effective, innovative suitable, and easily accessible intervention programs and pathways, and assist with the growth of a healthy aging population.

4. Conclusion

This article has examined the circumstances of aging and issues facing China, as well as the government's policy initiatives, accomplishments, and outlook for the country's future growth. The chance of developing dementia, a chronic illness, or impairment rises significantly with age, which presents great problems to China's medical and health care system as well as its health security system. A multifaceted elderly health care and security system that includes health education, preventive healthcare, disease diagnosis and treatment, nursing and rehabilitation, long-term care, integrated medical and elderly care, smart elderly care, and hospice care was first created by the Chinese Government in response to the country's population aging strategy. Even though these initiatives have been crucial in providing support, there are still many obstacles to overcome. These include uneven policies, unequal resource distribution, ineffective preventive measures, a lack of continuity and convenience in diagnostic and treatment, noticeable differences between urban and rural areas, and insufficient health security measures. China should prioritize early prevention, more ongoing, convenient, and cost-effective services, more equitable resource distribution, smarter technological applications, and a more welcoming social climate in the future.

Funding: None.

Conflict of Interest: The authors have no conflicts of interest to disclose.

References

1. National Bureau of Statistics of China. China Statistical Yearbook 2023; China Statistics Press: Beijing, 2023. (in Chinese)
2. Feng Z, Glinskaya E, Chen H, Gong S, Qiu Y, Xu J, Yip W. Long-term care system for older adults in China: Policy landscape, challenges, and future prospects. *Lancet*. 2020; 396:1362-1372.
3. Bai R, Liu Y, Zhang L, Dong W, Bai Z, Zhou M. Projections of future life expectancy in China up to 2035: A modelling study. *Lancet Public Health*. 2023; 8:e915-e922.
4. Han Y, Hu K, Wu Y, Fang Y. Future life expectancy with disability among elderly Chinese individuals: A forecast based on trends in stroke and dementia. *Public Health*. 2021; 198:62-68.
5. Li L, Du T, Hu Y. The effect of population aging on healthcare expenditure from a healthcare demand perspective among different age groups: Evidence from Beijing City in the People's Republic of China. *Risk Manag Healthc Policy*. 2020; 13:1403-1412.
6. Chen R, Hu Z, Wei L, Wilson K. Socioeconomic status and survival among older adults with dementia and depression. *Br J Psychiatry*. 2014; 204:436-440.
7. Chen WQ, Li N, Shi JF, Ren JS, Chen HD, Li J, Dai M, He J. Advancement of early diagnosis and treatment projects for cancer in urban areas of China. *China Cancer*. 2019; 28:23-25. (in Chinese)
8. Ren R, Qi J, Lin S, *et al*. The China Alzheimer Report 2022. *Gen Psychiatr*. 2022; 35:e100751.
9. National Office for Aging, Ministry of Civil Affairs, China. National Development Bulletin on Aging in 2022. https://www.gov.cn/lianbo/bumen/202312/content_6920261.htm (accessed June 15, 2024). (in Chinese)
10. Chen X, Giles J, Yao Y, *et al*. The path to healthy ageing in China: A Peking University-Lancet Commission. *Lancet*. 2022; 400:1967-2006.
11. Wang L. The impact of long-term care insurance pilot on the mental health of older adults: Quasi-experimental evidence from China. *SSM Popul Health*. 2024; 25:101632.
12. Yang S, Guo D, Bi S, Chen Y. The effect of long-term care insurance on healthcare utilization of middle-aged and older adults: Evidence from China Health and Retirement Longitudinal Study. *Int J Equity Health*. 2023; 22:228.
13. Zeng L, Zhong Y, Chen Y, Zhou M, Zhao S, Wu J, Dong B, Dou Q. Effect of long-term care insurance in a pilot city of China: Health benefits among 12,930 disabled older adults. *Arch Gerontol Geriatr*. 2024; 121:105358.
14. Li Q, Chen Y, Zhang Y, Liu X. Evaluation of China's long-term care insurance policies. *Front Public Health*. 2024; 12:1252817.
15. Shafei I, Khadka J, Balasubramanian M. Smart homes: Pioneering age-friendly environments in China for enhanced health and quality of life. *Front Public Health*. 2024; 12:1346963.
16. Feng WM. The development status, problems, and response strategies of smart elderly care in China. *J Chongqing Uni Tech (Social Science)*. 2024; 2:1-14. (in Chinese).

17. Tang R, Wang Z. The current status of medical and elderly care integration in China and its challenges to healthcare security governance. *China Medical Insurance*. 2024; 5:26-34. (in Chinese)
18. Feng W, Yu H, Wang J, Xia J. Application effect of the hospital-community integrated service model in home rehabilitation of stroke in disabled elderly: A randomised trial. *Ann Palliat Med*. 2021; 10:4670-4677.
19. Zhao WW, Guo CY, Yang JX, Zhou Zm Ji WG, Cheng WU. Research progress on hospice care practices. *Medicine and Philosophy*. 2024, 45:32–37. (in Chinese)
20. Gong XQ, Bai HN. Research on the policy diffusion of hospice care in Shanghai: Text analysis based on 56 hospice policies. *Chin J Health Policy*. 2022; 15:30-37. (in Chinese)

Received May 15, 2024; Revised June 17, 2024; Accepted June 29, 2024.

**Address correspondence to:*

Haiyin Wang, Shanghai Health Development Research Center (Shanghai Medical information Center), No. 181 Xinbei Road, Shanghai, China 201199.

E-mail: wanghaiyin@shdrc.org

The latest policies, practices, and hotspots in research in conjunction with the aging of Japan's population

Yuan Liu^{1,2}, Susumu Kobayashi², Kenji Karako^{3,*}, Peipei Song^{2,*}, Wei Tang²

¹ Shanghai Chest Hospital, Shanghai Jiao Tong University School of Medicine, Shanghai, China;

² National Center for Global Health and Medicine, Tokyo, Japan;

³ Department of Surgery, Graduate School of Medicine, The University of Tokyo, Tokyo, Japan.

SUMMARY Population aging is a global concern, and Japan currently has the world's highest proportion of an aging population. In 2020, the population age 65 and over accounted for 10% of the global population, while this proportion was 29% in Japan, and it is expected to reach 38.4% in 2065. The average life expectancy in Japan in 2022 was 81.05 for males and 87.09 for females. At the same time, Japan's healthy life expectancy continues to increase, and it is increasing at a faster rate than the average life expectancy, with males expected to live 72.68 years and females expected to live 75.38 years in 2019. This is causing the social role of elderly people in Japan to constantly change. The Japanese Government continues to adjust its policy orientation, to improve the health level and social participation of the elderly, improve the accessibility of long-term nursing services and the treatment of nursing professionals, and improve the pension system. By 2025, one-fifth of people in Japan are expected to suffer from dementia. Japan has implemented a series of policies to create a dementia-inclusive and less risky society. The proportion of the population ages 65 and over living alone in Japan increased from 4.3% among males and from 11.2% among females in 1980 to 15.0% among males and 22.1% among females in 2020, representing a sustained increase. Changes in the composition of the population have prompted sustained attention to the personalization and diversification of elderly care. At the same time, Japanese researchers continue to utilize scientific and information technology to innovate elderly care products, improve the efficiency of elderly care, and provide intelligent elderly care.

Keywords Japan, policy, aging, dementia, innovation

1. Population aging

The global phenomenon of population aging presents profound challenges to nations across the globe. The population over the age of 65 years is growing more rapidly than the population below that age. As a result, the share of the global population age 65 and over is projected to rise from 10% in 2022 to 16% in 2050 (1).

Japan has a superannuated population; people age ≥ 65 accounted for 29.0% of the country's population in 2022, which is the highest proportion in the world (2). The issue of population aging in Japan is expected to become even more severe over the next 40 years, with the proportion projected to rise to 38.4% by 2065 (3). The average life expectancy in Japan in 2022 has become 81.05 years for men and 87.09 years for women, representing the world's longest longevity (4). At the same time, Japan's healthy life expectancy continues to increase, and it is increasing at a faster rate than the

average life expectancy, with males expected to live 72.68 years and females expected to live 75.38 years in 2019 (2). This has led to a continuous evolution of the social roles of elderly individuals in Japan, with the changing demands for social participation and healthcare among the aging population. Maintaining the health and functional abilities of elderly individuals, as well as ensuring their quality of life and healthcare, has been a focal point of policy discussions and research in Japan, yielding internationally recognized results.

The challenge of population aging exists in both developed and developing regions. Providing economic security and healthcare for the elderly is a politically sensitive topic. Japan's decades-long efforts and systematic approach have resulted in higher levels of health among the elderly population and widespread access to healthcare and long-term care. Sharing Japan's experiences is crucial for other countries around the world. This study summarizes Japan's latest policy

practices and research trends since 2018, providing valuable insights for global responses to aging.

2. Recent support policies for population aging in Japan

2.1. Improving the social participation of the elderly

Japan has implemented a series of policy measures to enhance the level of health and social participation of the elderly population in order to create a sustainable aging society. In 2018, the Cabinet approved The Guideline of Measures for Ageing Society (5), providing comprehensive guidance for mid-to-long-term public measures to address an aging society. The document pointed out that the trend of defining individuals age 65 and over as elderly is no longer realistic as the physical age of elderly individuals tends to be younger. In 2021, the Act on Stabilization of Employment of Elderly Persons was revised to require employers to take measures to provide their employees with opportunities to work up to the age of 70 (6).

The Healthy Japan 21 strategy, spanning from the first term (2000-2012) to the second term (2013-2022), and subsequently the third term that was implemented in 2023, is committed to extending healthy life expectancy (7,8). Japan has also comprehensively promoted health by implementing a series of interventions such as diet and exercise (9) (Table 1).

2.2. Health care for the elderly

As the country's demographics change, the disease structure changes, and therefore the demand for health care changes. In order to ensure continuous and comprehensive access to long-term care for the elderly population, Japan is actively working to improve long-term care and personnel training. To enable the elderly population in need of medical and nursing care to continue living in familiar communities, Japan has implemented a series of measures to promote home medical care and nursing. These include the 8th National Medical Strategic Plan (10) and the Guidelines for Promoting Home Medicine and Nursing

Table 1. Key events in Japanese policies on population aging from 2018 to 2023

Classification	Year	Policies and Events
Social participation	2018	The Guideline of Measures for Ageing Society was approved. They reviewed standardization by age and aim to create an age-free society in which people of all ages can live and work happily.
	2020	The Dietary Reference Intakes for Japanese (2020) focuses on preventing malnutrition and physical weakness in elderly individuals.
	2021	The Act on Stabilization of Employment of Elderly Persons was revised to gradually extend retirement age to 70.
	2023	The third term of the Healthy Japan 21 strategy was announced with the continuation of extending healthy life expectancy as its ultimate goal.
Health care	2020	The 8 th National Medical Strategic Plan defines the functions and roles of "medical facilities that play an active role in home medical care" and "medical facilities necessary for home medical care".
	2020	Guidelines for Promoting Home Medicine and Nursing Collaboration Projects (Version 3) were announced, aimed to establish a community-based integrated care system.
	2021	Partial revisions were made to Long-term Care Insurance to establish a system to facilitate the provision of home medical care and nursing.
	2021	Nursing fees were modified to promote better treatment of caregivers' and better working conditions.
	2021	The Child and Family Care Leave Act was revised to relax requirements for fixed-term contract workers to take family care leave.
Economic security	2020	The National Pension Act was partially revised to enhance the functionality of the pension system.
	2021	The 8 th term of the Long-term Care Insurance Project Plan was released to facilitate the provision of insurance benefits for long-term care.
Dementia assistance	2018	The Ministerial Council on the Promotion of Dementia Policies was set up to further promote dementia policies.
	2019	The National Framework for Promotion of Dementia Policies was adopted at the Ministerial Council, using a whole-of-society approach to reduce the risk of dementia and provide a better quality of life for those living with dementia.
	2019	The Ministerial Council devised the Outline for the Promotion of Dementia Policies to enable people with dementia to continue to live their lives in their own way in the communities they are familiar with.
	2023	The "Basic Act on Dementia to Promote an Inclusive Society" was enacted to enable those with dementia to live in dignity with a sense of purpose.

Collaboration Projects (Version 3) (11) in 2020. In 2021, Long-Term Care Insurance was partially revised to create a system to facilitate the provision of home medical care and nursing (12). One of the key focuses of the modification of nursing fees in 2021 was to promote better treatment of caregivers and better working conditions (13). The Child and Family Care Leave Act was amended in 2021 to relax requirements for fixed-term contract workers to take family care leave in order to assist home caregivers in balancing work and care (14).

2.3. Economic security

Japan's social security systems, such as Pension Insurance, Medical Insurance, and Nursing Care Insurance, provide financial security for the elderly to receive social services. Since 2000, Japan has promoted a long-term care insurance system, financed by social insurance and taxes, to ensure that the burden on older persons is reduced (15). To maintain financial sustainability, Japan has been dynamically adjusting economic security policies. For instance, laws such as the National Pension Act (16) were amended in 2020 to enhance the functionality of the pension system. In 2021, the government released the 8th term of the Long-term Care Insurance Project Plan (17).

2.4. Dementia assistance

Long-term cognitive diseases such as dementia are on the rise as the population ages, and Japan has one of the highest rates of dementia in the world. With nearly 5 million Japanese living with dementia in 2015, and with one in five people in Japan expected to have dementia by 2025 and one-third of the population expected to live with the disease by 2060, the societal burden of dementia is unquestionably high (18). Japan hopes to create a dementia-inclusive and less risky society through a series of policies. In 2018, Japan established the Ministerial Council on the Promotion of Dementia Policies to promote dementia policies (19). In 2019, the Council adopted the National Framework for Promotion of Dementia Policies (20), which adopted a whole-of-society approach by considering multiple interwoven psychosocial, environmental, and healthcare dimensions to reduce the risk of dementia and provide a better quality of life for people with dementia. That same year, the Council devised the Outline for the Promotion of Dementia Policies, which is based on the concepts of "symbiosis" and "prevention" to enable people with dementia to continue to live their lives in their own way in the communities they are familiar with. The Basic Act on Dementia to Promote an Inclusive Society was enacted in 2023 to promote policies that enable people with dementia to live with greater dignity (21).

3. The latest hotspots in research on population aging in Japan

3.1. Health promotion and disease prevention

In order to create a healthy and vigorous population with long lives, Japan has been actively promoting disease prevention and health promotion, gradually shifting from a traditional focus on physical health to a focus on multiple dimensions of health, including physical, mental and social health, and actively promoting healthy lifestyles based on "nutrition, exercise, and recuperation." In recent years, the creation of nutritional and dietary support systems has been a hot topic of research in order to facilitate the independent living of the elderly and prevent them from becoming seriously ill. Exercise and nutritional interventions to prevent frailty in the elderly have also been a hot topic of research. To prevent malnutrition caused by oral muscle weakness, oral management in the elderly population is also a hot research topic. Rehabilitation systems for the acute, recovery, and chronic phases of disease are also a hot research topic in Japan in order to reduce the disease disability rate of common diseases in the elderly, such as stroke and myocardial infarction, and to help patients to better transition or prevent further deterioration.

3.2. Personalized aging and care

As the family structure of the elderly population changes and the disease spectrum changes, the needs of the elderly for elderly care continue to change. In 1980, the proportion of the population age 65 and over living alone in Japan was 4.3% for males and 11.2% for females, but this proportion increased to 15.0% for males and 22.1% for females by 2020, and it continues to rise (2). How to meet the medical needs and care needs of elderly people living alone is a topic of future research. Elderly people with a good financial base have higher demands and better purchasing power for elderly care, and the number of paid elderly care facilities has gradually increased in Japan in recent years. The provision of elderly care to special groups such as elderly persons with dementia or disabilities is also a continuing focus of research.

3.3. Technological innovation and smart elderly care

There are more serious problems in a superannuated population with a declining workforce, such as the growing demand for health care and long-term care and a shortage of health care workers. The government estimates that Japan will have a shortage of 370,000 nurses and other care professionals by 2025 (22). The Japanese Government continues to explore ways to use information and communications technology to improve the efficiency of care for the elderly and to

Table 2. Examples of technological innovations and smart elderly care in Japan

Classification	Example
Increasing social participation	An application for cellphones and computers that allows wheelchair users and those who are mobility-challenged to clearly see the accessibility of public spaces, sharing barrier-free-related information from all over Japan and hopefully around the world in the near future.
Improving social inclusion	A virtual reality (VR) tool that allows people to experience multiple symptoms of dementia in virtual reality from the perspective of a person with dementia, to increasing awareness and deepening understanding of dementia, and promoting better dementia care and dementia-friendly environments.
Health monitoring	A health management system that focuses on the vital statistics that caregivers monitor daily, helping them find any shifts at early stage and notifying the caregiver using an alert function, allowing individualized management of the health status of seniors.
Functional assistance	A wearable device that detects the expansion of the bladder using ultrasonic waves and predicts when the user needs to use the toilet and provides reminders, helping elders with bladder control issues maintain self-esteem and improving their quality of life.
Assisted care	Assisted care machines based on the "no-lift care" concept that allow caregivers to care for the elderly without relying solely on the caregivers' physical strength and that help seniors maintain their ability to carry out daily activities while receiving the care they need.
Dementia assistance	A jell sticker attached to a dementia patient's fingernail and toenail that features a QR code that can be read by a smartphone when they are disoriented to obtain the phone number of a family member, care facility, or other caregiver selected by the person and provide rescue accordingly.

utilize innovations in science and technology to create new initiatives for an aging society. Japan's Long-term Care Insurance included a robotic-assisted walker in its list of reimbursable technologies in 2016, and since then the list of approved robotic technologies has continued to expand (22). Table 2 lists some examples of technological innovations to address aging in Japan in recent years (23).

3.4. Integrated community-based care systems

Japan is also in the process of creating a community-based integrated care system by 2025, when the baby boomers will be age 75 and over (18). The purpose of this system is to comprehensively ensure the provision of healthcare, nursing care, preventive care, housing, and livelihood support to the elderly. In order to implement this community-based integrated care system, the government has proposed the concept of "mutual aid communities". People in the community (as well as various entities) must participate in and connect resources across generations and domains, beyond the "support providers" and "recipients" in various systems and areas. To achieve this concept, Japan is focusing on researching a reform framework that includes greater ability to solve regional problems, enhanced regional connections, enhanced community-based comprehensive support, and optimization of nursing professionals.

4. Conclusion

The current work has analyzed the state of population aging in Japan, the latest policies related to social participation of the elderly, medical care security,

economic security, support measures for dementia among special groups, and hotspots in research on population aging in Japan, such as promoting extended employment for the elderly, home-based elderly care, and technological innovation. Japan continues to reform its healthcare and nursing systems to improve the levels of services, to pay attention to personalized elderly care needs and services, to utilize advanced medical equipment, to promote a digital transformation of the healthcare system, to research new scientific technologies such as artificial intelligence and VR/AR, to create mutual aid communities, and to achieve satisfactory results in meeting the needs of the elderly. With the spatiotemporal changes in the demand for elderly care among the elderly population and the rapid advances in science and technology, policies and research priorities to address aging are also constantly evolving. However, there are still many problems that need to be urgently solved. Examples are how to ensure the elderly enjoy their old age and avoid forced labor in a social environment with "no retirement", alleviating the contradiction between continued advances in elderly care technology and the limited acceptance of new things by the elderly, and maintaining the financial sustainability of pension insurance to reduce the economic burden on the elderly. The use of new technologies to address aging is promising, but there are privacy and ethical concerns.

Funding: This work was supported by a grant from the Grants-in-Aid from the Ministry of Education, Science, Sports, and Culture of Japan (24K14216).

Conflict of Interest: The authors have no conflicts of interest to disclose.

References

- United Nations Department of Economic and Social Affairs. World Population Prospects 2022: Summary of Results. https://www.un.org/development/desa/pd/sites/www.un.org.development.desa.pd/files/undesa_pd_2022_wpp_key-messages.pdf (accessed April 11, 2024).
- Cabinet Office. White Paper on Population Aging (2023 version). <https://www8.cao.go.jp/kourei/whitepaper/w-2023/html/zenbun/index.html> (accessed April 11, 2024) (in Japanese).
- Song P, Tang W. The community-based integrated care system in Japan: Health care and nursing care challenges posed by super-aged society. *Biosci Trends*. 2019; 13:279-281.
- Ministry of Health, Labour, and Welfare of Japan. Life Table in 2022. <https://www.mhlw.go.jp/toukei/saikin/hw/life/life22/dl/life22-03.pdf> (accessed April 11, 2024) (in Japanese).
- Cabinet Office. The Guideline of Measures for Ageing Society. <https://www8.cao.go.jp/kourei/measure/taikou/h29/hon-index.html> (accessed April 11, 2024) (in Japanese).
- Ministry of Health, Labour, and Welfare of Japan. Act on Stabilization of Employment of Elderly Persons. <https://warp.da.ndl.go.jp/info:ndljp/pid/12312039/www.mhlw.go.jp/content/11600000/000694689.pdf> (accessed April 11, 2024) (in Japanese).
- Nomura S, Sakamoto H, Ghaznavi C, Inoue M. Toward a third term of Healthy Japan 21 - Implications from the rise in non-communicable disease burden and highly preventable risk factors. *Lancet Reg Health West Pac*. 2022; 21:100377.
- Ministry of Health, Labour, and Welfare of Japan. Healthy Japan 21 (the third term). https://www.mhlw.go.jp/stf/seisakunitsuite/bunya/kenkou_iryuu/kenkou/kenkouippon21_00006.html (accessed April 11, 2024) (in Japanese).
- Ministry of Health, Labour, and Welfare of Japan. Dietary Reference Intakes for Japanese (2020). https://www.mhlw.go.jp/stf/newpage_08517.html (accessed April 11, 2024) (in Japanese).
- Ministry of Health, Labour, and Welfare of Japan. The 8th National Medical Strategic Plan. <https://www.mhlw.go.jp/content/10800000/001106486.pdf> (accessed April 11, 2024) (in Japanese).
- Ministry of Health, Labour, and Welfare of Japan. Guidelines for Promoting Home Medicine and Nursing Collaboration Projects (Version 3). <https://www.mhlw.go.jp/content/12400000/000666660.pdf> (accessed April 11, 2024) (in Japanese).
- Ministry of Health, Labour, and Welfare of Japan. Summary of the Care Insurance System. https://www.mhlw.go.jp/stf/seisakunitsuite/bunya/hukushi_kaigo/kaigo_koureisha/gaiyo/index.html (accessed April 11, 2024) (in Japanese).
- Ministry of Health, Labour, and Welfare of Japan. The Modification of Nursing Fees in 2021. <https://www.mhlw.go.jp/content/12404000/000753776.pdf> (accessed April 12, 2024) (in Japanese).
- Ministry of Health, Labour, and Welfare of Japan. Child and Family Care Leave Act. <https://www.mhlw.go.jp/stf/seisakunitsuite/bunya/0000130583.html> (accessed April 12, 2024) (in Japanese).
- Tamiya N, Noguchi H, Nishi A, Reich MR, Ikegami N, Hashimoto H, Shibuya K, Kawachi I, Campbell JC. Population ageing and wellbeing: Lessons from Japan's long-term care insurance policy. *Lancet*. 2011; 378:1183-1192.
- Ministry of Health, Labour, and Welfare of Japan. Outline of the Amended Pension System Act. https://www.mhlw.go.jp/stf/seisakunitsuite/bunya/0000147284_00006.html (accessed April 13, 2024) (in Japanese).
- Ministry of Health, Labour, and Welfare of Japan. The 8th term of the Long-term Care Insurance Project Plan. <https://www.mhlw.go.jp/content/12300000/000598356.pdf> (accessed April 13, 2024) (in Japanese).
- Ishihara M, Matsunaga S, Islam R, Shibata O, Chung UI. A policy overview of Japan's progress on dementia care in a super-aged society and future challenges. *Glob Health Med*. 2024; 6:13-18.
- Prime Minister's Office of Japan. Ministerial Council on the promotion of dementia care policies, 2018. https://japan.kantei.go.jp/98_abe/actions/201812/_00054.html (accessed April 21, 2024) (in Japanese).
- Baba H, Aung MN, Miyagi A, Masu A, Yokobori Y, Kiyohara H, Otake E, Yuasa M. Exploring the contribution of Japan's experience in addressing rapid aging in Asia: Focus on dementia care. *Glob Health Med*. 2024; 6:19-32.
- Ministry of Health, Labour, and Welfare of Japan. The Basic Act on Dementia to Promote an Inclusive Society (Outline). <https://www.japaneselawtranslation.go.jp/outline/92/905R510.pdf> (accessed April 21, 2024) (in Japanese).
- Plackett B. Tackling the crisis of care for older people: Lessons from India and Japan. *Nature*. 2022; 601:S12-s14.
- The Asia Health and Wellbeing Initiative. Healthy aging prize for Asian innovation. <https://ahwin.org/innovative-cases/> (accessed May 12, 2024).

Received May 14, 2024; Revised June 9, 2024; Accepted June 11, 2024.

*Address correspondence to:

Kenji Karako, Department of Surgery, Graduate School of Medicine, The University of Tokyo, Tokyo 113-8655, Japan.
E-mail: tri.leafs@gmail.com

Peipei Song, National Center for Global Health and Medicine, Tokyo 162-8655, Japan.
E-mail: psong@it.ncgm.go.jp

Released online in J-STAGE as advance publication June 12, 2024.

Trends in the treatment of advanced pancreatic cancer

Hirokazu Momose, Shohei Kudo, Tomoyuki Yoshida, Nobuhiro Hasui, Ryota Matsuki, Masaharu Kogure, Yoshihiro Sakamoto*

Department of Hepato-Biliary-Pancreatic Surgery, Kyorin University Hospital, Tokyo, Japan.

SUMMARY Pancreatic cancer (PC) has the poorest prognosis among digestive cancers; only 15-20% of cases are resectable at diagnosis. This review explores multidisciplinary treatments for advanced PC, emphasizing resectability classification and treatment strategies. For locally advanced unresectable PC, systemic chemotherapy using modified FOLFIRINOX and gemcitabine with albumin-bound paclitaxel is standard, while the role of chemoradiation is debated. Induction chemotherapy followed by chemoradiation may be a promising therapy. Conversion surgery after initial chemotherapy or chemoradiotherapy offers favorable survival, however criteria for conversion need further refinements. For metastatic PC, clinical trials using immune checkpoint inhibitors and molecular targeted therapies are ongoing. Multidisciplinary approaches and further research are crucial for optimizing treatment and improving outcomes for advanced PC.

Keywords pancreatic cancer, multidisciplinary treatment, conversion surgery

1. Introduction

Pancreatic cancer (PC) has the poorest prognosis among digestive cancers; only 15-20% of cases are resectable at diagnosis, whereas 30-40% are locally advanced and 50-60% involve distant metastases that are initially unresectable (1). In PC, resection is the only treatment that offers the possibility of a cure; however, long-term prognosis cannot be expected with resection alone. Therefore, multidisciplinary treatment is recommended. In this chapter, we review the multidisciplinary treatment for advanced PC.

2. Establishing the definition of resectability for PC

In the early 2000s, attempts were made to classify PC based on their resectability. The 2004 NCCN guidelines first categorized PC, and further objective classification based on the anatomical extension of computed tomography (CT) images was proposed by the M.D. Anderson Cancer Center in 2006 (2). All PCs were classified as resectable (R), borderline resectable (BR), or unresectable (UR) based on local extension and the presence or absence of distant metastasis. In 2016, the international consensus on the classification of BR PC was based on anatomical configurations on CT imaging (Table 1) (3). Currently, the treatment strategy for PC is determined by the resectability status at diagnosis, with a multidisciplinary treatment strategy being key to

successful treatment.

3. Multidisciplinary treatment for UR-locally advanced (LA) PC

3.1. Chemotherapy and chemoradiation (CRT) for UR-LA PC

UR-LA PC accounts for 10-20% of all PCs (2). To achieve disease control, initial treatment typically consists of chemotherapy regimens such as modified FOLFIRINOX (mFFX) or gemcitabine and albumin-bound paclitaxel (GnP) (4). However, the role of radiation in UR-LA treatment remains controversial. Two randomized controlled trials of chemotherapy and CRT for UR-LA PC have been previously reported (Table 2) (5,6). There have been reports of chemotherapy significantly improving overall survival (OS) (median survival 13.0 months vs. 8.6 months, $p = 0.03$) (5) and significantly worsening OS (median survival 9.2 months vs. 11.1 months, $p = 0.017$) (6), and currently, there is no definitive conclusion on the superiority of chemotherapy and CRT. However, the chemotherapy regimens used in the chemotherapy groups of these two RCTs were both GEM alone, and there is a demand for better treatment outcomes for UR-LA PC with more potent chemotherapy regimens. The results of a randomized phase II trial (JCOG1407) comparing mFFX with GnP as a first-line treatment

Table 1. The international consensus on the classification of BR PC defined based on the anatomical configurations on computed tomography imaging

Resectable (R)	<ul style="list-style-type: none"> • SMV/PV: no tumor contact or unilateral narrowing • SMV/PV: no tumor contact or unilateral narrowing
Borderline resectable (BR)	Subclassified according to SMV/PV involvement alone or arterial invasion.
BR-PV (SMV/PV involvement alone)	<ul style="list-style-type: none"> • SMV/PV: tumor contact ≥ 180 or bilateral narrowing/occlusion, not exceeding the inferior border of the duodenum. • SMA, CA, CHA: no tumor contact/invasion
BR-A (arterial involvement)	<ul style="list-style-type: none"> • SMA, CA, CHA: no tumor contact/invasion • CHA: tumor contact without showing tumor contact of the PHA and/or CA. (The involvement of the aorta is categorized as unresectable. Presence of variant arterial anatomy is not taken into consideration)
Unresectable: UR	Subclassified according to the status of distant metastasis
Locally advanced (LA)	<ul style="list-style-type: none"> • SMV/PV: bilateral narrowing/occlusion, exceeding the inferior border of the duodenum. • SMA, CA: tumor contact/invasion of ≥ 180 degree. • CHA: tumor contact/invasion showing tumor contact/invasion of the PHA and/or CA. • Ao: tumor contact or invasion
Metastatic (M)	<ul style="list-style-type: none"> • Distant metastasis

SMV, superior mesenteric vein; PV, portal vein; SMA, superior mesenteric artery; CA, celiac artery; CHA, common hepatic artery; PHA, proper hepatic artery.

Table 2. Results of two RCTs comparing chemotherapy alone and chemoradiation for unresectable, locally advanced pancreatic cancer

Author	Country/Year	Regimen	Number of patients	Median PFS (months)	Median OS (months)
Chauffert <i>et al.</i>	France/2008	60Gy/30Fr and GEM vs. GEM alone	119	7.2 vs. 11.6, $p = 0.025$	8.6 vs. 13.0, $p = 0.03$
Loehrer <i>et al.</i>	USA/2011	50.4Gy/28Fr and GEM vs. GEM alone	71	6.0 vs. 6.7	11.1 vs. 9.2, $p = 0.017$

GEM, gemcitabine; PFS, progression-free survival; OS, overall survival.

for UR-LA PC were reported in 2023 in Japan. The 1-year OS was 77.4% (95% confidence interval [CI], 64.9-86.0) and 82.5% (95% CI, 70.7-89.9), median OS was 23.0 months (19.3-29.3) and 21.3 months (18.2-24.1), median progression-free survival (PFS) was 11.2 months (95% CI, 9.9-15.9) and 9.4 months (95% CI, 7.4-12.8), and response rate was 30.9% (95% CI, 19.1-44.8) and 57.1% (95% CI, 41.0-72.3) in the mFFX and GnP arms, respectively. The 1-year survival and response rates were better in the GnP group, whereas the median OS and PFS were better in the mFFX group (7). It is necessary to discuss how the results of this study can be integrated into clinical treatment strategies.

3.2. Induction chemotherapy before CRT for UR-LA PC

UR-LA PC may potentially have distant metastases, and administration of induction chemotherapy could allow the early identification of cases in which distant metastases emerge during the initial phase of treatment (8). Therefore, favorable treatment outcomes can be achieved by administering potent induction chemotherapy to control potential distant metastases, followed by local control through CRT. Table 3 shows the results of trials of induction chemotherapy before CRT (9-12).

In the LAP07 randomized clinical trial, no improvement in OS was observed after induction chemotherapy with a combination of GEM and erlotinib (9).

In a prospective multicenter phase II trial (LAPACT trial), in which six cycles of induction chemotherapy (GnP) were administered for UR-LA PC, 58% (62/107) of patients completed induction chemotherapy. The disease control rate using induction chemotherapy was 77.6%, and the response rate was 33.6%, both of which were considered favorable. Subsequent treatments included CRT in 17% (18/107) and surgery in 16% (17/107) of patients. The median OS was 18.8 months (10). In a phase II randomized trial (JCOG1106 trial) that evaluated the effectiveness of induction chemotherapy with GEM alone for 12 weeks before CRT with S-1, the median OS for the group that received induction chemotherapy with GEM alone prior to CRT with S-1 was 17.2 months, compared to 19.0 months for the group without induction chemotherapy, showing no significant difference (hazard ratio [HR] (95% CI), 1.255 (0.816-1.930)) (11). Takada *et al.* conducted a retrospective study of 45 patients with UR-LA PC, including 25 who received GnP therapy as induction chemotherapy and 20 who received chemotherapy alone (12). They reported that the CRT group had a better prognosis than the chemotherapy-

Table 3. Trials on induction chemotherapy before chemoradiation for unresectable, locally advanced pancreatic cancer

Author	Country	Year	Design	Induction chemotherapy regimen	Treatment after chemotherapy	Number of patients	Median PFS (months) CRT vs. CTx	Median OS (months) CRT vs. CTx
Hummel <i>et al.</i>	USA	2016	Phase III, RCT	GEM and Erlotinib or GEM alone	50Gy/30Fr and capecitabine	269	9.9 vs. 8.4, $p = 0.06$	15.2 vs. 16.5, $p = 0.83$
Philip <i>et al.</i>	International	2020	Phase II	GnP	GnP or CRT or surgery	107	10.9	18.8
Ioka <i>et al.</i>	Japan	2021	Phase II, RCT	GEM	50.4Gy/28Fr and S-1	100	10.1 vs. 10.4, HR (95% CI) = 1.034 (0.689-1.551)	19 vs. 17.2, HR (95% CI) = 1.255 (0.816-1.930)
Takada <i>et al.</i>	Japna	2021	Retrospective	GnP	60Gy/25fr and GEM or S-1	45	17.9 vs. 7.6, $p = 0.044$	29.2 vs. 17.4, $p < 0.001$

RCT, randomized controlled trial; GEM, gemcitabine; GnP, gemcitabine and nab-paclitaxel; CRT, chemoradiation therapy; N/A, not applicable; CTx, chemotherapy; HR, hazard ratio.

alone group (OS 29.2 months vs. 17.4 months, $p < 0.001$). It is expected that by administering CRT during a potent chemotherapy regimen, in addition to local control achieved through CRT, there will be a reduction in the adverse events associated with chemotherapy or an extension of the time until these events worsen. Therefore, it is necessary to accumulate evidence on the efficacy of induction chemotherapy with potent chemotherapeutic regimens.

3.3. Conversion surgery (CS) for UR-LA PC

Surgical resection of initially UR PC after remission following chemo(radio)therapy is defined as CS.

The rate of CS for UR-LA PC varied according to previous reports. A meta-analysis of 13 trials of FFX for UR-LA PC reported that 91 of 325 patients (28%) underwent CS, achieving 74% R0 resection (13). In a retrospective study of 454 cases in which mFFX or Gemcitabine GnP was administered for UR-LA PC, 38 patients (16%) underwent CS, achieving 89% R0 resection. The independent prognostic factors were normalized CA19-9 concentration, modified Glasgow prognostic score of 0, tumor shrinkage after chemotherapy, chemotherapy duration ≥ 8 months, and resection (14). In a study of patients who underwent CS for UR-LA PC, Nagai *et al.* reported that the prognosis was significantly better and the time to postoperative recurrence was significantly longer in cases where all three tumor markers (CA19-9, CEA, and DUPAN-2) were at normal levels preoperatively than in cases with elevated preoperative tumor markers (15). CS for UR-LA PC requires further accumulation of evidence regarding the criteria and timing for considering resection in the future.

4. Case

A 56-year-old woman was diagnosed with UR-LA pancreatic head cancer involving the common hepatic artery (CHA) (Figure 1A) and portal vein (PV) (Figure 1B). The patient underwent 19 courses of GnP therapy. Postchemotherapy CT revealed tumor shrinkage (Figure 2A) and regression of the soft tissue shadow around the CHA (Figure 2B). Additionally, CA19-9 levels decreased from 9880 U/mL to 800 U/mL after chemotherapy. It was determined that technical and oncological R0 resections were feasible. Subtotal stomach-preserving pancreaticoduodenectomy with CHA resection and reconstruction using the splenic artery and PV resection and reconstruction using a left renal vein graft were performed (Figure 3A, 3B). The operating time was 13 h and 34 min, with an intraoperative blood loss of 756 mL. The postoperative course was uneventful, and the patient was discharged on the 18th postoperative day. The patient has achieved recurrence-free survival for 10 months postoperatively.

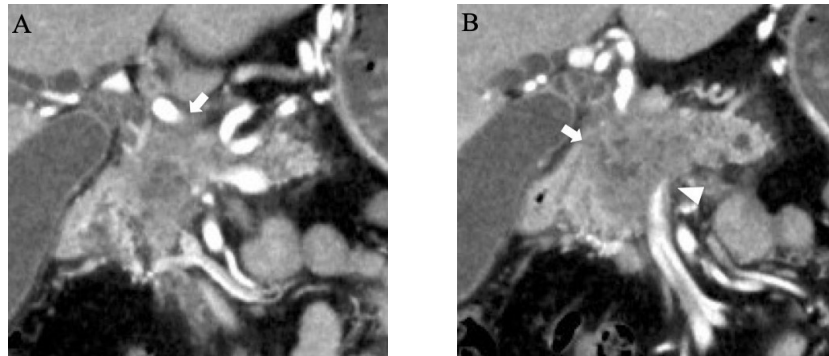


Figure 1. CT scan before chemotherapy. (A) Hepatobiliary and Pancreatic Oncology Group of Japan Clinical Oncology Group (JCOG). A randomized phase II study of modified FOLFIRINOX versus gemcitabine plus nab-paclitaxel for locally advanced pancreatic cancer (JCOG1407). (B) The arrow indicates a hypo-vascular mass in the head and body of the pancreas. The arrowhead points to suspected invasion of the tumor into the portal vein.

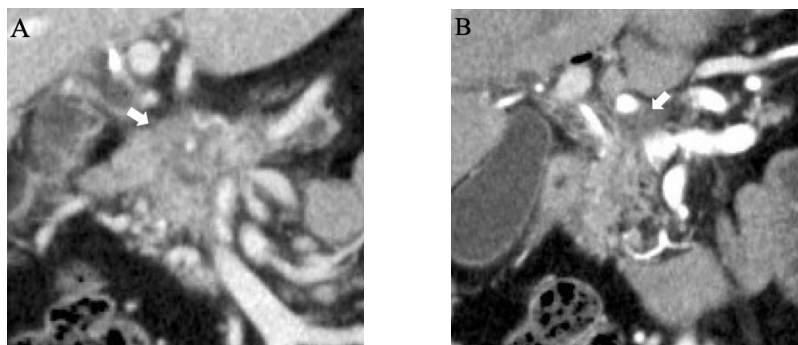


Figure 2. Preoperative CT scan. (A) After chemotherapy, the tumor has shrunk (arrow). (B) The low-density area around the CHA remains after chemotherapy (arrow).

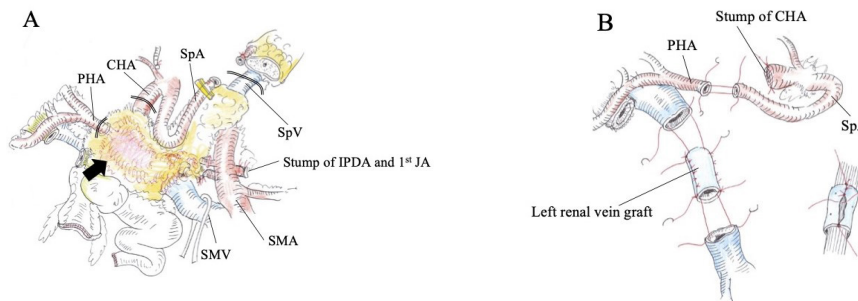


Figure 3. Operation record. (A) The tumor in the head and body of the pancreas (arrow) had invaded from the common hepatic artery (CHA) to the proper hepatic artery (PHA). The PHA, CHA, and portal vein were resected en bloc along with the tumor. The double lines indicate the sites of vascular transection. CHA, common hepatic artery; PHA, proper hepatic artery; SpA, splenic artery; SpV, splenic vein; SMV, superior mesenteric vein; SMA, superior mesenteric artery; IPDA, inferior pancreaticoduodenal artery; 1st JA, 1st jejunal artery. (B) In the arterial reconstruction, the splenic artery was anastomosed to the proper hepatic artery. A left renal vein graft was used for portal vein reconstruction. CHA, common hepatic artery; PHA, proper hepatic artery; SpA, splenic artery.

5. Multidisciplinary treatment for UR-metastasis (M) PC

5.1. Immune checkpoint inhibitors for UR-M PC

In immunotherapy, CD8+ T cells are the primary agents that induce tumor shrinkage. The tumor microenvironment within tumor tissues can be broadly classified into "hot (inflamed)" and "cold (non-inflamed)" based on the presence or absence of tumor-infiltrating lymphocytes, respectively, including CD8+ T cells. Hot tumors have a higher response rate to

immune checkpoint inhibitors (16). PC is known to contain a large number of stromal components that result in poor infiltration of T cells (cold tumors) and a low tumor mutational burden. Consequently, PC respond poorly to immune checkpoint inhibitors. Furthermore, the abundance of stromal components in PC may impede drug delivery, potentially hindering the antitumor effects of cytotoxic chemotherapy and immune checkpoint inhibitors. Currently, the development of immune checkpoint inhibitors with antitumor effects is in progress. Table 4 shows the results of clinical trials of immune checkpoint inhibitors

as monotherapy or combination therapy (17-19).

In a phase II trial of ipilimumab (anti-CTLA-4), 27 patients were enrolled (UR-M PC, 20; UR-LA PC, 7), and tumor shrinkage was observed in three patients, but the response rate was 0% (17).

In a phase I trial of BMS-936559 (anti-PD-L1 antibody), 207 patients were enrolled, including 14 patients with PC. No response was reported in PC; however, response rates for malignant melanoma, non-small cell lung cancer (squamous cell carcinoma), non-small cell lung cancer (non-squamous cell carcinoma), mesothelioma, and renal cell carcinoma were 17%, 8%, 11%, 6%, and 12% respectively (18).

In a randomized phase II trial for patients with metastatic PC, the combination therapy of durvalumab (anti-PD-L1 antibody) and tremelimumab (anti-CTLA-4) was compared with Durvalumab alone; 32 patients were enrolled in the combination therapy group, and 33 patients in the Durvalumab alone group. Response rates were 3.1% and 0%, respectively. There was no difference in the median PFS and median OS (19).

These findings indicated that immune checkpoint inhibitors alone are not effective against PC. In the future, it will be necessary to evaluate biomarker expression to identify patients most likely to benefit from immune checkpoint inhibitors.

5.2. Combination of immune checkpoint inhibitors and cytotoxic chemotherapy for UR-M PC

Clinical trials are currently being conducted to evaluate the efficacy of combination therapies using immune checkpoint inhibitors and cytotoxic anticancer drugs. Table 5 summarizes the main results of the clinical trials (20-24).

Thirty-eight patients were enrolled in a phase I trial of combination therapy with tremelimumab (anti-CTLA-4) and GEM for PC with distant metastases that had not been previously treated with chemotherapy. Among the 28 patients in whom efficacy could be evaluated, two (7.1%) showed a response, and the median OS was 7.4 months (20).

A phase Ib/II trial targeting solid tumors was conducted using combination therapy with pembrolizumab and GnP. Seventeen patients were enrolled in this PC cohort study. Twelve (70.6%) patients received first-line treatment. The response rate, median PFS, and median OS were 27.3%, 9.1 months, and 15.0 months, respectively (21).

A phase Ib trial of combination therapy with ipilimumab (anti-CTLA-4) and GEM for advanced PC enrolled 21 patients (UR-M PC, 20; UR-LA PC, 1). Eleven patients (52%) received second-line treatment, and three patients (14%) received third-line treatments. The response rate, median PFS, and median OS were 14%, 2.78 months, and 6.90 months, respectively (22).

Table 4. Results of clinical trials on immune checkpoint inhibitors as monotherapy or combination therapy for unresectable metastatic pancreatic cancer

Author	Year	Country	Design	Regimen	Number of patients	Response rate	Median PFS (95% CI)	Median OS (95% CI)
Royal <i>et al.</i>	2010	USA	Phase II	Ipilimumab	27	0%	NA	NA
Brahmer <i>et al.</i>	2012	USA	Phase I	BMS-936559	14	0%	NA	NA
O'Reilly <i>et al.</i>	2019	USA	Phase II, RCT	Durvalumab vs. Durvalumab and Tremelimumab	65	0% vs. 3.1%	1.5 months (1.3-1.5 months) vs. 1.5 months (1.2-1.5 months)	3.6 months (2.7-6.1 months) vs. 3.1 months (2.2-6.1 months)

PFS, progression-free survival; OS, overall survival; RCT, randomized controlled trial; NA, not applicable.

Table 5. Clinical trials on a combination of immune checkpoint inhibitors and cytotoxic chemotherapy for unresectable metastatic pancreatic cancer

Author	Year	Country	Design	Regimen	Number of patients	Response rate	Median PFS (months)	Median OS (months)
Aglietta <i>et al.</i>	2014	Italy	Phase I	Tremelimumab and GEM	38	7.1%	NA	7.4
Weiss	2019	USA	Phase Ib/II	Pembrolizumab and GnP	17	27.3%	9.1	15
Kamath <i>et al.</i>	2020	USA	Phase Ib	Ipilimumab and GEM	21	14%	2.78	6.9
Renouf <i>et al.</i>	2022	Canada	Phase II	Durvalumab and tremelimumab and GnP vs. GnP	180	30.3% vs. 20.0%	5.5 vs. 5.4, $p = 0.91$	9.8 vs. 8.8, $p = 0.72$
Fu <i>et al.</i>	2023	China	Phase II, RCT	Sintilimumab and mFFX vs. mFFX	110	50.0% vs. 23.9%	5.9 vs. 5.7, $p > 0.05$	10.9 vs. 10.8, $p > 0.05$

PFS, progression-free survival; OS, overall survival; RCT, randomized controlled trial; GEM, gemcitabine; GnP, gemcitabine and nab-paclitaxel; mFFX, modified FOLFIRINOX.

A randomized phase II trial (CCTG PA.7 trial) was conducted to assess the additive effects of durvalumab and tremelimumab on GnP as a first-line treatment for PC with distant metastases. A total of 119 and 61 patients were allocated to the four-drug combination and GnP groups, respectively. The primary endpoint, median OS, was 9.8 months in the four-drug combination group and 8.8 months in the GnP group (HR: 0.94, 90% CI: 0.71-1.25), showing no additive effects of durvalumab and tremelimumab. The response rate and median PFS were 30.3% and 5.4 months, respectively, in the four-drug combination group compared to 23.0% and 5.4 months, respectively, in the GnP group (23).

A randomized phase II trial (CISPD3 trial) was conducted to assess the additive effect of sintilimab on mFFX in PC with distant metastases that had not been treated with chemotherapy or developed resistance to gemcitabine-based first-line treatment. A total of 55 patients were enrolled in each group. The primary endpoint, median OS, was 10.9 months in the sintilimab and mFFX combination group compared to 10.8 months in the mFFX group (HR: 1.07, 95% CI: 0.69-1.68), showing no additive effect of sintilimab. However, the response rates and median PFS were 50.0% and 5.9 months in the sintilimab and mFFX combination group, respectively, and 23.9% and 5.7 months, respectively, in the mFFX group, with a significant difference in the response rates (24).

Cytotoxic anticancer drugs are expected to enhance the effects of immune checkpoint inhibitors. However, the results of these clinical trials showed that the effectiveness of gemcitabine alone, GnP, and mFFX therapies remained unchanged, and no additive effect of immune checkpoint inhibitors on cytotoxic chemotherapy was observed in PC.

5.3. Molecular targeted therapy for UR-M PC

Few molecular targeted therapies have shown efficacy against PC. However, in recent years, promising therapeutic target proteins have been identified for PC, and their development is progressing.

A randomized phase III trial (NCIC CTG PA.3 trial) comparing GEM and placebo therapy with GEM and erlotinib combination therapy for PC with local advancement or distant metastases enrolled 569 patients. The final analysis was conducted after observing 486 deaths, and the primary endpoint, OS, was significantly better in the erlotinib combination group (HR: 0.82, 95% CI: 0.69-0.99, $p = 0.038$). However, in the erlotinib combination group, there were more adverse events, including rash in 72% of patients and interstitial lung disease in 2.1% (25).

In a randomized phase III (POLO trial), that assessed the efficacy of the PARP inhibitor olaparib in patients with unresectable PC and germline BRCA gene mutations, 154 patients were enrolled. The patients

were allocated to the olaparib and placebo groups in a 3:2 ratio. The primary endpoint, median PFS, was 7.4 months for the olaparib group compared to the placebo group, with an HR of 0.53 (95% CI 0.35-0.82, $p < 0.001$), demonstrating the superiority of maintenance therapy with olaparib (26).

In recent years, promising therapeutic target proteins for PC have been discovered and new targeted therapies are currently under development.

The development of drugs targeting CLDN18.2 is underway. CLDN18.2 is selectively expressed in tight junctions of the stomach and pancreas. In normal cells, it is located within tight junctions, making it difficult for anti-CLDN18.2 antibodies to reach it, even if they are present in the bloodstream. In contrast, cancer cells exhibit disrupted cell polarity, allowing antibody drugs to bind to CLDN18.2. Zolbetuximab is a monoclonal IgG1 antibody that binds to CLDN18.2, and induces cell death through antibody-dependent cellular cytotoxicity and complement-dependent cytotoxicity. In the SPOTLIGHT (27) and GLOW (28) trials targeting unresectable advanced gastric cancer, combination therapy with cytotoxic anticancer drugs and zolbetuximab was shown to be significantly superior in terms of OS. Against this background, a randomized phase II trial (NCT03816163) is underway to compare combination therapy of zolbetuximab and GnP with GnP therapy alone in patients with PC with distant metastases and high CLDN18.2 expression.

Results from phase I/II trials of sotorasib and adagrasib, antibody drugs targeting the KRAS p.12C mutant protein, have been reported.

In a single-arm Phase II trial targeting KRAS G12C-mutated advanced PC, 38 patients received sotorasib. The objective response rate was 21%, median PFS was 4.0 months, and median OS was 6.9 months (29).

In a phase I/II trial (KRYSTAL-1 trial) targeting KRAS G12C-mutant solid tumors, 12 of 42 patients with PC were administered adagrasib. The objective response rate, disease control rate, and median PFS was 50.0%, 100%, and 6.6 months, respectively (30). Among KRAS mutations other than KRAS G12C, drugs that can bind to the G12D mutation are also being developed and phase I clinical trials are being conducted (NCT05382559).

5.4. CS for UR-M PC

There are few reports of CS for PC with synchronous metastases, which included only selected patients and had poor prognoses after surgery with an approximately 10-month median OS (31). A small number of patients responded remarkably well to the novel chemotherapy approach, and metastatic tumors were no longer detectable on imaging studies. Table 6 shows the CS results for UR-M (liver) PC (32-35).

Frigerio *et al.* (32) administered chemotherapy to patients with PC with liver-only metastases and

Table 6. Results of clinical trials on conversion surgery for unresectable pancreatic cancer with liver metastasis

Author	Year	Country	Design	Regimen	Number of patients	Response rate	Median PFS (months)	Median OS (months)
Frigerio <i>et al.</i>	2022	Italy	Retrospective	FFX/GnP/GEM	52	86.5	23.9	37.2
Bachelier <i>et al.</i>	2022	France	Retrospective	FFX	92	50	5.4	12.7
Satoi <i>et al.</i>	2023	Japan	Retrospective	Multi regimen	10	NA	7.8	20.9
Takeda <i>et al.</i>	2023	Japan	Retrospective	mFFX/GnP/S-IROX	13	100	14.0	54.6

FFX, FOLFIRINOX; mFFX, modified FOLFIRINOX; GnP, gemcitabine and nab-paclitaxel; S-IROX, S-1 and Irinotecan, PFS, progression-free survival; OS, overall survival; NA, not applicable.

investigated the prognosis of 52 patients who achieved complete regression of the metastatic component and underwent pancreatectomy. The authors reported a median OS of 23.0 months.

Bachelier *et al.* (33) reported that a median OS of 92 patients with PC and synchronous liver metastases who underwent resection after neoadjuvant chemotherapy was 18.26 months.

Satoi *et al.* (34) reported a comparative study of patients with PC and synchronous liver metastases ($n = 49$), including those who underwent CS ($n = 10$), upfront surgery with or without short-term neoadjuvant chemotherapy for oligometastases and occult metastases limited to the liver ($n = 8$), and chemotherapy for R or BR diseases with occult liver-only metastases ($n = 31$). The median survival time from the initial treatment was significantly better in the CS group, (36.7 months) than in the other two groups. Additionally, CS was the only significant independent prognostic factor in the total cohort (HR, 0.173; $p = 0.002$). Takeda *et al.* (35) reported that patients with oligometastasis to the liver had a favorable survival duration of 13.2 months, which was significantly better than 8.2 months of patients with polymetastasis to the liver. The former group underwent CS more frequently than the latter (12% vs. 1.3%), and the MST in patients who underwent CS was 54.6 months.

alone; however, the criteria for performing CS vary between institutions.

Furthermore, it must be considered that CS is more challenging than standard pancreatic resection and carries a higher risk of postoperative severe complications (23% and 40.2%, respectively) (33 35).

6. Conclusion

Despite these improvements, PC continues to pose substantial challenges owing to its poor prognosis and high rate of initially unresectable cases. Multidisciplinary approaches incorporating potent chemotherapy regimens, chemoradiation, and innovative strategies, such as immune checkpoint inhibitors and molecular targeted therapies, are being explored to improve outcomes. CS has shown promise in patients with initially UR-LA or M PC, achieving notable survival benefits. However, the criteria and timing of CS require further investigation to optimize patient selection and outcomes.

Funding: None.

Conflict of Interest: The authors have no conflicts of interest to disclose.

References

- Gillen S, Schuster T, Meyer Zum Büschenfelde C, Friess H, Kleeff J. Preoperative/neoadjuvant therapy in pancreatic cancer: a systematic review and meta-analysis of response and resection percentages. *PLoS Med.* 2010; 7:e1000267.
- Varadhachary GR, Tamm EP, Abbruzzese JL, Xiong HQ, Crane CH, Wang H, Lee JE, Pisters PW, Evans DB, Wolff RA. Borderline resectable pancreatic cancer: definitions, management, and role of preoperative therapy. *Ann Surg Oncol.* 2006; 13:1035-1046.
- Isaji S, Mizuno S, Windsor JA, Bassi C, Fernández-Del Castillo C, Hackert T, Hayasaki A, Katz MHG, Kim SW, Kishiwada M, Kitagawa H, Michalski CW, Wolfgang CL. International consensus on definition and criteria of borderline resectable pancreatic ductal adenocarcinoma 2017. *Pancreatol.* 2018; 18:2-11.
- Pancreatic Cancer, Version 1.2021. National Comprehensive Cancer Network; 2024.
- Chauffert B, Mornex F, Bonnetain F, Rougier P, Mariette C, Bouché O, Bosset JF, Aparicio T, Mineur L, Azzedine A, Hammel P, Butel J, Stremsdoerfer N, Maingon P, Bedenne L. Phase III trial comparing intensive induction chemoradiotherapy (60 Gy, infusional 5-FU and intermittent cisplatin) followed by maintenance gemcitabine with gemcitabine alone for locally advanced unresectable pancreatic cancer. Definitive results of the 2000-01 FFCD/SFRO study. *Ann Oncol.* 2008; 19:1592-1599.
- Loehrer PJ Sr, Feng Y, Cardenas H, Wagner L, Brell JM, Cella D, Flynn P, Ramanathan RK, Crane CH, Alberts SR, Benson AB 3rd. Gemcitabine alone versus gemcitabine plus radiotherapy in patients with locally advanced pancreatic cancer: an Eastern Cooperative Oncology Group trial. *J Clin Oncol.* 2011; 29:4105-4112.
- Ozaka M, Nakachi K, Kobayashi S, *et al.* Hepatobiliary and Pancreatic Oncology Group of Japan Clinical Oncology Group (JCOG). A randomised phase II study of modified FOLFIRINOX versus gemcitabine plus nab-paclitaxel for locally advanced pancreatic cancer (JCOG1407). *Eur J Cancer.* 2023; 181:135-144.
- Karabıcak I, Satoi S, Yanagimoto H, Yamamoto T, Hirooka S, Yamaki S, Kosaka H, Inoue K, Matsui Y, Kon M. Risk factors for latent distant organ metastasis detected by staging laparoscopy in patients with radiologically defined locally advanced pancreatic ductal adenocarcinoma. *J Hepatobiliary Pancreat Sci.* 2016; 23:750-755.

9. Hammel P, Huguet F, van Laethem JL, Goldstein D, Glimelius B, Artru P, Borbath I, Bouché O, Shannon J, André T, Mineur L, Chibaudel B, Bonnetain F, Louvet C; LAP07 Trial Group. Effect of Chemoradiotherapy vs Chemotherapy on Survival in Patients With Locally Advanced Pancreatic Cancer Controlled After 4 Months of Gemcitabine With or Without Erlotinib: The LAP07 Randomized Clinical Trial. *JAMA*. 2016; 315:1844-1853.
10. Philip PA, Lacy J, Portales F, *et al.* Nab-paclitaxel plus gemcitabine in patients with locally advanced pancreatic cancer (LAPACT): a multicentre, open-label phase 2 study. *Lancet Gastroenterol Hepatol*. 2020; 5:285-294.
11. Ioka T, Furuse J, Fukutomi A, *et al.* Hepatobiliary and Pancreatic Oncology Group (HBPOG) of Japan Clinical Oncology Group (JCOG). Randomized phase II study of chemoradiotherapy with versus without induction chemotherapy for locally advanced pancreatic cancer: Japan Clinical Oncology Group trial, JCOG1106. *Jpn J Clin Oncol*. 2021; 51:235-243.
12. Takada R, Ikezawa K, Daiku K, *et al.* The Survival Benefit of Chemoradiotherapy following Induction Chemotherapy with Gemcitabine Plus Nab-Paclitaxel for Unresectable Locally Advanced Pancreatic Cancer. *Cancers (Basel)*. 2021; 13:4733.
13. Suker M, Beumer BR, Sadot E, *et al.* FOLFIRINOX for locally advanced pancreatic cancer: a systematic review and patient-level meta-analysis. *Lancet Oncol*. 2016; 17:801-810.
14. Ushida Y, Inoue Y, Oba A, Mie T, Ito H, Ono Y, Sato T, Ozaka M, Sasaki T, Saiura A, Sasahira N, Takahashi Y. Optimizing Indications for Conversion Surgery Based on Analysis of 454 Consecutive Japanese Cases with Unresectable Pancreatic Cancer Who Received Modified FOLFIRINOX or Gemcitabine Plus Nab-paclitaxel: A Single-Center Retrospective Study. *Ann Surg Oncol*. 2022; 29:5038-5050.
15. Nagai M, Nakamura K, Terai T, Kohara Y, Yasuda S, Matsuo Y, Doi S, Sakata T, Sho M. Significance of multiple tumor markers measurements in conversion surgery for unresectable locally advanced pancreatic cancer. *Pancreatol*. 2023; 23:721-728.
16. Yarchoan M, Hopkins A, Jaffee EM. Tumor Mutational Burden and Response Rate to PD-1 Inhibition. *N Engl J Med*. 2017; 377:2500-2501.
17. Royal RE, Levy C, Turner K, Mathur A, Hughes M, Kammula US, Sherry RM, Topalian SL, Yang JC, Lowy I, Rosenberg SA. Phase 2 trial of single agent Ipilimumab (anti-CTLA-4) for locally advanced or metastatic pancreatic adenocarcinoma. *J Immunother*. 2010; 33:828-833.
18. Brahmer JR, Tykodi SS, Chow LQ, *et al.* Safety and activity of anti-PD-L1 antibody in patients with advanced cancer. *N Engl J Med*. 2012; 366:2455-2465.
19. O'Reilly EM, Oh DY, Dhani N, Renouf DJ, Lee MA, Sun W, Fisher G, Hezel A, Chang SC, Vlahovic G, Takahashi O, Yang Y, Fitts D, Philip PA. Durvalumab With or Without Tremelimumab for Patients With Metastatic Pancreatic Ductal Adenocarcinoma: A Phase 2 Randomized Clinical Trial. *JAMA Oncol*. 2019; 5:1431-1438
20. Aglietta M, Barone C, Sawyer MB, Moore MJ, Miller WH Jr, Bagalà C, Colombi F, Cagnazzo C, Gioeni L, Wang E, Huang B, Fly KD, Leone F. A phase I dose escalation trial of tremelimumab (CP-675,206) in combination with gemcitabine in chemotherapy-naïve patients with metastatic pancreatic cancer. *Ann Oncol*. 2014; 25:1750-1755.
21. Weiss GJ, Blaydorn L, Beck J, Bornemann-Kolatzki K, Urnovitz H, Schütz E, Khemka V. Phase Ib/II study of gemcitabine, nab-paclitaxel, and pembrolizumab in metastatic pancreatic adenocarcinoma. *Invest New Drugs*. 2018; 36:96-102.
22. Kamath SD, Kalyan A, Kircher S, Nimeiri H, Fought AJ, Benson A 3rd, Mulcahy M. Ipilimumab and Gemcitabine for Advanced Pancreatic Cancer: A Phase Ib Study. *Oncologist*. 2020; 25:e808-e815.
23. Renouf DJ, Loree JM, Knox JJ, *et al.* The CCTG PA.7 phase II trial of gemcitabine and nab-paclitaxel with or without durvalumab and tremelimumab as initial therapy in metastatic pancreatic ductal adenocarcinoma. *Nat Commun*. 2022; 13:5020.
24. Fu Q, Chen Y, Huang D, *et al.* Sintilimab Plus Modified FOLFIRINOX in Metastatic or Recurrent Pancreatic Cancer: The Randomized Phase II CISP3 Trial. *Ann Surg Oncol*. 2023; 30:5071-5080.
25. Moore MJ, Goldstein D, Hamm J, *et al.* National Cancer Institute of Canada Clinical Trials Group. Erlotinib plus gemcitabine compared with gemcitabine alone in patients with advanced pancreatic cancer: a phase III trial of the National Cancer Institute of Canada Clinical Trials Group. *J Clin Oncol*. 2007; 25:1960-1966.
26. Golan T, Hammel P, Reni M, *et al.* Maintenance Olaparib for Germline *BRCA*-Mutated Metastatic Pancreatic Cancer. *N Engl J Med*. 2019; 381:317-327.
27. Shitara K, Lordick F, Bang YJ, *et al.* Zolbetuximab plus mFOLFOX6 in patients with CLDN18.2-positive, HER2-negative, untreated, locally advanced unresectable or metastatic gastric or gastro-oesophageal junction adenocarcinoma (SPOTLIGHT): a multicentre, randomised, double-blind, phase 3 trial. *Lancet*. 2023; 401:1655-1668.
28. Shah MA, Shitara K, Ajani JA, *et al.* Zolbetuximab plus CAPOX in CLDN18.2-positive gastric or gastroesophageal junction adenocarcinoma: the randomized, phase 3 GLOW trial. *Nat Med*. 2023; 29:2133-2141.
29. Strickler JH, Satake H, George TJ, *et al.* Sotorasib in *KRAS* p.G12C-Mutated Advanced Pancreatic Cancer. *N Engl J Med*. 2023; 388:33-43.
30. Ou SI, Jänne PA, Leal TA, Rybkin II, Sabari JK, Barve MA, Bazhenova L, Johnson ML, Velastegui KL, Cilliers C, Christensen JG, Yan X, Chao RC, Papadopoulos KP. First-in-Human Phase I/IB Dose-Finding Study of Adagrasib (MRTX849) in Patients With Advanced *KRAS*^{G12C} Solid Tumors (KRYSTAL-1). *J Clin Oncol*. 2022; 40:2530-2538.
31. Bellon E, Gebauer F, Tachezy M, Izbicki JR, Bockhorn M. Pancreatic cancer and liver metastases: state of the art. *Updates Surg*. 2016; 68:247-251.
32. Frigerio I, Malleo G, de Pastena M, Deiro G, Surci N, Scopelliti F, Esposito A, Regi P, Giardino A, Allegrini V, Bassi C, Girelli R, Salvia R, Butturini G. Prognostic Factors After Pancreatectomy for Pancreatic Cancer Initially Metastatic to the Liver. *Ann Surg Oncol*. 2022; 29:8503-8510.
33. Bachellier P, Addeo P, Averous G, Dufour P. Resection of pancreatic adenocarcinomas with synchronous liver metastases: A retrospective study of prognostic factors for survival. *Surgery*. 2022; 172:1245-1250.
34. Satoi S, Yamamoto T, Hashimoto D, Yamaki S, Matsui Y, Ikeura T, Boku S, Shibata N, Tsybulskyi D, Sekimoto

- M. Oncological role of surgical resection in patients with pancreatic ductal adenocarcinoma with liver-only synchronous metastases in a single-center retrospective study. *J Gastrointest Oncol.* 2023; 14:2587-2599.
35. Takeda T, Sasaki T, Okamoto T, Kasuga A, Matsuyama M, Ozaka M, Inoue Y, Takahashi Y, Saiura A, Sasahira N. Outcomes of pancreatic cancer with liver oligometastasis. *J Hepatobiliary Pancreat Sci.* 2023; 30:229-239.

Received May 29, 2024; Revised June 22, 2024; Accepted June 25, 2024.

**Address correspondence to:*

Yoshihiro Sakamoto, Department of Hepato-Biliary-Pancreatic Surgery, Kyorin University Hospital, 6-20-2 Shinkawa, Mitaka-city, Tokyo 181-8611, Japan.

E-mail: yosakamo@ks.kyorin-u.ac.jp

Revealing the gut microbiome mystery: A meta-analysis revealing differences between individuals with autism spectrum disorder and neurotypical children

Changjiang Yang¹, Hongli Xiao¹, Han Zhu¹, Yijie Du^{2,*}, Ling Wang^{3,4,5,*}

¹ Faculty of Education, East China Normal University, Shanghai, China;

² Qingpu Traditional Chinese Medicine Hospital, Shanghai, China;

³ Laboratory for Reproductive Immunology, Obstetrics and Gynecology Hospital of Fudan University, Shanghai, China;

⁴ The Academy of Integrative Medicine, Fudan University, Shanghai, China;

⁵ Shanghai Key Laboratory of Female Reproductive Endocrine-related Diseases, Shanghai, China.

SUMMARY The brain-gut axis intricately links gut microbiota (GM) dysbiosis to the development or worsening of autism spectrum disorder (ASD). However, the precise GM composition in ASD and the effectiveness of probiotics are unclear. To address this, we performed a thorough meta-analysis of 28 studies spanning PubMed, PsycINFO, Web of Science, Scopus, and MEDLINE, involving 1,256 children with ASD and 1042 neurotypical children, up to February 2024. Using Revman 5.3, we analyzed the relative abundance of 8 phyla and 64 genera. While individuals with ASD did not exhibit significant differences in included phyla, they exhibited elevated levels of *Parabacteroides*, *Anaerostipes*, *Faecalibacterium*, *Clostridium*, *Dorea*, *Phascolarctobacterium*, *Lachnoclostridium*, *Catenibacterium*, and *Collinsella* along with reduced percentages of *Barnesiella*, *Odoribacter*, *Paraprevotella*, *Blautia*, *Turicibacter*, *Lachnospira*, *Pseudomonas*, *Parasutterella*, *Haemophilus*, and *Bifidobacterium*. Notably, discrepancies in *Faecalibacterium*, *Clostridium*, *Dorea*, *Phascolarctobacterium*, *Catenibacterium*, *Odoribacter*, and *Bifidobacterium* persisted even upon systematic exclusion of individual studies. Consequently, the GM of individuals with ASD demonstrates an imbalance, with potential increases or decreases in both beneficial and harmful bacteria. Therefore, personalized probiotic interventions tailored to ASD specifics are imperative, rather than a one-size-fits-all approach.

Keywords autism spectrum disorder (ASD), gut microbiota, meta-analysis, neurotypical children

1. Introduction

Autism spectrum disorder (ASD) is a neurodevelopmental disorder emerging in early childhood, marked by social interaction and communication impairments, repetitive behaviors, and potential comorbidities including sleep, immune, gastrointestinal disorders, and endocrine imbalances. Its prevalence is rising, with about 1 in 100 children affected globally as of 2022, according to the World Health Organization (WHO) (1). Nonetheless, ASD presents with heterogeneous clinical manifestations, and its etiology and pathogenesis are multifaceted and intricate. Although research suggests that ASD has a complex etiology involving both genetic and environmental factors (2), specific causes are still not well understood.

Extensive research has revealed that the development and progression of ASD may be closely linked to gut microbiota dysbiosis. Clinical investigations have

frequently observed that children with ASD often experience gastrointestinal symptoms (GIS) like diarrhea, constipation, and abdominal pain linked to disrupted GM. These GIS have been found in 9 to 91% of individuals with ASD and are correlated with the severity of clinical symptoms (3). The exact causal relationship between ASD and GIS is still unclear, but numerous studies have indicated a certain association between them. Fortunately, the "microbiota-gut-brain axis" mechanism provides novel insights into understanding this connection (4). The gut-brain axis is a crucial bidirectional communication pathway between the brain and the gastrointestinal tract, with GM acting as key regulators. They can influence brain function through the enteric nervous system (ENS), endocrine system, metabolic system, and immune system. Disruptions in the dynamic equilibrium of GM within the human body lead to peripheral neurotransmitter imbalances, abnormal secretion of metabolites, or activation of immune

responses, ultimately resulting in elevated levels of peripheral inflammatory mediators capable of affecting neurodevelopment through circulation or penetration of the blood-brain barrier (5). In other words, changes in GM composition may contribute to gastrointestinal disturbances and exacerbate ASD symptoms (6-8).

Interestingly, numerous studies have documented notable variation in the composition and quantity of GM between ASD and neurotypical children (9), but there is no consensus on the dysregulation of GM in ASD. Moreover, research on the effectiveness of prebiotics, probiotics, and fecal microbiota transplantation in managing ASD has yielded mixed results (10-12). Consequently, analyzing current clinical data and increasing sample sizes are essential to better understanding the changes in GM in individuals with ASD and to provide insights for developing treatments involving probiotics, prebiotics, or fecal transplantation.

Thus far, four published meta-analysis have examined the association between GM and ASD, yielding inconsistent conclusions. These studies reported varied findings, including a decreased presence of *Akkermansia*, *Bifidobacterium*, *Bacteroides*, *Enterococcus* and *Escherichia coli* compared to typically developing children, and an increased prevalence of *Faecalibacterium* and *Lactobacillus*, with a slight elevation in *Ruminococcus* and *Clostridium* (13). Moreover, another meta-analysis performed in 2020 noted a higher abundance of Bacteroidetes, Firmicutes, and Actinobacteria along with specific genera like *Bacteroides*, *Clostridium*, *Faecalibacterium*, *Parabacteroides*, and *Phascolarctobacterium*, but a decreased proportion of *Bifidobacterium* and *Coprococcus* (14). Conversely, a 2022 meta-analysis found no significant correlation for the phyla Actinobacteria, Bacteroidetes, Firmicutes, and Proteobacteria but did report significantly lower levels of *Bifidobacterium* and *Streptococcus* in ASD (15). Moreover, the latest meta-analysis published in 2024 found decreased levels of *Bifidobacterium* and *Parabacteroides* in comparison to controls while observing elevated levels of *Bacteroides*, *Clostridium*, and *Faecalibacterium* (16). To date, published meta-analysis have covered only a limited range of GM, precluding a comprehensive understanding of GM in ASD.

To address conflicting findings regarding the composition of GM in ASD versus neurotypical controls and to provide data on the association between ASD and GM, our meta-analysis integrated data from recent studies encompassing the full spectrum of tested GM, comprising approximately 8 phyla and 64 genera, to statistically derive significant conclusions about variations in gut microbial composition. These findings are anticipated to make a valuable contribution in the advancement of a potential set of biomarkers for the diagnosis of ASD or the identification of targets for therapy.

2. Methods

To ensure the transparency and reliability of our findings, we diligently followed the guidelines outlined by PRISMA (17), which provide a comprehensive framework for performing meta-analyses in a systematic and standardized manner.

2.1. Literature search

Our meta-analysis involved an exploration of diverse databases such as MEDLINE, PubMed, PsycINFO, Scopus, and Web of Science. The search terms were combined using Boolean logic operators: (autism OR autism spectrum disorder OR ASD OR autistic disorder) AND (microbiota OR microflora OR stool OR fecal OR microbiome). The search options used in the Scopus database included "title, abstract, and keywords," whereas the PubMed database relied on searching through "title/abstract," and the "abstract" was searched for in other databases. Moreover, the searches encompassed English publications without any restrictions on the year of publication. To guarantee a thorough examination of relevant literature, we diligently examined the references of systematic reviews and meta-analysis that explored differences in GM among ASD versus neurotypical children.

2.2. Selection criteria

The studies were selected based on the inclusion criteria outlined below: (1) Participants consisted of individuals diagnosed with ASD, with neurotypical individuals constituting the control group; (2) Studies comparing the composition of GM in individuals; (3) Studies examining the relative abundance (RA) of GM, including at least the phylum and/or genus level of microbiota; and (4) Studies using stools samples for analysis.

Exclusion of studies was based on the following criteria: (1) Animal model studies; (2) Studies focusing solely on GM in blood, urine, or saliva; (3) Reviews, meta-analyses, books, conferences, or editorial materials; and (4) non-English publications.

A point worth emphasizing us that a considerable number of studies fulfilling the inclusive criteria were not included due to incomplete data or only presenting figures without specific data (*e.g.*, missing values for RA, Mean, or SD) despite attempts to obtain this information through direct communication with either the corresponding author or first author.

2.3. Data extraction and study quality

The data presented in Table 1 were extracted from included studies by two researchers working independently: First authors' surnames (publication years), the subjects' country, details on children with

ASD and NT children (sample size, gender, mean age \pm SD), samples of extracted DNA, and details on GM (microbiological assessments, units). Importantly, our meta-analysis comprehensively incorporated all relevant data on GM from the included studies to thoroughly investigate the composition of GM in ASD.

The Newcastle-Ottawa Scale (NOS) was utilized to evaluate the methodological quality of the included studies in our meta-analysis, which primarily focused on assessing observational research such as cohort and case-control studies (18). The NOS uses a "star system" to evaluate three dimensions: Selection, Comparability, and Exposure (for case-control studies)/Outcome (for cohort studies). It consists of 8 items with a maximum rating of 9 stars. The quality was classified as high (7 – 9 stars), moderate (4 – 6 stars), or low (below 4 stars).

To ensure the reliability of extracted study data and evaluate the quality of the NOS, two researchers collaborated to extract data from a single study, resolving any discrepancies through consensus. After achieving an impressive rate of consistency of 99%, they subsequently performed the task independently. In addition, for accuracy, our meta-analysis compared the extracted microbial data with published meta-analyses and data were double-checked for any inconsistencies.

2.4. Statistical analysis

The included studies reported the relative abundance (RA), mean, standard deviation (SD), standard error (SE), or confidence interval of GM in children with ASD and NT children. RA and SE were used to standardize the data in order to calculate the overall percentage of GM from various phyla and genera in both the ASD and NT groups. In cases where SE was not directly available, we derived it using the formula $SE = SD/\sqrt{n}$.

Review Manager 5.3 was used to assess effect sizes, heterogeneity, and sensitivity analysis. (1) Heterogeneity was assessed using the Chi-Square test and I^2 . $P < 0.10$ in the Chi-square test suggests significant heterogeneity among the included studies. I^2 values of 25%, 50%, and 75% indicate slight, moderate, and high levels of heterogeneity, respectively. In situations where there are inconsistencies between the results of the Chi-square test and I^2 , priority is given to assessing studies based on I^2 . (2) Calculation of Effect Sizes. A random-effects model is utilized when $I^2 \geq 50\%$ ($P < 0.10$); otherwise, a fixed-effects model is selected. The standardized mean difference (SMD) was used as the measure of effect size in our meta-analysis. An $SMD > 0$ indicates a higher relative abundance of GM in the ASD compared to the NT group, while an $SMD < 0$ suggests a lower average abundance of GM in the ASD group. SMDs of approximately 0.20, 0.50, and 0.80 represent small, medium, and large effect sizes, respectively. (3) Sensitivity analysis in our meta-analysis was performed through a systematic exclusion of individual studies.

If the consistency of the subgroup difference remained relatively stable even after excluding a particular study, this suggested limited susceptibility and enhanced the reliability of our results. In particular, the design of our included studies, specifically cohort and case-control studies, precluded the possibility of performing a publication bias analysis in our meta-analysis. Typically, publication bias analysis is used to verify the accuracy and representativeness of study results by comparing effect sizes across different groups (19). However, our meta-analysis primarily focused on subgroup analyses comparing the abundance of GM in individuals with ASD to NT children, without the inclusion of any comparison groups.

3. Results

The step-by-step process for article screening is depicted in Figure 1. The articles underwent a rigorous review process, including the examination of titles, abstracts, and full texts. A comprehensive screening was then conducted using predefined criteria for inclusion and exclusion. As a result, 28 articles were deemed eligible for inclusion (20-47). A point of note is that although an additional 24 articles initially met the inclusion criteria of our meta-analysis, they were ultimately excluded due to the presentation of only images without providing accurate data or a lack of response despite attempts to contact the authors.

3.1. Characteristics of the included studies

The details regarding the included studies in our meta-analysis can be found in Table 1. Most of the studies were conducted in China (ten), followed by seven in the US, three in Italy, two in Australia, and one each in Japan, Spain, India, Tunisian, Uruguay, and Russia. The sample sizes ranged from 6 to 143, with 1,256 individuals with ASD and 1042 neurotypical children between the ages of 2 to 37 years. Most studies utilized 16S rRNA gene sequencing to analyze GM differences, with two studies using culture-based methods, four using a polymerase chain reaction (PCR), and two using shotgun metagenomic sequencing. Stool samples were gathered for analysis in each of the included studies. Microbiota analysis primarily focused on the phylum and genus levels, and a wide range of microbes was reported in terms of Relative Abundance (RA) or percentage.

3.2. Study quality

We performed an in-depth analysis of the sample selection and study design of the included studies, subsequently establishing criteria to evaluate their quality using the NOS. Our primary considerations regarding selection included (1) whether the studies provided comprehensive

Table 1. The characteristics of included studies in the meta-analysis

Study	ASD			NT			Sample			Details on Microbiota	
	Country	n	Gender (M/F)	Age (years)	n	Gender (M/F)	Age (years)	Sample	Microbiology Assessment	Outcomes	Unit
Finegold (2010)	USA	19	-	2-13	8	5/3	2-13	stool	Pyrosequencing	Phylum: Bacteroidetes, Firmicutes, Proteobacteria, Actinobacteria, Cyanobacteria, Fusobacteria, Verrucomicrobia, Tenericutes Genus: <i>Akkermansia</i> , <i>Bacteroides</i> , <i>Bifidobacterium</i> , <i>Clostridium</i> , <i>Faecalibacterium</i> , <i>Parabacteroides</i> , <i>Ruminococcus</i>	RA
Wang (2011)	Australia	23	21/2	10.25 ± 0.75	9	4/5	9.5 ± 1.25	stool	qPCR	Genus: <i>Akkermansia</i> , <i>Bacteroides</i> , <i>Bifidobacterium</i> , <i>Faecalibacterium</i> , <i>Clostridium</i>	RA
Adam (2011)	USA	58	50/8	6.91 ± 3.4	39	18/21	7.7 ± 4.4	Stool	Culture	Genus: <i>Lactobacillus</i> , <i>Bifidobacterium</i> , <i>Enterococcus</i>	RA/CFU
Gondalia (2012)	Australia	51	42/9	2-12	53	19/34	2-12	Stool	Culture	Phylum: Bacteroidetes, Firmicutes, Proteobacteria, Actinobacteria, Cyanobacteria, Fusobacteria, Verrucomicrobia, Tenericutes Genus: <i>Anaerostipes</i> , <i>Anaerotruncus</i> , <i>Bacteroides</i> , <i>Bifidobacterium</i> , <i>Blautia</i> , <i>Clostridium</i> , <i>Roseburia</i> , <i>Faecalibacterium</i> , <i>Parabacteroides</i> , <i>Ruminococcus</i> , <i>Sutterella</i> , <i>Veillonella</i> , <i>Coproccoccus</i> , <i>Dialister</i> , <i>Dorea</i> , <i>Phascolarctobacterium</i>	RA
Williams (2012)	USA	23	-	-	9	-	-	Stool	16S rRNA genes sequencing/PCR	Genus: <i>Sutterella</i>	RA
Angelis (2013)	Italy	10	-	4-10	10	-	4-10	Stool	Pyrosequencing	Genus: <i>Akkermansia</i> , <i>Bacteroides</i> , <i>Bifidobacterium</i> , <i>Clostridium</i> , <i>Faecalibacterium</i> , <i>Parabacteroides</i> , <i>Ruminococcus</i>	CFU/RA
Kang (2013)	USA	20	17/3	6.7 ± 2.7	20	18/2	8.3 ± 4.4	stool	qPCR	Phylum: Bacteroidetes, Firmicutes, Proteobacteria, Actinobacteria, Cyanobacteria, Fusobacteria, Verrucomicrobia, Tenericutes Genus: <i>Akkermansia</i> , <i>Anaerostipes</i> , <i>Anaerotruncus</i> , <i>Bacteroides</i> , <i>Bifidobacterium</i> , <i>Blautia</i> , <i>Clostridium</i> , <i>Faecalibacterium</i> , <i>Parabacteroides</i> , <i>Ruminococcus</i> , <i>Sutterella</i> , <i>Veillonella</i> , <i>Coproccoccus</i> , <i>Dialister</i> , <i>Dorea</i> , <i>Phascolarctobacterium</i> , <i>Roseburia</i>	RA
Son (2015)	USA	59	52/7	10.3 ± 1.8	44	21/23	10.0 ± 1.8	stool	qPCR	Genus: <i>Sutterella</i> , <i>Bacteroidetes</i> , <i>Prevotella</i>	RA

Note: ASD: Autism spectrum disorder; NT: Neurotypical children; M/F: male/female; RA: Relative Abundance; CFU: Colony Forming Unit

Table 1. The characteristics of included studies in the meta-analysis (continued)

Study	ASD			NT		Sample	Details on Microbiota				
	Country	n	Gender (M/F)	Age (years)	Gender (M/F)		Age (years)	Microbiology Assessment	Outcomes	Unit	
Inoue (2016)	Japan	6	-	3-5	6	-	3-5	stool	16S rRNA gene sequencing	Genus: <i>Akkermansia</i> , <i>Anaerostipes</i> , <i>Anaerotruncus</i> , <i>Bacteroides</i> , <i>Bifidobacterium</i> , <i>Blautia</i> , <i>Clostridium</i> , <i>Faecalibacterium</i> , <i>Parabacteroides</i> , <i>Ruminococcus</i> , <i>Sutterella</i> , <i>Veillonella</i> , <i>Coproccoccus</i> , <i>Dialister</i> , <i>Dorea</i> , <i>Phascolarctobacterium</i> , <i>Roseburia</i>	RA
Strati (2017)	Italy	40	31/9	11.1 ± 6.8	40	28/12	9.2 ± 7.9	stool	16S rRNA gene sequencing	Phylum: Bacteroidetes, Firmicutes, Proteobacteria, Actinobacteria, Cyanobacteria, Fusobacteria, Verrucomicrobia Genus: <i>Akkermansia</i> , <i>Anaerostipes</i> , <i>Anaerotruncus</i> , <i>Bacteroides</i> , <i>Bifidobacterium</i> , <i>Blautia</i> , <i>Clostridium</i> , <i>Faecalibacterium</i> , <i>Parabacteroides</i> , <i>Ruminococcus</i> , <i>Sutterella</i> , <i>Veillonella</i> , <i>Coproccoccus</i> , <i>Dialister</i> , <i>Dorea</i> , <i>Phascolarctobacterium</i> , <i>Roseburia</i>	RA
Berding (2018)	USA	26	19/7	4.1 ± 1.6	32	19/13	4.8 ± 1.8	Stool	Real-time PCR	Phylum: Bacteroidetes, Firmicutes, Clostridiales, Streptophyta Genus: <i>Clostridiaceae</i> , <i>Clostridium</i> , <i>SMB53</i> , <i>Blautia</i> , <i>Roseburia</i> , <i>Butyrivibrio</i> , <i>Butyrivibrio</i> , <i>Faecalibacterium</i> , <i>Dialister</i> , <i>Bilophila</i> , <i>Bifidobacterium</i> , <i>C. perfringens</i>	RA
Coretti (2018)	Italy	11	9/2	2-4	14	8/6	2-4	Stool	16S rRNA gene sequencing	Phylum: Bacteroidetes, Firmicutes, Proteobacteria, Actinobacteria Genus: <i>Bacteroides</i> , <i>Bifidobacterium</i> , <i>Blautia</i> , <i>Faecalibacterium</i> , <i>Parabacteroides</i> , <i>Ruminococcus</i> , <i>Coproccoccus</i> , <i>Roseburia</i>	RA
Kang (2018)	USA	23	22/1	10.1 ± 4.1	21	15/6	8.4 ± 3.4	Stool	16S rRNA gene sequencing	Genus: <i>Faecalibacterium</i> , <i>Haemophilus</i> , <i>Prevotella</i>	RA
Pulitkkan (2018)	India	30	28/2	9.5 ± 3.25	24	15/9	9.5 ± 3.13	Stool	16S rRNA gene sequencing	Genus: <i>Lactobacillus</i>	RA
Zhang (2018)	China	35	29/6	4.9 ± 1.5	6	5/1	4.6 ± 1.1	Stool	16S rRNA sequencing	Phylum: Bacteroidetes Genus: <i>Veillonella</i> , <i>Streptococcus</i> , <i>Escherichia</i>	RA
Ma (2019)	China	45	39/6	7.04 ± 1.19	45	39/6	7.27 ± 1.07	Stool	16S rRNA gene sequencing	Phylum: Bacteroidetes, Firmicutes, Proteobacteria, Actinobacteria, Cyanobacteria, Fusobacteria, Verrucomicrobia, Tenericutes Genus: <i>Bacteroides</i> , <i>Bifidobacterium</i> , <i>Blautia</i> , <i>Clostridium</i> , <i>Faecalibacterium</i> , <i>Parabacteroides</i> , <i>Ruminococcus</i> , <i>Coproccoccus</i> , <i>Phascolarctobacterium</i> , <i>Roseburia</i>	RA

Note: ASD: Autism spectrum disorder; NT: Neurotypical children; M/F: male/female; RA: Relative Abundance; CFU: Colony Forming Unit

Table 1. The characteristics of included studies in the meta-analysis (continued)

Study	ASD		NT		Sample	Microbiology Assessment		Details on Microbiota		Unit	
	Country	n	Gender (M/F)	Age (years)		Gender (M/F)	n	Age (years)	Microbiology Assessment		Outcomes
Plaza-Diaz (2019)	Spain	48	-	2-6	57	-	2-6	Stool	16S rRNA gene amplicon sequencing	Phylum: Bacteroidetes, Firmicutes, Proteobacteria, Actinobacteria, Verrucomicrobia Genus: Akkermansia, Bacteroides, Veillonella Bifidobacterium, Clostridium, Faecalibacterium, Parabacteroides, Ruminococcus	RA
Dan (2020)	China	143	130/13	4.94 ± 0.16	143	127/16	5.19 ± 0.17	Stool	16S rRNA gene sequencing	Genus: Bacteroides, Prevotella, Paraprevotella Phascolarctobacterium,	RA
Zou (2020)	China	48	38/10	2-7	48	24/24	4	Stool	16S rRNA gene sequencing	Phylum: Bacteroidetes, Firmicutes, Proteobacteria, Verrucomicrobia Genus: Clostridium XlIIa, Bacteroides, Prevotella, Eisenbergiella, Lachnospiraceae incertae sedis...	RA
Ding (2020)	China	77	59/18	3.21 ± 0.96	50	39/11	3.58 ± 1.21	Stool	16S rRNA gene sequencing	Genus: Lachnospiraceae, Clostridiales, Dorea, Erysipelotrichaceae, Collinsella, Lachnoclostridium, Bacteroides, Faecalibacterium, Parasutterella, Paraprevotella	RA
Averina (2020)	Russia	36	30/6	3.72 ± 0.61	21	14/7	3.58 ± 0.63	Stool	shotgun metagenome sequencing	Genus: Barnesiella, Parabacteroides	RA
Chen (2021)	China	138	117/21	6.11 ± 2.00	60	27/33	6.65 ± 2.22	Stool	16S rRNA gene sequencing	Genus: Prevotella, Bacteroides, Faecalibacterium, Sutterella, Megamonas, Coprococcus, Collinsella, Desulfovibrio	RA
Deng (2022)	China	45	39/6	5.95 ± 2.36	45	21/24	6.13 ± 0.90	Stool	16S rRNA gene sequencing	Phylum: Bacteroidetes, Genus: Agathobacter, Massilia, Proteobacteria, Gammaaproteobacteria, Massilia, Megamonas, Sphingomonas, Agathobacter, Blautia	RA
Wong (2022)	China	92	30/62	8.2	112	32/80	8.47	Stool	16S rRNA gene sequencing	Phylum: Firmicutes: Bacteroidetes Genus: Bifidobacterium, Dorea, Blautia, Collinsella, Bacteroides, Alistipes, Parabacteroides, Sutterella	RA
Chamtouri (2023)	Tunisian	28	22/6	7.93 ± 2.05	28	22/6	7.29 ± 2.09	Stool	16S rRNA gene sequencing	Genus: Bacteroides, Lachnoclostridium, Megamonas, Collinsella, Subdoligranulum...	RA
Pang (2023)	China	19	14/5	17-32	19	14/5	19-37	Stool	16S rRNA gene sequencing	Phylum: Proteobacteria Genus: Agathobacter, Akkermansia, Alistipes, Anaerobutyricum, Anaerostipes, Bifidobacterium... (18)	RA

Note: ASD: Autism spectrum disorder; NT: Neurotypical children; M/F: male/female; RA: Relative Abundance; CFU: Colony Forming Unit

Table 1. The characteristics of included studies in the meta-analysis (continued)

Study	ASD			NT		Sample			Details on Microbiota	
	Country	n	Gender (M/F)	Age (years)	n	Gender (M/F)	Age (years)	Microbiology Assessment	Outcomes	Unit
Dubourdieu (2023)	Uruguay	30	-	3-12	28	-	3-12	16S rDNA gene sequencing	Genus: <i>Bifidobacterium</i> , <i>Clostridium glycolicum</i> , <i>Roseburia</i> , <i>Faecalibacterium</i> , <i>Eubacterium ventriosum</i> , <i>Flavonifractor plautii</i>	RA
Wang (2023)	China Russia	43 30	- -	2-7 3-5	31 20	- -	2-7 3-5	Shotgun metagenomic sequencing	Genus: <i>Bacteroides</i> , <i>Faecalibacterium</i> , <i>Eubacterium</i> , <i>Bifidobacterium</i> , <i>Alistipes</i> , <i>Prevotella...</i> (91)	RA

Note: ASD: Autism spectrum disorder; NT: Neurotypical children; M/F: male/female; RA: Relative Abundance; CFU: Colony Forming Unit

information on the diagnostic criteria for ASD and (2) whether NT children were recruited from community settings or hospitals. In term of comparability, our key focus lay in assessing whether studies controlled for factors such as age, gastrointestinal comorbidities, probiotic or prebiotic treatments, and special diets. Our primary examination of exposure/outcome centered on the methods used for fecal sample preservation and analytical techniques. In addition, the response rate was not addressed in any of the included studies, so all studies were awarded a star in this criterion.

Ultimately, all included studies were assessed to be of medium to good quality. Specifically, 21 studies were deemed to be of good quality, while 7 studies were categorized as medium quality. Regarding selection criteria, the majority of included studies provided comprehensive descriptions of the screening criteria for ASD, such as DSM-5, ICD-10, or CARS, as shown in Table 3. However, two articles briefly mentioned the inclusion of diagnosed ASD without providing specific details regarding diagnostic criteria (23,37). In addition, there was insufficient information in 7 articles (21,23,29,38,42,47,48) regarding the location of the children in the control group. Regarding comparability, all studies rigorously matched age across subgroups, but 16 studies that did not explicitly address gastrointestinal comorbidities in participants (20,23-25,29,33,35,38-41,43-45,47,49), and 7 studies did not explicitly control for probiotic or prebiotic treatments or special diets (21-23,37,41,42,49). Regarding Exposure/Outcome, all studies used rigorous scientific protocols for the preservation of fecal samples and they all utilized effective analytical techniques, including culture, PCR, and pyrosequencing, in both cohorts.

3.3. Mean effect size and between-study heterogeneity

The mean effect sizes according to our meta-analysis, which includes data at both the phylum and genus levels of GM, are shown in Table 2. The meta-analysis revealed no significant differences between children with ASD and NT children across the bacterial phyla Actinobacteria, Bacteroidetes, Cyanobacteria, Firmicutes, Fusobacteria, Proteobacteria, Tenericutes, and Verrucomicrobia. Notably, the overall effect size for two subgroups, except for Cyanobacteria, was statistically significant across Actinobacteria, Bacteroidetes, Firmicutes, Fusobacteria, Proteobacteria, Tenericutes, and Verrucomicrobia, ranging from 2.18 for Fusobacteria to 34.86 for Firmicutes. This indicated that both groups might have a greater abundance of Actinobacteria, Bacteroidetes, Proteobacteria, and Verrucomicrobia, along with a lower abundance of Firmicutes, Fusobacteria, and Tenericutes. Moreover, between-study heterogeneity was high, ranging between 25% and 100%, while heterogeneity within subgroups when comparing both phyla was zero.

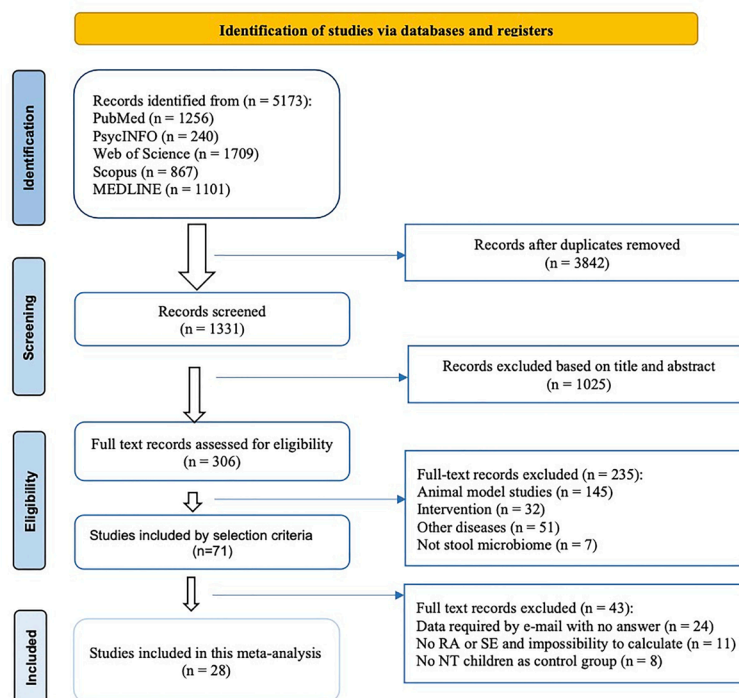


Figure 1 Flow Diagram for selection of studies (PRISMA flow diagram).

Figure 1. Flow diagram for selection of studies (PRISMA flow diagram).

3.3.1. Bacterial genera that were more abundant in individuals with ASD than controls

Parabacteroides: As shown in Table 2, 18 studies were included in the random-effects meta-analysis for *Parabacteroides*. The RA of *Parabacteroides* was 0.18% (95% CI: 0.13, 0.23) in the ASD group, compared to 0.09% (95% CI: 0.06, 0.12) in the NT group. High between-study heterogeneity was observed in both subgroups ($I^2 = 95\%$ and 96% , respectively), as well as in the comparison between the two groups ($I^2 = 89\%$). The overall effect size was large and highly significant ($Z = 7.90$, $P < 0.001$). In addition, there was a difference in the bacterial percentage of 2, suggesting higher levels of *Parabacteroides* in children with ASD compared to NT individuals.

Anaerostipes: The meta-analysis for *Anaerostipes* included 11 studies, indicating that 0.27% (95% CI: 0.19, 0.35) of the detected microbiota were attributed to *Anaerostipes* in the ASD group, while 0.08% (95% CI: 0.05, 0.11) were attributed in the NT group. Very high between-study heterogeneity was observed ($I^2 = 98\%$) in both groups. In addition, high heterogeneity persisted in the comparison between the two groups ($I^2 = 94.40\%$). The effect size was large and significant ($Z = 8.74$, $P < 0.001$). Moreover, the difference in bacterial percentage for *Anaerostipes* was 3.38, showing that children with ASD exhibited greater levels of *Anaerostipes* in comparison to NT individuals.

Faecalibacterium: The relative abundance of *Faecalibacterium* was evaluated across 22 trials. In

children diagnosed with ASD, the percentage was 2.28% (95% CI: 2.04, 2.52) in contrast to 1.04% (95% CI: 0.88, 1.19) in the NT group. High between-study heterogeneity was noted in both the ASD (99%) and NT (98%) groups, as well as between the subgroups ($I^2 = 98.60\%$). The effect size was large and significant ($Z = 22.82$, $P < 0.001$). A difference in bacterial percentage of 2.19 indicates that individuals with ASD had higher levels of *Faecalibacterium* than those without ASD.

Clostridium: Fourteen studies were included in the meta-analysis of *Clostridium*, yielding the following results: A relative abundance of 1.27% in the ASD group (95% CI: 0.97, 1.57) compared to 0.31% in the NT group (95% CI: 0.21, 0.41). Significant between-study heterogeneity was observed in both the ASD and control groups, with percentages of 97% and 98%, respectively, and heterogeneity remained very high (97.10%) when comparing the subgroups. The effect size was large and statistically significant ($Z = 9.79$, $P < 0.001$). The difference in bacterial percentage for *Clostridium* was significantly higher, by a factor of 4.10, among individuals with ASD compared to the NT group.

Dorea: Our meta-analysis included 12 studies on *Dorea*, revealing the following findings: the relative abundance of *Dorea* was 0.50% (95% CI: 0.33, 0.67) in children with ASD and 0.05% (95% CI: 0.03, 0.07) in the control group. Heterogeneity among studies was high at 97% and 98% in the ASD and the control group, respectively, while it decreased to 96.40% when comparing the two groups. The effect size was significant and of a large magnitude ($Z = 9.93$, $P < 0.001$). The

Table 2. Results of the meta-analysis comparing ASD and neurotypical children at the phylum and genus levels

	Included Studies			ASD			NT			Overall Effect			Subgroup Differences		
	Studies	Overall Relative Abundance	95% CI	Between-study I ²	Overall Relative Abundance	95% CI	Between-study I ²	Overall Effect	Z	p	f	p	f	p	
															Overall Relative Abundance
Bacteroidetes	5	30.35	8.21 – 52.48	100	28.55	7.04 – 50.06	99	24.85	<0.00001	0	0.91	0	0.91		
<i>Bacteroides</i>	24	3.72	3.31 – 4.13	99	3.35	2.93 – 3.76	99	22.13	<0.00001	37.4	0.21	37.4	0.21		
<i>Parabacteroides</i>	18	0.18	0.13 – 0.23	95	0.09	0.06 – 0.12	96	7.90	<0.00001	89	0.003	89	0.003		
<i>Alistipes</i>	12	0.19	0.10 – 0.28	95	0.19	0.12 – 0.27	97	6.14	<0.00001	0	0.91	0	0.91		
<i>Prevotella</i>	15	0.04	0.01 – 0.07	87	0.07	0.02 – 0.12	81	3.85	0.0001	19.8	0.26	19.8	0.26		
<i>Fusobacterium</i>	7	0.01	-0.01 – 0.04	65	0.00	-0.00 – 0.01	78	1.91	0.06	0	0.38	0	0.38		
<i>Barnesiella</i>	7	0.08	0.02 – 0.13	82	0.28	0.11 – 0.44	78	4.56	<0.00001	79.5	0.03	79.5	0.03		
<i>Odoribacter</i>	9	0.09	0.05 – 0.13	97	0.18	0.12 – 0.24	82	7.01	<0.00001	82.8	0.02	82.8	0.02		
<i>Paraprevotella</i>	8	0.00	0.00 – 0.01	11	0.03	0.01 – 0.05	52	3.08	0.002	80	0.03	80	0.03		
<i>Pseudobutyrvibrio</i>	4	0.04	-0.01 – 0.09	98	0.01	-0.00 – 0.02	97	2.84	0.005	29.6	0.23	29.6	0.23		
<i>Intestinimonas</i>	3	0.01	0.00 – 0.02	33	0.03	0.01 – 0.05	67	4.72	<0.00001	53	0.14	53	0.14		
<i>Butyrivimonas</i>	7	0.02	0.01 – 0.03	4	0.03	0.01 – 0.06	77	3.75	0.0002	21.2	0.26	21.2	0.26		
<i>Allisonella</i>	5	0.02	0.00 – 0.04	91	0.01	0.00 – 0.02	93	3.78	0.0002	16	0.28	16	0.28		
Firmicutes	5	40.27	6.98 – 73.56	100	43.04	10.66 – 75.41	100	34.86	<0.00001	0	0.91	0	0.91		
<i>Anaerostipes</i>	11	0.27	0.19 – 0.35	98	0.08	0.05 – 0.11	98	8.74	<0.00001	94.4	< 0.00001	94.4	< 0.00001		
<i>Anaerotruncus</i>	9	0.02	0.01 – 0.04	78	0.02	0.01 – 0.04	84	5.31	<0.00001	0	0.87	0	0.87		
<i>Blautia</i>	14	0.09	0.06 – 0.13	99	0.20	0.15 – 0.25	99	8.35	<0.00001	91.9	0.0005	91.9	0.0005		
<i>Faecalibacterium</i>	22	2.28	2.04 – 2.52	99	1.04	0.88 – 1.19	98	22.82	<0.00001	98.6	< 0.00001	98.6	< 0.00001		
<i>Ruminococcus</i>	13	0.19	0.12 – 0.26	96	0.17	0.12 – 0.22	97	7.43	<0.00001	0	0.72	0	0.72		
<i>Veillonella</i>	9	0.02	-0.00 – 0.03	79	0.05	0.01 – 0.03	87	3.47	0.0005	56.2	0.13	56.2	0.13		
<i>Clostridium</i>	14	1.27	0.97 – 1.57	97	0.31	0.21 – 0.41	98	9.79	<0.00001	97.1	< 0.00001	97.1	< 0.00001		
<i>Coprococcus</i>	17	0.04	0.03 – 0.05	97	0.05	0.04 – 0.07	97	10.00	<0.00001	72.8	0.06	72.8	0.06		
<i>Dialister</i>	8	0.01	-0.01 – 0.04	83	0.01	-0.01 – 0.02	88	1.64	0.10	0	0.77	0	0.77		
<i>Dorea</i>	12	0.50	0.33 – 0.67	97	0.05	0.03 – 0.07	98	9.93	<0.00001	96.4	< 0.00001	96.4	< 0.00001		
<i>Phascolarctobacterium</i>	13	0.11	0.07 – 0.16	91	0.01	0.00 – 0.02	88	5.08	<0.00001	94.4	< 0.00001	94.4	< 0.00001		
<i>Roseburia</i>	14	0.06	0.04 – 0.09	94	0.04	0.02 – 0.06	97	6.77	<0.00001	53.8	0.14	53.8	0.14		
<i>Enterococcus</i>	10	0.07	0.01 – 0.12	80	0.08	0.01 – 0.16	86	2.74	0.006	0	0.74	0	0.74		
<i>Lactobacillus</i>	12	0.04	0.02 – 0.07	96	0.07	0.02 – 0.13	86	4.40	<0.0001	0	0.33	0	0.33		
<i>Eubacterium</i>	11	0.23	0.16 – 0.30	97	0.25	0.15 – 0.34	98	8.88	<0.00001	0	0.84	0	0.84		
<i>Holdemania</i>	6	0.01	0.00 – 0.02	82	0.01	0.00 – 0.01	73	4.37	<0.0001	0	0.32	0	0.32		
<i>Lachnoclostridium</i>	8	0.47	0.36 – 0.57	99	0.24	0.17 – 0.30	99	13.90	<0.00001	92.5	0.0003	92.5	0.0003		
<i>Streptococcus</i>	11	0.08	0.04 – 0.13	93	0.09	0.04 – 0.14	92	4.23	<0.0001	0	0.88	0	0.88		
<i>Turicibacter</i>	11	0.01	0.00 – 0.02	88	0.04	0.01 – 0.06	88	4.07	<0.0001	76.6	0.04	76.6	0.04		
<i>Catenibacterium</i>	6	0.12	0.08 – 0.17	97	0.01	0.00 – 0.02	95	5.24	<0.0001	95.2	< 0.00001	95.2	< 0.00001		
<i>Fusicatenibacter</i>	7	0.67	0.45 – 0.89	98	0.61	0.36 – 0.87	98	10.17	<0.00001	0	0.73	0	0.73		
<i>Holdemania</i>	5	0.03	0.01 – 0.05	99	0.01	0.00 – 0.03	89	3.30	0.0010	54.6	0.14	54.6	0.14		
<i>Lachnospira</i>	8	0.07	0.02 – 0.11	89	0.26	0.08 – 0.43	95	5.86	<0.00001	76.2	0.04	76.2	0.04		
<i>Lactococcus</i>	6	0.03	0.01 – 0.05	35	0.02	0.01 – 0.02	0	5.17	<0.00001	0	0.33	0	0.33		

Note: ASD: autism spectrum disorder; NT: neurotypical children; Phyla are emphasized in bold font, while genera are italicized and organized based on their respective phyla.

Table 2. Results of the meta-analysis comparing ASD and neurotypical children at the phylum and genus levels (continued)

	Included Studies	ASD			NT			Overall Effect			Subgroup Differences		
		Overall Relative Abundance	95% CI	Between-study I ²	Overall Relative Abundance	95% CI	Between-study I ²	Z	p	I ²	p	p	
<i>Monoglobus</i>	3	0.01	0.00 - 0.01	3	0.00	-0.00 - 0.01	69	3.24	0.001	49	0.16		
<i>Megamonas</i>	13	0.01	-0.00 - 0.01	86	0.04	0.00 - 0.08	86	2.89	0.004	64.4	0.09		
<i>Megasphaera</i>	10	0.02	0.00 - 0.04	56	0.00	-0.00 - 0.00	24	2.37	0.02	70.1	0.07		
<i>Flavonifractor</i>	7	0.06	0.04 - 0.08	99	0.06	0.04 - 0.08	98	9.28	<0.00001	0	0.66		
<i>Acidaminococcus</i>	6	0.01	-0.00 - 0.01	44	0.00	-0.01 - 0.01	6	1.42	0.15	0	0.66		
<i>Butyrivibrio</i>	6	0.01	0.00 - 0.02	94	0.01	0.00 - 0.03	95	2.90	0.004	0	0.71		
<i>Gemmiger</i>	4	0.64	0.19 - 1.09	91	0.70	0.26 - 1.15	94	4.52	<0.00001	0	0.85		
<i>Intestinibacter</i>	5	0.03	-0.00 - 0.07	96	0.01	-0.00 - 0.03	95	2.93	0.003	9.6	0.29		
<i>Subdoligranulum</i>	7	0.02	-0.01 - 0.05	95	0.01	0.00 - 0.02	96	3.35	0.0008	0	0.40		
<i>Collinsella</i>	7	1.04	0.64 - 1.44	98	0.23	0.12 - 0.34	96	6.19	<0.00001	93.3	0.0001		
<i>Oscillospira</i>	6	0.14	0.07 - 0.22	94	0.17	0.11 - 0.24	97	6.99	<0.00001	0	0.52		
<i>Slackia</i>	5	0.19	-0.03 - 0.41	92	0.07	-0.01 - 0.16	79	3.32	0.0009	0	0.33		
<i>Dialister</i>	10	0.02	-0.00 - 0.04	90	0.06	0.02 - 0.10	89	2.57	0.01	67.7	0.08		
<i>Coprococcus</i>	6	0.01	0.00 - 0.02	64	0.04	0.01 - 0.08	88	3.40	0.0007	63.9	0.10		
Proteobacteria	5	1.89	0.32 - 3.46	97	1.28	0.41 - 2.15	98	4.93	<0.00001	0	0.50		
<i>Sutterella</i>	14	0.02	0.01 - 0.03	95	0.04	0.02 - 0.05	94	5.00	<0.00001	65.3	0.09		
<i>Escherichia/Shigella</i>	12	0.34	0.21 - 0.47	91	0.35	0.22 - 0.49	92	7.77	<0.00001	0	0.90		
<i>Pseudomonas</i>	6	0.00	-0.02 - 0.02	96	0.06	0.02 - 0.10	97	2.61	0.009	84.0	0.01		
<i>Klebsiella</i>	9	0.01	0.00 - 0.02	73	0.05	-0.01 - 0.11	75	3.19	0.001	44.1	0.18		
<i>Parasutterella</i>	8	0.03	0.01 - 0.04	87	0.11	0.05 - 0.17	80	5.98	<0.00001	85.3	0.009		
<i>Enterobacter</i>	6	0.00	-0.00 - 0.01	65	0.02	-0.01 - 0.05	72	1.83	0.07	0	0.40		
<i>Haemophilus</i>	11	0.04	0.02 - 0.06	83	0.13	0.06 - 0.20	65	5.23	<0.00001	83.8	0.01		
<i>Citrobacter</i>	5	0.01	-0.00 - 0.02	84	0.13	-0.05 - 0.30	51	2.63	0.009	44.6	0.18		
<i>Desulfovibrio</i>	9	0.01	0.00 - 0.02	39	0.01	0.00 - 0.03	61	4.67	<0.00001	0	0.90		
<i>Blifilifactor</i>	6	0.03	0.01 - 0.05	89	0.06	0.04 - 0.09	74	5.11	<0.00001	66.2	0.09		
Actinobacteria	5	4.35	2.06 - 6.64	97	4.55	1.56 - 7.54	98	4.87	<0.00001	0	0.92		
<i>Bifidobacterium</i>	22	0.46	0.37 - 0.55	99	1.48	1.25 - 1.71	99	16.56	<0.00001	98.5	< 0.00001		
<i>Actinomyces</i>	6	0.03	0.01 - 0.04	96	0.04	0.01 - 0.06	96	4.51	<0.00001	0	0.46		
Cyanobacteria	3	0.00	-0.00 - 0.01	82	0.01	-0.01 - 0.04	93	1.66	0.10	0	0.43		
Fusobacteria	3	0.91	-1.23 - 3.06	80	0.50	-0.42 - 1.43	89	2.18	0.03	0	0.73		
<i>Fusobacterium</i>	3	0.03	-0.03 - 0.10	77	0.02	-0.03 - 0.08	62	1.33	0.18	0	0.80		
Verrucomicrobia	4	0.27	-0.14 - 0.68	89	0.32	-0.23 - 0.86	79	2.15	0.03	0	0.88		
<i>Akkermansia</i>	14	0.21	0.10 - 0.32	87	0.11	0.02 - 0.20	82	3.98	<0.0001	48.8	0.16		
Tenericutes	3	0.00	0.00 - 0.00	100	0.00	0.00 - 0.00	25	2.19	0.03	0	0.45		

Note: ASD: autism spectrum disorder; NT: neurotypical children; Phyla are emphasized in bold font, while genera are italicized and organized based on their respective phyla.

Table 3. Quality assessment of included studies

Study	Selection (max = ★★★★★)			Comparability (max = ★★★)		Exposure (max = ★★★)		Quality score
	Adequate definition of cases	Representativeness of the cases	Selection of controls	Definition of controls	Controls for important factor	Ascertainment of exposure	Same method of ascertainment for cases and controls	
Finegold (2010)	★	★	★	★	★	★	★	8
Wang (2011)	★	★	★	★	★★	★	★	9
Adam (2011)	★	★	-	★	★	★	★	6
Gondalia (2012)	★	★	-	-	★	★	★	7
Williams (2012)	★	-	-	-	★	★	★	4
Angelis (2013)	★	★	★	★	★★	★	★	9
Kang (2013)	★	★	★	-	★	★	★	7
Son (2015)	★	★	★	★	★★	★	★	9
Inoue (2016)	★	★	★	-	★★	★	★	8
Strati (2017)	★	★	-	-	★	★	★	6
Berding (2018)	★	★	★	★	★★	★	★	9
Coretti (2018)	★	★	★	★	★★	★	★	9
Kang (2018)	★	★	★	-	★★	★	★	8
Pulikkan (2018)	★	★	★	★	★★	★	★	8
Zhang (2018)	★	★	★	-	★★	★	★	8
Ma (2019)	★	★	-	★	★	★	★	7
Plaza-Diaz (2019)	★	★	★	★	★	★	★	8
Dan (2020)	★	-	★	★	★	★	★	7
Zou (2020)	★	★	-	-	★	★	★	6
Ding (2020)	★	★	★	★	★	★	★	8
Averina (2020)	★	★	★	★	★	★	★	8
Chen (2021)	★	★	★	★	★	★	★	8
Deng (2022)	★	★	★	★	★	★	★	8
Wong (2022)	★	★	-	-	★	★	★	6
Chamtouri (2023)	★	★	★	-	★	★	★	7
Pang (2023)	★	★	★	-	★	★	★	7
Dubourdieu (2023)	★	★	-	-	★	★	★	6
Wang (2023)	★	★	-	-	-	★	★	5

Note: each item within the Selection and Exposure categories of a study is eligible for a maximum of one star (one point). For the Comparability category, a study can earn up to two stars.

difference in bacterial percentage for *Dorea* was notably higher by a factor of 10 among individuals with ASD in comparison to the NT group.

Phascolarctobacterium: The meta-analysis of *Phascolarctobacterium*, which included 13 studies, yielded the following findings: 0.11% (95% CI: 0.07, 0.16) was observed in children with ASD, while 0.01% (95% CI: 0.00, 0.02) was observed in the control group. High between-study heterogeneity was observed in the ASD group ($I^2 = 91\%$) and the control group ($I^2 = 88\%$). Similarly, high heterogeneity was noted when comparing the two groups ($I^2 = 94.40\%$). The effect size was significant and large ($Z = 5.08, P < 0.001$).

Lachnospirillum: Eight studies were included in the meta-analysis of *Lachnospirillum*. The results were as follows: 0.47% (95% CI: 0.36, 0.57) was observed among children diagnosed with ASD, and 0.24% (95% CI: 0.17, 0.30) was observed in the NT group. Considerable heterogeneity was observed within both the ASD and control groups ($I^2 = 99\%$). Similarly, high heterogeneity was noted when comparing the two groups ($I^2 = 92.50\%$). A significant and large effect was evident in the meta-analysis of *Lachnospirillum* ($Z = 13.90, P < 0.001$).

Catenibacterium: The 6 trials included in the meta-analysis of *Catenibacterium* revealed that the level of *Catenibacterium* was 0.12% in the ASD group (95% CI: 0.08, 0.17) and 0.01% in the NT group (95% CI: 0.00, 0.02). There was very high heterogeneity observed ($I^2 = 97\%$ in the ASD group and 95% in the NT group) among the included studies and also between the subgroups ($I^2 = 95.20\%$). Nevertheless, the overall effect size was large and significant ($Z = 5.24, P < 0.001$).

Collinsella: The meta-analysis of *Collinsella*, using a random-effects model and incorporating 7 studies, indicated a proportion 1.04% (95% CI: 0.64, 1.44) in the ASD group and 0.23% (95% CI: 0.12, 0.34) in the NT group. However, there was considerable heterogeneity among the included studies, with high levels noted in both the ASD group ($I^2 = 98\%$) and NT group ($I^2 = 96\%$), as well as between the subgroups ($I^2 = 93.30\%$). Despite these variations, the overall effect size was found to be large ($Z = 6.19, P < 0.001$).

3.3.2. Bacterial genera that were less abundant in individuals with ASD than controls

Barnesiella: The relative abundance of *Barnesiella* was evaluated in 7 trials. In children with ASD, the percentage was 0.08 % (95% CI: 0.02, 0.13), while it was 0.28% in the NT group (95% CI: 0.11, 0.44). Considerable heterogeneity was observed both between studies (82% and 78%, respectively) and within subgroups ($I^2 = 79.50\%$). The effect size indicated a moderate yet significant impact ($Z = 4.56, P < 0.001$).

Odoribacter: The meta-analysis of *Odoribacter*, which included 9 studies, yielded the following findings:

the relative abundance of *Odoribacter* in children with ASD was 0.09% (95% CI: 0.05, 0.13), while it was 0.18% (95% CI: 0.12, 0.24) in the NT group. High heterogeneity was noted both within the ASD group ($I^2 = 97\%$) and the control group ($I^2 = 82\%$). Similarly, when comparing the two groups, a significant and substantial effect size was noted ($Z = 7.01, P < 0.001$), accompanied by considerable heterogeneity ($I^2 = 82.80\%$).

Paraprevotella: Meta-analysis of *Paraprevotella* revealed no presence of *Paraprevotella* in individuals with ASD (95% CI: 0.00, 0.01), while it accounted for approximately 0.03% in the NT group (95% CI: 0.01, 0.05). The included studies exhibited a low to medium level of heterogeneity ($I^2 = 11\%$ in the ASD group and 52% in the NT group) both within and between subgroups ($I^2 = 80\%$). Despite this variability, there was a significant and substantial overall effect size ($Z = 3.08, P = 0.002$).

Blautia: A total of 14 studies were included in the meta-analysis performed on *Blautia*. The findings indicated that the percentage was 0.09% (95% CI: 0.06, 0.13) among children diagnosed with ASD, while a relative abundance of 0.20% (95% CI: 0.15, 0.25) was found in the NT group. Both the ASD and control groups exhibited significant heterogeneity ($I^2 = 99\%$). When these two groups were compared, a high level of heterogeneity was also noted ($I^2 = 91.90\%$). The meta-analysis revealed a substantial and statistically significant effect for *Blautia* ($Z = 8.35, P < 0.001$).

Turicibacter: We performed a meta-analysis of 11 studies on *Turicibacter* and found that the relative abundance in individuals with ASD was 0.01% (95% CI: 0.00, 0.02), while it was 0.04% (95% CI: 0.01, 0.06) in NT children. Both groups showed significant heterogeneity among studies, with percentages of 88%, which remained high at 76.60% when comparing subgroups. The effect size was large and statistically significant ($Z = 4.07, P < 0.001$). In addition, a lower relative abundance of Clostridium bacteria was observed in individuals with ASD compared to the NT group.

Lachnospira: The relative abundance of *Lachnospira* was assessed in 8 trials. Among ASD children, the relative abundance was 0.07% (95% CI: 0.02, 0.11), while it was 0.26% (95% CI: 0.08, 0.43) in the NT group. High heterogeneity between studies was observed both in the ASD (89%) and NT (95%) groups, as well as among subgroups ($I^2 = 76.20\%$). The effect size was large and significant ($Z = 5.86, P < 0.001$). The difference in bacterial percentage for *Lachnospira* (-3.71) indicated that individuals with ASD exhibited lower levels compared to NT children.

Pseudomonas: As shown in Table 2, the random-effects meta-analysis of *Pseudomonas* included six studies. The findings revealed that the levels of *Pseudomonas* in the ASD group were zero (95% CI: -0.02, 0.02), while they were slightly higher at 0.06% (95% CI: 0.02, 0.10) in the NT group. Both subgroups

exhibited considerable heterogeneity among studies ($I^2 = 96\%$ and 97% , respectively), as the comparison between the two subgroups also indicated ($I^2 = 84\%$). The overall effect size was large and highly significant ($Z = 2.61$, $P = 0.009$).

Parasutterella: Our meta-analysis included 8 studies on *Parasutterella*, which yielded the following findings: the relative abundance of *Parasutterella* was estimated to be 0.03% (95% CI: 0.01, 0.04) in children with ASD and 0.11% (95% CI: 0.05, 0.17) in the control group. Notably, there was a considerable level of heterogeneity among the studies, which was as high as 87% and 80% for children with ASD and the control group, respectively; however, this heterogeneity decreased to approximately 85.30% when comparing these two groups together. The effect size revealed significant results of a large magnitude ($Z = 5.98$, $P < 0.001$). Moreover, individuals with ASD had a lower factor (-3.67) difference in bacterial percentage for *Parasutterella* compared to NT children.

Haemophilus: A meta-analysis of *Haemophilus* was performed in 11 studies, yielding the following results: 0.04% in the ASD group (95% CI: 0.02, 0.06) and 0.13% in the NT group (95% CI: 0.06, 0.20). Both the ASD and control groups exhibited significant heterogeneity among studies, with percentages of 83% and 65% , respectively, which remained consistently high (83.80%) even when comparing subgroups. The effect size was found to be substantial and statistically significant ($Z = 5.23$, $P < 0.001$).

Bifidobacterium: In the meta-analysis of *Bifidobacterium*, which included 22 studies, a significantly lower level of *Bifidobacterium* was observed in children with ASD (0.46% , 95% CI: 0.37, 0.55) compared to NT children (1.48% , 95% CI: 1.25, 1.71). Despite substantial heterogeneity among both ASD group studies ($I^2 = 99\%$) and NT group studies ($I^2 = 99\%$), as well as subgroups ($I^2 = 98.50\%$), the overall effect size remained large and statistically significant ($Z = 16.56$, $P < 0.001$).

3.3.3. Bacterial genera that did not differ between individuals with ASD and controls

As shown in Table 2, the comparison between ASD and NT children did not yield statistically significant differences concerning specific bacterial genera. However, *Bacteroides* was more abundant in both children with ASD (3.72% , 95% CI: 3.31, 4.13) and the control group (3.35% , 95% CI: 2.93, 3.76), with a consistent heterogeneity of 99% within both groups. *Fusicatenibacter* and *Gemmiger* were found in lower percentages among the studied microbiota, accounting for $0.50\% - 1.00\%$ overall in both the ASD and control groups, respectively, whereas all other genera were found in even lower proportions ($< 0.50\%$) within the studied microbiota across both groups collectively. High

heterogeneity was noted within subgroups, while slight to moderate heterogeneity was observed in intergroup comparisons.

3.4. Sensitivity analysis

The consistency of the effect size was evaluated in our meta-analysis by performing a sensitivity analysis, systematically excluding each study. As detailed in Table 4, significant differences in *Faecalibacterium*, *Clostridium*, *Dorea*, *Phascolarctobacterium*, *Catenibacterium*, *Odoribacter*, and *Bifidobacterium* between children with ASD and NT children persisted even after sequentially excluding each study. In addition, near-significant differences between children with ASD and NT children persisted in *Anaerostipes*, *Collinsella* and *Paraprevotella* following the sequential exclusion of each study. A point worth noting is that the subgroup differences in *Turicibacter* and *Lachnospira* were found to be highly sensitive, as non-significant differences within these two subgroups were observed in more than five of the excluded studies. Moreover, the studies conducted by Strati (29), Dan (37), and Deng (43) were most frequently excluded due to their potential influence on the significant difference between children with ASD and NT children.

4. Discussion

Our meta-analysis encompassed 28 studies, with a particular emphasis on the most recent studies (44,45,47,49), and it offered a most comprehensive overview of the GM in children diagnosed with ASD, highlighting their differences. By pooling data from these medium- to high-quality studies, we analyzed the relative abundance of GM across 8 phyla and 64 genera within a sample size of 1,256 children with ASD and 1,042 NT children. Our findings revealed that individuals with ASD exhibited a significantly higher relative abundance of *Anaerostipes*, *Catenibacterium*, *Clostridium*, *Collinsella*, *Dorea*, *Faecalibacterium*, *Lachnoclostridium*, *Parabacteroides*, and *Phascolarctobacterium* and a lower relative abundance of *Barnesiella*, *Blautia*, *Bifidobacterium*, *Haemophilus*, *Odoribacter*, *Paraprevotella*, *Pseudomonas*, *Parasutterella*, *Lachnospira*, and *Turicibacter*. Importantly, the significant differences in the relative abundance of *Faecalibacterium*, *Clostridium*, *Dorea*, *Phascolarctobacterium*, *Catenibacterium*, *Odoribacter*, and *Bifidobacterium* between individuals with ASD and NT controls were systematically confirmed by individually excluding studies. Given that this study exclusively examined GM data from individuals diagnosed with ASD, data were for single groups without comparison groups, and a non-normal distribution was evident. Therefore, we decided not to evaluate publication bias in our meta-analysis.

4.1. Persisting significant differences in GM between individuals with ASD and controls

Our findings consistently confirmed significant differences between children with ASD and NT children in *Faecalibacterium*, *Clostridium*, *Dorea*, *Phascolarctobacterium*, *Catenibacterium*, *Odoribacter* and *Bifidobacterium*. In these GM, the differences in *Faecalibacterium*, *Clostridium*, *Phascolarctobacterium* and *Bifidobacterium* between the two groups were in line with those in previous meta-analyses (13-16). Notably, our meta-analysis is the first to consistently find significant differences in bacterial *Dorea*, *Catenibacterium* and *Odoribacter* between the two groups.

Regarding *Dorea*, some studies have suggested that it might have an inflammatory effect in ASD (50) since it has been positively correlated with pro-inflammatory cytokines like TNF- α and it has been negatively correlated with the anti-inflammatory cytokines TGF- β and IL-10 (51). However, other studies suggested a protective effect of *Dorea* against ASD, possibly related to its ability to alleviate tropomyosin (Tm)-induced allergic responses (52,53). Regarding *Catenibacterium*, Wu *et al.* previously proposed *Catenibacterium* as a potential biomarker in patients with ASD (54). However, scant attention has been devoted to elucidating the mechanism between *Catenibacterium* and ASD. An animal study found that phobic dogs exhibited an increased abundance of *Catenibacterium* (55). Moreover, studies revealed significant differences in the abundance of *Catenibacterium* across nativity, race/ethnicity (56), and socioeconomic status (57). Regarding *Odoribacter*, several studies suggested a potential association between a higher percentage of *Odoribacter* and ASD (58). Wang *et al.* suggested that *Odoribacter* might play a role in regulating serotonergic and glutamatergic synapse metabolism in mice with VPA-induced ASD (48). Other studies suggested that *Odoribacter* is involved in the production of short-chain fatty acids (SCFAs), which exhibit neuroactive and anti-inflammatory effects and which have been linked to worsening ASD symptoms at high levels (59,60). However, research into the association between *Dorea*, *Catenibacterium*, and *Odoribacter* and ASD is still in its preliminary stages. Caution is advised when interpreting these results.

4.2. Imbalance of gut microbiota in children with ASD

The main issues associated with dysbiosis in ASD involve an increased presence of harmful bacteria along with decreased levels of beneficial bacteria (13,14). Contrary to this perspective, our findings revealed an increasing abundance of certain beneficial bacteria, including *Faecalibacterium*, *Phascolarctobacterium*, and *Lachnoclostridium*, while some harmful bacteria like *Pseudomonas*, *Parasutterella*, and *Haemophilus*

tended to decrease. In addition, significant differences in certain bacteria with indeterminate functions, such as *Catenibacterium* and *Odoribacter*, were also noted. Our study suggested that dysbiosis in the GM of individuals with ASD may manifest as either an increase or decrease in the abundance of beneficial or harmful bacteria, thereby disrupting the overall structure of the microbial community.

This dysbiosis is believed to play a significant role in the pathophysiology of ASD. An important point to note is that while an overabundance of beneficial bacteria might intuitively seem positive, it can, in fact, disrupt the delicate balance of the gut microbial community. This imbalance can lead to a range of issues including digestive disturbances, immune reactions, and nutritional deficiencies (61). Many pathogens can exist within a normal, healthy microbiome for extended periods without causing harm. Contrary to expectations, commensal organisms can also cause disease and often carry genes associated with virulence (62). These findings challenge the traditional division between pathogens and commensals, revealing instead a dynamic spectrum of microbial behaviors. Therefore, simply boosting beneficial bacteria without addressing the specific dysbiosis present in ASD may not be effective and could potentially exacerbate existing problems.

This underscores the necessity for a more targeted approach to probiotic therapy in ASD. Rather than using conventional probiotics or prebiotics in a generalized manner, supplementation needs to be tailored to address the specific microbial imbalances observed in individuals with ASD. This targeted supplementation should aim to restore a healthy balance of gut bacteria, which may involve introducing specific beneficial strains that are deficient or underrepresented in the GM of individuals with ASD.

By addressing the dysbiosis in a more precise and tailored manner, probiotic therapy holds the potential to alleviate gastrointestinal symptoms and improve immune function and overall health and well-being in individuals with ASD. However, additional research is required to deepen our understanding of the complex interplay between the GM and ASD and to identify the most effective probiotic interventions for this population.

5. Limitations of this study

Our meta-analysis had several limitations. First, due to the unavailability of data from a substantial portion of the studies that met our inclusion criteria, our meta-analysis could not fully capitalize on the breadth of available study data. Second, considering the dynamic nature of GM composition and its susceptibility to various factors such as host region, sex, age, disease, drug treatment, dietary habits, lifestyle, and BMI, the inclusion of studies from diverse geographical locations worldwide might account for the high between-study

heterogeneity observed. Third, our meta-analysis was limited to assessing the abundance of bacteria in fecal samples from individuals with ASD at the phylum and genus levels, potentially underestimating the overall diversity of GM. A point worth emphasizing is that fecal samples exclusively collect bacteria released from the intestinal lining, potentially offering a narrower view compared to that obtained through biopsies. In addition, focusing solely on evaluating microbial abundance might lead to an underestimation of bacterial diversity.

6. Conclusion

Our meta-analysis indicated that dysbiosis of the GM in ASD may involve more intricate changes beyond a simple reduction in beneficial bacteria and an increase in harmful bacteria. In essence, children with ASD exhibited a higher abundance of *Parabacteroides*, *Anaerostipes*, *Faecalibacterium*, *Clostridium*, *Dorea*, *Phascolarctobacterium*, *Lachnoclostridium*, *Catenibacterium*, and *Collinsella* and a lower abundance of *Barnesiella*, *Odoribacter*, *Paraprevotella*, *Blautia*, *Turicibacter*, *Lachnospira*, *Pseudomonas*, *Parasutterella*, *Haemophilus*, and *Bifidobacterium* compared to NT children. Notably, significant differences in the relative abundance of *Faecalibacterium*, *Clostridium*, *Dorea*, *Phascolarctobacterium*, *Catenibacterium*, *Odoribacter*, and *Bifidobacterium* between individuals with ASD and NT controls remained consistently stable even after sequentially excluding single studies. However, given the complex pathophysiology of ASD and the susceptibility of GM to factors such as living conditions, lifestyle, and diet, validating our findings is imperative, particularly by taking into account potential factors that may influence the composition of human GM, such as geographical location, dietary patterns, medication usage, and underlying diseases, and exploring whether disruption of GM is associated with specific subpopulations of ASD.

Funding: This work was supported by a project of the National Natural Science Foundation of China (grant no. 82374243 to L Wang) and a project of National Key R&D Program (grant no. 2021YFC2501405 to YJ Du).

Conflict of Interest: The authors have no conflicts of interest to disclose.

References

1. Zeidan J, Fombonne E, Scora J, Ibrahim A, Durkin MS, Saxena S, Yusuf A, Shih A, Elsabbagh M. Global prevalence of autism: A systematic review update. *Autism Research*. 2022; 15:778-790.
2. Masini E, Loi E, Vega-Benedetti AF, Carta M, Doneddu G, Fadda R, Zavattari P. An overview of the main genetic, epigenetic and environmental factors involved in autism spectrum disorder focusing on synaptic activity. *International Journal of Molecular Sciences*. 2020; 21:8290.
3. Leader G, Abberton C, Cunningham S, Gilmartin K, Grudzien M, Higgins E, Joshi L, Whelan S, Mannion A. Gastrointestinal symptoms in autism spectrum disorder: A systematic review. *Nutrients*. 2022; 14:1471.
4. Wang Q, Yang Q, Liu X. The microbiota–gut–brain axis and neurodevelopmental disorders. *Protein & Cell*. 2023; 14:762-775.
5. Agirman G, Yu KB, Hsiao EY. Signaling inflammation across the gut-brain axis. *Science*. 2021; 374:1087-1092.
6. Chernikova MA, Flores GD, Kilroy E, Labus JS, Mayer EA, Aziz-Zadeh L. The brain-gut-microbiome system: Pathways and implications for autism spectrum disorder. *Nutrients*. 2021; 13:4497.
7. Dargenio VN, Dargenio C, Castellana S, De Giacomo A, Laguardia M, Schettini F, Francavilla R, Cristofori F. Intestinal barrier dysfunction and microbiota–gut–brain axis: Possible implications in the pathogenesis and treatment of autism spectrum disorder. *Nutrients*. 2023; 15:1620.
8. Gonçalves CL, Doifode T, de Rezende VL, da Costa MA, Rhoads JM, Soutullo CA. The many faces of microbiota–gut–brain axis in autism spectrum disorder. *Life Sciences*. 2023; 122357.
9. Gong XR, You XR, Guo MR, Ding XY, Ma BX. Children autism spectrum disorder and gut microbiota: A bibliometric and visual analysis from 2000 to 2023. *Medicine*. 2023; 102:e36794.
10. Martínez-González AE, Andreo-Martínez P. Prebiotics, probiotics and fecal microbiota transplantation in autism: A systematic review. *Revista de Psiquiatría y Salud Mental (English Edition)*. 2020; 13:150-164.
11. Tan Q, Orsso CE, Deehan EC, Kung JY, Tun HM, Wine E, Madsen KL, Zwaigenbaum L, Haqq AM. Probiotics, prebiotics, synbiotics, and fecal microbiota transplantation in the treatment of behavioral symptoms of autism spectrum disorder: A systematic review. *Autism Research*. 2021; 14:1820-1836.
12. Song W, Zhang M, Teng L, Wang Y, Zhu L. Prebiotics and probiotics for autism spectrum disorder: A systematic review and meta-analysis of controlled clinical trials. *Journal of Medical Microbiology*. 2022; 71:001510.
13. Xu M, Xu X, Li J, Li F. Association between gut microbiota and autism spectrum disorder: A systematic review and meta-analysis. *Frontiers in Psychiatry*. 2019; 10:473.
14. Iglesias-Vázquez L, Van Ginkel Riba G, Arija V, Canals J. Composition of gut microbiota in children with autism spectrum disorder: A systematic review and meta-analysis. *Nutrients*. 2020; 12:792.
15. Andreo-Martínez P, Rubio-Aparicio M, Sánchez-Meca J, Veas A, Martínez-González AE. A meta-analysis of gut microbiota in children with autism. *Journal of Autism and Developmental Disorders*. 2022; 52:1374-1387.
16. Lin P, Zhang Q, Sun J, Li Q, Li D, Zhu M, Fu X, Zhao L, Wang M, Lou X. A comparison between children and adolescents with autism spectrum disorders and healthy controls in biomedical factors, trace elements, and microbiota biomarkers: A meta-analysis. *Frontiers in Psychiatry*. 2024; 14:1318637.
17. Shamseer L, Moher D, Clarke M, Ghersi D, Liberati A, Petticrew M, Shekelle P, Stewart LA. Preferred reporting items for systematic review and meta-analysis protocols (PRISMA-P) 2015: Elaboration and explanation. *BMJ*. 2015; 349.

18. Wells GA, Shea B, O'Connell D, Peterson J, Welch V, Losos M, Tugwell P. The Newcastle-Ottawa Scale (NOS) for assessing the quality of nonrandomised studies in meta-analyses. 2000.
19. Page MJ, Moher D, Bossuyt PM, Boutron I, Hoffmann TC, Mulrow CD, Shamseer L, Tetzlaff JM, Akl EA, Brennan SE. PRISMA 2020 explanation and elaboration: Updated guidance and exemplars for reporting systematic reviews. *BMJ*. 2021; 372.
20. Finegold SM, Dowd SE, Gontcharova V, Liu C, Henley KE, Wolcott RD, Youn E, Summanen PH, Granpeesheh D, Dixon D. Pyrosequencing study of fecal microflora of autistic and control children. *Anaerobe*. 2010; 16:444-453.
21. Adams JB, Johansen LJ, Powell LD, Quig D, Rubin RA. Gastrointestinal flora and gastrointestinal status in children with autism—comparisons to typical children and correlation with autism severity. *BMC gastroenterology*. 2011; 11:1-13.
22. Wang L, Christophersen CT, Sorich MJ, Gerber JP, Angley MT, Conlon MA. Low relative abundances of the mucolytic bacterium *Akkermansia muciniphila* and *Bifidobacterium* spp. in feces of children with autism. *Applied and Environmental Microbiology*. 2011; 77:6718-6721.
23. Williams BL, Hornig M, Parekh T, Lipkin WI. Application of novel PCR-based methods for detection, quantitation, and phylogenetic characterization of *Sutterella* species in intestinal biopsy samples from children with autism and gastrointestinal disturbances. *MBio*. 2012; 3:10.1128/mbio.00261-00211.
24. Gondalia SV, Palombo EA, Knowles SR, Cox SB, Meyer D, Austin DW. Molecular characterisation of gastrointestinal microbiota of children with autism (with and without gastrointestinal dysfunction) and their neurotypical siblings. *Autism Research*. 2012; 5:419-427.
25. Kang DW, Park JG, Ilhan ZE, Wallstrom G, LaBaer J, Adams JB, Krajmalnik-Brown R. Reduced incidence of *Prevotella* and other fermenters in intestinal microflora of autistic children. *PloS one*. 2013; 8:e68322.
26. De Angelis M, Piccolo M, Vannini L, Siragusa S, De Giacomo A, Serrazanetti DI, Cristofori F, Guerzoni ME, Gobetti M, Francavilla R. Fecal microbiota and metabolome of children with autism and pervasive developmental disorder not otherwise specified. *PloS one*. 2013; 8:e76993.
27. Son JS, Zheng LJ, Rowehl LM, Tian X, Zhang Y, Zhu W, Litcher-Kelly L, Gadow KD, Gathungu G, Robertson CE. Comparison of fecal microbiota in children with autism spectrum disorders and neurotypical siblings in the simons simplex collection. *PloS one*. 2015; 10:e0137725.
28. Inoue R, Sakaue Y, Sawai C, Sawai T, Ozeki M, Romero-Pérez GA, Tsukahara T. A preliminary investigation on the relationship between gut microbiota and gene expressions in peripheral mononuclear cells of infants with autism spectrum disorders. *Bioscience, Biotechnology, and Biochemistry*. 2016; 80:2450-2458.
29. Strati F, Cavalieri D, Albanese D, De Felice C, Donati C, Hayek J, Jousson O, Leoncini S, Renzi D, Calabrò A. New evidences on the altered gut microbiota in autism spectrum disorders. *Microbiome*. 2017; 5:1-11.
30. Coretti L, Paparo L, Riccio MP, Amato F, Cuomo M, Natale A, Borrelli L, Corrado G, De Caro C, Comegna M. Gut microbiota features in young children with autism spectrum disorders. *Frontiers in Microbiology*. 2018; 9:3146.
31. Berding K, Donovan SM. Diet can impact microbiota composition in children with autism spectrum disorder. *Frontiers in Neuroscience*. 2018; 12:394954.
32. Kang DW, Ilhan ZE, Isern NG, Hoyt DW, Howsmon DP, Shaffer M, Lozupone CA, Hahn J, Adams JB, Krajmalnik-Brown R. Differences in fecal microbial metabolites and microbiota of children with autism spectrum disorders. *Anaerobe*. 2018; 49:121-131.
33. Pulikkan J, Maji A, Dhakan DB, Saxena R, Mohan B, Anto MM, Agarwal N, Grace T, Sharma VK. Gut microbial dysbiosis in Indian children with autism spectrum disorders. *Microbial Ecology*. 2018; 76:1102-1114.
34. Zhang M, Ma W, Zhang J, He Y, Wang J. Analysis of gut microbiota profiles and microbe-disease associations in children with autism spectrum disorders in China. *Scientific Reports*. 2018; 8:13981.
35. Ma B, Liang J, Dai M, Wang J, Luo J, Zhang Z, Jing J. Altered gut microbiota in Chinese children with autism spectrum disorders. *Frontiers in Cellular and Infection Microbiology*. 2019; 9:40.
36. Plaza-Díaz J, Gómez-Fernández A, Chueca N, Torre-Aguilar MJdl, Gil Á, Perez-Navero JL, Flores-Rojas K, Martín-Borreguero P, Solís-Urra P, Ruiz-Ojeda FJ. Autism spectrum disorder (ASD) with and without mental regression is associated with changes in the fecal microbiota. *Nutrients*. 2019; 11:337.
37. Dan Z, Mao X, Liu Q, Guo M, Zhuang Y, Liu Z, Chen K, Chen J, Xu R, Tang J. Altered gut microbial profile is associated with abnormal metabolism activity of autism spectrum disorder. *Gut Microbes*. 2020; 11:1246-1267.
38. Zou R, Xu F, Wang Y, Duan M, Guo M, Zhang Q, Zhao H, Zheng H. Changes in the gut microbiota of children with autism spectrum disorder. *Autism Research*. 2020; 13:1614-1625.
39. Ding X, Xu Y, Zhang X, Zhang L, Duan G, Song C, Li Z, Yang Y, Wang Y, Wang X. Gut microbiota changes in patients with autism spectrum disorders. *Journal of Psychiatric Research*. 2020; 129:149-159.
40. Averina OV, Kovtun AS, Polyakova SI, Savilova AM, Rebrikov DV, Danilenko VN. The bacterial neurometabolic signature of the gut microbiota of young children with autism spectrum disorders. *Journal of Medical Microbiology*. 2020; 69:558-571.
41. Chen Z, Shi K, Liu X, Dai Y, Liu Y, Zhang L, Du X, Zhu T, Yu J, Fang S. Gut microbial profile is associated with the severity of social impairment and IQ performance in children with autism spectrum disorder. *Frontiers in Psychiatry*. 2021; 12:789864.
42. Wong OW, Lam AM, Or BP, Mo FY, Shea CK, Lai KY, Ma SL, Hung SF, Chan S, Kwong TN. Disentangling the relationship of gut microbiota, functional gastrointestinal disorders and autism: A case-control study on prepubertal Chinese boys. *Scientific Reports*. 2022; 12:10659.
43. Deng W, Wang S, Li F, Wang F, Xing YP, Li Y, Lv Y, Ke H, Li Z, Lv PJ. Gastrointestinal symptoms have a minor impact on autism spectrum disorder and associations with gut microbiota and short-chain fatty acids. *Frontiers in Microbiology*. 2022; 13:1000419.
44. Chamtouri M, Gaddour N, Merghni A, Mastouri M, Arbolya S, De Los Reyes-Gavilán CG. Age and severity-dependent gut microbiota alterations in Tunisian children with autism spectrum disorder. *Scientific Reports*. 2023; 13:18218.
45. Pang X, Zhang Q, Wang Y, Zhan Y, Guo M, Chen B,

- Li Q, Zheng H. Characteristics of the gut microbiota in young adults with autism spectrum disorder. *Journal of Integrative Neuroscience*. 2023; 22:141.
46. Wang H, Liu S, Xie L, Wang J. Gut microbiota signature in children with autism spectrum disorder who suffered from chronic gastrointestinal symptoms. *BMC pediatrics*. 2023; 23:476.
 47. Mendive Dubourdieu P, Guerendiain M. Understanding the link between gut microbiota, dietary intake, and nutritional status in children with autism and typical development. *Frontiers in Nutrition*. 2023; 10:1202948.
 48. Wang J, Cao Y, Hou W, Bi D, Yin F, Gao Y, Huang D, Li Y, Cao Z, Yan Y. Fecal microbiota transplantation improves VPA-induced ASD mice by modulating the serotonergic and glutamatergic synapse signaling pathways. *Translational Psychiatry*. 2023; 13:17.
 49. Wang W, Fu P. Gut microbiota analysis and *in silico* biomarker detection of children with autism spectrum disorder across cohorts. *Microorganisms*. 2023; 11:291.
 50. Li Y, Deng Q, Liu Z. The relationship between gut microbiota and insomnia: A bi-directional two-sample Mendelian randomization research. *Frontiers in Cellular and Infection Microbiology*. 2023; 13.
 51. Chen YY, Fei F, Ding LL, Wen SY, Ren CF, Gong AH. Integrated gut microbiome and metabolome analysis reveals the inhibition effect of *Lactobacillus plantarum* CBT against colorectal cancer. *Food & Function*. 2024; 15:853-865.
 52. Li Z, Liu S, Liu F, Dai N, Liang R, Lv S, Bao L. Gut microbiota and autism spectrum disorders: A bidirectional Mendelian randomization study. *Frontiers in Cellular and Infection Microbiology*. 2023; 13.
 53. Abujamel TS, Al-Otaibi NM, Abuaish S, AlHarbi RH, Assas MB, Alzahrani SA, Alotaibi SM, El-Ansary A, Aabed K. Different alterations in gut microbiota between *Bifidobacterium longum* and fecal microbiota transplantation treatments in propionic acid rat model of autism. *Nutrients*. 2022; 14:608.
 54. Wu T, Wang H, Lu W, Zhai Q, Zhang Q, Yuan W, Gu Z, Zhao J, Zhang H, Chen W. Potential of gut microbiome for detection of autism spectrum disorder. *Microbial Pathogenesis*. 2020; 149:104568.
 55. Mondo E, Barone M, Soverini M, D'amico F, Cocchi M, Petrulli C, Mattioli M, Marliani G, Candela M, Accorsi P. Gut microbiome structure and adrenocortical activity in dogs with aggressive and phobic behavioral disorders. *Heliyon*. 2020; 6.
 56. Peters BA, Yi SS, Beasley JM, Cobbs EN, Choi HS, Beggs DB, Hayes RB, Ahn J. US nativity and dietary acculturation impact the gut microbiome in a diverse US population. *The ISME Journal*. 2020; 14:1639-1650.
 57. Ahn J, Kwak S, Usyk M, Beggs D, Choi H, Ahdoot D, Wu F, Maceda L, Li H, Im E-O. Sociobiome-individual and neighborhood socioeconomic status influence the gut microbiome in a multi-ethnic population in the US. *Research Square*. 2023.
 58. Srikantha P, Mohajeri MH. The possible role of the microbiota-gut-brain-axis in autism spectrum disorder. *International Journal of Molecular Sciences*. 2019; 20:2115.
 59. Bull-Larsen S, Mohajeri MH. The potential influence of the bacterial microbiome on the development and progression of ADHD. *Nutrients*. 2019; 11:2805.
 60. Gkougka D, Mitropoulos K, Tzanakaki G, Panagouli E, Psaltopoulou T, Thomaidis L, Tsolia M, Sergentanis TN, Tsitsika A. Gut microbiome and attention deficit/hyperactivity disorder: A systematic review. *Pediatric Research*. 2022; 92:1507-1519.
 61. Chu J, Feng S, Guo C, Xue B, He K, Li L. Immunological mechanisms of inflammatory diseases caused by gut microbiota dysbiosis: A review. *Biomedicine & Pharmacotherapy*. 2023; 164:114985.
 62. Wiles TJ, Guillemin K. The other side of the coin: What beneficial microbes can teach us about pathogenic potential. *Journal of Molecular Biology*. 2019; 431:2946-2956.
- Received May 11, 2024; Revised June 12, 2024; Accepted June 16, 2024.
- *Address correspondence to:*
Ling Wang, Laboratory for Reproductive Immunology, Obstetrics and Gynecology Hospital of Fudan University, 419 Fangxie Road, Shanghai 200011, China.
E-mail: dr.wangling@fudan.edu.cn
- Yijie Du, Qingpu Traditional Chinese Medicine Hospital, 95 Qingan Road Shanghai, China.
E-mail: xdzy2004@163.com
- Released online in J-STAGE as advance publication June 18, 2024.

Revealing the enhancement effect of social capital on the individual performance of core members in elderly caring organizations: A study from Anhui, China

Shuo Ding^{1,§}, Fuqin Xu^{1,§}, Guoqing Liu¹, Xin Zheng¹, Lanlan Zhao¹, Otsen Benjamin^{1,2}, Ziwon Xu¹, Jiajie Zhao¹, Sanyuan Hao¹, Ren Chen^{1,3,*}

¹School of Health Services Management, Anhui Medical University, Hefei, Anhui, China;

²Registrars' Department, University of Cape Coast, Cape Coast Ghana;

³Key Laboratory of Public Health Social Governance, Philosophy and Social Sciences of Anhui Province, Hefei, Anhui, China.

SUMMARY Aging is a challenge to global development. This challenge is particularly significant for China because it has the largest elderly population worldwide. The proportion of aging population continues to increase, and solely relying on government efforts to meet the needs of the elderly is inadequate. Hence, involvement of social organizations in elderly care services is needed. Their core members exhibit higher sense of responsibility and identification with the organization than regular members, thus profoundly affecting organizational development. Based on the Social Capital Theory, this study employed a multistage stratified random sampling method to examine the social capital stock of elderly social organizations and their core members across six cities in Anhui Province, China. Chi-square tests analyzed the relationship between the core members' demographic factors and individual performance. Independent-sample *t*-tests assessed the relationship between social capital and individual performance. Finally, binary logistic regression models determined the factors influencing the individual performance of core members. Social networks within core members' social capital and the internal social capital of elderly caring social organizations (ESOs) affect the individual performance of core members. Therefore, organizations should provide more training opportunities for core members to expand their networks. Cultivating a shared language and vision as components of social capital can enhance organizational cohesion and operational stability.

Keywords elderly care, organizational management, social capital

1. Introduction

China is a developing country with an aging society. It not only has the largest elderly population in the world but also one of the fastest growing aging rates (1). Data from the Seventh National Population Census in 2020 show that 18.70% of China's population is aged 60 years and above, while 13.50% is aged 65 years and above, approaching a moderate level of aging (2). China's aging population is projected to peak by the mid-21st century, with the proportion of the population aged 65 years and above approaching 30% of the total population. The daunting trend of population aging poses significant challenges to existing healthcare insurance systems and elderly care services (3). Strengthening the construction of elderly care service systems is an indispensable path to address population aging. Thus, strengthening the elderly care service systems is indispensable. Social

organizations (SOs) are citizen groups outside the government and market systems and are characterized by organization, private ownership, non-profit orientation, autonomy, and voluntarism. Elderly caring social organizations (ESOs) are non-profit groups dedicated to serving seniors through community services, volunteer coordination, and care facility establishment aimed at enhancing quality of life and happiness through socialized care and support (4). As one of the main service entities, ESOs play a crucial role in elderly care services to address the goals pertaining to healthy aging. As of 2022, in Jiangsu Province, which is one of the highly populated areas in China, there were 2,192 elderly care institutions and 730,000 beds in Jiangsu Province. Of these, 70% were operated or managed by social forces (5). The Chinese government has recently begun considering the role of SOs in elderly care services as significant. As early as 2013, the "Several Opinions on Accelerating

the Development of the Elderly Service Industry" mentioned the need to fully leverage the leading role of SOs, encouraging the participation of social capital to meet the diverse needs of elderly care services (6). The "14th Five-Year Plan" for the development of national elderly care and the establishment of a pension service system released in 2021 explicitly proposed the complete mobilization of the enthusiasm of SOs to provide elderly care services and guide and the promotion of the standardized development of social organizations (7). Therefore, enhancing the efficiency and quality of elderly care services provided by SOs is an effective approach to address the pressure of population aging in China.

Despite government policies providing support, the underdevelopment and overall weak capabilities of SOs continue to constrain their growth in China. These organizations still face challenges, such as insufficient development resources, inadequate internal growth, an incomplete performance evaluation system, and lack of external support. These internal and external deficiencies result in SOs not fully leveraging their inherent advantages to participate in elderly care services (8). Relevant studies have shown that the accumulation and cultivation of social capital facilitate the development of SOs (9-11). The origin of the Social Capital Theory can be traced back to the field of Sociology in the 19th century. One of its main contributors, Robert Putnam, defined social capital as follows: "Social capital refers to the features of networks, trust, and norms within social organizations, which enhance social efficiency by facilitating coordinated actions among individuals and groups (12)." Social capital can be divided into organizational and personal social capital. The core elements of social capital, such as social networks, trust, social support, and norms, are essential for the survival and development of SOs. By accumulating and nurturing organizational social capital, organizations can strengthen their connections with external resources and support; they can also acquire more partners and opportunities, thereby enhancing their influence and sustainable development capabilities (13). Developing personal social capital at the individual level is crucial in expanding the network of relationships and accessing the resources necessary for personal growth. This is particularly vital for managers and leaders because social capital provides them with valuable information and influence, thereby improving their performance and leadership skills. This enables them to effectively acquire the knowledge and resources required to establish outstanding organizations, ultimately enhancing organizational performance (14).

In summary, applying the Social Capital Theory to promote the development of SOs has theoretical compatibility. Although this theory has been applied to elderly care services, existing research primarily focused on exploring the social capital of service recipients, namely the elderly (15-17). Research concentrating

on the core members of ESOs remains limited. The core members of an organization typically include its founders, leaders, legal representatives, and key management personnel. As pivotal figures within an organization, core members significantly influence the organization's development (18). Despite this, there is a lack of research on the relationship between core members' performance and social capital. The impact of social capital on their performance is unknown. Therefore, this study selected core members of ESOs as research subjects to explore the relationship between social capital at different levels and core members' performance. This exploration has vital implications for improving elderly care service provisions, meeting diverse elderly care needs, and promoting healthy aging.

2. Methods

2.1. Study design and data collection

This study was conducted in China's Anhui Province from November to December 2019. Anhui Province is situated in southeast China. By the end of 2019, the elderly population aged 60 years and above in Anhui reached 11.72 million, accounting for 18.41% of the resident population, ranking among the highly populated provinces nationwide (19). Anhui actively encourages participation in social capital in public services, such as healthcare, sanitation, and elderly care to expand the supply of public products and services. The immense demand for social services offers ample space for the development of SOs. The province has 1,572 SOs in elderly care (20), providing abundant research samples for this study and representing a typical province for researching ESOs. The on-site survey utilized a multistage stratified sampling approach. In the first stage, two cities were selected from each of the northern, central, and southern regions of the Anhui Province based on geographical and economic factors. For the northern region, Fuyang and Suzhou cities were chosen; Lu'an and Huainan cities were selected for the central region; and the cities of Anqing and Chizhou were included for the southern region. Six cities were surveyed. Supplementary Document 1 (<http://www.biosciencetrends.com/action/getSupplementalData.php?ID=202>) provides the geographical location information of the survey sites. In the second stage, officials responsible for elder care services in the Civil Affairs Bureau of each selected city were interviewed. These interviews sought to gather information about the ESOs in each city and to identify all administrative districts, totaling 15 districts. Third, half of the SOs listed in the ESO register of each district's Civil Affairs Bureau were randomly selected for this study. The core members of these organizations were the study participants. The core members included founders, leaders, legal representatives, and key management personnel. If an organization had three or fewer core

Table 1. The individual performance of core members in ESOs

Performance 1	Have you received any recognition in the field of elderly care services?
Performance 2	Has the team you led received any recognition in the field of elderly care services?
Performance 3	Have you and your team been featured in the media for your involvement in elderly care services?
Performance 4	Have you been appointed as a member of the association in the field of elderly care services?
Performance 5	Have you participated in discussions or drafting of local elderly care service standards?

members, all the core members of that organization were included in the survey. However, in organizations with more than three core members, only three members were randomly selected for the survey.

Survey administration was coordinated by civil affairs bureaus in each city and district. The trained survey team comprised postgraduate students from Anhui Medical University.

Face-to-face surveys were conducted with the assistance of ESO staff members. The study participants received advanced notifications prior to the interviews. Each participant was informed about the study's objectives and procedures, and informed consent was obtained. A total of 305 valid responses were collected from 49 ESOs. Relevant details can be found in other studies (9,21).

2.2. Measurement

2.2.1. Social capital

Social capital was the main independent variable in this study. Its measurement included three aspects, namely the social capital of core individuals, social capital within organizations, and social capital outside organizations.

In the field of elderly care, core individuals' social capital refers to the total resources obtained by individuals through their social relationships, trust, support, and other means during organizational activities. The Core Individual Social Capital Scale has four dimensions, namely social networks, trust, social support, cohesion, and sense of belonging. Organizational internal social capital refers to the sum of tangible and potential resources embedded within an organization, obtained through network relationships, and possessed by individuals or the organization. It comprises five dimensions, namely networks (formal and informal), trust, support, norms, common language, and vision. Organizational external social capital is the network of synergy and cooperation established between organizations, the government, and other organizations, and the reciprocal symbiotic relationship formed in this network. It has five dimensions, namely participation, trust, support, norms, common language, and vision. All three social capital measurement questionnaires use a five-point Likert scale (1 = completely disagree; 5 = completely agree). The score for each dimension of social capital is the sum of the scores of the respective subdimensions. Higher scores indicate higher social capital. In this study, the Cronbach's alpha coefficient

was 0.86 for the Core Personal Social Capital Scale, 0.92 for the Internal Organizational Social Capital Scale, and 0.93 for the External Organizational Social Capital Scale. The application and measurement details of the scale can be found in published articles (9,21,22). Supplementary Document 2 (<http://www.biosciencetrends.com/action/getSupplementalData.php?ID=202>) provides the detailed information on the survey questionnaire.

2.2.2. Core members' performance

The individual performance of core members was the dependent variable in this study. We used a self-developed questionnaire to assess the individual performance of the core members. As shown in Table 1, we employed five questions to evaluate individual performance (Performances 1 to 5). The responses to each question were either "yes" or "no." These indicators served as crucial references for the individual performances by reflecting the members' industry recognition and professional influence in elderly care services. All questions were finalized through multiple rounds of expert assessment, ensuring a high degree of objectivity in evaluating the achievements of core members in senior care services. Furthermore, this questionnaire has been used in similar studies; its reliability and validity have been confirmed in previous publications (22). In this study, the Cronbach's alpha for individual performance was 0.615, which meets the minimum acceptable limit of 0.6 (23).

2.2.3. Other variables

The sociodemographic variables included in this study were, gender (male, female), age (≤ 40 , 41-49, ≥ 50), marital status (unmarried, widowed or divorced, married). Information regarding the basic work details of core members also included the years of service in the organization (≤ 1 , 2-5, > 5), the years of experience in elderly care (≤ 1 , 2-5, > 5), professional qualification (no, yes), attendance of management training program (no, yes), attendance of skill-based training program (no, yes), and type of work (part-time, full-time).

2.3. Statistical analysis

Descriptive statistics were used to characterize the samples using SPSS 26.0. Continuous variables were reported as mean \pm standard deviation, while categorical variables were reported as percentages (%).

Sociodemographic factors and individual performances among the core ESO members were subjected to a univariate analysis using the chi-squared test. A *t*-test was employed to discern the variations in internal, external, and individual social capital across core members exhibiting different levels of performance. Finally, the variables that showed statistical significance in the Chi-square and the *t*-test analyses were incorporated into a multiple regression model using the Stepwise Forward Method. In this model, the five individual performance indicators were treated as dependent variables, with the positive outcomes from the univariate analysis serving as independent variables. Statistical significance was set at $P < 0.05$.

3. Results

3.1. Results of demographic data

A total of 308 questionnaires were collected from the core members of the organizations, of which 305 were considered valid, resulting in a questionnaire response rate of 99.02%. Table 2 summarizes the sociodemographic characteristics of the members. The majority were males (57.7%), and over half of the members were aged 50 years and above (50.1%). Only 90 individuals (29.5%) had an educational background of junior high school or below.

The vast majority (92.1%) of core members reported being married, and a considerable proportion (38.4%) had worked in the organization for two to five years. Of the core members, 39.1% had worked in elderly care for over 5 years, 84.9% did not possess any professional qualification certificates, and 93.8% worked full-time. A greater proportion participated in the management training program (70.2%) and skill-based training program (67.9%).

3.2. Results of univariate analysis

3.2.1. Univariate analysis of sociodemographic factors and individual performance among core members

Table 3 illustrates the impact of core members' sociodemographic factors on individual performance. The independent variables were the sociodemographic factors of core members, while the dependent variable was the individual performance of core members, consisting of five variables (Performance 1 to Performance 5).

Performances 1-5 were characterized by a majority of male core members. They had over five years of experience in elderly care and had received both management and skill-based training. Most of the core members who achieved *Performance 1* had professional qualifications, spent ≥ 5 years in their current organization, and were also married. In *Performance 2*, more than half of the core members worked full-

Table 2. Sociodemographic characteristics of core members

Variables	N (%)
Gender	
Male	176 (57.7)
Female	129 (42.3)
Age (years)	
≤ 40	71 (23.3)
41-49	81 (26.6)
≥ 50	153 (50.1)
Education	
Junior high school and below	90 (29.5)
Senior high school	113 (37.0)
College degree and above	102 (33.5)
Marital status	
Unmarried, widowed, or divorced	24 (7.9)
Married	281 (92.1)
Years of service in the organization	
≤ 1	99 (32.5)
2-5	117 (38.4)
> 5	89 (29.2)
Years of engaged in elderly care	
≤ 1	76 (24.9)
2-5	110 (36.1)
> 5	119 (39)
Professional Qualification	
No	259 (84.9)
Yes	46 (15.1)
Attending management training program	
No	91 (29.8)
Yes	214 (70.2)
Attending skill-based training program	
No	98 (32.1)
Yes	207 (67.9)
Type of work	
Part-time	19 (6.2)
Full-time	286 (93.8)

time. Most core members who attained *Performance 3* possessed college-level degrees or above, had additional professional qualifications, and spent two to five years of service in the current organization. A greater proportion of core members who achieved *Performance 5* had a college-level degree or higher and professional qualifications.

3.2.2. Univariate analysis of sociodemographic factors and individual performance among core members

Table 4 presents the univariate analysis results of core members' social capital scores across various dimensions of individual performance. The findings indicate:

CmSC was statistically significant in all the Performances 1, 2, 3, 4, and 5 ($t = 3.28$, $P = 0.001$; $t = 3.487$, $P = 0.001$; $t = 3.699$, $P < 0.001$; $t = 2.218$, $P = 0.028$; and $t = 2.325$, $P = 0.021$, respectively).

Social networks in CmSC across Performance 1, 2, 3, and 5 were statistically significant ($t = 4.861$, $P < 0.001$, $t = 4.388$, $P < 0.001$, $t = 3.916$, $P < 0.001$, and $t = 3.243$, $P = 0.001$, respectively). CmSC cohesiveness and sense of belonging were statistically significant for Performances 3 and 4 ($t = 3.103$, $P = 0.002$ and $t = 2.218$, $P = 0.028$, respectively). The total ISC was statistically significant

Table 3. Univariate analysis results of individual performance of core members

Variables	Performance 1		Performance 2		Performance 3		Performance 4		Performance 5	
	Yes	No	Yes	No	Yes	No	Yes	No	Yes	No
Gender										
Male	50	126	88	88	90	86	30	146	33	143
Female	32	97	42	87	81	48	36	93	23	106
χ^2	0.492		9.26		4.105		5.179		0.042	
P	0.483		0.002		0.043		0.023		0.837	
Age(years)										
≤ 40	19	52	25	46	48	23	19	52	17	54
41-49	22	40	26	36	38	24	15	47	13	49
≥ 50	41	131	79	93	85	87	32	140	26	146
χ^2	3.145		2.376		7.611		2.271		2.965	
P	0.077		0.305		0.022		0.321		0.227	
Education										
Junior high school and below	18	72	39	51	35	55	16	74	10	80
Senior high school	33	80	48	65	68	45	22	91	20	93
College degree and above	31	71	43	59	68	34	28	74	26	76
χ^2	3.118		0.029		16.209		3.137		6.647	
P	0.077		0.986		< 0.001		0.077		0.036	
Marital status										
Unmarried, widowed, or divorced	2	22	7	17	12	12	3	21	7	17
Married	80	201	123	158	159	122	63	218	49	232
χ^2	4.561		1.929		0.389		1.283		2.029	
P	0.033		0.165		0.533		0.257		0.154	
Professional Qualification										
Yes	64	138	86	116	126	76	53	149	44	158
No	18	85	44	59	45	58	13	90	12	91
χ^2	7.005		0.001		9.671		7.459		4.672	
P	0.008		0.981		0.002		0.006		0.031	
Attending management training program										
Yes	73	141	109	105	130	84	57	157	47	167
No	9	82	21	70	41	50	9	82	9	82
χ^2	19.057		20.261		6.383		10.559		6.208	
P	< 0.001		< 0.001		0.012		0.001		0.013	
Attending skill-based training program										
Yes	69	138	97	110	128	79	54	153	44	163
No	13	85	33	65	43	55	12	86	12	86
χ^2	13.627		4.729		8.708		7.515		3.603	
P	< 0.001		0.03		0.003		0.006		0.058	
Years of service in the organization										
≤ 1	18	81	32	67	43	56	15	84	18	81
2-5	30	87	46	71	70	47	28	89	18	99
> 5	34	55	52	37	58	31	23	66	20	69
χ^2	9.706		13.907		10.079		3.747		1.697	
P	0.008		0.001		0.006		0.154		0.428	
Years of engaged in elderly care										
≤ 1	7	69	20	56	30	46	7	69	11	65
2-5	29	81	46	64	68	42	30	80	18	92
> 5	46	73	64	55	73	46	29	90	27	92
χ^2	20.48		14.352		11.318		9.505		2.546	
P	< 0.001		0.001		0.003		0.009		0.28	
Type of work										
Part-time	1	18	4	15	7	12	3	16	2	17
Full-time	81	205	126	160	164	122	63	223	54	232
χ^2	4.819		3.855		3.04		0.124		0.83	
P	0.028		0.05		0.081		0.725		0.362	

for Performances 3 and 5 ($t = 3.380$, $P = 0.001$, and $t = 2.906$, $P = 0.004$). Additionally, the subdimensions of the ISC informal network ($t = 2.374$, $P = 0.018$), ISC support ($t = 3.985$, $P < 0.001$), ISC norms ($t = 2.289$, $P = 0.023$), and ISC common language and vision ($t = 2.643$, $P = 0.009$) were statistically significant in Performance 3. Similarly, for Performance 5, ISC support ($t = 2.445$, $P = 0.016$), ISC common language and vision ($t = 4.010$, P

< 0.001), and Performances 3 and 5 showed statistically significant associations with the respective total ESC ($t = 2.012$, $P < 0.045$, $t = 2.579$, $P = 0.010$). Sub-dimensions of Performance 3: ESC trust ($t = 2.191$, $P = 0.029$) and ESC norm scores ($t = 2.028$, $P = 0.044$). Similarly, ESC participation ($t = 3.143$, $P = 0.002$), ESC support ($t = 3.341$, $P = 0.001$), and ESC common language and vision scores ($t = 2.019$, $P = 0.046$) were significantly

Table 4. Univariate analysis results of individual performance of core members and various dimensions of social capital

Social capital indicators	Performance 1			Performance 2			Performance 3		
	Yes	No	P	Yes	No	P	Yes	No	P
Core member social capital (CmSC)									
Total Score	22.16 ± 3.79	20.64 ± 2.97	3.280	21.79 ± 3.47	20.49 ± 3.02	0.001	21.65 ± 3.21	20.28 ± 3.21	0.001
From social network	3.59 ± 2.59	2.07 ± 1.84	4.861	3.12 ± 2.42	2.01 ± 1.83	<0.001	2.89 ± 2.29	1.95 ± 1.88	<0.001
From trust	10.49 ± 1.79	10.69 ± 0.95	0.979	10.63 ± 1.48	10.65 ± 1.02	0.330	10.73 ± 1.32	10.52 ± 1.11	0.882
From social support	4.93 ± 0.97	4.76 ± 1.11	1.254	4.89 ± 0.98	4.74 ± 1.14	0.211	4.83 ± 1.06	4.78 ± 1.09	0.223
From cohesiveness and sense of belonging	3.15 ± 0.41	3.11 ± 0.45	0.666	3.15 ± 0.39	3.10 ± 0.47	0.506	3.19 ± 0.35	3.23 ± 0.35	0.264
Internal organizational social capital (ISC)									
Total Score	20.81 ± 1.84	20.6 ± 1.95	0.854	20.85 ± 3.47	20.51 ± 3.02	0.394	20.99 ± 1.56	20.23 ± 2.24	0.129
From informal network	1.54 ± 0.39	1.48 ± 0.48	1.139	1.55 ± 2.42	1.47 ± 1.83	0.256	1.55 ± 0.43	1.43 ± 0.47	0.133
From formal network	1.86 ± 0.36	1.92 ± 0.32	-1.400	1.90 ± 1.48	1.91 ± 1.02	0.163	1.90 ± 0.34	1.90 ± 0.33	0.825
From trust	5.04 ± 0.44	5.04 ± 0.51	-0.019	5.07 ± 0.98	5.02 ± 1.14	0.985	5.08 ± 0.42	5.00 ± 0.57	0.435
From support	4.48 ± 0.49	4.35 ± 0.74	1.697	4.45 ± 0.39	4.34 ± 0.47	0.091	4.53 ± 0.43	4.20 ± 0.88	0.160
From norms	4.33 ± 0.4	4.3 ± 0.43	0.519	4.34 ± 1.87	4.28 ± 1.95	0.604	4.36 ± 0.34	4.24 ± 0.51	0.253
From common language and vision	3.56 ± 0.37	3.5 ± 0.41	1.222	3.55 ± 0.42	3.49 ± 0.48	0.224	3.57 ± 0.32	3.45 ± 0.47	0.202
External organizational social capital (ESC)									
Total Score	25.35 ± 3.22	24.9 ± 3.45	1.030	25.01 ± 0.36	25.03 ± 0.32	0.304	25.38 ± 3.04	24.57 ± 3.76	0.967
From participation	6.73 ± 1.55	6.49 ± 1.55	1.203	6.52 ± 0.44	6.58 ± 0.53	0.230	6.68 ± 1.49	6.40 ± 1.66	0.740
From trust	9.31 ± 1.22	9.15 ± 1.28	0.952	9.22 ± 0.60	9.18 ± 0.73	0.342	9.34 ± 1.11	9.01 ± 1.42	0.802
From support	2.33 ± 0.6	2.29 ± 0.71	0.528	2.31 ± 0.38	2.30 ± 0.45	0.598	2.33 ± 0.67	2.26 ± 0.70	0.851
From participation	2.57 ± 0.3	2.59 ± 0.27	-0.546	2.59 ± 0.38	2.58 ± 0.41	0.586	2.62 ± 0.23	2.55 ± 0.33	0.704
From common language and vision	4.4 ± 0.58	4.38 ± 0.59	0.370	4.37 ± 3.37	4.39 ± 3.41	0.712	4.41 ± 0.54	4.35 ± 0.64	0.770

Table 4. Univariate analysis results of individual performance of core members and various dimensions of social capital (Continued)

Social capital indicators	t	P	Performance 4		t	P	Performance 5		t	P
			Yes	No			Yes	No		
Core member social capital (CmSC)										
Total Score	3.699	< 0.001	21.60 ± 3.02	20.89 ± 3.33	1.566	0.118	21.60 ± 3.02	20.89 ± 3.33	2.325	0.021
From social network	3.916	< 0.001	2.75 ± 2.06	2.40 ± 2.20	1.145	0.253	2.75 ± 2.06	2.40 ± 2.20	3.243	0.001
From trust	1.527	0.128	10.84 ± 0.63	10.58 ± 1.35	2.218	0.028	10.84 ± 0.63	10.58 ± 1.35	-1.140	0.259
From social support	0.428	0.669	4.79 ± 1.17	4.81 ± 1.05	-0.157	0.875	4.79 ± 1.17	4.81 ± 1.05	1.800	0.073
From cohesiveness and sense of belonging	3.103	0.002	3.03 ± 0.53	3.09 ± 0.46	2.515	0.013	3.23 ± 0.35	3.09 ± 0.46	2.649	0.009
Internal organizational social capital (ISC)										
Total Score	3.380	0.001	21.00 ± 1.72	20.56 ± 1.97	1.631	0.104	21.00 ± 1.72	20.56 ± 1.97	2.906	0.004
From informal network	2.374	0.018	1.61 ± 0.39	1.47 ± 0.47	2.397	0.018	1.61 ± 0.39	1.47 ± 0.47	1.909	0.057
From formal network	-0.002	0.998	1.89 ± 0.37	1.91 ± 0.33	-0.312	0.755	1.89 ± 0.37	1.91 ± 0.33	0.900	0.369
From trust	1.241	0.216	5.08 ± 0.41	5.03 ± 0.52	0.586	0.558	5.08 ± 0.41	5.03 ± 0.52	0.948	0.344
From support	3.985	< 0.001	4.49 ± 0.62	4.36 ± 0.70	1.522	0.131	4.49 ± 0.62	4.36 ± 0.70	2.445	0.016
From norms	2.289	0.023	4.34 ± 0.33	4.30 ± 0.44	0.781	0.436	4.34 ± 0.33	4.30 ± 0.44	1.097	0.274
From common language and vision	2.643	0.009	3.59 ± 0.33	3.50 ± 0.41	1.936	0.055	3.59 ± 0.33	3.50 ± 0.41	4.010	< 0.001
External organizational social capital (ESC)										
Total Score	2.012	0.045	25.37 ± 3.07	24.93 ± 3.47	0.945	0.345	25.37 ± 3.07	24.93 ± 3.47	2.579	0.010
From participation	1.535	0.126	6.79 ± 1.48	6.49 ± 1.59	1.380	0.169	6.79 ± 1.48	6.49 ± 1.59	3.143	0.002
From trust	2.191	0.029	9.42 ± 1.05	9.13 ± 1.31	1.898	0.060	9.42 ± 1.05	9.13 ± 1.31	1.097	0.273
From support	0.891	0.374	2.24 ± 0.67	2.32 ± 0.68	-0.802	0.423	2.24 ± 0.67	2.32 ± 0.68	3.341	0.001
From participation	2.028	0.044	2.54 ± 0.30	2.60 ± 0.27	-1.412	0.161	2.54 ± 0.30	2.60 ± 0.27	0.171	0.864
From common language and vision	0.904	0.367	4.37 ± 0.65	4.39 ± 0.57	-0.179	0.858	4.37 ± 0.65	4.39 ± 0.57	2.019	0.046

associated with Performance 5. Performance 4 was significantly associated with ISC informal social networks ($t = 2.397, P = 0.018$)

3.3. Results of binary logistic regression analysis

Significant variables identified in the univariate analysis were included in the multiple-factor regression model, and the analysis was conducted using the Stepwise Forward Method. Table 5 summarizes the results.

Performance 1: The results of binary logistic regression analysis (Table 5) indicate that not attending management training program and not attending skill-based training program decreased the likelihood

achieving performance 1 at OR = 0.34 (95% CI = 0.151–0.788) and OR = 0.38 (95% CI = 0.174–0.831), respectively. However, having 2.5 years (OR = 6.474, 95% CI = 2.477–16.923) and over 5 years (OR = 3.927, 95% CI = 1.463–10.542) of engagement in elderly care increased the likelihood of achieving Performance 1. Additionally, working full time (OR = 8.911, 95% CI = 1.038–76.464), possessing a strong social network (OR = 1.36, 95% CI = 1.186–1.559), and being married (OR = 5.621, 95% CI = 1.169–2.703) increased the likelihood of attaining Performance 1.

Performance 2: In the bivariate analysis, being a female core member (OR = 0.483, 95% CI = 0.286–

Table 5. Multifactor analysis of factors influencing the individual performance of core members

Variables	P	OR	95%CI
<i>Performance 1</i>			
Attending management training program			
Yes (<i>ref</i>)		1.000	
No	0.012	0.344	0.151-0.788
Attending skill-based training program			
Yes (<i>ref</i>)		1.000	
No	0.015	0.380	0.174-0.831
Years of engaged in elderly care			
≤ 1 (<i>ref</i>)		1.000	
2-5	0.007	3.927	1.463-10.542
> 5	< 0.001	6.474	2.477-16.923
Type of work			
Part-time (<i>ref</i>)		1.000	
Full-time	0.046	8.911	1.038-76.464
CmSC Social network	< 0.001	1.360	2.477-16.923
Marital status			
Unmarried, widowed, or divorced		1.000	
Married	0.031	5.621	1.169-2.703
<i>Performance 2</i>			
Gender			
Male (<i>ref</i>)		1.000	
Female	0.007	0.483	0.286-0.817
Attending management training program			
Yes (<i>ref</i>)		1.000	
No	< 0.001	0.332	0.184-0.598
Type of work			
Part-time (<i>ref</i>)		1.000	
Full-time	0.036	3.728	1.091-12.739
CmSC Social network	< 0.001	1.254	1.106-1.421
<i>Performance 3</i>			
Years of engaged in elderly care			
≤ 1 (<i>ref</i>)		1.000	
2-5	0.001	2.903	1.527-5.521
> 5	0.001	3.127	1.625-6.017
CmSC Social network	0.015	1.179	1.186-1.559
ISC Support	0.001	2.102	1.369-3.227
<i>Performance 4</i>			
Attending management training program			
Yes (<i>ref</i>)		1.000	
No	0.001	0.283	0.132-0.611
Professional Qualification			
Yes (<i>ref</i>)		1.000	
No	0.016	0.425	0.211-0.854
<i>Performance 5</i>			
Professional Qualification			
Yes (<i>ref</i>)		1.000	
No	0.012	0.393	0.19-0.814
CmSC Social network	0.005	1.050	1.015-1.087
ISC common language and vision	0.020	4.227	1.259-14.186

Table 6. Summary of the individual performance model for core members

Variables	Performance 1	Performance 2	Performance 3	Performance 4	Performance 5
Attending management training program	√	√		√	
Attending skill-based training program	√				
Professional qualification				√	√
Years of engaged in elderly care	√		√		
Type of work	√	√			
Marital status	√				
Gender		√			
CmSC Social network	√	√	√		√
ISC Support			√		
ISC common language and vision					√

0.817) and not receiving management training (OR = 0.332, 95% CI = 0.184–0.598) decreased the likelihood of achieving Performance 2. In contrast, working full time (OR = 3.728, 95% CI = 1.091–12.739) and having a high social network score (OR = 1.254, 95% CI = 1.106–1.421) increased the chances of Performance 2.

Performance 3: As shown in Table 5, having 2-5 years (OR = 3.127, 95%CI = 1.625–6.017) and over 5 years (OR = 2.903, 95% CI = 1.527–5.521) of engagement in elderly care increased the chances of Performance 3. Likewise, high CmSC social network score (OR = 1.179, 95% CI = 1.186–1.559) and high ISC support (OR = 2.102, 95% CI = 1.369–3.227) increased the likelihood of Performance 3.

Performance 4: Not receiving management training and not possessing professional qualifications decreased the chances of achieving good Performance 4 (OR = 0.283, 95% CI = 0.132–0.611 and OR = 0.425, 95% CI = 0.211–0.854), respectively.

Performance 5: The results show that not having professional qualifications (OR = 0.393, 95% CI = 0.19–0.814) decreased the chance of performance 5. Conversely, a one-point increase in CmSC social network score (OR = 1.05, 95% CI = 1.015–1.087) and a one-point increase in ISC common language and vision (OR = 4.227, 95% CI = 1.259–14.186) increased the likelihood of Performance 5.

Summary of personal performance model: Summarizing the binary logistic regression results in Table 6, we observed that the most influential factor affecting the individual performance of core members was the CmSC's social network. Other significant influencing factors included attending management training programs, obtaining professional qualifications, years of engagement in elderly care, and type of work.

4. Discussion

This study investigated the relationship between organizational social capital stock and how the social capital possessed by core members influences individual performance. This study found significant associations between social capital and individual performance attributable to factors, such as attending management

training programs, skill-based training programs, professional qualifications, sex, marriage, type of work, CmSC social network, ISC support, ISC common language and vision, and the years of experience in elderly care.

The fast-aging population of China (24) has resulted in a swift expansion of the elderly population coupled with their comparatively diminished health conditions, which has generated substantial demands for elderly care. Therefore, ESOs witness unprecedented opportunities and challenges (25). This double-edged scenario highlights the crucial role of the core members of ESOs in influencing the operations and quality of services (26). Exploring strategies to enhance the performance of key members is of paramount significance in elevating the service quality of elderly care organizations, refining their capacity to meet service demands, and mitigating the challenges associated with elderly care services. This study adopted a social capital perspective and examined the factors that influence core members' individual performances. The subsequent sections discuss how different dimensions of social capital and other variables affect the performance of ESOs' core members.

4.1. Social Capital and Individual Performance

Our analysis suggests that core members' social networks predominantly influence their performance. Those with higher social network scores perform more extensively in elderly care. This is consistent with the results of previous studies (27-28). We argue that core members with high social networks are more likely to enjoy media reporting and, in some instances, receive awards for their contributions to elderly care. They may also participate in drafting or discussing the local elderly care service standards. Wide social networks serve as proxies for accessing resources, including those essential for task completion and experiential information related to tasks (29). Social networks help individuals acquire and assimilate potentially valuable knowledge (30). All these, in turn, facilitate organizational development and recognition in the professional sphere. A study in the Netherlands showed that the most successful managers in businesses spend 70% more time participating in social

network activities than less successful ones (31).

In the organizational social capital dimension, our research indicates that elements like support, a common language, and a shared vision within the organization's internal social capital can influence individual performance. Specifically, core individuals who receive more support from ESOs have a greater likelihood of both themselves and their teams being covered by media reports. This is attributed to the support, both material and non-material, provided by ESOs, such as opportunities for training or further education, which leads to the professional development of the employees. Consequently, competence was enhanced and performance improved. Noteworthy accomplishments frequently attract the attention of the media and public. Media coverage contributes to the construction of a positive organizational image of ESOs, enhancing the organization's reputation and influence. This fosters support for employees within an organization (32).

A common language and vision reflect the extent to which members of an organization possess a common understanding of the professional knowledge and skills needed to conduct their work as well as their identification with the organization's goals and mission. A strong reserve of professional knowledge and experience in the elderly service industry gives core members the opportunity to participate in the drafting and discussion of local standards for elderly services. Identification with the philosophy and values of the SO for the elderly makes them willing participants in the formulation of policies and standards related to elderly services, thus promoting the alignment of these policies and standards with the organization's philosophy and goals (33).

However, in contrast to previous findings (34-35), this study did not identify a positive influence of external social capital on individual performance. One possible explanation is that external social capital refers to tangible and potential resources derived from an organization's collaborative networks established with external stakeholders (36). In Anhui, ESOs face challenges, such as high entry barriers and an underdeveloped coordination mechanism (37). Thus, there are few connections between ESOs and governments. This scarcity results in a limited reserve of external social capital, making it challenging to influence performance. Additionally, differences in the questionnaires used to measure external social capital may be an implicit factor contributing to this result.

4.2. Other variables influencing individual performance

Regarding the sociodemographic factors of core members, factors like training participation, possession of qualifications or certifications, and years of experience in elderly care services significantly influenced their performance of core members. Previous studies have

established the significant impact of training on employee performance (38). Business training stands out as a key avenue for enhancing the job skills and professional knowledge of core members, thereby boosting their capacity to adapt to change. Heightened ability is often positively associated with improved job performance. Core members who lack professional certifications often exhibit poorer job performance. One significant reason for this is that, within ESOs, employees without certifications typically engage in lower-level positions, affording them fewer opportunities to receive training in elderly care service management and skills (39). Consequently, this contributes to lower job performance. For core members with extensive experience in elder care services, prolonged involvement in the field resulted in a wealth of practical knowledge. They availed of increased training opportunities, established deeper social networks, and attained higher levels of expertise and skills. Consequently, these aspects positively affect job performance. Additionally, variables like gender, marital status, and job type exert varying degrees of influence on the individual performance of core members.

Furthermore, it's important to note that the outbreak of the COVID-19 pandemic has resulted in a lack of survey data on elderly caring social organizations during this period. As a result, this study is unable to investigate the impact of the COVID-19 pandemic on the core members of these organizations. However, existing literature suggests that social capital can mitigate the disruptive effects of the pandemic, reducing its impact on individuals (40). Therefore, in the current context of normalized epidemic prevention and control measures, this research still offers valuable insights into performance enhancement strategies for core members of elderly caring social organizations.

4.3. Countermeasures and proposals

In light of the research outcomes, we recommend the following to enhance the performance of core members in elderly social organizations:

First, organizations should provide comprehensive support for the professional development of core members. This involves actively guiding and encouraging active participation in various professional training programs to continually enhance job capabilities. Moreover, it is crucial to expand interpersonal networks in elderly services. Actively fostering relationships with other organizations is essential for preventing the loss of social capital. Leveraging the advantages of social media is instrumental. Through online platforms, core members can exchange and share experiences with elderly services, establish communication channels with peers, and broaden their social networks.

Second, enhancing external engagement is imperative. This involves actively participating in government initiatives such as public service procurement projects

and collaborating with the government, higher education institutions, volunteer organizations, and other relevant entities to cultivate robust partnerships. This promotes synergistic development and increases the reserves of external social capital.

Finally, we suggest retention strategies and practices for core members with extensive experience and prolonged service. This may include the provision of additional career development opportunities, greater remuneration, and improved benefits. Employees with a long history of elderly services often have valuable experience and knowledge that can be shared for succession. This is instrumental in maintaining organizational stability and improving operational efficiency in ESOs.

However, we acknowledge some limitations of this study. First, because of the COVID-19 pandemic, elderly care facilities across regions implemented access restrictions, thereby limiting the conduct of surveys during the pandemic period. Consequently, this study did not incorporate survey data on social capital during the COVID-19 pandemic. Thus, it is a cross-sectional study that is unable to ascertain the impact of the COVID-19 pandemic on social capital. Second, the inherent limitations of cross-sectional studies render it impractical to establish a causal relationship between social capital and individual performance. Finally, the research sample was drawn solely from the Anhui Province, which may hinder generalizability.

5. Conclusions

The personal social networks of core members within elderly social organizations and certain elements of internal social capital within the organization can influence their job performance of these core members. Enhancing the social capital of core members can assist ESOs in obtaining more developmental resources, thereby improving the overall performance of the organization. Therefore, at the individual level, SOs should enhance the job capabilities of core members by providing more training opportunities and establishing online platforms to broaden their social networks. At the organizational level, ESOs should actively seek interactions with the external environment, increase their external social capital reserves through project engagement and collaboration, and strengthen organizational cohesion by establishing a common language and vision to enhance operational stability.

Acknowledgements

The authors sincerely thank the provincial and local Civil Affairs Department of Anhui Province, Anhui-based elderly caring social organizations, and all study participants for their valuable contributions to this research.

Funding: This study was funded by the National Science Foundation of China (NO.71874002 and NO.72174001) and Scientific Research Projects for Higher Education of Anhui Province(2023AH10036).

Conflict of Interest: The authors have no conflicts of interest to disclose.

Declarations

Ethics approval and consent to participate: In this study, ethics approval was obtained from the Biomedical Ethics Committee of Anhui Medical University with reference number No. 20180181 before the commencement of data collection. All participants provided written informed consent before participating in the study. Participants were informed of the study's purpose, procedures, potential risks, and benefits, and their right to withdraw at any time without penalty. Confidentiality and anonymity were maintained throughout the study, and all data collected were stored securely to protect participants' privacy. In addition, all methods used in our study are in accordance with the Declaration of Helsinki.

Availability of data and materials: The datasets used during the current study are available from the corresponding author on reasonable request.

Additional documents: Supplementary Document 1 illustrates the geographical positions of Anhui Province and the respective locations of the survey sites, detailing the reliability and validity of each dimension. Supplementary Document 2 offers a concise overview of the scales employed in this study.

References

1. Man W, Wang S, Yang H. Exploring the spatial-temporal distribution and evolution of population aging and social-economic indicators in China. *BMC Public Health*. 2021; 21:966.
2. National Bureau of Statistics. "The Seventh National Population Census.". https://www.stats.gov.cn/zt_18555/zdtjgz/zgrkpc/dqcrkpc/ (accessd March 29, 2024). (in Chinese)
3. Fang EF, Xie C, Schenkel JA, *et al*. A research agenda for ageing in China in the 21st century (2nd edition): Focusing on basic and translational research, long-term care, policy and social networks. *Ageing Res Rev*. 2020; 64:101174.
4. Yang Y. The Role of NGOs in Enabling Elderly Activity and Care in the Community: a Case Study of Silver Wings in South Korea. *J Cross Cult Gerontol*. 2018; 33:217-228.
5. Civil Affairs Bureau of Jiangsu Province. Overview of data on civil affairs operations. <http://mzt.jiangsu.gov.cn/col/col178570/index.html> (accessd March 29, 2024). (in Chinese)
6. The State Council. Opinions on Accelerating the

- Development of the Elderly Service Industry. https://www.gov.cn/zhengce/zhengceku/2013-09/13/content_7213.htm (accessed March 29, 2024). (in Chinese)
7. National Development and Reform Commission. "14th Five-Year Plan" for the development of national elderly care and the establishment of the pension service system. https://www.gov.cn/zhengce/content/2022-02/21/content_5674844.htm (accessed March 29, 2024). (in Chinese)
 8. Zhang X, Laiti M. The Action Logic of Social Capital Construction of Grassroots Elderly Organizations in the Context of Government Purchasing--The Case of Organization S in District Y of M City. *Social development research*. 2017; 1:94-110. (in Chinese)
 9. Tang L, Bai Z, Ji K, Zhu Y, Chen R. Correlations of external social capital in social organizations providing integrated eldercare services with medical care in China. *BMC Health Serv Res*. 2022; 22:101.
 10. Wang D, Mei G, Xu X, Zhao R, Ma Y, Chen R, Qin X, Hu Z. Chinese non-governmental organizations involved in HIV/AIDS prevention and control: Intra-organizational social capital as a new analytical perspective. *Biosci Trends*. 2016; 10:418-423.
 11. Andrews R. Organizational social capital, structure and performance. *human relations*. 2010; 63:583-608.
 12. Leonardi R, Nanetti RY, Putnam RD. *Making democracy work: Civic traditions in modern Italy*. Princeton university press Princeton, NJ, USA, 2001.
 13. Pretty J, Ward H. Social capital and the environment. *World development*. 2001; 29:209-227.
 14. Subramony M, Segers J, Chadwick C, Shyamsunder A. Leadership development practice bundles and organizational performance: The mediating role of human capital and social capital. *Journal of business research*. 2018; 83:120-129.
 15. Kishimoto Y, Suzuki E, Iwase T, Doi H, Takao S. Group involvement and self-rated health among the Japanese elderly: an examination of bonding and bridging social capital. *BMC Public Health*. 2013; 13:1189.
 16. Cain CL, Wallace SP, Ponce NA. Helpfulness, Trust, and Safety of Neighborhoods: Social Capital, Household Income, and Self-Reported Health of Older Adults. *Gerontologist*. 2018; 58:4-14.
 17. Adjaye-Gbewonyo D, Rebok GW, Gross AL, Gallo JJ, Underwood CR. Assessing urban-rural differences in the relationship between social capital and depression among Ghanaian and South African older adults. *PLoS One*. 2019; 14:e0218620.
 18. Zhou Y, Zhou Y, Zhang L, Zhao X, Chen W. Effects of Top Management Team Characteristics on Patent Strategic Change and Firm Performance. *Front Psychol*. 2021; 12:762499.
 19. Anhui Bureau of Statistics. 2020 Anhui Province Census Yearbook. <http://tjj.ah.gov.cn/ssah/qwfbjd/rksj/147987521.html> (accessed March 29, 2024). (in Chinese)
 20. Civil Affairs Bureau of Anhui Province. Anhui Social Organization Public Service Platform. <http://www.ahnpo.cn/> (accessed March 29, 2024). (in Chinese)
 21. Wang Z, Zhang X, Liu L, Tang L, Zhu Y, Bai Z, Chen R. Factors related to the social network of core members of elderly care service social organizations: a cross-sectional study. *BMC Health Serv Res*. 2022; 22:1147.
 22. Wang Z, Chen X, Ji K, Sang L, Bai Z, Chen R. Relationship between social network and individual performance of core members from aged care services social organizations: cross-sectional study. *BMC Geriatr*. 2023; 23:108.
 23. Kusuma IY, Triwibowo DN, Pratiwi ADE, Pitaloka DAE. Rasch Modelling to Assess Psychometric Validation of the Knowledge about Tuberculosis Questionnaire (KATUB-Q) for the General Population in Indonesia. *Int J Environ Res Public Health*. 2022; 19.
 24. Bao J, Zhou L, Liu G, Tang J, Lu X, Cheng C, Jin Y, Bai J. Current state of care for the elderly in China in the context of an aging population. *BioScience Trends*. 2022; 16:107-118.
 25. Chu LW, Chi I. Nursing homes in China. *J Am Med Dir Assoc*. 2008; 9:237-243.
 26. Wang D, Xu X, Mei G, Ma Y, Chen R, Qin X, Hu Z. The Relationship Between Core Members' Social Capital and Perceived and Externally Evaluated Prestige and Cooperation Among HIV/AIDS-Related Civil Society Organizations in China. *Evaluation & the Health Professions*. 2017; 40:61-78.
 27. Tavakoli Taba S, Hossain L, Heard R, Brennan P, Lee W, Lewis S. Personal and Network Dynamics in Performance of Knowledge Workers: A Study of Australian Breast Radiologists. *PLoS One*. 2016; 11:e0150186.
 28. Sparrowe RT, Liden RC, Wayne SJ, Kraimer ML. Social networks and the performance of individuals and groups. *Academy of management journal*. 2001; 44:316-325.
 29. Carter DR, DeChurch LA, Braun MT, Contractor NS. Social network approaches to leadership: an integrative conceptual review. *J Appl Psychol*. 2015; 100:597-622.
 30. Cross R, Cummings JN. Tie and network correlates of individual performance in knowledge-intensive work. *Academy of management journal*. 2004; 47:928-937.
 31. Van der Heijden BIJM, Kruyen PM, Notelaers G. The Importance of Intra-Organizational Networking for Younger Versus Older Workers: Examining a Multi-Group Mediation Model of Individual Task Performance Enhancement. *Frontiers in Psychology*. 2020; 11.
 32. Kioussis S, Popescu C, Mitrook M. Understanding influence on corporate reputation: An examination of public relations efforts, media coverage, public opinion, and financial performance from an agenda-building and agenda-setting perspective. *Journal of Public Relations Research*. 2007; 19:147-165.
 33. Ryan S. The relationship between shared vision, cohesion, role clarity, mutual trust and transformational leadership within a team setting. Stellenbosch: Stellenbosch University, 2012.
 34. Galunic C, Ertug G, Gargiulo M. The positive externalities of social capital: Benefiting from senior brokers. *Academy of Management Journal*. 2012; 55:1213-1231.
 35. Chen Z, Chen D, Peng MY, Li Q, Shi Y, Li J. Impact of Organizational Support and Social Capital on University Faculties' Working Performance. *Front Psychol*. 2020; 11:571559.
 36. Laursen K, Masciarelli F, Prencipe A. Regions matter: How localized social capital affects innovation and external knowledge acquisition. *Organization science*. 2012; 23:177-193.
 37. Xu X, Zhang W, Wang D, Chen R, Ma Y, Qin X. A Reflection on the Development of Integrated Medical and Care Facilities for the Elderly Based on Social Capital Theory. *Chinese Health Service Management*. 2017; 34:630-632. (in Chinese)
 38. Otero I, Salgado JF, Moscoso S. Criterion Validity of Cognitive Reflection for Predicting Job Performance and

- Training Proficiency: A Meta-Analysis. *Front Psychol.* 2021; 12:668592.
39. Hao Q, Wu S, Ying L, Luo L, Dong D, Dong B. Current dilemmas of nursing homes in Chengdu: a cross-sectional survey. *J Am Med Dir Assoc.* 2012; 13:406.e409-412.
40. Laurence J, Kim HH. Individual and community social capital, mobility restrictions, and psychological distress during the COVID-19 pandemic: a multilevel analysis of a representative US survey. *Soc Sci Med.* 2021; 287:114361.

Received March 21, 2024; Revised April 26, 2024; Accepted

June 7, 2024.

[§]These authors contributed equally to this work.

**Address correspondence to:*

Ren Chen, School of Health Services Management, Anhui Medical University and Key Laboratory of Public Health Social Governance, Philosophy and Social Sciences of Anhui Province, Hefei 230032, Anhui, China.

E-mail: chenren2006@hotmail.com

Released online in J-STAGE as advance publication June 12, 2024.

A predictive radiotranscriptomics model based on DCE-MRI for tumor immune landscape and immunotherapy in cholangiocarcinoma

Lu Chen^{1,6,§}, Guotao Yin^{2,§}, Ziyang Wang^{3,4,6,§}, Zifan Liu^{3,6}, Chunxiao Sui^{3,6}, Kun Chen^{3,6}, Tianqiang Song^{1,6}, Wengui Xu^{3,6}, Lisha Qi^{5,6,*}, Xiaofeng Li^{3,6,*}

¹Department of Hepatobiliary Cancer, Liver Cancer Research Center, Tianjin Medical University Cancer Institute and Hospital, Tianjin, China;

²Department of Radiology, Qilu Hospital of Shandong University, Jinan, Shandong, China;

³Department of Molecular Imaging and Nuclear Medicine, Tianjin Medical University Cancer Institute and Hospital, Tianjin, China;

⁴Department of Nuclear Medicine, Tianjin Cancer Hospital Airport Hospital, Tianjin, China;

⁵Department of Pathology, Tianjin Medical University Cancer Institute and Hospital, Tianjin, China;

⁶National Clinical Research Center for Cancer, Tianjin Key Laboratory of Cancer Prevention and Therapy, Tianjin's Clinical Research Center for Cancer, Tianjin, China.

SUMMARY This study aims to determine the predictive role of dynamic contrast-enhanced magnetic resonance imaging (DCE-MRI) derived radiomic model in tumor immune profiling and immunotherapy for cholangiocarcinoma. To perform radiomic analysis, immune related subgroup clustering was first performed by single sample gene set enrichment analysis (ssGSEA). Second, a total of 806 radiomic features for each phase of DCE-MRI were extracted by utilizing the Python package Pyradiomics. Then, a predictive radiomic signature model was constructed after a three-step features reduction and selection, and receiver operating characteristic (ROC) curve was employed to evaluate the performance of this model. In the end, an independent testing cohort involving cholangiocarcinoma patients with anti-PD-1 Sintilimab treatment after surgery was used to verify the potential application of the established radiomic model in immunotherapy for cholangiocarcinoma. Two distinct immune related subgroups were classified using ssGSEA based on transcriptome sequencing. For radiomic analysis, a total of 10 predictive radiomic features were finally identified to establish a radiomic signature model for immune landscape classification. Regarding to the predictive performance, the mean AUC of ROC curves was 0.80 in the training/validation cohort. For the independent testing cohort, the individual predictive probability by radiomic model and the corresponding immune score derived from ssGSEA was significantly correlated. In conclusion, radiomic signature model based on DCE-MRI was capable of predicting the immune landscape of cholangiocarcinoma. Consequently, a potentially clinical application of this developed radiomic model to guide immunotherapy for cholangiocarcinoma was suggested.

Keywords cholangiocarcinoma, DCE-MRI, radiotranscriptomics, tumor immune landscape, immunotherapy

1. Introduction

Cholangiocarcinoma is the second most common primary liver malignancy after hepatocellular carcinoma (HCC) worldwide, accounting for approximately 10%–20% of all primary liver cancers (1). Increasing evidences show that its morbidity and mortality rates have steadily risen in the past decades (2). Despite tremendous progress in advanced treatment, the prognosis of cholangiocarcinoma patients remains dismal, with a 5-year overall survival (OS) rate ranging from 14% to 40% (3). Because most of cholangiocarcinoma patients are already in the

advanced clinical stage with the occurrence of early invasion and metastasis at the time of original diagnosis, which leads to minor eligibility for surgical resection (4), development of novel treatment strategies for cholangiocarcinoma is urgently needed.

Currently, immunotherapy is emerging as a promising therapeutic strategy for various types of cancers (5). Particularly with the clinical application of immune checkpoint blockade (ICB) treatment in a couple of types of cancer, including melanoma (6), lymphoma (7) and non-small cell lung cancer (NSCLC) (8), tumor immunotherapy has revolutionized the management

of cancer patients in recent decades. As reviewed in an updated report regarding immunotherapy for cholangiocarcinoma, several novel immunotherapeutic approaches, such as adoptive cell transfer therapy, cancer vaccines and ICB treatment combined with other targeted therapy, are currently under investigation (9,10). Unfortunately, only 20-50% of patients with advanced solid tumors significantly benefit from ICB therapy, mainly due to intrinsic heterogeneity in tumor (11). Therefore, it is of necessity to identify robust predictive biomarkers for selection of potentially responsive patients prior to immunotherapy (12,13).

Previous reports proved predictive roles of tumor immune landscape in tumor immunotherapy, reflected in a remarkably significant association between the status of tumor-infiltrating lymphocytes (TILs) (14) or programmed death-ligand 1 (PD-L1) (15) in tumor microenvironment (TME) and therapeutic efficacy to ICB treatment. However, tumor immunophenotype is currently assessed by immunohistochemistry (IHC) assay (16) and flow cytometric analyses, which mainly depends on biopsy specimen availability. Given the complexity of the staining procedure, lack of standardization and subjectivity of results interpretation and the spatio-temporal heterogeneity in tumorous tissues, a noninvasive, repeatable and reliable method is urgently needed to overcome these deficiencies. Dynamic contrast-enhanced magnetic resonance imaging (DCE-MRI) is one of the most commonly used imaging modalities in clinical practice for cholangiocarcinoma (17). Apart from conventional parameters based on MRI images, radiomic analysis and deep learning algorithms based on MRI images also exhibited a predictive power in prediction of tumor immune status for multiple types of cancer, including cholangiocarcinoma (18,19).

Radiomics, emerging as a novel technique, allows for a high-throughput analysis to extract the hidden non-visual features and establish corresponding descriptive or predictive models to characterize the intrinsic heterogeneous nature of tumors reflected in medical images (20). However, with the rapid development of radiomics, the biological rationale underlying the high predictive power of established radiomic models is increasingly required, which is not only an important tendency but also a challenge for radiomic studies in future (21). Radiomics combined with genomics or associated transcriptomics is significantly helpful to reintroduce biological meaning into radiomics. That was the very reason why we chose to perform radiotranscriptomics but not traditional radiomics in the study. Though TIL score and/or PD-1/PD-L1 status is predictive of the tumor immune landscape, a comprehensive characterization of the tumor immunophenotype is needed to substantially improve the prospect of tumor immunotherapy. With the development of next-generation sequencing techniques and the rise of bioinformatic analysis, distinct immune subtypes in

the TME of cholangiocarcinoma were characterized based on transcriptome sequencing, representing the comprehensive tumor immune landscape (22,23).

For radiotranscriptomics in the present investigation, transcriptomic signature was used as a starting point to identify the predictive imaging radiomic signature. In other words, tumor immune subgroups classification for cholangiocarcinoma was first achieved based on transcriptome sequencing data by an unsupervised clustering method. Then, quantitative radiomic features were extracted and selected to establish a potentially predictive radiomic signature model for tumor immune subgroups classification in cholangiocarcinoma. Finally, the predictive power of this developed radiomic signature model was evaluated by the value of area under the curve (AUC) based on receiver operating characteristic (ROC) analysis. Furthermore, cholangiocarcinoma patients with immunotherapy who underwent transcriptome sequencing after surgery and DCE-MRI examination prior to treatment were also included as an independent testing cohort to test the potential of this model in prediction of immunotherapy. Promisingly, this constructed radiomic signature model based on DCE-MRI was able to noninvasively and comprehensively characterize the local tumor immune landscape, and then guide immunotherapy for cholangiocarcinoma in clinical practice.

2. Materials and Methods

2.1. Patients selection

All recruited patients eligible for this present investigation met the following strict criteria: (1) patients with biopsy-proven diagnosis of cholangiocarcinoma after surgical resection; (2) patients who underwent preoperative liver DCE-MRI within 1 month of surgery; (3) patients without preoperative adjuvant treatment, such as chemotherapy, radiotherapy, molecular targeted therapy and other treatment; (4) patients who underwent specimen transcriptome sequencing and IHC staining for immune cells infiltration. The exclusion criteria were as follows: (1) patients without complete clinicopathologic information; (2) patients without qualified MRI images for tumor segmentation; (3) patients without valid sample transcriptome sequencing data or tumoral IHC assay results. A total of 365 cholangiocarcinoma patients were screened to recruit eligible candidates who underwent preoperative DCE-MRI examination and postoperative transcriptome sequencing. Among cholangiocarcinoma candidates undergoing transcriptome sequencing after surgery ($n = 72$), cholangiocarcinoma patient with complete preoperative DCE-MRI information ($n = 44$) was used as training cohort ($n = 34$) (3-fold cross-validation, 50 repetition) and independent testing cohort ($n = 10$) to construct and evaluate a preliminary radiotranscriptomics model for

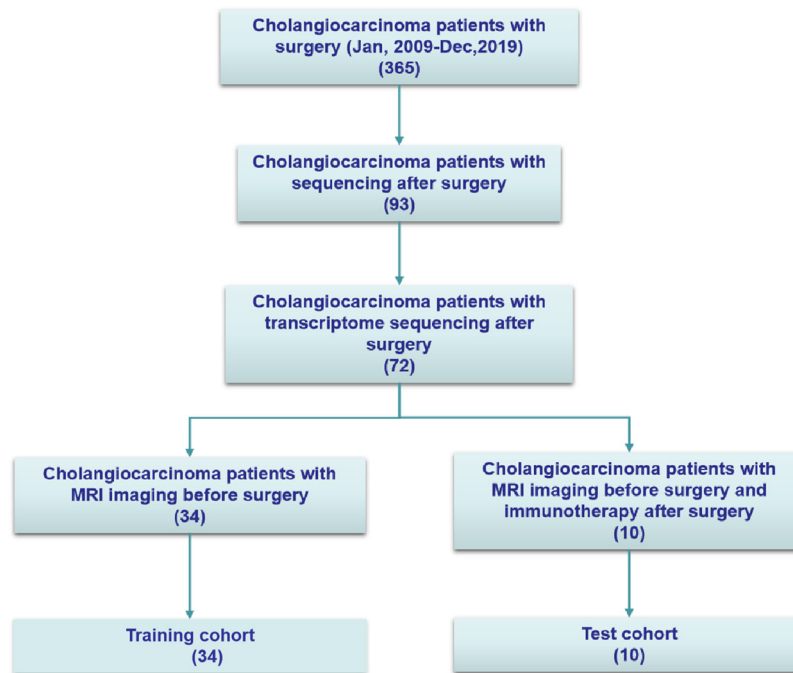


Figure 1. The flowchart of cholangiocarcinoma patients' enrollment in the study.

immunotherapy. The inclusion and exclusion flowchart for the patient enrollment in the study is represented in Figure. 1. The clinicopathological characteristics of these included cholangiocarcinoma patients based on immune-related subgroup clustering are summarized in Table 1. This retrospective study was approved by the our institutional ethics review committee (EK20240068), and the written informed consent requirement was waived because of the retrospective nature of this study. This study conforms to the provisions of the Declaration of Helsinki (as revised in 2013) and the provisions of the ICMJE recommendations and the CONSORT 2010 guidelines.

2.2. MRI acquisition

All MR examinations were performed by using a 3.0-T whole-body MRI system (Discovery MR750; GE Medical Systems, Milwaukee, WI) equipped with a quadrature body coil. Axial dynamic contrast-enhanced magnetic resonance imaging (DCE-MRI) (3D liver acquisition with volume acceleration-extended volume, LAVA-XV) consisted of non-contrast agent-enhanced, arterial phase (20-35 seconds), portal phase (60 seconds), 3-minute transitional phase and 20-minute delayed hepatobiliary phase images. The contrast agent, gadolinium diethylenetriaminepentaacetic acid (Gd-DTPA; Bayer Healthcare, Berlin, Germany) (0.1 mmol/kg), was automatically administered intravenously at the second phase of the DCE-MRI protocol at 2 mL/sec by using a power injector system, followed by a 20 mL saline flush at the same rate. These images were obtained using a breath-hold T1-weighted three-dimensional with fat suppression fast spoiled gradient echo sequence.

Repetition time/echo time (TR/TE) = 4/1.8 ms, number of excitations: (NEX) = 0.7, bandwidth = 142.9 kHz, thickness = 4mm, slice gap = -2mm, field of view (FOV) = 26 cm, matrix = 220×192, flip angle (FA) = 12°.

2.3. Immunotherapy and transcriptome sequencing for cholangiocarcinoma

A total of 10 advanced cholangiocarcinoma patients with postoperative transcriptome sequencing data were enrolled for immunotherapy in combination with systematic chemotherapy in the present investigation. Sintilimab were administered intravenously at a dose of 3 mg/kg every 3 weeks for at least 4 courses of treatment until disease progression or unacceptable toxic events. Therapy response was evaluated by radiological assessment (using computed tomography or magnetic resonance imaging) at baseline and then every 12 weeks during treatment or follow-up. The primary endpoint was the proportion of patients with disease control at week 12, including complete response (CR), partial response (PR), stable disease (SD) and progressive disease (PD) according to Response Evaluation Criteria In Solid Tumors (RECIST) v1.1 criteria. CR, PR and SD were categorized into the "clinical benefit (CB)" group, whereas PD was categorized into the "non-clinical benefit (NCB)" group for immunotherapy response evaluation. For transcriptome sequencing, each well-preserved fresh frozen block was first used to isolate Ribonucleic Acid (RNA) using the RNeasy Mini Kit (Qiagen) according to the manufacturer's instruction. After the construction of RNA-sequencing (RNA-seq) libraries using NEBNext Ultra RNA Library (New England Biolabs), 150-bp paired-end reads were checked for quality and sequenced

Table 1. Clinicopathologic characteristics of cholangiocarcinoma patients included in the study

Parameters	Immune-related classification		P
	Subgroup 1 (n = 17), n (%)	Subgroup 2 (n = 17), n (%)	
Location			0.29
ICC	9 (52.9)	12 (70.6)	
ECC	8 (47.1)	5 (29.4)	
Gender			0.72
Female	6 (35.3)	7 (41.2)	
Male	11 (64.7)	10 (58.8)	
Age (year)			0.73
< 60	7 (41.2)	8 (47.1)	
≥ 60	10 (58.8)	9 (52.9)	
Tumor size (cm)			0.78
< 3	6 (35.3)	8 (47.1)	
≥ 3 < 5	4 (23.5)	3 (17.6)	
≥ 5	7 (41.2)	6 (35.3)	
Lesion number			1.00
One	16 (94.1)	16 (94.1)	
More than one	1 (5.9)	1 (5.9)	
Differentiation			0.89
Low	1 (5.9)	2 (11.8)	
Medium-low	9 (52.9)	7 (41.2)	
Medium	6 (35.3)	7 (41.2)	
High	1 (5.9)	1 (5.9)	
Perineural invasion			0.99
Absence	13 (76.5)	13 (76.5)	
Presence	4 (23.5)	4 (23.5)	
Vascular invasion			0.99
Absence	14 (82.4)	15 (88.2)	
Presence	3 (17.6)	2 (11.8)	
Lymph node metastasis			0.99
Absence	15 (88.2)	14 (82.4)	
Presence	2 (11.8)	3 (17.6)	
CEA (µg/L) median (IQR)	2.48 (1.41-3.49)	2.53 (1.57-2.81)	0.94
CA199 (U/ml) median (IQR)	6.07 (14.62-331.03)	45.59 (22.77-214.90)	0.91
TBIL (µmol/L) median (IQR)	13.00 (10.35-77.90)	23.30 (12.00-68.03)	0.30
DBIL (µmol/L) median (IQR)	2.70 (1.73-36.18)	6.35 (2.33-34.50)	0.25
HBV infection			0.99
Absence	13 (76.5)	14 (82.4)	
Presence	4 (23.5)	3 (17.6)	
AJCC 8 th TNM			0.98
I	8 (47.1)	9 (52.9)	
II	5 (29.4)	4 (23.5)	
III	3 (17.6)	3 (17.6)	
IV	1 (5.9)	1 (5.9)	
CD3 ⁺ T infiltration			0.002
High	13 (76.5)	4 (23.5)	
Low	4 (23.5)	13 (76.5)	
CD8 ⁺ T infiltration			0.02
High	12 (70.6)	5 (29.4)	
Low	5 (29.4)	12 (70.6)	
FOXP3 ⁺ T infiltration			0.04
Positive	5 (29.4)	0 (0)	
Negative	12 (70.6)	17 (100)	

ICC: Intrahepatic cholangiocarcinoma; ECC: Extrahepatic cholangiocarcinoma; CEA: Carcinoma Embryonic Antigen; CA199: Carbohydrate antigen 199; HBV: Hepatitis B virus; HCV: Hepatitis C virus; TBIL: Total bilirubin; DBIL: Direct bilirubin; AJCC: American Joint Committee on Cancer; CD3/4/8: Cluster of differentiation 3/4/8; FOXP3: Forkhead box protein 3; IQR: Interquartile range.

with Illumina Novaseq (Illumina).

2.4. Immune-related subgroup clustering for cholangiocarcinoma based on transcriptome sequencing data

First, RNA-sequencing data from the included cholangiocarcinoma patients were first standardized

for further analysis. Then, immune-related subgroup clustering for cholangiocarcinoma was performed by using gene set enrichment analysis (GSEA) and the K-means algorithm. Briefly, a total of 29 immune-associated gene sets were chosen to represent tumor immunity as previously reported by literature, and the gene set variation analysis (GSVA) package was used for

single sample gene set enrichment analysis (ssGSEA) of the 29 immune gene sets. K-means algorithm, a classical unsupervised learning algorithm of artificial intelligence, was used for subgroup clustering in R software version 3.6.0 (<https://www.r-project.org/>) by 50 iterations. The total within the sum of square and average silhouette width was calculated using R package factoextra to determine the optimal number of clustering. Afterwards, the ConsensusClusterPlus package in R software was used for consensus clustering and subgroup screening of ssGSEA scores. In addition, a principal component analysis (PCA) plot was also drawn to verify the reliability of the consensus clusters. In the end, the heatmap package in R software was used for heatmap visualization of the ssGSEA scores for the aforementioned 29 immune gene sets based on subgroup clustering to illustrate the distinct immune characteristics of different subgroups.

2.5. Immunohistochemical analysis for the tumor-infiltrating lymphocytes in cholangiocarcinoma

Streptavidin-biotin-peroxidase staining was performed to determine the immune landscape in the tumorous tissue of cholangiocarcinoma. Briefly, paraffin embedding slides were first deparaffinized, rehydrated and pretreated with microwaves and blocking according to typical protocols. Then, the slides were incubated with a series of primary antibodies against several immunological markers overnight at 4°C according to the manufacturer's instructions, including CD3, CD8 and FOXP3. Finally, signals on the slides were revealed using 3,3-diaminobenzidine (DAB) buffer as substrate after incubation with appropriate horseradish peroxidase (HRP)-conjugated secondary antibodies (1:2000; Santa Cruz Biotechnology, Inc., Dallas, TX) for 1 hour at room temperature. Three most independent and representative fields in tissues for each case were selected and photographed ($\times 200$ magnification) to evaluate the levels of T lymphocyte infiltrations with an Olympus digital camera. Then, the numbers of infiltrating lymphocytes in each field were automatically and recorded as previously described (24) using Image pro plus 6.0 software (Media Cybernetics Inc.). The averages of infiltration were calculated and used for statistical analysis.

2.6. Radiomics workflow

The radiomics workflow in the study mainly consists of (1) Lesion segmentation, (2) radiomic features extraction, (3) radiomic features reduction and selection; (4) radiomic signature/model construction and clinical use. The detailed workflow of the radiotranscriptomics is schemed in Figure. 2. The 3D Slicer version 4.10.2 (open-source software; <https://www.slicer.org/>) was used for semiautomatic segmentation. The volume of interest (VOI) segmentation and subsequent radiomic

features extraction for each lesion were performed in a blinded fashion by two radiologists with > 10 years' experience (reader 1 and reader 2) based on multiple images per phase of DCE-MRI, and only indicator lesion was delineated if multiple lesions existed. Radiomic features extraction was performed by utilizing open-source Python package Pyradiomics 1.2.0 (<http://www.radiomics.io/pyradiomics.html>). Both original features and wavelet features were extracted in the study. A total of 806 radiomic features were generated for each VOI based on per phase of MRI, including shape features, first-order statistic features, second-order features, higher-order statistic features and wavelet features. Radiomic features reduction and selection were performed to select the most informative features to construct radiomic models. In the present investigation, three steps were adopted to avoid or reduce overfitting and selection bias. Firstly, the intra-class coefficients (ICCs) with a threshold of 0.95 were used to select the stable features that were not easily affected by the process of delineation. Then, spearman correlation analysis with a Spearman correlation coefficient of 0.75 was performed to reduce the redundancy between selected radiomic features. Third, the Man-Whitney *U* test ($p < 0.05$) was used to identify the informative radiomic features that significantly differ between the two immune-related subgroups. Lastly, a support vector machine with rbf kernel was employed to establish the radiomic model. Due to the limited sample size, three-fold cross-validation was performed and repeated 50 times in the training set. Furthermore, the calibration performance was also evaluated by the Hosmer-Lemeshow test. To test the predictive power of the established radiomic model in immune related subgroup classification and immunotherapy, another 10 cholangiocarcinoma patients with ICB treatment were recruited as an independent testing cohort.

2.7. Statistical analysis

For all continuous variables, normal distribution and variance homogeneity were first assessed. Those with a normal distribution were expressed as mean and standard deviation (mean \pm SD), while those with non-normal distributions were expressed as medians and interquartile range. The inter-group statistical differences for numerical variables were determined by the *t*-test (normal distribution), the Mann-Whitney *U* test/ or Wilcoxon Rank Sum tests (non-normal distribution), while the chi-square test or Fisher's exact test was used for categorical variables. Inter-observer agreement was used to assess the reliability of the MRI evaluation using the Kappa test, and the performance of the developed radiomic model based on DCE-MRI in immune profiling for cholangiocarcinoma was quantified by receiver operating characteristic (ROC) curve analysis and justified by the calibration curve. The area under the curve (AUC) of the ROC curve, classification accuracy, sensitivity

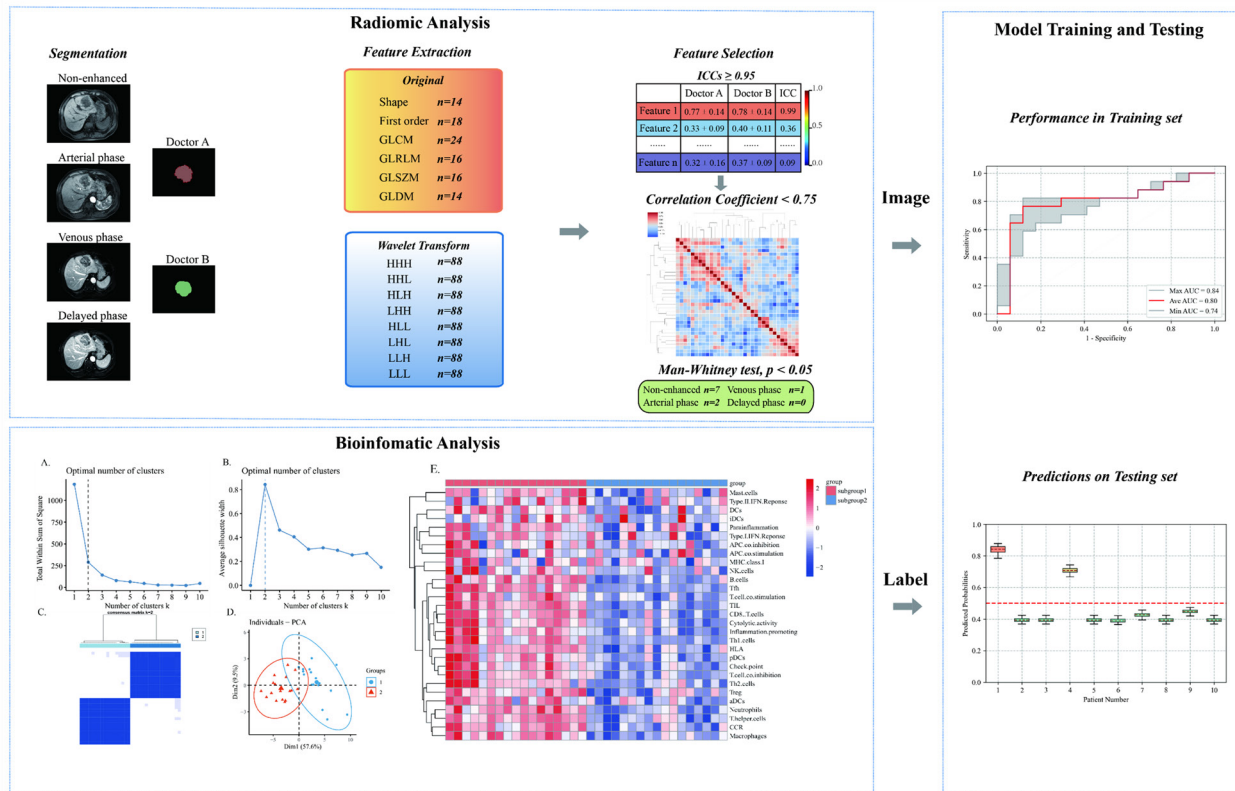


Figure 2. The detailed workflow of radiotranscriptomic analysis in the study. First, a bioinformatics analysis based on transcriptome sequencing data was performed to classify the immune-related subgroup, which was used as a label for subsequent radiomic analysis. Second, based on the label aforementioned, a radiomic analysis was conducted to establish a radiomic signature model, which mainly consists of VOI segmentation, radiomic features extraction, three-step features reduction and selection. Finally, a ROC analysis was performed to evaluate the power of the developed radiomic model in the prediction of immune landscape and immunotherapy for cholangiocarcinoma in both the training set and the testing set.

and specificity were also calculated by using Python (Version 3.6, <https://www.jianshu.com/p/b48d6bad9aaf>) for constructed radiomic model. The above statistical analyses were conducted using the software Python (Version 3.6, <https://www.jianshu.com/p/b48d6bad9aaf>) and IBM SPSS Statistics v. 20.0 (Armonk, NY). A P value of less than 0.05 is considered as statistically significant.

3. Results

3.1. Immune-related subgroup clustering for cholangiocarcinoma based on transcriptome sequencing data

For each included cholangiocarcinoma sample ($n = 34$), the gene set variation analysis (GSVA) package was used for single sample gene set enrichment analysis (ssGSEA) to obtain scores for a total of 29 immune-associated gene sets representing multiple immune cell types, functions and pathways. The K-means algorithm was used to determine the optimal cluster number. As shown in Figure. 3A and Figure. 3B, corresponding to both the turning point on the total within the sum of square (elbow method) and maximum average silhouette width (Silhouette Coefficient method), $k = 2$ was suggested as the optimal number of immune-related subgroup clustering for cholangiocarcinoma.

The R package Consensus Cluster Plus was used to perform consensus matrix analysis for validation of the consensus clustering when $k = 2$ (Figure. 3C). Additionally, the principal component analysis (PCA) plots also showed the reliability of the consensus clusters based on the subgroup screening of ssGSEA scores (Figure. 3D). Ultimately, the distinct immune characteristics of the identified two subgroups were visualized in a heat map based on the ssGSEA scores for aforementioned 29 immune gene sets (Figure. 3E). As shown, the extent of immune cell infiltration in subgroup 1 was remarkably higher than that in subgroup 2 ($P < 0.05$).

3.2. Immune characteristics validation of the identified two immune-related subgroups

Based on the aforementioned immune-related subgroup clustering for cholangiocarcinoma, an IHC assay was performed to validate the differences in immune characteristics between the two subgroups. Consistent with the results illustrated in the heat map mentioned above, subgroup 1 was characterized by higher infiltrations for various types of immune cells compared to subgroup 2. As shown in the representative IHC images (Figure. 4A), for subgroup 1, which was considered as an immune-hot subtype, the densities of

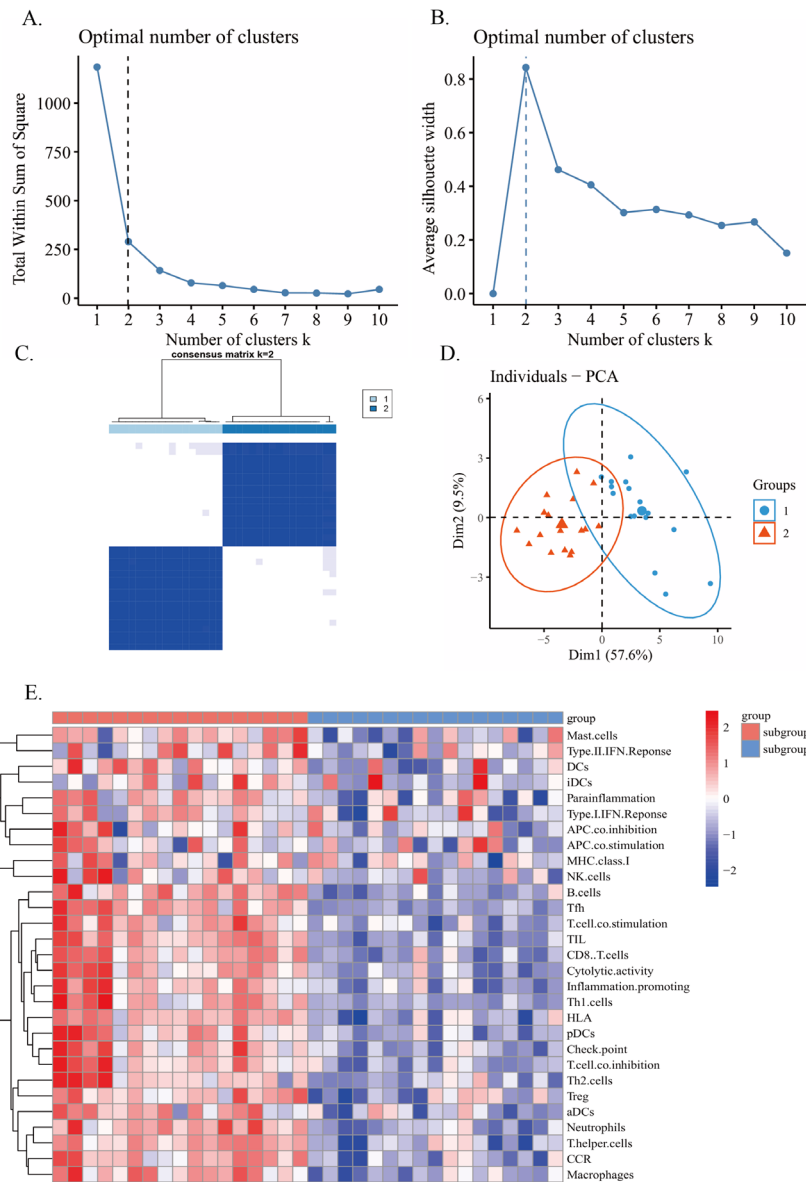


Figure 3. A bioinformatic analysis for immune-related subgroup clustering for cholangiocarcinoma recruited in the study based on transcriptome sequencing data. (A) The curve of the total within sum of squared error under corresponding cluster number k by using elbow method reached the "elbow point" when $k = 2$. **(B)** The curve of average silhouette width under corresponding cluster number k by using silhouette coefficient calculation, and the maximum of average silhouette width was achieved when $k = 2$. **(C)** The consensus clustering of immune-related subgroup of cholangiocarcinoma when $k = 2$. **(D)** The principal component analysis (PCA) plots of clustered samples of cholangiocarcinoma. (subgroup 1: blue; subgroup2: red). **(E)** The visualization of the distinct immune characteristics of the classified subgroups based on ssGSEA scores calculated by a GSVA package in the form of heat map.

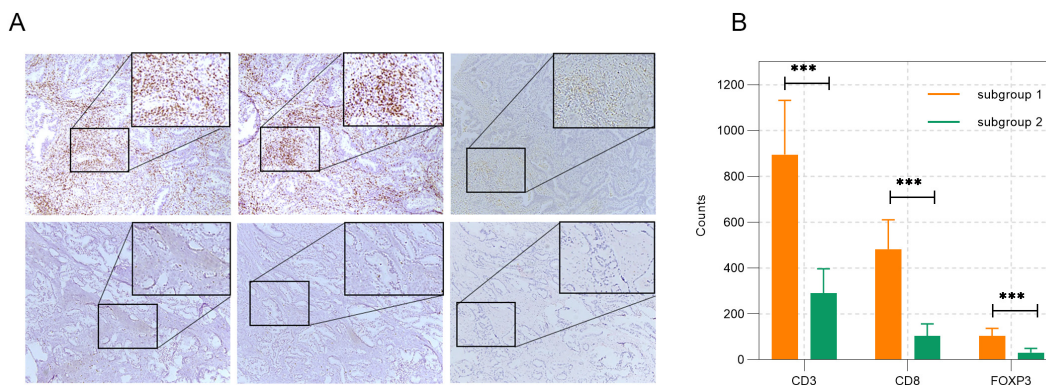


Figure 4. Validation of the immune-related subgroup clustering by IHC assay. (A) Representative IHC images of multiple immune cell infiltrations in cholangiocarcinoma for subgroup 1 (upper) and subgroup 2 (lower), including $CD3^+$ T (left), $CD8^+$ T (middle), and $FOXP3^+$ T cells (right). **(B)** The differences of $CD3^+$ T, $CD8^+$ T, and $FOXP3^+$ T cell infiltration in cholangiocarcinoma between subgroup 1 and subgroup 2 were summarized in the histogram.

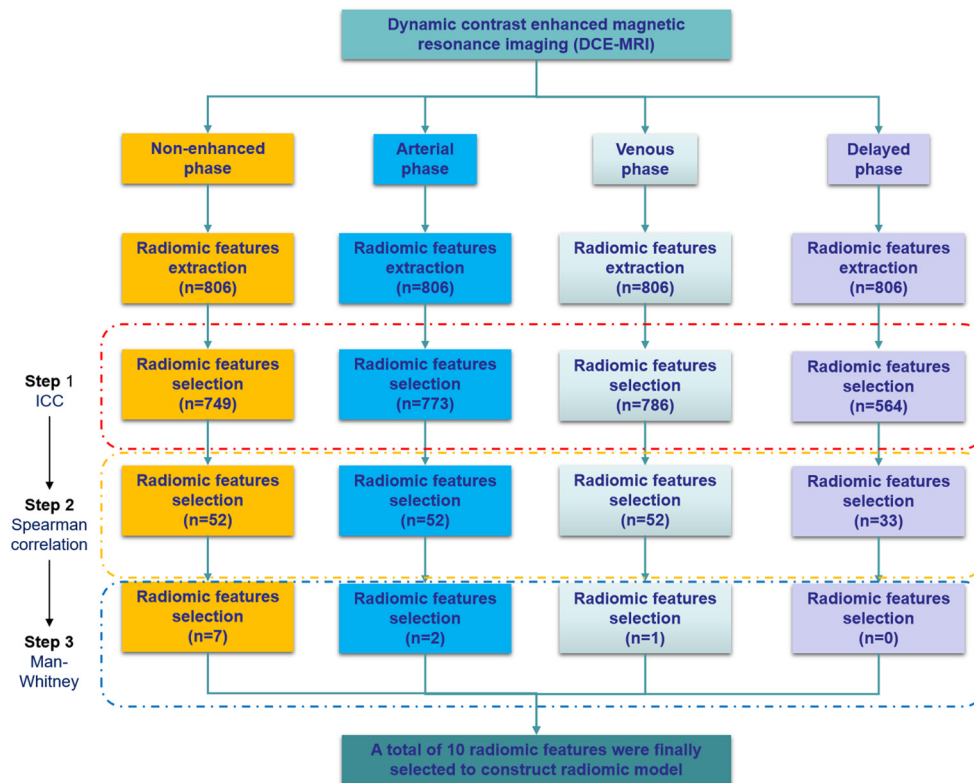


Figure 5. The flowchart of radiomic features extraction, reduction and selection. First, the delineation of VOI in each phase of DCE-MRI for all the included cholangiocarcinoma patients was performed by using 3D Slicer, including the non-enhanced phase, the arterial phase, the venous phase and the delayed phase. Second, a total of 806 radiomic features were generated per lesion in each phase of DCE-MRI for individual cholangiocarcinoma patients. Then, to select the most informative radiomic features to build the radiomic model, three-step radiomic features reduction (ICC analysis, spearman correlation analysis and Man-Whitney U test) was performed for each phase of DCE-MRI. In the end, a total of 10 radiomic features from four phases of DEC-MRI were finally selected.

infiltrating CD3⁺ T ($P < 0.001$), CD8⁺ T ($P < 0.001$), and FOXP3⁺ T ($P < 0.001$) were dramatically higher than that in subgroup 2 which represented an immune-cold or immunodeficient subtype (Figure. 4B), suggesting a potential sensitivity to immune checkpoint blockade (ICB) treatment for subgroup 1 but not subgroup 2.

3.3. Extraction and selection of radiomic features derived from DCE-MRI images

Before radiomic features extraction, semiautomatic segmentation by using the 3D Slicer was first performed to delineate the VOI in each phase of dynamic contrast enhancement (DCE) images of MRI, including non-enhanced phase, arterial phase, venous phase and delayed phase. A total of 806 radiomic features were generated per lesion in each phase of DCE-MRI, including shape features ($n = 14$), (b) first-order statistics ($n = 18$), (c) gray-level co-occurrence matrix (GLCM) features ($n = 24$), (d) gray-level dependence matrix (GLDM) features ($n = 14$), (e) gray-level run-length matrix (GLRLM) features ($n = 16$), (f) gray-level size-zone matrix (GLSZM) features ($n = 16$) and wavelet features ($n = 704$). A three-step procedure for radiomic features reduction and selection

were utilized to select the most informative radiomic features for immune related subgroup classification for cholangiocarcinoma based on each phase of DCE-MRI, including ICC analysis, spearman correlation analysis and Man-Whitney U test. In the end, a total of 10 radiomic features were selected to build the model. The detailed outcome for each radiomic features reduction and selection step is flowcharted in Figure. 5. To illustrate the differences in predictive radiomic features between subgroup 1 and subgroup 2. Representative DCE-MRI images, including the non-enhanced phase, arterial phase and portal venous phase, are presented in Figure. 6. The original DCE-MRI images are shown in Figure. 6A, and the upper row and the lower row is for subgroup 1 and subgroup 2, respectively. The generated images depicting the activities of predictive radiomic features within the VOI from representative cholangiocarcinoma patients from subgroup 1 and subgroup 2 are placed in Figure. 6B. As shown, the predictive radiomic feature based on MRI images from non-enhanced phase in subgroup 1 was significantly increased in contrast with that in subgroup 2. Especially, in comparison with subgroup 2, the predictive radiomic feature based on MRI images from portal venous phase was remarkably enhanced in subgroup 1.

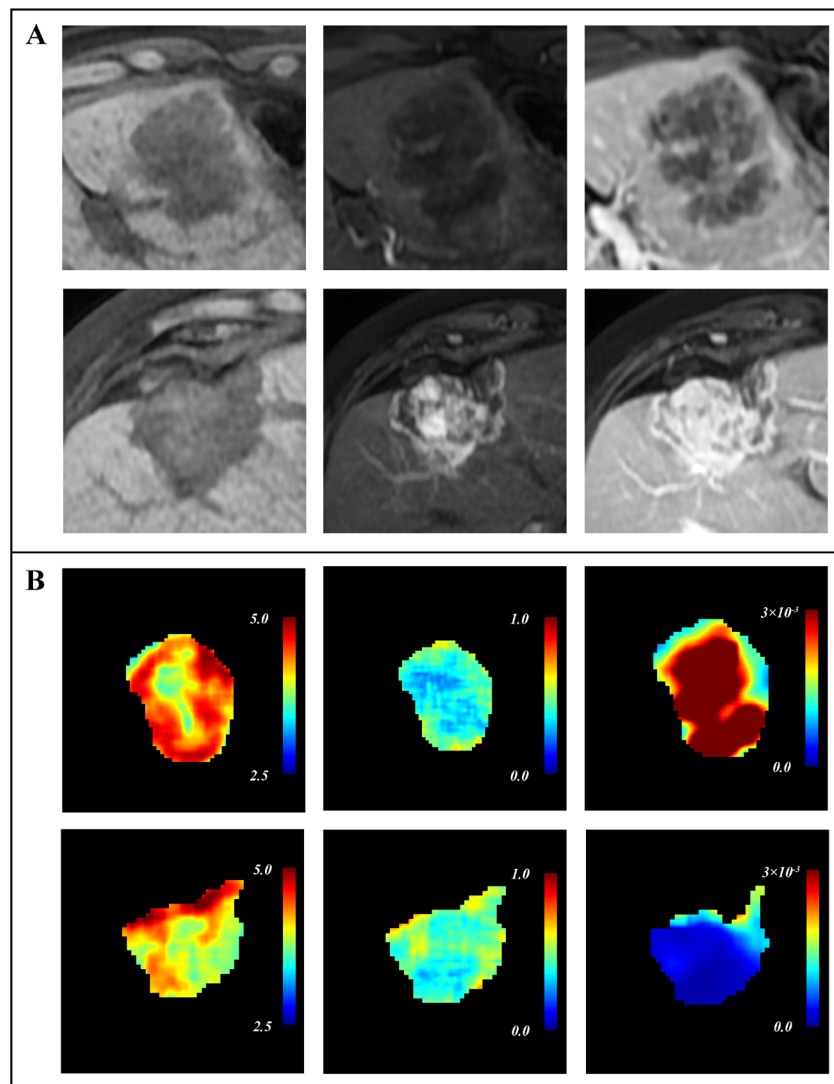


Figure 6. Representative multiple-phase images of DCE-MRI in subgroup 1 and subgroup 2 with pseudo-color delineation of predictive radiomic features. (A) The representative original DCE-MRI images from subgroup 1 (upper) and subgroup 2 (lower). The left column is for the non-enhanced phase, the middle column is for the arterial phase and the right column is for the portal venous phase. (B) The generated pseudo-color delineation of predictive radiomic features within the VOI of representative cholangiocarcinoma patients from subgroup 1 and subgroup 2. The left column is for the non-enhanced phase, the middle column is for the arterial phase and the right column is for the portal venous phase.

3.4. The predictive power of the constructed multivariate radiomic model in immune-related subgroup classification for cholangiocarcinoma

A support vector machine with rbf kernel was employed to establish the radiomic model by using the finally selected 10 radiomic features. The ROC curve (Figure. 7A) and the decision curve (Figure. 7B) were drawn to evaluate the predictive power of the developed radiomic model in immune related subgroup classification for cholangiocarcinoma. In order to make the results stable and reliable, three-fold cross-validation was performed and repeated 50 times in the training set. As shown, the mean AUC of the ROC curve for the training set was 0.80 (95% CI 0.64-0.93), with a classification accuracy of 76.47%, a classification sensitivity of 70.59% and a classification specificity of 82.35%. In addition, the 50 prediction results of every patient in the training/

validation set based on immune-related subgroup clustering were displayed through the violin box diagram (Figure. 7C). As indicated, the predictive probabilities in subgroup 1 were dramatically higher than that in subgroup 2 ($P < 0.01$). The stability of this predictive radiomic model was justified by the Chi-Square Goodness-of-Fit test ($\chi^2 = 0.233$, $p = 0.629$) and evaluated by calibration curve analysis which suggested a high level of stability (Figure. 7D).

3.5. The potential clinical translation of the established radiomic model for immunotherapy of cholangiocarcinoma

To test the predictive role of the established radiomic model in immunotherapy for cholangiocarcinoma, a total of 10 cholangiocarcinoma patients who underwent both transcriptome sequencing and ICB treatment after

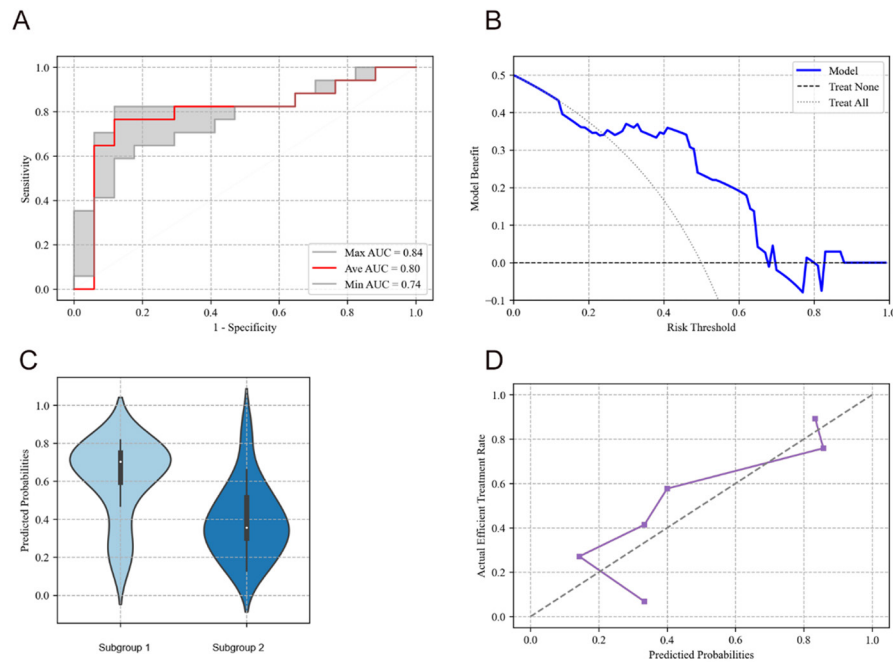


Figure 7. Evaluation of the established radiomic model in prediction of immune-related subgroup classification for cholangiocarcinoma. A ROC curve (A) and a decision curve (B) were drawn to evaluate the predictive power of the developed radiomic model. (C) Moreover, the violin box diagram displayed the distribution of the repeated 50 times predicted probabilities of being recognized as immune-related subgroup 1. (D) The stability of this predictive radiomic model was evaluated by calibration curve analysis.

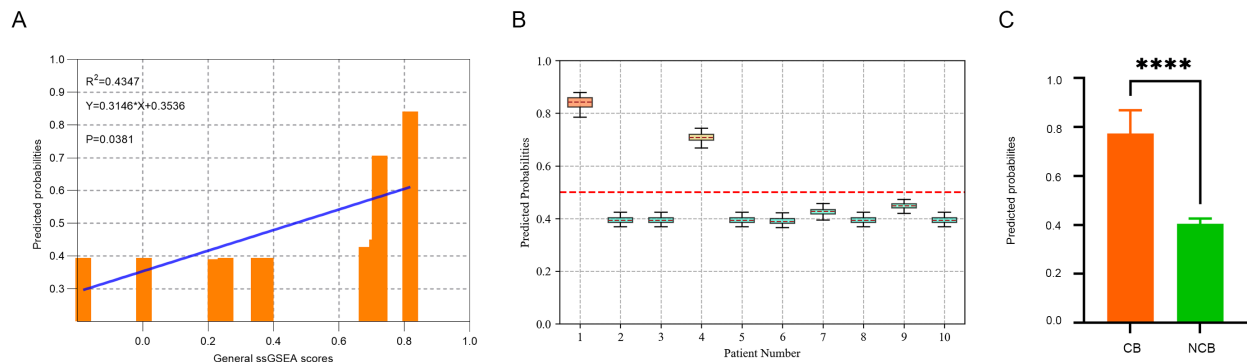


Figure 8. The performance of the established radiomic model in an independent testing cohort. (A) As shown in the diagram of regression analysis, the predictive probability of immune-hot subgroup 1 by radiomic model based on DCE-MRI was positively correlated with the immune scores derived from ssGSEA. (B) The individual predictive probability to be recognized as immune-hot subgroup 1 for each cholangiocarcinoma patient in the testing cohort ($n=10$) was calculated by the established radiomic model. (C) The relationship between the status of actual response to ICB treatment (CB vs NCB) and the predicted probability of being immune-related subgroup 1 for was tested by Mann-Whitney U test.

surgery with complete DCE-MRI information before treatment were included as an independent testing cohort. Regression analysis indicated that the individual probability of being predicted as immune-hot subgroup 1 by radiomics based on DCE-MRI was positively correlated with corresponding individual immune score derived from ssGSEA (Figure. 8A). As exhibited in Figure. 8B, the individual predictive probability of being recognized as immune-hot subgroup 1 for each cholangiocarcinoma patient was calculated by using the established radiomic model. Among the 10 candidates, patients NO.1 and NO.4 with predictive probabilities higher than 0.5 were considered as immune-hot subgroup

1, whereas other patients with predictive probabilities lower than 0.5 were predicted as immune-cold or immune-deficient subgroup 2 (Figure. 8B). Expectedly, based on the actual therapeutic effect evaluation for immunotherapy, patients NO.1 and NO.4 were divided into "clinical benefit (CB)" group who were with partial response (PR). In contrast, other patients were categorized into the "non-clinical benefit (NCB)" group with progressive disease (PD). The relationship between the status of actual response to ICB treatment (CB vs NCB) and the predicted probability of being immune-related subgroup 1 for individual cholangiocarcinoma patient was tested by Mann-Whitney U test (Figure. 8C,

$P < 0.0001$), which further verified that the established radiomic signature model was potentially predictive of immunotherapy for cholangiocarcinoma.

4. Discussion

Immunotherapy is emerging as a potentially promising treatment strategy for cholangiocarcinoma (25). To further improve the clinical benefit of immunotherapy for cholangiocarcinoma, a noninvasive and accurate selection of potentially responsive patient candidates prior to treatment is urgently required (26,27). In the present investigation, an established radiomic signature model based on DCE-MRI was potentially predictive of immune-related subgroup classification for cholangiocarcinoma, allowing for a noninvasive and reliable characterization of local tumor immune landscape to guide immunotherapy for cholangiocarcinoma.

The local immune landscape plays an important role in individualized treatment and precision medicine, particularly for tumor immunotherapy (5). On the one hand, characterization of the local tumor immune landscape is needed to guide tumor immunotherapy; On the other hand, a comprehensive and precise determination of tumor immune status is challenging. Currently, immune-related subgroup classification based on transcriptome sequencing is becoming a trend to predict potential response to tumor immunotherapy prior to treatment. Especially, distinct immune-associated subtypes in human cholangiocarcinoma (22,23,28) and hepatocellular carcinoma (27) were reported previously based on sequencing data. In our study, two immune-related subgroups clustering was attained based on tumor mRNA sequencing data through a K-means algorithm, a classical unsupervised learning algorithm of artificial intelligence. These classified two subgroups characterized by different immune landscapes represented potential responder and non-responder to immunotherapy for cholangiocarcinoma, respectively. Multiomic analyses also demonstrated a noticeable advantage of personalized treatment based on TME profiling over molecular targeting therapy based on tumor heterogeneity profiling, considering the more feasibility and the longer-lasting therapeutic effect of the former than the latter (28-30). However, similar to IHC assay and flow cytometric assay for tumor immune status determination, transcriptome sequencing was also an invasive approach and dependent on specimen availability. With the development of computing techniques and big data processing algorithms, radiomics and derivative radiogenomics or radiotranscriptomics based on both medical images and sequencing data are emerging as a noninvasive, repetitive and reliable method to reveal the underlying biological and molecular mechanism for heterogeneity reflected in radiological features (31,32). Though the studies with regard to the biological validation of radiomic findings are increasingly required to conduct, we have to keep in

mind that the level of biological insight and analytical tools used in genomics or transcriptomics are largely not available for radiomics. As the field of radiomics grows, more and more relationships between radiomic features and radiomic meaning are being revealed, and a relevant database platform is expected to establish.

In the study, a large amount of radiomic features captured in the DCE-MRI images were extracted and selected to build a multivariate radiomic signature model to predict immune-related subgroup classification. As shown in the results of ROC analysis, the constructed radiomic signature model was able to discriminate between different immune-related subgroups with an AUC of up to 0.80. Among the finally selected 10 radiomic features for construction of the predictive model in the study, five of them were from original texture features, whereas the other five were from wavelet radiomic features. Additionally, the selected radiomic features consist of 7 from the non-enhanced phase, 2 from the arterial phase and 1 from the venous phase. Consistently, it was found that the predictive radiomic signature was mainly composed by maximum, median, entropy, kurtosis, emphasis, correlation and non-uniformity. All of these features contributed to reflect the heterogeneity captured in the DCE-MRI images from different aspects, suggesting that the established radiomic model was capable of predicting the immune status in TME by quantitatively characterizing heterogeneity reflected in the DCE-MRI images. Although predictive radiomic models based on MRI for immunotherapy were already previously reported for several types of cancer, such as breast cancer (33), MRI-derived radiomics with regard to immunotherapy for cholangiocarcinoma was rare. Though investigations conducted by Zhang *et al* (18,19) mainly focused on the relationship between MRI-derived radiomic signature and immunophenotyping and survival for cholangiocarcinoma, only the status of PD-1/PD-L1 status and CD8⁺ T cells infiltration were determined to represent the immune profile for cholangiocarcinoma. However, patient clustering based on a comprehensive characterization of the TME to perform subsequent radiomic analysis needs to be improved in their studies. In the present study, radiotranscriptomics but not radiomics was performed to identify the potential association between tumor immune profile and developed radiomic signature model based on MRI for cholangiocarcinoma. Study from Wang *et al*. (34) also revealed a link between radiomic biomarker and TME in breast cancer, consistent with our investigation. However, only MRI images from one single phase, usually arterial phase, were commonly used to establish radiomic signature model by previous investigations (17,18). The radiomic model developed in our study was based on four phase images of DCE-MRI. Presumably, multi-phase DCE-MRI radiomics was able to provide more information about heterogeneity in TME in contrast with radiomics from single-phase images. As reported by

Li *et al.*, machine learning based on multi-phase images, DCE-MRI outperformed single-phase MRI in early prediction of pathological complete response (pCR) to neoadjuvant therapy (NAT) in human epithelial growth factor receptor 2 (HER2) positive invasive breast cancer (35).

Noticeably, an independent testing cohort of cholangiocarcinoma patients with immunotherapy who underwent both tumor transcriptome sequencing and DCE-MRI examination prior to treatment were also enrolled in the study to validate the predictive power of the constructed radiomic signature model in immunotherapy for cholangiocarcinoma. As shown, the significant relationship between the predictive probability of being immune-related subgroup 1 by this established model and actual therapeutic response state to immunotherapy highly suggested the capacity of this model to effectively predict immunotherapy for cholangiocarcinoma.

Apart from MRI-derived radiomics, artificial intelligence (AI) techniques based on other clinical imaging modalities were also helpful to tumor immunotherapy, especially for ^{18}F -Fluorodeoxyglucose positron emission tomography/computed tomography (^{18}F -FDG PET/CT) imaging (36,37). As known, both attenuated tumor immunity and tumor metabolic reprogramming, which are also intimately correlated, are important hallmarks of tumor (38,39). In our previous work, immunosuppression in HCC could be induced by metabolic modulation (40). Accordingly, ^{18}F -FDG PET images, which could provide metabolic information in tumors, is promisingly predictive of the immune profile in TME and potentially applied in tumor immunotherapy. Consistently, PET-derived radiomics was also reported to be able to reveal transcriptomics in cancer (41). Furthermore, the predictive roles of AI analysis based on PET/CT images in immune profiling, immunotherapy response and survival for NSCLC were suggested by previous investigations (42,43). With the development of immuno-PET techniques and AI techniques, direct integration of them is expected to accurately predict tumor immunotherapy (44,45).

Despite the encouraging results in this study, several limitations in the current work need to be addressed. First, only cholangiocarcinoma patients with preoperative DCE-MRI and postoperative transcriptome sequencing and IHC staining for immune cell infiltration were included, which resulted in a limited sample size for radiomic analysis. However, this primary radiotranscriptomic analysis shed light on the biological validation of established predictive radiomic models for immunotherapy in cholangiocarcinoma, because relevant investigation is rare due to the lack of simultaneous collection of imaging data and tumor mRNA sequencing data for cholangiocarcinoma from other research groups and public database, such as the Cancer Genome Atlas (TCGA) with imaging information from The cancer

Imaging Archive (TCIA). Additionally, the potential overfitting of this predictive radiomic model was prevented by cross-validation with repetition for 50 times and inclusion of an independent testing cohort, and the analytical results from both the Chi-Square Goodness-of-Fit test and calibration curve analysis suggested a low likelihood of overfitting for this model. For sure, a prospective trial in the near future is needed to verify the results; Second, limited by the small sample size of this single-center study, a further study with a larger training cohort and external test cohorts from multi-center was warranted to confirm the conclusion obtained in the work. Then, TILs representation in cholangiocarcinoma specimens was only evaluated by IHC assay, an immunologic function assay was not performed to analyze the functional status of immune cells in local TME. With a sufficient size of specimen, cytometric analyses based on fresh isolation of TILs from tissue samples would partially address this issue. In the end, a comprehensive model involving both radiomic features and clinicopathological parameters was expected to develop to noninvasively predict the response probability to immunotherapy for cholangiocarcinoma.

5. Conclusion

The local tumor immune microenvironment is increasingly accepted as a vital factor influencing the sensitivity and outcome of tumor immunotherapy. Thus, characterization of the immune status in TME prior to tumor immunotherapy allows for the selection of potentially responsive candidates who would benefit from immunotherapy. An immune-related subgroup classification based on RNA sequencing data is capable of providing comprehensive information for immune profiling in cholangiocarcinoma. Furthermore, the developed radiomic model based on DCE-MRI in the study is potentially applied as a noninvasive, repetitive and reliable approach to predict the immune-related subgroup classification and response probability to immunotherapy for cholangiocarcinoma.

Funding: This work was supported by a grant from the national natural science foundation of China (grant nos. 82272074, 82373365), the natural science foundation of our city (21JCQNJC01290), the health science and technology project in our city (TJWJ2022MS008), the key medical discipline (Pathology) construction project in our city (TJYXZDXK-012A), the Key Medical Discipline (Specialty) construction project (TJYXZDXK-009A) and the accurate diagnosis of tumor and pharmacotherapy technology construction project in our institution (grant nos. ZLJZZDYYWZL11 and ZLJZZDYYWZL03).

Conflict of Interest: The authors have no conflicts of interest to disclose.

References

- Bray F, Ferlay J, Soerjomataram I, Siegel RL, Torre LA, Jemal A. Global cancer statistics 2018: GLOBOCAN estimates of incidence and mortality worldwide for 36 cancers in 185 countries. *CA Cancer J Clin.* 2018; 68:394-424.
- Siegel RL, Miller KD, Fuchs HE, Jemal A. Cancer Statistics, 2021. *CA Cancer J Clin.* 2021; 71:7-33.
- Bridgewater J, Galle PR, Khan SA, Llovet JM, Park JW, Patel T, Pawlik TM, Gores GJ. Guidelines for the diagnosis and management of intrahepatic cholangiocarcinoma. *J Hepatol.* 2014; 60:1268-1289.
- Rizvi S, Khan SA, Hallemeier CL, Kelley RK, Gores GJ. Cholangiocarcinoma-evolving concepts and therapeutic strategies. *Nat Rev Clin Oncol.* 2018; 15:95-111.
- Sadeghi Rad H, Monkman J, Warkiani ME, Ladwa R, O'Byrne K, Rezaei N, Kulasinghe A. Understanding the tumor microenvironment for effective immunotherapy. *Med Res Rev.* 2021; 41:1474-98.
- Charalampakis N, Papageorgiou G, Tsakatikas S, Fioretzaki R, Kole C, Kykalos S, Tolia M, Schizas D. Immunotherapy for cholangiocarcinoma: A 2021 update. *Immunotherapy.* 2021; 13:1113-1134.
- Al-Rajabi R, Sun W. Immunotherapy in cholangiocarcinoma. *Curr Opin Gastroenterol.* 2021; 37:105-111.
- Carlino MS, Larkin J, Long GV. Immune checkpoint inhibitors in melanoma. *Lancet.* 2021; 398:1002-1014.
- Kline J, Godfrey J, Ansell SM. The immune landscape and response to immune checkpoint blockade therapy in lymphoma. *Blood.* 2020; 135:523-533.
- Lin A, Wei T, Meng H, Luo P, Zhang J. Role of the dynamic tumor microenvironment in controversies regarding immune checkpoint inhibitors for the treatment of non-small cell lung cancer (NSCLC) with EGFR mutations. *Mol Cancer.* 2019; 18:139.
- Bashash D, Zandi Z, Kashani B, Pourbagheri-Sigaroodi A, Salari S, Ghaffari SH. Resistance to immunotherapy in human malignancies: Mechanisms, research progresses, challenges, and opportunities. *J Cell Physiol.* 2022; 237:346-372.
- Gibney GT, Weiner LM, Atkins MB. Predictive biomarkers for checkpoint inhibitor-based immunotherapy. *Lancet Oncol.* 2016; 17:e542-e551.
- Ren D, Hua Y, Yu B, *et al.* Predictive biomarkers and mechanisms underlying resistance to PD1/PD-L1 blockade cancer immunotherapy. *Mol Cancer.* 2020; 19:19.
- Paijens ST, Vledder A, de Bruyn M, Nijman HW. Tumor-infiltrating lymphocytes in the immunotherapy era. *Cell Mol Immunol.* 2021; 18:842-859.
- Patel SP, Kurzrock R. PD-L1 Expression as a Predictive Biomarker in Cancer Immunotherapy. *Mol Cancer Ther.* 2015; 14:847-856.
- Xia T, Li K, Niu N, *et al.* Immune cell atlas of cholangiocarcinomas reveals distinct tumor microenvironments and associated prognoses. *J Hematol Oncol.* 2022; 15:37.
- Min JH, Kim YK, Choi SY, Kang TW, Lee SJ, Kim JM, Ahn S, Cho H. Intrahepatic Mass-forming Cholangiocarcinoma: Arterial Enhancement Patterns at MRI and Prognosis. *Radiology.* 2019; 290(3):691-699.
- Zhang J, Wu Z, Zhao J, Liu S, Zhang X, Yuan F, Shi Y, Song B. Intrahepatic cholangiocarcinoma: MRI texture signature as predictive biomarkers of immunophenotyping and survival. *Eur Radiol.* 2021; 31:3661-3672.
- Zhang J, Wu Z, Zhang X, Liu S, Zhao J, Yuan F, Shi Y, Song B. Machine learning: an approach to preoperatively predict PD-1/PD-L1 expression and outcome in intrahepatic cholangiocarcinoma using MRI biomarkers. *ESMO Open.* 2020; 5:e000910.
- Mayerhoefer ME, Materka A, Langs G, Häggström I, Szczypiński P, Gibbs P, Cook G. Introduction to Radiomics. *J Nucl Med.* 2020; 61:488-495.
- Job S, Rapoud D, Dos Santos A, *et al.* Identification of Four Immune Subtypes Characterized by Distinct Composition and Functions of Tumor Microenvironment in Intrahepatic Cholangiocarcinoma. *Hepatology.* 2020; 72:965-981.
- Huang X, Tang T, Zhang G, Liang T. Identification of tumor antigens and immune subtypes of cholangiocarcinoma for mRNA vaccine development. *Mol Cancer.* 2021; 20:50.
- Li S, Xu F, Li H, Zhang J, Zhong A, Huang B, Lai M. S100A8+ stroma cells predict a good prognosis and inhibit aggressiveness in colorectal carcinoma. *Oncimmunology.* 2016; 6:e1260213.
- Fiste O, Ntanasis-Stathopoulos I, Gavriatopoulou M, Lontos M, Koutsoukos K, Dimopoulos MA, Zagouri F. The Emerging Role of Immunotherapy in Intrahepatic Cholangiocarcinoma. *Vaccines (Basel).* 2021; 9:422.
- Du Y, Qi Y, Jin Z, Tian J. Noninvasive imaging in cancer immunotherapy: The way to precision medicine. *Cancer Lett.* 2019; 466:13-22.
- Deutsch E, Paragios N. Radiomics to predict response to immunotherapy, bridging the gap from proof of concept to clinical applicability? *Ann Oncol.* 2019; 30:879-881.
- Chen S, Xie Y, Cai Y, *et al.* Multiomic Analysis Reveals Comprehensive Tumor Heterogeneity and Distinct Immune Subtypes in Multifocal Intrahepatic Cholangiocarcinoma. *Clin Cancer Res.* 2022; 28:1896-1910.
- Ho DW, Tsui YM, Chan LK, *et al.* Single-cell RNA sequencing shows the immunosuppressive landscape and tumor heterogeneity of HBV-associated hepatocellular carcinoma. *Nat Commun.* 2021; 12:3684.
- Zhang Q, Lou Y, Yang J, *et al.* Integrated multiomic analysis reveals comprehensive tumour heterogeneity and novel immunophenotypic classification in hepatocellular carcinomas. *Gut.* 2019; 68:2019-2031.
- Martin-Serrano MA, Kepecs B, Torres-Martin M, *et al.* Novel microenvironment-based classification of intrahepatic cholangiocarcinoma with therapeutic implications. *Gut.* 2023; 72:736-748.
- Jeong WK, Jamshidi N, Felker ER, Raman SS, Lu DS. Radiomics and radiogenomics of primary liver cancers. *Clin Mol Hepatol.* 2019; 25:21-29.
- Saini A, Breen I, Pershad Y, Naidu S. Radiogenomics and Radiomics in Liver Cancers. *Diagnostics (Basel).* 2018; 9:4.
- Bian T, Wu Z, Lin Q, Mao Y, Wang H, Chen J, Chen Q, Fu G, Cui C, Su X. Evaluating Tumor-Infiltrating Lymphocytes in Breast Cancer Using Preoperative MRI-Based Radiomics. *J Magn Reson Imaging.* 2022; 55:772-784.
- Wang X, Xie T, Luo J, Zhou Z, Yu X, Guo X. Radiomics predicts the prognosis of patients with locally advanced breast cancer by reflecting the heterogeneity of tumor

- cells and the tumor microenvironment. *Breast Cancer Res.* 2022; 24:20.
35. Li Q, Xiao Q, Li J, Wang Z, Wang H, Gu Y. Value of Machine Learning with Multiphases CE-MRI Radiomics for Early Prediction of Pathological Complete Response to Neoadjuvant Therapy in HER2-Positive Invasive Breast Cancer. *Cancer Manag Res.* 2021; 13:5053-5062.
 36. Mu W, Tunali I, Gray JE, Qi J, Schabath MB, Gillies RJ. Radiomics of 18F-FDG PET/CT images predicts clinical benefit of advanced NSCLC patients to checkpoint blockade immunotherapy. *Eur J Nucl Med Mol Imaging.* 2020; 47:1168-1182.
 37. Mu W, Jiang L, Shi Y, Tunali I, Gray JE, Katsoulakis E, Tian J, Gillies RJ, Schabath MB. Non-invasive measurement of PD-L1 status and prediction of immunotherapy response using deep learning of PET/CT images. *J Immunother Cancer.* 2021; 9:e002118.
 38. RRenner K, Singer K, Koehl GE, Geissler EK, Peter K, Siska PJ, Kreutz M. Metabolic Hallmarks of Tumor and Immune Cells in the Tumor Microenvironment. *Front Immunol.* 2017; 8:248.
 39. Bader JE, Voss K, Rathmell JC. Targeting Metabolism to Improve the Tumor Microenvironment for Cancer Immunotherapy. *Mol Cell.* 2020; 78:1019-1033.
 40. Li X, Zhang Y, Ma W, Fu Q, Liu J, Yin G, Chen P, Dai D, Chen W, Qi L, Yu X, Xu W. Enhanced glucose metabolism mediated by CD147 contributes to immunosuppression in hepatocellular carcinoma. *Cancer Immunol Immunother.* 2020; 69:535-548.
 41. Tixier F, Cheze-le-Rest C, Schick U, Simon B, Dufour X, Key S, Pradier O, Aubry M, Hatt M, Corcos L, Visvikis D. Transcriptomics in cancer revealed by Positron Emission Tomography radiomics. *Sci Rep.* 2020; 10:5660.
 42. Polverari G, Ceci F, Bertaglia V, Reale ML, Rampado O, Gallio E, Passera R, Liberini V, Scapoli P, Arena V, Racca M, Veltri A, Novello S, Deandreis D. 18F-FDG Pet Parameters and Radiomics Features Analysis in Advanced Nsclc Treated with Immunotherapy as Predictors of Therapy Response and Survival. *Cancers (Basel).* 2020; 12:1163.
 43. Tong H, Sun J, Fang J, Zhang M, Liu H, Xia R, Zhou W, Liu K, Chen X. A Machine Learning Model Based on PET/CT Radiomics and Clinical Characteristics Predicts Tumor Immune Profiles in Non-Small Cell Lung Cancer: A Retrospective Multicohort Study. *Front Immunol.* 2022; 13:859323.
 44. Liberini V, Laudicella R, Capozza M, Huellner MW, Burger IA, Baldari S, Terreno E, Deandreis D. The Future of Cancer Diagnosis, Treatment and Surveillance: A Systemic Review on Immunotherapy and Immuno-PET Radiotracers. *Molecules.* 2021; 26:2201.
 45. Derclé L, Sun S, Seban RD, *et al.* Emerging and Evolving Concepts in Cancer Immunotherapy Imaging. *Radiology.* 2023; 306:32-46.
- Received May 8, 2024; Revised June 7, 2024; Accepted June 9, 2024.
- §These authors contributed equally to this work.
- *Address correspondence to:
Xiaofeng Li and Lisha Qi, Tianjin Medical University Cancer Institute and Hospital, Huan-Hu-Xi Road, Ti-Yuan-Bei, He Xi District, Tianjin 300060, PR China.
E-mail: Xli03@tmu.edu.cn (Xiaofeng Li); Lqi01@tmu.edu.cn (Lisha Qi)
- Released online in J-STAGE as advance publication June 10, 2024.

Establishment of nomogram prediction model of contrast-enhanced ultrasound and Gd-EOB-DTPA-enhanced MRI for vessels encapsulating tumor clusters pattern of hepatocellular carcinoma

Feiqian Wang^{1,2}, Kazushi Numata^{2,*}, Akihiro Funaoka², Xi Liu³, Takafumi Kumamoto², Kazuhisa Takeda², Makoto Chuma², Akito Nozaki², Litao Ruan¹, Shin Maeda⁴

¹Department of Ultrasound, The First Affiliated Hospital of Xi'an Jiaotong University, Xi'an, Shaanxi, China;

²Gastroenterological Center, Yokohama City University Medical Center, Yokohama, Kanagawa, Japan;

³Department of Pathology, The First Affiliated Hospital of Xi'an Jiaotong University, Xi'an, Shaanxi, China;

⁴Division of Gastroenterology, Yokohama City University Graduate School of Medicine, Yokohama, Kanagawa, Japan.

SUMMARY To establish clinical prediction models of vessels encapsulating tumor clusters (VETC) pattern using preoperative contrast-enhanced ultrasound (CEUS) and gadolinium-ethoxybenzyl-diethylenetriamine pentaacetic acid magnetic resonance imaging (EOB-MRI) in patients with hepatocellular carcinoma (HCC). A total of 111 resected HCC lesions from 101 patients were included. Preoperative imaging features of CEUS and EOB-MRI, postoperative recurrence, and survival information were collected from medical records. The best subset regression and multivariable Cox regression were used to select variables to establish the prediction model. The VETC-positive group had a statistically lower survival rate than the VETC-negative group. The selected variables were peritumoral enhancement in the arterial phase (AP), hepatobiliary phase (HBP) on EOB-MRI, intratumoral branching enhancement in the AP of CEUS, intratumoral hypoenhancement in the portal phase of CEUS, incomplete capsule, and tumor size. A nomogram was developed. High and low nomogram scores with a cutoff value of 168 points showed different recurrence-free survival rates and overall survival rates. The area under the curve (AUC) and accuracy were 0.804 and 0.820, respectively, indicating good discrimination. Decision curve analysis showed a good clinical net benefit (threshold probability > 5%), while the Hosmer-Lemeshow test yielded excellent calibration ($P = 0.6759$). The AUC of the nomogram model combining EOB-MRI and CEUS was higher than that of the models with EOB-MRI factors only (0.767) and CEUS factors only (0.7). The nomogram verified by bootstrapping showed AUC and calibration curves similar to those of the nomogram model. The Prediction model based on CEUS and EOB-MRI is effective for preoperative noninvasive diagnosis of VETC.

Keywords vessels encapsulating tumor clusters, diagnosis, hepatocellular carcinoma, contrast-enhanced ultrasound, gadolinium-ethoxybenzyl-diethylenetriamine, pentaacetic acid magnetic resonance imaging

1. Introduction

Approximately 40–70% hepatocellular carcinoma (HCC) patients suffer from postoperative recurrence within 5 years (1). The intrahepatic metastasis rate was 78.5%, according to an autopsy study of 240 patients with HCC in Japan (2). Because metastasis and recurrence of HCC can seriously affect the survival of patients, its mechanism has been extensively explored. Vessels encapsulating tumor clusters (VETC) patterns are a recently discovered tumor vascular growth pattern (3). VETC coating provides an "integrated ecosystem" that

can protect or shield tumor cells from anoikis (apoptosis upon loss of attachment to the extracellular matrix), shearing forces in the bloodstream, and immunological attack (3). Thus, it has a very strong invasion potential. VETC patterns have been reported to be able to predict the response and prognosis after various treatments for HCC, including transcatheter artery chemoembolization (TACE) benefit (4,5), liver transplantation (6), and sorafenib (7). VETC was independently associated with early recurrence within 2 years (hazard ratio [HR]: 1.52, $P = 0.023$), disease-free survival (HR: 1.66, $P = 0.002$), and overall survival (OS) (HR: 2.26, $P = 0.001$)

(8). Currently, the diagnosis of VETC patterns can only be assessed by histopathological staining of surgically resected tissue with endothelial cell-specific markers such as cluster of differentiation (CD)34 and CD31. In addition, for patients who cannot be treated with surgical resection, a histopathology-based VETC diagnosis cannot be obtained. Therefore, it is of great clinical significance to use a modality independent of pathology to accurately diagnose VETC, especially to predict VETC before surgery.

Among all imaging modalities, contrast-enhanced ultrasound (CEUS) using Sonazoid agent and magnetic resonance imaging using gadolinium-ethoxybenzyl-diethylenetriamine penta-acetic acid (EOB-MRI) have been highlighted as breakthrough imaging modalities for HCC diagnosis (9). CEUS and EOB-MRI have the widely recognized advantages of nonradiation, noninvasive, good repeatability, and few side effects (10). The microbubbles of contrast agents are not metabolized by the liver and kidney; thus, CEUS is safer than enhanced CT and MRI for patients with poor liver and kidney function. The Japan Society of Hepatology (JSH) and European Association for the Study of the Liver (EASL) guidelines recommend EOB-MRI and CEUS as first- and second-line approaches for liver cancer diagnosis, respectively (11,12). Chinese guidelines recommend CEUS as a first-line examination for high-risk populations of HCC (13). In real-world practice, some indicators in EOB-MRI have been reported to be associated with the occurrence of VETC in patients with HCC (14,15). However, the reported diagnostic strategy based on MRI features is not good enough to provide a satisfactory diagnosis (pooled accuracy was 57.6–74%) (16). Sonazoid agents are pure blood pool microbubbles that cannot enter the stroma (10). Therefore, it can be used to evaluate blood perfusion and microcirculation. We previously found that EOB-MRI is more likely to miss the detection of intratumoral hypervascularity than CEUS in small lesions ($P = 0.012$), heterogeneity ($P = 0.013$), and slight enhancement in arterial phase (AP) ($P = 0.009$) (17). Regrettably, there is very little English literature on the application of CEUS for the preoperative diagnosis of VETC (18,19). By combining two or more imaging techniques, multimodal imaging is believed to enhance the diagnostic accuracy by overcoming the limitations of independent techniques and providing a large amount of information to minimize the risk of false positives or negatives (20). As the quality of CEUS images is easily affected by lung gas and depth of the target lesion, we considered multimodal imaging of EOB-MRI and CEUS as a way to research VETC patterns.

Therefore, the primary aim of our study was to estimate the value of preoperative multimodal imaging using CEUS and EOB-MRI for predicting VETC patterns. Compared to conventional prediction approaches, nomograms present an excellent graphical

easy-to-interpret visualization; by combining patients' characteristics and statistical models constructed based on diagnostic tests, higher accuracy can be achieved, facilitating the clinical decision-making process (21). In order for our study to be adapted to clinical needs (individualized and easy to use), the secondary aim was to establish a clinical predictive model of VETC patterns.

2. Materials and Methods

2.1. Patients Enrollment

Between September 2007 and December 2021, 196 patients with 218 HCC lesions were enrolled in this study. The inclusion criteria were as follows: (1) adult patients (≥ 18 years old); (2) non-pregnancy and/or non-lactation; (3) clear pathological diagnosis of HCC; and (4) definite diagnosis of VETC pattern according to the gold standard of CD34 staining in surgical specimens. The exclusion criteria were as follows: (1) either CEUS or EOB-MRI not performed within one month before hepatectomy ($N/n = 43/47$); (2) Child-Pugh grade C ($N/n = 12/12$); (3) already treated HCC lesions ($N/n = 13/15$); (4) history of other cancers ($N/n = 10/13$); (5) poor image quality, which affected the analysis of the indicators ($N/n = 8/8$); and (6) incomplete preoperative serological data ($N/n = 7/10$). After the above screening, 101 HCC patients with 111 lesions were included in this study, including 24 VETC-positive lesions and 87 VETC-negative lesions (Figure 1). This study was approved by the Ethics Review Board (No. F220700009 on June 27, 2022) of Yokohama City University Medical Center, Japan. The requirement for informed consent was waived owing to the retrospective nature of the study.

The general baseline demographic data (including age, sex, etiology of hepatitis of patients, degree of liver fibrosis, and size of the lesion) and preoperative serological indicators (including α -fetoprotein (AFP), serum albumin (Alb), total bilirubin (T-BIL), prothrombin time (Pt), platelet counts (Plt), prothrombin induced by vitamin K absence II (PIVKA-II), and indocyanine green 15 min retention (ICG-R15)) were obtained by retrospectively searching the electronic medical record system.

2.2. Grayscale US and CEUS examination

A LOGIQ E9 US system (GE Healthcare, Milwaukee, WI, USA) equipped with native tissue harmonic grayscale imaging and CEUS functions was used. Convexes and microconvexities with frequencies of 1–6 MHz and 2–5 MHz, respectively, were used. A 0.2 mL dose of perfluorobutane microbubbles (Sonazoid®, Daiichi Sankyo, Tokyo, Japan) was injected into the antecubital vein (0.2 mL/s *via* a 24-gauge cannula, followed by 2 mL of 5% glucose). CEUS images were acquired during three contrast phases: AP, portal phase

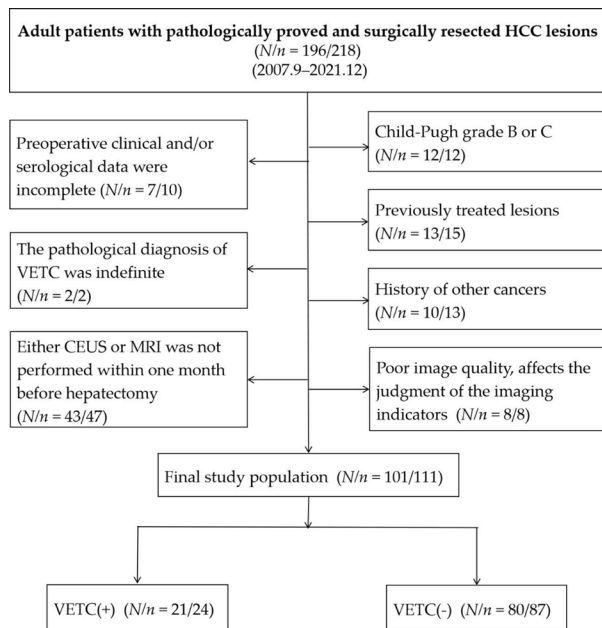


Figure 1. Flowchart of the study population. HCC: hepatocellular carcinoma; VETC: vessels encapsulating tumor clusters; CEUS: Contrast-enhanced ultrasound; EOB-MRI: Gadolinium-Ethoxybenzyl-Diethylenetriamine Penta-Acetic Acid magnetic-resonance imaging.

(PP), and postvascular phase (PVP) (10–50 and 80–120 s, and 10 min after injection, respectively). Low mechanical index mode (0.2–0.3) was used for CEUS examination.

2.3. EOB-MRI examination

MR was performed using a 1.5 T whole-body imager (Avant; Siemens Medical Systems, Erlangen, Germany). A power injector (Spectris Solaris EP; MEDRAD, Bayer Schering Pharma AG, Berlin, Germany) was used to inject 0.1 mmol/kg of Gd-EOB-DTPA (Primovist; Bayer Schering Pharma AG, Berlin, Germany) at 1 mL/s through a catheter placed in the antecubital vein, followed by flushing with 20 mL of sterile saline solution at 2 mL/s. AP, PP, late-phase, and hepatobiliary phase (HBP) scanning was performed at 25–30 s, 70–85 s, 180 s, and 20 min after initiation of the contrast injection, respectively. Images were obtained using fat-suppressed volumetric interpolated breath-hold examination (FS VIBE) T1-weighted sequences (TR, 6.2 ms; TE, 3.15 ms; flip angle, 20°; bandwidth, 260 Hz/pix; matrix, 166 × 320; acquisition time, 20 s). In addition, a fast low-angle shot (FLASH) T1-weighted sequence (TR, 115 ms; TE, 4.76 ms; flip angle, 70°; bandwidth, 260 Hz/pix; matrix, 192 × 256; acquisition time, 20 s × 3) was performed.

2.4. Interpretation of Key Imaging Features

Two doctors (F. W. and A.F., with 11 and 5 years of experience in abdominal imaging diagnosis, respectively) independently evaluated the image features of CEUS and EOB-MRI, respectively. When there were inconsistent

results between the two doctors after the first image analysis, a final decision was made by an expert (K. N., with 35 years of experience in liver imaging diagnosis).

The CEUS imaging features included the following: 1) Size: the largest axial diameter on the grayscale images. If the lesion was indistinct (especially if it was isoechogenic) on the grayscale US image, size measurement on the AP or PVP of the CEUS images could be performed. 2) AP enhancement degree: hyper-/iso-enhancement (comprising more than half of the lesion area). 3) PP enhancement degree: iso-/hypo-enhancement (comprising more than half of the lesion area). 4) PVP enhancement degree: iso-/hypo-enhancement (comprising more than half of the lesion area). 5) Tumor margin (regular/irregular): "Irregular" margin is ill-defined, uneven, and/or lobulated while "regular" margin is well-defined, smooth, and round. 6) Intratumoral branching enhancement: thick or thin continuous strip-like, branching, separation-like enhancement in AP. 7) Intratumoral homogeneity: "homogeneous" enhancement was defined as a whole and diffuse enhancement of the lesion, while "heterogeneous" enhancement was defined as two or more enhancement echoes mixed enhancement of the lesion.

The EOB-MRI features included the following: 1) Intratumoral hyperenhancement in AP: high/iso- or low (compared with the background liver parenchyma). 2) Intratumoral hypoenhancement in HBP: low/iso- or high (compared to background liver parenchyma). 3) Peritumoral irregular hyperenhancement in AP: existence of a visible portion adjacent to the lesion enhanced at the AP. 4) Peritumoral hypoenhancement in HBP: Peritumoral parenchymal enhancement with a wedge-shaped or bud-shaped protrusion in HBP. 5) Presence of capsule: thin uniform ring-like enhancement surrounding the tumor (which was different from that of the lesion or surrounding tissue) on the AP or HBP images. 6) Incomplete capsule: A certain area of the capsule is disrupted or even disappears. 7) Intratumoral homogeneity, "homogeneous" enhancement was defined as a whole and diffuse enhancement of the lesion, while "heterogeneous" enhancement was defined as the mixed enhancement of two or more enhancement echoes of the lesion.

2.5. Histopathologic Examination

A senior pathologist (X.L., working in the field of liver pathological diagnosis for 12 years) reviewed all surgical specimens to identify VETC patterns. The VETC pattern is defined as the presence of sinusoid-like vessels that form web-like networks and encapsulate individual tumor clusters on imaging with CD34 immunostaining (21). Cases with a visible VETC pattern in whole or part of the CD34 slides were identified as VETC positivity, and those without any VETC pattern were identified as VETC negativity (Figure 2).

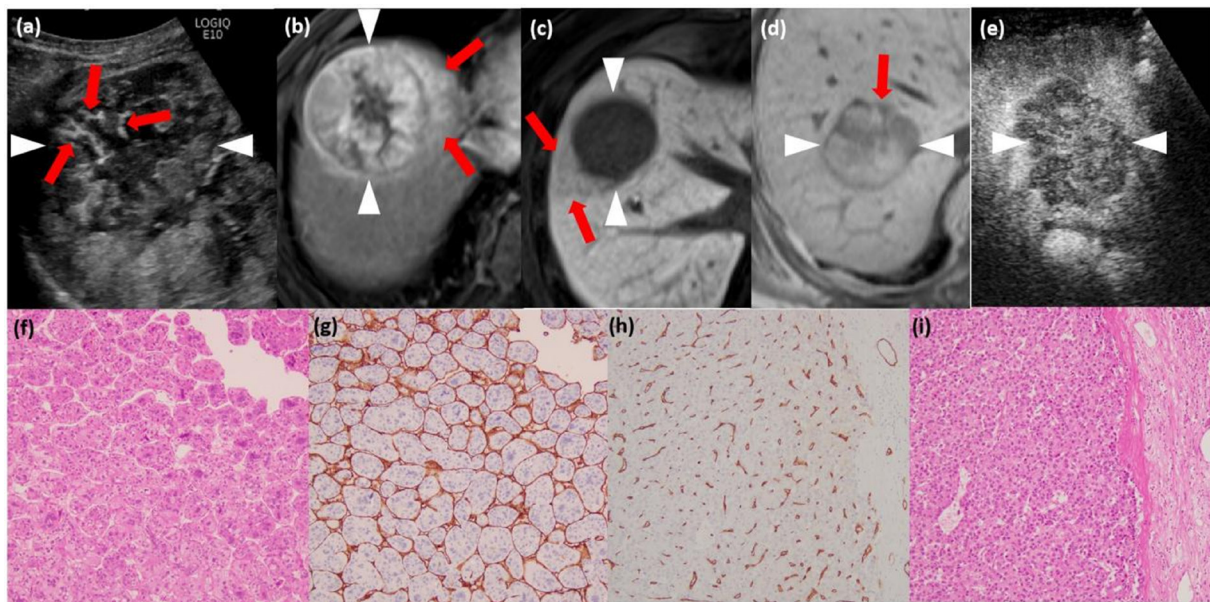


Figure 2. Typical imaging features and histological photos. (a) shows branching enhancement in AP of CEUS (arrow). (b) shows peritumoral hyperenhancement in AP of EOB-MRI (arrow) and intratumoral "heterogeneous" enhancement. (c) exhibit peritumoral hypoenhancement in HBP of EOB-MRI (arrow) and intratumoral "homogeneous" enhancement. (d) exhibit incomplete capsule of the lesion (arrow) and intratumoral "heterogeneous" enhancement in HBP of EOB-MRI. (e) shows irregular margin in PVP of CEUS and "heterogeneous" enhancement. Arrowheads in (a) to (e) represent the lesion. (f) and (i) are based on Hematoxylin & Eosin stain, while (g) and (h) are immunohistochemical staining for CD34. (f-g) are a case of VETC positive. (h-i) are another case of VETC negative. (Original magnifications x 100). For VETC positive lesion, endothelial cells envelope the HCC cell clusters and formed spider webs (g), whereas VETC-negative lesion shows only sparse cord-like vessels (h).

2.6. Survival analysis

Patients were followed up by telephone, outpatient visits, and rehospitalization. OS and progression-free survival (PFS) were defined as the interval from the date of operation to the date of last living visit or death and the date of recurrence, respectively. Recurrence was confirmed by CEUS, contrast-enhanced computed tomography (CECT), EOB-MRI, positron emission tomography (PET)-CT, and/or pathological diagnosis such as tumor biopsy. The endpoint for follow-up was March 31, 2024.

2.7. Statistical Analysis

The enumeration data between the VETC-positive and VETC-negative groups were calculated using the chi-square test. Non-normally distributed data are presented as medians and quartiles, and the Mann-Whitney *U* test was used to compare intergroup differences. Continuous variables that showed normal distribution were presented as mean \pm standard deviation and compared using Student's *t*-test. The interobserver variability for radiological features was assessed using the kappa analysis ($\kappa=0.00-0.20$, poor agreement; $\kappa=0.21-0.40$, fair agreement; $\kappa=0.41-0.60$, moderate agreement; $\kappa=0.61-0.80$, good agreement; $\kappa=0.81-1.0$, excellent agreement). Baseline and survival data were analyzed on the basis of patients and non-lesions. When a patient has multiple HCC lesions, the patient is defined as VETC-positive if at least one lesion is VETC-positive. In contrast, the

patient was defined as VETC-negative when all HCC lesions were negative for VETC. Univariate analysis was used to assess the significance of each variable in discriminating the presence of VETC in the training cohort. The selection method of best subset regression (BSR) was used to identify independent predictors and rule out potential confounding variables. The final nomogram model was developed. For the validation process, the receiver operator characteristic curve (ROC) was plotted, the area under the ROC curve (AUC) was estimated, and intergroup differences in the AUC were compared using the DeLong test. Survival curves were plotted using the Kaplan-Meier method. Differences in PFS and OS were calculated using log-rank tests. All statistical analyses were performed using STATA 15.0, R 4.0.3, and MedCalc. Statistical significance was set $P < 0.05$.

3. Results

3.1. Baseline Characteristics

Baseline patient characteristics are summarized in Table 1. The 111 lesions included 87 VETC-negative and 24 VETC-positive. The incidence of VETC was 21.6% at the base of the lesion. The incidence of VETC was 20.8% (21/101) on patient base. The baseline patient characteristics are shown in Table 1. There were no statistical differences in demographic or serological indicators between the VETC-positive and VETC-negative groups.

Table 1. Demographic and serological characteristics of HCC patients^{1,2}

	All n=101	VETC-positive n = 21	VETC-negative n = 80	P value ³
<i>Demographic characteristics</i>				
Age ([median, Q], years)	69.0 (63.0, 75.0)	66.0 (63.0, 74.0)	69.0 (62.8, 75.2)	0.728
Gender (male/female)	81/20	17/4	64/16	1.000
Etiology (HCV/HBV/others ³)	11/47/43	1/11/9	10/36/34	0.688
Cirrhosis (No/Yes)	52/49	12/9	40/40	0.736
<i>Serological characteristics</i>				
AFP ([median, Q], mg/mL)	11.0 (4.00, 137)	11.0 (4.00,342)	11.5 (4.00,129)	0.546
Alb (x±s, g/dL)	4.18±0.51	4.31±0.58	4.14±0.48	0.211
T-BIL ([median, Q], mg/dL)	0.90 (0.70, 1.10)	0.90 (0.60, 1.40)	0.90 (0.70, 1.10)	0.493
PT-INR [median, Q]	1.04 (0.97, 1.12)	1.02 (0.97, 1.12)	1.04 (0.98, 1.11)	0.700
Platelets ([median, Q], 10 ¹⁰ /L]	15.4 (10.7, 20.0)	15.6 (11.8, 23.9)	15.1 (10.6, 19.9)	0.610
PIVKA-II ([median, Q], mAU/mL)	94.0 (28.0, 629)	133 (35.0, 2020)	92.0 (28.0, 613)	0.467
ICG-R15 ([median, Q], %)	15.1 (10.4, 22.1)	12.9 (8.40, 18.9)	15.6 (11.0, 22.8)	0.175

¹Abbreviations: HCC, Hepatocellular carcinoma; VETC, vessels encapsulating tumor clusters; HCV, hepatitis C virus; HBV, hepatitis B virus. AFP, alpha-fetoprotein; Alb, serum albumin; T-BIL, total bilirubin; PT, prothrombin time; INR, international normalized ratio; PIVKA-II, prothrombin induced by vitamin K absence II; ICG-R15: Indocyanine green 15 min retention. x±s: mean ±standard deviation; Q:1st quartile, 4th quartile. ²The groupings of VETC and statistics in this table are based on patients. ³"Others" included etiologies of alcoholic liver disease, non-HBV non-HCV, nonalcoholic steatohepatitis, and primary biliary cirrhosis.

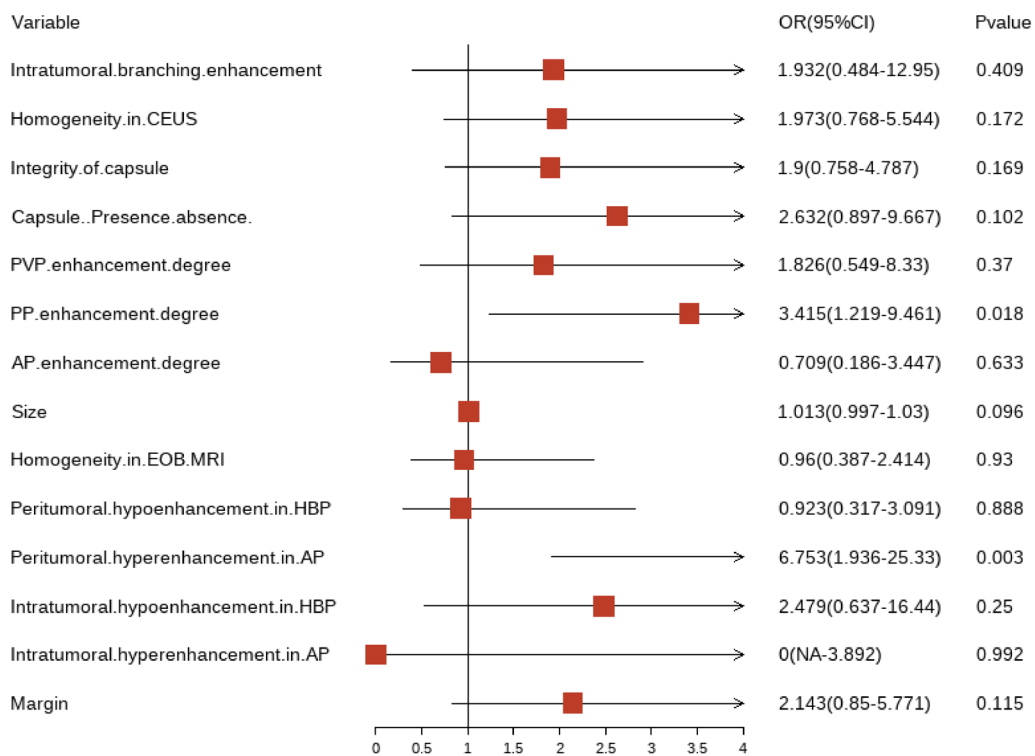


Figure 3. Forest plot demonstrating the univariate regression model for predicting VETC. Abbreviations: CEUS, contrast-enhanced ultrasound; AP, arterial phase; PP, portal phase; PVP, postvascular phase; HBP, hepatobiliary phase; EOB-MRI, magnetic-resonance imaging using gadolinium-ethoxybenzyl-diethylenetriamine penta-acetic acid; OR, odds ratio; VETC, vessels encapsulating tumor clusters.

3.2. Potential risk factors of VETC selection

The interobserver agreement for the radiological features indicated for the VETC patterns was good to excellent between the two doctors (F. W. and A.F.). The kappa values ranged from 0.663 to 0.955 (Table S1, <http://www.biosciencetrends.com/action/getSupplementalData.php?ID=203>).

As shown in Figure 3, an initial variable screening was first performed using univariate analysis. When selecting possible risk factors for establishing a clinical prediction model, the first step of univariate analysis cannot be based on $P < 0.05$ as a general statistical analysis. A typical entry criterion of P -value threshold should be relaxed (such as 0.15 (22), 0.2 (23), 0.25 (24)) to allow more factors that may be relevant to VETC to

Table 2. Final predictors for the risk of VETC in HCC patients¹

Characteristics	Estimate	SE	Z	P	OR	VIF	Tolerance
(Intercept)	-7.666	1.952	-3.927	< 0.001	0.002		
Peritumoral hyperenhancement in AP (presence)	2.386	0.861	2.772	0.006	10.871	1.427	0.7006110
Peritumoral hypoenhancement in HBP (presence)	1.790	0.865	2.070	0.038	5.991	1.715	0.5830635
Size	0.023	0.012	1.874	0.061	1.023	1.570	0.6369370
Enhancement degree in PP (hypo)	1.393	0.613	2.274	0.023	4.027	1.080	0.9262363
Integrity of capsule (incomplete)	1.043	0.543	1.920	0.055	2.839	1.064	0.9394779
Intratumoral branching enhancement in CEUS (presence)	1.702	1.042	1.634	0.102	5.487	1.223	0.8169957

¹Abbreviations: HCC, Hepatocellular carcinoma; AP, arterial phase; PP, portal phase; HBP, hepatobiliary phase; CEUS, contrast-enhanced ultrasound; SE, standard error; OR, odds ratio; VIF, variance inflation factor; VETC, vessels encapsulating tumor clusters. All VIF values were < 2.

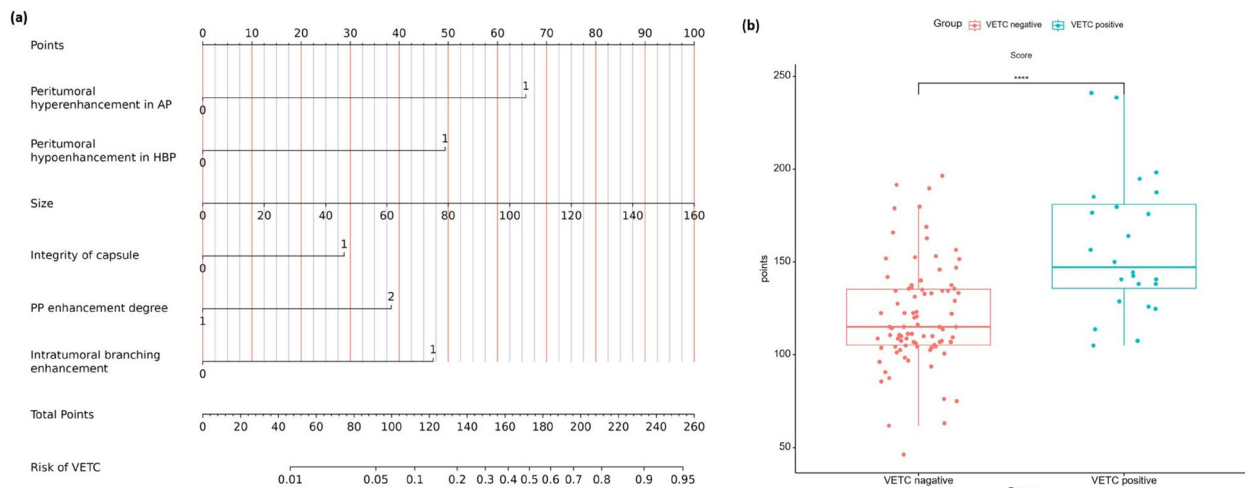


Figure 4. Nomogram and nomoscore for predicting the probability of VETC. (a) The constructed nomogram for predicting VETC. **(b)** A boxplot of nomoscore between VETC positive and negative group. Abbreviations: AP, arterial phase; HBP, hepatobiliary phase; PP, portal phase; VETC, vessels encapsulating tumor clusters.

enter subsequent screening. Therefore, the variables with a *P*-value of less than 0.2 (seven imaging features of "size," "margin," "capsule (presence/absence)," "integrity of capsule," "PP enhancement degree," "homogeneity in CEUS" and "peritumoral hyperenhancement in AP") were chosen for subsequent analysis. In addition, "peritumoral hypoenhancement in HBP" (25) has been considered a key aggressive imaging feature in published studies. SonoVue is a pure blood-pool contrast agent that does not enter the vascular space. Because the images of CEUS totally reflect intravascular contrast perfusion rather than stroma, we wanted to explore whether the spatial pattern of contrast-enhanced perfusion could reflect the pathological pattern of vascular encapsulation of VETC. Furthermore, some CEUS perfusion modes (such as "arterial enhancing modes with a fissure or flakiness style" (25), "fine network of many hyperenhancing lines" (26)) have been studied in HCC progression and invasion. After careful consideration, we included "peritumoral hypoenhancement in HBP" and "intratumoral branching enhancement," which yielded *P* value of more than 0.2, in the follow-up multivariate and BSR analysis. The "PP enhancement degree," "peritumoral hyperenhancement in AP," "branching

enhancement," "integrity of capsule," "peritumoral hypoenhancement in HBP" and "size" were identified as effective sets of factors. Our final model with these six variables had an Akaike information criterion (AIC) of 106.4, the smallest AIC compared to a model with any other combination of factors (radiological features). No significant statistical collinearity was observed for any of the 6 variables (Table 2).

3.3. Development and presentation of the prediction model

Based on the findings of the above regression analysis, we obtained the following regression equation: $\text{Logit}(P) = -7.666 + 2.386 \times \text{"peritumoral hyperenhancement in AP"} + 1.790 \times \text{"peritumoral hypoenhancement in HBP"} + 1.393 \times \text{"PP enhancement degree"} + 0.023 \times \text{"size"} + 1.043 \times \text{"integrity of capsule"} + 1.702 \times \text{"branching enhancement"}.$

The model was visualized in the form of a nomogram (Figure 4a). The nomogram included a preliminary score for each of the six predictors (ranging from 0 to 100). These scores were summed to obtain the total score (range, 0–260), which translates into the

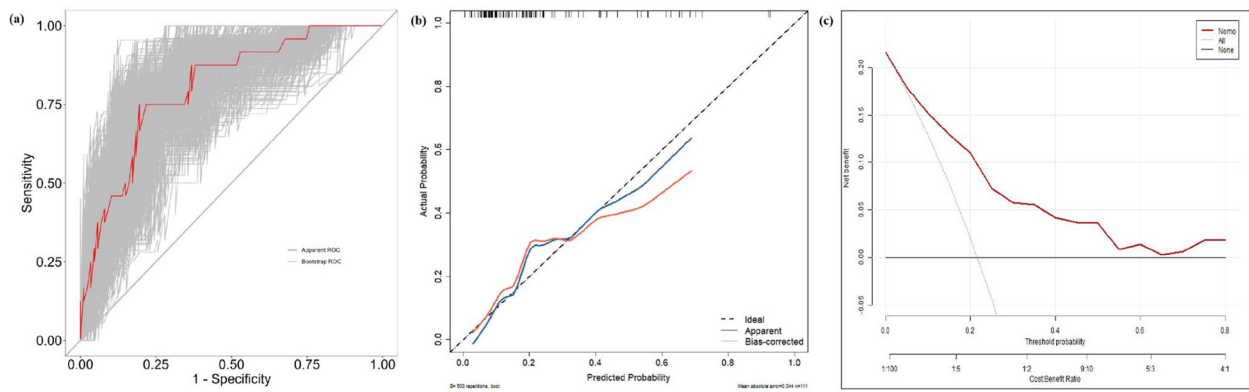


Figure 5. valuation and assessment of our model. (a) AUC by receiver operating characteristic curve (ROC) analysis by bootstrapping. Many of the gray curves are AUC made by repeated sampling 500 times. The red curve is the average AUC of 500 curves. **(b)** Calibration curves (blue curve is nomogram model while red curve is bootstrap validation). **(c)** Decision curve analysis (DCA). The DCA demonstrated that the threshold probability of the prediction model is approximately more than 5%.

individual probability (1–95%) of VETC for HCC lesions. For clinical application, according to the nomogram algorithm, the nomoscore was calculated for each lesion and plotted to assess risk stratification of the established nomogram (Figure 4b). For the VETC-negative and -positive lesion groups, the median (range) score values were 115 (46.3–196.4) and 147.5 (105.0–241.1), respectively. We observed a marked difference in the nomoscore profiles between the positive and VETC-negative groups ($P < 0.001$). The model is made available as an easy-to-use online calculator (<https://wangfeiqian126.shinyapps.io/dynnomapp/>) (Figure S1, <http://www.biosciencetrends.com/action/getSupplementalData.php?ID=203>).

3.4. Validation and assessment of model performance

The AUC of our nomogram model was 0.804 (95% confidence interval [CI], 0.707–0.901; $P < 0.05$; Figure S2 (<http://www.biosciencetrends.com/action/getSupplementalData.php?ID=203>)). Logit (P) accuracy was 0.820. Sensitivity and specificity were 0.375 and 0.943, respectively. The Hosmer-Lemeshow test was used to evaluate the goodness-of-fit of the logistic regression model, and the results showed that the regression equation was highly matched ($\chi^2 = 5.7439$, $df = 8$, $P = 0.6759$). Decision curve analysis (DCA) revealed that using the nomogram to predict VETC would probably add more benefit than treating all or no patients (Figure 5).

Some published studies used bootstrapping as their only validation (27-31) as bootstrapping is an ideal internal validation method for smaller sample sizes or for larger numbers of candidate predictors (32). Because of the small sample size included in this study, all data were used for modeling without splitting the training and validation sets. Bootstrapping (500 bootstrap replicates) was performed in the internal validation phase of our model. The AUC and calibration curves with bootstrapping did not change much when compared with

those of our model (Figure 5 a, b).

3.5. Comparison of EOB-MRI model, CEUS model and combined model

We built models using the total imaging features of EOB-MRI (seven factors) and CEUS (seven factors). Our multimodal model, which combined factors of EOB-MRI and CEUS (six selected factors), yielded a higher AUC (0.804) than the EOB-MRI model (0.767) and CEUS model (0.7) (Figure 6). However, there was no statistical difference between their AUCs (multimodal model vs. EOB-MRI model, $P = 0.3921$; multimodal model vs. CEUS model, $P = 0.0933$).

3.6. A novel nomogram-based prognostic risk assessment

The median follow-up duration of all the 101 patients was 60.3 months (range, 3.7–146.3 months). The median time to recurrence was 33.9 months (range: 1–143.4 months).

The 3-, 5-, and 8-year OS rates were lower in the VETC-positive group than in the VETC-negative group (69.2% vs. 88.0%, 62.6% vs. 77.0%, and 42.4% vs. 65.1%, respectively; $P = 0.027$; Figure 7a). Similarly, the 1-, 3-, 5-, and 8-year PFS rates were lower in the VETC-positive group than in the VETC-negative group (61.9% vs. 73.6%, 40.4% vs. 64.1%, 26.9% vs. 43.6%, and 11.5% vs. 33.6%, respectively; $P = 0.041$; Figure 7b).

To further confirm the validity of our VETC-related nomogram for predicting prognosis, we stratified all 101 patients into two risk groups according to the nomoscore. They were low-risk group: $0 \leq$ nomoscore ≤ 168 ; and high-risk group: nomoscore >168 . Kaplan-Meier survival curves for OS and PFS in the two risk groups according to the nomoscore were plotted (Figure 7c, d), which showed an obvious grading ability based on our nomogram ($P < 0.05$). In other words, the prognosis would be good when the total score calculated

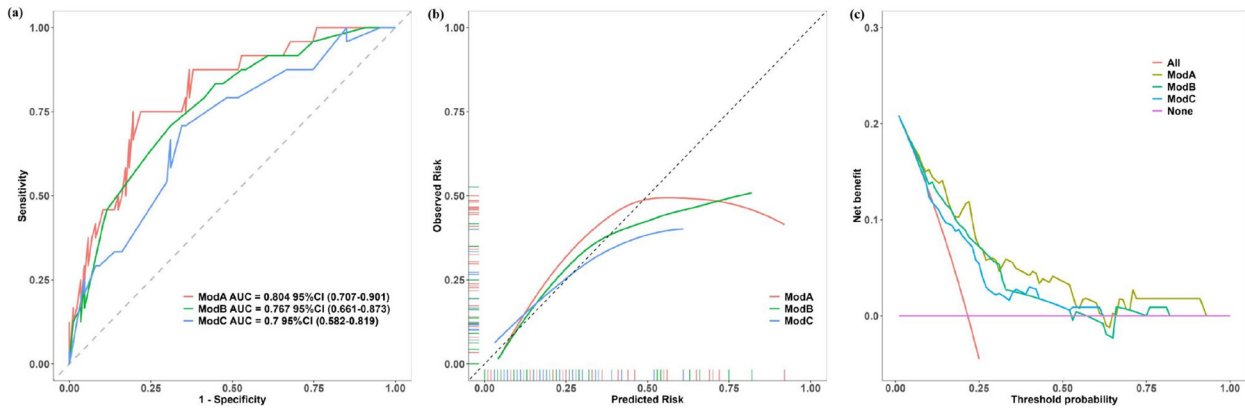


Figure 6. Comparison of three models. Model A is our final model with imaging factors of EOB-MRI and CEUS combined. Model B is EOB-MRI model. Model C is CEUS model. (a) AUC by receiver operating characteristic curve (ROC) analysis. Model A had the highest AUC. (b) Calibration curves. (c) Decision curve analysis (DCA). DCA showed that combined EOB-MRI and CEUS features had maximum clinical practicability. Abbreviations: HCC, Hepatocellular carcinoma; VETC, vessels encapsulating tumor clusters.

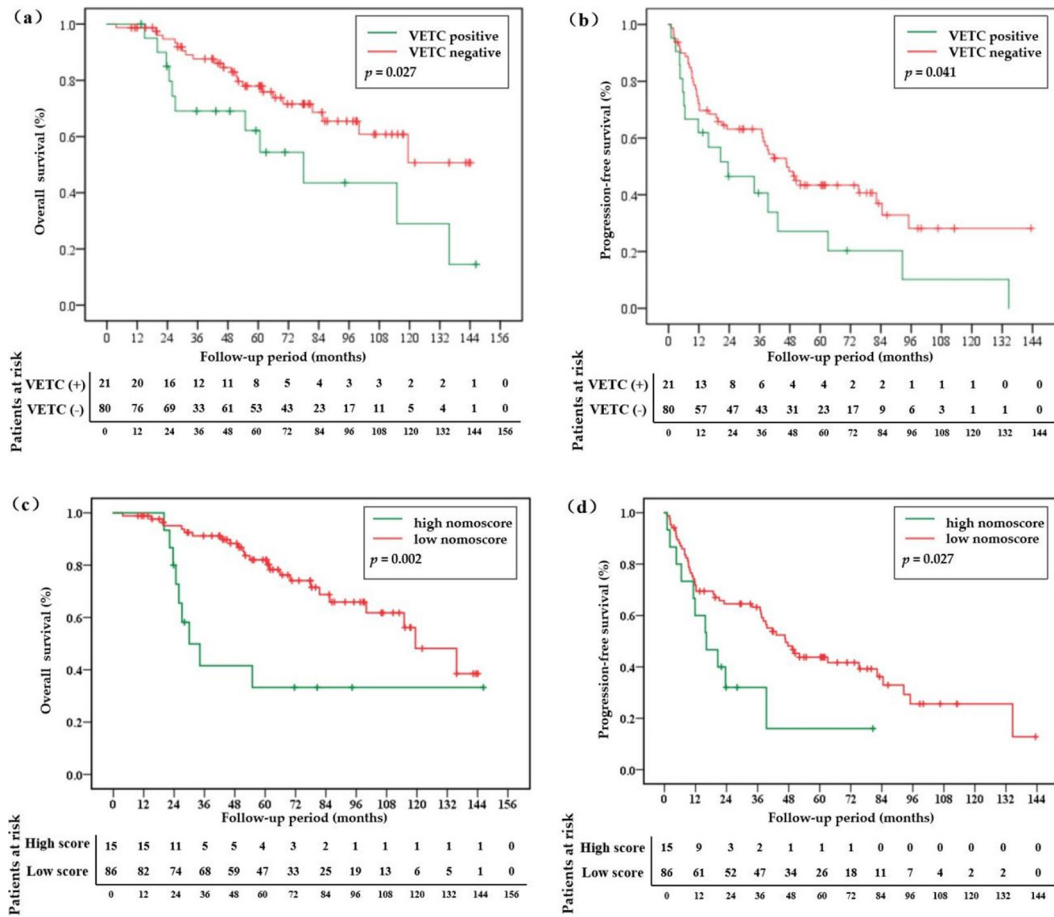


Figure 7. Survival rate curves of patients with HCC lesions of different VETC status and nomoscore risk stratification based on Kaplan-Meier survival analysis. OS (a) and PFS (b) are different between VETC positive and negative groups, with a p value of 0.027 and 0.041, respectively. According to our calculated nomoscore, OS (c) and PFS (d) among the low-risk and high-risk groups are different. Abbreviations: OS, Overall survival; PFS, Progression-free survival; HCC, Hepatocellular carcinoma; VETC, vessels encapsulating tumor clusters.

by "peritumoral hyperenhancement in AP," "peritumoral hypoenhancement in HBP," "PP enhancement degree," "size," "integrity of capsule" and "branching enhancement" was less than 168, but worse when the score was more than 168.

4. Discussion

Our study demonstrated that "size," "peritumoral hyperenhancement in AP," "peritumoral hypoenhancement in HBP," "integrity of the

capsule (incomplete)," "PP enhancement degree (hypoenhancement)," and "branching enhancement in AP of CEUS" can potentially predict VETC-positive HCC.

It is interesting that although VETC occurs within the lesion, peritumoral imaging features can predict VETC. Consistent with our findings, a published study showed that the peritumoral radiomics model yielded an incremental predictive value over the intratumoral model (AUC of peritumoral model=0.972, AUC of intratumoral model=0.919) ($P = 0.044$) (14). Abnormal peritumoral enhancement, regardless of AP or HBP, is widely recognized as a key independent risk factor for microvascular invasion (MVI) (33). MVI and VETC are the classical EMT-dependent and newly discovered EMT-independent patterns of hematogenous metastasis in HCC tumor cells, respectively (3). Regarding tumor behavior, for MVI, individual cancer cells separated from the primary site actively crossed the vessel wall and entered the vessel, while the tumor cluster passively was squeezed into the vessel in the VETC pattern. In short, tumor invasion and metastasis by the VETC pattern is simpler, easier, and more direct than MVI; thus, VETC has a higher invasive potential than MVI. MVI can be observed in up to 80% of VETC-positive tumors (3). Some researchers consider MVI and VETC to be synergistic (34). Therefore, it is not surprising that peritumoral imaging features, which are closely related to MVI, can predict VETC.

HCC lesions with the VETC pattern were found to have a higher intratumoral microvessel density than those without the VETC pattern (35). These blood vessels are considered to originate from tumor-associated dysplasia rather than from a normal vascular bed. Morphologically and structurally, tumor vasculature is characterized by dilated, tortuous, and disorganized blood vessels (36). They lack an endothelial basement membrane and form arteriovenous fistulas. These immature, unstable, and highly heterogeneous vessels have a high functional permeability (36). In this situation, the contrast agent is prone to rapid washout. Thus, one possible explanation for PP hypoenhancement is the large amount of abnormal angiogenesis in the VETC of HCC.

Previous studies have shown that large tumor size is related to VETC (8,35). As the tumor expands in size, the diffusion distance from the existing supplying vessels increases, leading to hypoxia. Hypoxia stimulates intratumoral vascular proliferation (35). As described below, increased intratumoral vessel density is closely related to VETC development. From this perspective, the correlation between tumor size and VETC suggests that tumor proliferation (an increase in lesion size on ultrasound images) may be one of the causes of VETC.

CEUS is the most sensitive tool for detecting intratumoral arterial vascularity (11). In agreement with our findings of branching enhancement in AP of CEUS, it was reported that HCC having VETC exhibits a "crack-and-tendon-like filling" characteristic throughout the AP

of CEUS until the contrast agent reaches its peak (19). Theoretically, the imageological branching enhancement during the AP of CEUS may reflect the microscopic pattern of the web-like vascular networks of VETC.

Tumor capsules, which we observed in the images, were mainly composed of fibroblasts and endothelial cells. They can act as barriers to the infiltration of peritumoral immune cells (37). However, Wu. R *et al.* found that the incomplete capsule of HCC lesions may result in reduced intratumoral spatial continuity of tumor cells and, through a complex mechanism, redistribution of peritumoral immune cells (38). Therefore, a radiologic incomplete capsule has been found to promote tumor invasion in many studies (39). VETC indicates that the cancer nests are surrounded, cut, and extruded by a network of blood vessels, which may suggest a discontinuity in the spatial structure of tumor cells. When VETC develops, the cancer cells are thought to easily escape from the immune response because genes representing effective immune responses are less enriched in the VETC positive group than in the negative group (40). These findings suggest that incomplete capsules may contribute to VETC and promote peritumoral invasion by altering tumor immunity.

Few VETC studies have combined CEUS with CEMRI. The choice of radiological modality (CT, US/CEUS, or MRI) depends on the patient, institutional, and regional factors (41). According to the HCC management guidelines of some countries, the diagnosis of HCC should be based on typical imaging features on at least two of the three imaging modalities, including contrast-enhanced computed tomography (CECT), MRI or EOB-MRI, and CEUS (42). However, some cases of pathologically early HCC are typically hypovascular and thus unlikely to be detected by CECT (11). Therefore, as 62% of HCC cases are in Barcelona Clinic Liver Cancer (BCLC) stages 0 and A in Japan (43), CEUS and EOB-MRI are the two main screening modalities for high-risk patients in Japan. In other words, both EOB-MRI and CEUS are routine preoperative examinations in Japan, with or without VETC evaluation. As some discrepancies were found between CEUS and EOB-MRI in evaluating the features of HCC (44), we believe the diagnostic strategy of their combination would be of great necessity. Furthermore, our study shows that the combination of EOB-MRI and CEUS has a better diagnostic effect on VETC according to all aspects we assessed (discrimination by AUC, calibration by Hosmer-Lemeshow analysis, and net benefit gain by DCA). Encouragingly, the combination of CEUS and EOB-MRI provides rich useful diagnostic information (VETC in our study, MVI (45), histological grade (46)) other than the diagnosis of HCC.

Consistent with some published VETC studies (6,47), our study also found that the presence of VETC had a long-term effect on survival. The VETC-positive and-negative groups had different OS and PFS. Thus, the

early diagnosis of VETC may be of great importance in predicting the prognosis of patients with HCC.

This study had some limitations. First, there was a potential for selection bias due to the retrospective nature of the study. Second, the sample size of this study was small and there was no external validation group to confirm the stability and applicability of the prediction model. Finally, the patients were all Japanese, with a relatively low incidence of VETC compared with published research in other countries (3). The results of our research are not representative of the situation in Asia or the world. Our study is the first multimodal imaging study to combine EOB-MRI and CEUS; in particular, we achieved excellent diagnostic efficiency. Therefore, we believe our study has important reference value for the preoperative diagnosis of VETC. More importantly, EOB-MRI and CEUS are routine liver cancer diagnostic and therapeutic steps implemented in accordance with liver cancer guidelines. These are not redundant diagnostic methods specifically added for the diagnosis of VETC. Therefore, real-world clinical work does not significantly increase the financial and time burden of patients and physicians. Furthermore, the visual and easy-to-use nomogram and nomoscore proposed in this paper can not only predict the VETC status of HCC lesions but also predict the survival condition of patients. The results of this study have great application prospects in clinical settings.

5. Conclusion

Combining CEUS and EOB-MRI, imaging features with peritumoral enhancement on AP and HBP of EOB-MRI, intratumoral branching enhancement in AP of CEUS, intratumoral hypoenhancement in PP of CEUS, incomplete capsule, and size show a satisfactory performance of VETC prediction in HCC. This study provides a promising approach for the noninvasive preoperative prediction of VETC using enhanced imaging.

Funding: This research was supported by the National Natural Science Foundation of China (No. 82102074) and Beijing Xisike Clinical Oncology Research Foundation of China (No. Y-Young2022-0162).

Conflict of Interest: The authors have no conflicts of interest to disclose.

References

- Wen T, Jin C, Facciorusso A, Donadon M, *et al.* Multidisciplinary management of recurrent and metastatic hepatocellular carcinoma after resection: an international expert consensus. *Hepatobiliary Surgery and Nutrition.* 2018; 7: 353-371.
- Lin YL, Li Y. Study on the hepatocellular carcinoma model with metastasis. *Genes & Diseases.* 2020; 7: 336-350.
- Liu K, Dennis C, Prince DS, Marsh-Wakefield F, Santhakumar C, Gamble JR, Strasser SI, McCaughan GW. Vessels that encapsulate tumour clusters vascular pattern in hepatocellular carcinoma. *JHEP Reports.* 2023; 5:100792.
- Wang JH, Li XS, Tang HS, Fang RY, Song JJ, Feng YL, Guan TP, Ruan Q, Wang J, Cui SZ. Vessels that encapsulate tumor clusters (VETC) pattern predicts the efficacy of adjuvant TACE in hepatocellular carcinoma. *Journal of Cancer Research and Clinical Oncology.* 2023; 149:4163-4172.
- Lin W, Lu L, Zheng R, Yuan S, Li S, Ling Y, Wei W, Guo R. Vessels encapsulating tumor clusters: a novel efficacy predictor of hepatic arterial infusion chemotherapy in unresectable hepatocellular carcinoma. *Journal of Cancer Research and Clinical Oncology.* 2023; 149:17231-17239.
- Dennis C, Prince DS, Moayed-Alaei L, Remash D, Carr-Boyd E, Bowen DG, Strasser SI, Crawford M, Pulitano C, Kench J, McCaughan GW, McKenzie C, Liu K. Association between vessels that encapsulate tumour clusters vascular pattern and hepatocellular carcinoma recurrence following liver transplantation. *Frontiers in Oncology.* 2022; 12:997093.
- Fang JH, Xu L, Shang LR, Pan CZ, Ding J, Tang YQ, Liu H, Liu CX, Zheng JL, Zhang YJ, Zhou ZG, Xu J, Zheng LM, Chen MS, Zhuang SM. Vessels that encapsulate tumor clusters (VETC) pattern is a predictor of sorafenib benefit in patients with hepatocellular carcinoma. *Hepatology.* 2019; 70:824-839.
- Renne SL, Woo HY, Allegra S, Rudini N, Yano H, Donadon M, Vigano L, Akiba J, Lee HS, Rhee H, Park YN, Roncalli M, Tommaso LD. Vessels encapsulating tumor clusters (VETC) is a powerful predictor of aggressive hepatocellular carcinoma. *Hepatology.* 2020; 71:183-195.
- Kudo M. Breakthrough Imaging in Hepatocellular Carcinoma. *Liver Cancer.* 2016; 5: 47-54.
- Wang F, Numata K, Nihonmatsu H, Okada M, Maeda S. Application of new ultrasound techniques for focal liver lesions. *Journal of Medical Ultrasonics.* 2020; 47:215-237.
- Kudo M, Kawamura Y, Hasegawa K, Tateishi R, Kariyama K, Shiina S, Toyoda H, Imai Y, Hiraoka A, Ikeda M, *et al.* Management of hepatocellular carcinoma in Japan: JSH Consensus Statements and Recommendations 2021 Update. *Liver Cancer.* 2021; 10:181-223.
- EASL Clinical Practice Guidelines: Management of hepatocellular carcinoma. *Journal of Hepatology.* 2018; 69:182-236.
- General Office, N.H.C. Standard for diagnosis and treatment of primary liver cancer (2022 edition). *Journal of Clinical Hepatology.* 2022; 38:288-303.
- Yu Y, Fan Y, Wang X, Zhu M, Hu M, Shi C, Hu C. Gd-EOB-DTPA-enhanced MRI radiomics to predict vessels encapsulating tumor clusters (VETC) and patient prognosis in hepatocellular carcinoma. *European Radiology.* 2022; 32:959-970.
- Fan Y, Yu Y, Hu M, Wang X, Du M, Guo, L, Hu, C. Imaging features based on Gd-EOB-DTPA-enhanced MRI for predicting vessels encapsulating tumor clusters (VETC) in patients with hepatocellular carcinoma. *The British Journal of Radiology.* 2021; 94:20200950.
- Hong SB, Choi SH, Kim SY, Shim JH, Lee SS, Byun JH, Park SH, Kim KW, Kim S, Lee NK. MRI features for predicting microvascular invasion of hepatocellular

- carcinoma: A systematic review and meta-analysis. *Liver Cancer*. 2021; 10:94-106.
17. Wang F, Numata K, Chuma M, Miwa H, Moriya S, Ogushi K, Okada M, Otani M, Inayama Y, Maeda S. A study on the inconsistency of arterial phase hypervascularity detection between contrast-enhanced ultrasound using sonazoid and gadolinium-ethoxybenzyl-diethylenetriamine penta-acetic acid magnetic resonance imaging of hepatocellular carcinoma lesions. *Journal of Medical Ultrasonics*. 2021; 48:215-224.
 18. Xu W, Huang B, Zhang R, Zhong X, Zhou W, Zhuang S, Xie X, Fang J, Xu M. Diagnostic and prognostic ability of contrast-enhanced ultrasound and biomarkers in hepatocellular carcinoma subtypes. *Ultrasound in Medicine and Biology*. 2024; 50:617-626.
 19. Lan CY, Ling B, Guo WW, Yin W, Zhong XG, Han YM, Dong XF. The relationship between vimentin protein expression in endothelial cells and contrast-enhanced ultrasound characters in VETC (+) hepatocellular carcinoma. *Zhonghua Zhong Liu Za Zhi*. 2018; 40:105-109. (in Chinese).
 20. Van der Horst G, Buijs JT, Van der Pluijm G. Pre-clinical molecular imaging of "the seed and the soil" in bone metastasis. In *Bone Cancer*, Elsevier. 2015:557-570.
 21. Lee W, Lam S, Zhang Y, Yang R, Cai J. Review of methodological workflow, interpretation and limitations of nomogram application in cancer study. *Radiation Medicine and Protection*. 2022; 3:200-207.
 22. Yang K, Xie W, Zhang X, Wang Y, Shou A, Wang Q, Tian J, Yang J, Li G. A nomogram for predicting late radiation-induced xerostomia among locoregionally advanced nasopharyngeal carcinoma in intensity modulated radiation therapy era. *Aging (Albany NY)*. 2021; 13:18645-18657.
 23. Dong N, Wang S, Li X, Li W, Gao N, Pang L, Xing J. Prognostic nomogram for the severity of acute organophosphate insecticide self-poisoning: a retrospective observational cohort study. *BMJ Open*. 2021; 11:e42765.
 24. Guner R, Kayaaslan B, Hasanoglu I, *et al.* Development and validation of nomogram to predict severe illness requiring intensive care follow up in hospitalized COVID-19 cases. *BMC Infectious Diseases*. 2021; 21:1004.
 25. Zhang L, Yu X, Wei W, Pan X, Lu L, Xia J, Zheng W, Jia N, Huo L. Prediction of HCC microvascular invasion with gadobenate-enhanced MRI: correlation with pathology. *European Radiology*. 2020; 30:5327-5336.
 26. Giorgio A, Calisti G, Di Sarno A, Farella N, De Stefano G, Scognamiglio U, Giorgio V. Characterization of dysplastic nodules, early hepatocellular carcinoma and progressed hepatocellular carcinoma in cirrhosis with contrast-enhanced ultrasound. *Anticancer Research*. 2011; 31:3977-3982.
 27. Xie W, Liu M, Okoli C, Zeng L, Huang S, Ye X, Liu F, Wang J. Construction and evaluation of a predictive model for compassion fatigue among emergency department nurses: A cross-sectional study. *International Journal of Nursing Studies*. 2023; 148:104613.
 28. Liang W, Zhang K, Cui J, Xi H, Cai A, Li J, Liu Y, Liu J, Zhang W, Wang P, Wei B, Chen L. Nomogram to predict prolonged postoperative ileus after gastrectomy in gastric cancer. *World Journal of Gastroenterology*. 2019; 25:5838-5849.
 29. Ding N, Zhang J, Wang P, Wang F. A novel machine learning model for predicting clinical pregnancy after laparoscopic tubal anastomosis. *BMC Pregnancy Childbirth*. 2023; 23:537.
 30. Van Straalen JW, Giancane G, Amazrhar Y, *et al.* A clinical prediction model for estimating the risk of developing uveitis in patients with juvenile idiopathic arthritis. *Rheumatology (Oxford)*. 2021; 60:2896-2905.
 31. Jatuworapruk K, Grainger R, Dalbeth N, Taylor WJ. Development of a prediction model for inpatient gout flares in people with comorbid gout. *Annals of the Rheumatic Diseases*. 2020; 79:418-423.
 32. Shipe ME, Deppen SA, Farjah F, Grogan E.L. Developing prediction models for clinical use using logistic regression: an overview. *Journal of Thoracic Disease*. 2019; 11:S574-S584.
 33. Hu F, Zhang Y, Li M, Liu C, Zhang H, Li X, Liu S, Hu X, Wang J. Preoperative Prediction of Microvascular Invasion Risk Grades in Hepatocellular Carcinoma Based on Tumor and Peritumor Dual-Region Radiomics Signatures. *Frontiers in Oncology*. 2022; 12:853336.
 34. Qu Q, Liu Z, Lu M, Xu L, Zhang J, Liu M, Jiang J, Gu C, Ma Q, Huang A, Zhang X, Zhang T. Preoperative Gadoteric Acid-Enhanced MRI Features for Evaluation of Vessels Encapsulating Tumor Clusters and Microvascular Invasion in Hepatocellular Carcinoma: Creating Nomograms for Risk Assessment. *Journal of Magnetic Resonance Imaging*. 2023 (Online ahead of print).
 35. Huang CW, Lin SE, Huang SF, Yu MC, Tang JH, Tsai CN, Hsu HY. The vessels that encapsulate tumor clusters (VETC) pattern is a poor prognosis factor in patients with hepatocellular carcinoma: an analysis of microvessel density. *Cancers (Basel)*. 2022; 14:5428.
 36. Taskaeva I, Bgatova N. Microvasculature in hepatocellular carcinoma: an ultrastructural study. *Microvascular Research*. 2021; 133, 104094.
 37. Rahmzade R. Redefinition of tumor capsule: Rho-dependent clustering of cancer-associated fibroblasts in favor of tensional homeostasis. *Medical Hypotheses*. 2020; 135, 109425.
 38. Wu R, Guo W, Qiu X, *et al.* Comprehensive analysis of spatial architecture in primary liver cancer. *Science Advances*. 2021; 7:g3750.
 39. Zhu F, Yang F, Li J, Chen W, Yang W. Incomplete tumor capsule on preoperative imaging reveals microvascular invasion in hepatocellular carcinoma: a systematic review and meta-analysis. *Abdominal Radiology*. 2019; 44:3049-3057.
 40. Zhang P, Ono A, Fujii Y, *et al.* The presence of vessels encapsulating tumor clusters is associated with an immunosuppressive tumor microenvironment in hepatocellular carcinoma. *International Journal of Cancer*. 2022; 151:2278-2290.
 41. Granata V, Grassi R, Fusco R, Belli A, Cutolo C, Pradella S, Grazzini G, La Porta M, Brunese MC, De Muzio F, Ottaiano A, Avallone A, Izzo F, Petrillo A. Diagnostic evaluation and ablation treatments assessment in hepatocellular carcinoma. *Infectious Agents and Cancer*. 2021; 16:53.
 42. Cho Y, Kim BH, Park JW. Overview of Asian clinical practice guidelines for the management of hepatocellular carcinoma: an Asian perspective comparison. *Clinical and Molecular Hepatology*. 2023; 29:252-262.
 43. Kudo, M. Management of hepatocellular carcinoma in Japan as a world-leading model. *Liver Cancer*. 2018; 7:134-147.
 44. Yang J, Jiang H, Xie K, Bashir MR, Wan H, Huang J, Qin Y, Chen J, Lu Q, Song B. Profiling hepatocellular carcinoma

- aggressiveness with contrast-enhanced ultrasound and gadoxetate disodium-enhanced MRI: an intra-individual comparative study based on the Liver Imaging Reporting and Data System. *European Journal of Radiology*. 2022; 154:110397.
45. Zheng R, Zhang X, Liu B, Zhang Y, Shen H, Xie X, Li S, Huang G. Comparison of non-radiomics imaging features and radiomics models based on contrast-enhanced ultrasound and Gd-EOB-DTPA-enhanced MRI for predicting microvascular invasion in hepatocellular carcinoma within 5 cm. *European Radiology*. 2023; 33:6462-6472.
46. Wang F, Numata K, Nakano M, Tanabe M, Chuma M, Nihonmatsu H, Nozaki A, Ogushi K, Luo W, Ruan L, Okada M, Otani M, Inayama Y, Maeda S. Diagnostic value of imaging methods in the histological four grading of hepatocellular carcinoma. *Diagnostics (Basel)*. 2020; 10:321.
47. Kawasaki J, Toshima T, Yoshizumi T, Itoh S, Mano Y, Wang H, Iseda N, Harada N, Oda Y, Mori M. Prognostic impact of vessels that encapsulate tumor cluster (VETC) in patients who underwent liver transplantation for hepatocellular carcinoma. *Annals of Surgical Oncology*. 2021; 28:8186-8195.

Received May 2, 2024; Revised June 2, 2024; Accepted June 7, 2024.

**Address correspondence to:*

Kazushi Numata, Gastroenterological Center, Yokohama City University Medical Center, 4-57 Urafune-cho, Minami-ku, Yokohama, Kanagawa 232-0024, Japan.

E-mail: kz-numa@urahp.yokohama-cu.ac.jp

Released online in J-STAGE as advance publication June 12, 2024.

Suppression of STK39 weakens the MASLD/MASH process by protecting the intestinal barrier

Qing Xu^{1,§}, Fei Liu^{2,§}, Zhenru Wu¹, Menglin Chen¹, Yongjie Zhou^{3,*}, Yujun Shi^{1,3,*}

¹Institute of Clinical Pathology & Department of Pathology, Key Laboratory of Transplant Engineering and Immunology, NHC, West China Hospital, Sichuan University, Chengdu, China;

²Department of Biliary Surgery, West China Hospital, Sichuan University, Chengdu, China;

³Laboratory of Liver Transplantation, West China Hospital, Sichuan University, Chengdu, China.

SUMMARY STK39 is reportedly a critical negative regulator of intestinal barrier. Pharmacological targeting of STK39 is expected to protect the intestinal barrier and thereby weaken metabolic dysfunction-associated steatohepatitis (MASH); Proximal colon biopsy tissues from patients with metabolic dysfunction-associated steatotic liver disease (MASLD) and those without MASLD were analyzed for STK39 expression. Wildtype (WT) mice and systemic STK39 gene knockout (STK39^{-/-}) male mice were fed a normal diet or a high-fat methionine-choline deficient diet (HFMCD) for 8 weeks. The MASH mice were grouped and treated with ZT-1a (a STK39 inhibitor) or vehicle intraperitoneal injection during the procedure of HFMCD induction. Liver and intestinal tissues were collected for further examination; Colon tissues from patients with MASLD exhibited higher levels of STK39 than those from subjects without MASLD. Knockout of STK39 diminished CD68⁺ Kupffer cells and α -SMA⁺ hepatic stellate cells infiltration in mouse MASH model. Treatment with ZT-1a also prevented severe steatohepatitis in a mouse MASH model, including milder histological and pathological manifestations (lobular inflammation and fibrosis) in the liver. Interestingly, Inhibition of STK39 had minimal effects on hepatic lipid metabolism. The reduced liver injury observed in mice with STK39 inhibition was linked to significant decreases in mucosal inflammation, tight junction disruption and intestinal epithelial permeability to bacterial endotoxins; Collectively, we have revealed that inhibiting STK39 prevents the progression of MASH by protecting the intestinal epithelial barrier.

Keywords STK39, ZT-1a, MASLD/MASH, intestinal barrier

1. Introduction

Globally, nonalcoholic fatty liver disease (MASLD) and nonalcoholic steatohepatitis (MASH), both diet-related, are among the most prevalent causes of chronic liver disease (1). It is estimated that 20% of MASLD patients develop MASH, and 15% MASH patients progress to cirrhosis (2). Despite the fact that most MASLD/MASH patients remain asymptomatic, they face an elevated risk of developing hepatocellular carcinoma (3). This poses a considerable hindrance to the development of therapeutic strategies and biomarkers for advanced MASH.

The possible involvement of impaired intestinal epithelial permeability in the pathogenesis of MASH has been emphasized by several recent studies (4-7). The intestinal barrier serves as a protective shield against potentially harmful metabolites, bacteria, and their antigens. Consequently, immunologic regulation of the commensal microbiota and the intestinal barrier is

crucial and has been preserved throughout evolution (8). Elevated intestinal epithelial permeability is associated with increased serum endotoxin levels, a powerful inducer of hepatic inflammation, in both human and animal models (9). In recent years, diet, particularly a high-fat diet (HFD), has emerged as one of the most significant factors affecting the function of the intestinal epithelial barrier and leading to endotoxemia in healthy individuals (10). Moreover, human MASH and MASH-related cirrhosis often exhibit increased intestinal epithelial permeability and small intestinal bacterial overgrowth (7). However, it remains unclear whether the persistent systemic inflammation observed in MASH patients is a consequence or a contributing factor to intestinal epithelial barrier dysfunction.

The tight junctions (TJs) of intestinal epithelium cells form a crucial component of the intestinal barrier (11). The physiological functions of the TJ proteins are sustained by three essential proteins: zonula occludens-1

(ZO-1), Occludin, and claudins (12). Damage to the TJs barrier due to high-fat diet contributes to the progression of MASLD/MASH. A human study revealed that patients with MASLD exhibit increased gut epithelial permeability, decreased levels of tight junction proteins (such as ZO-1, claudin 1, and Occludin), and elevated inflammation levels; these alterations are closely linked to the occurrence and progression of MASLD (13). A meta-analysis indicated that, compared to healthy volunteers, patients with MASLD and MASH are more prone to having enhanced intestinal permeability (14). The increased gut permeability heightens the liver's exposure to intestine-derived bacterial products (such as LPS, short-chain fatty acids, bile acids, cytokines, and ethanol), which exacerbate hepatic inflammation and fibrosis by activating toll-like receptor (TLR) signaling and the inflammasome (15,16). Therefore, it is necessary and particularly crucial to prevent MASLD/MASH by maintaining TJs function. TJ proteins, the most important intercellular junctions of intestinal epithelial cells (IECs), seal the paracellular space between adjacent IECs (17). TJ proteins regulate the transport of water, ions, and solutes through the paracellular pathway and prevent the passage of immunogenic macromolecules, particularly gut bacterial metabolites (18). Previous research has shown that upregulation of ZO-1 and Occludin can inhibit the increase in intestinal permeability and attenuate MASLD (19). Therefore, drugs that prevent TJ protein disruption are widely considered an effective approach for MASLD/MASH therapies.

Serine/threonine kinase 39 (STK39), a member of MAP4K family, comprises an N-terminal series of proline/alanine repeats (PAPA box), followed by a catalytic domain, a nuclear localization signal, a potential caspase cleavage motif, and a C-terminal regulatory region. STK39 is present in both the nucleus and the cytoplasm (20). Recent studies have demonstrated that STK39 knockout mice exhibit a significant increase in intestinal transepithelial resistance, a marked decrease in paracellular permeability to fluorescent isothiocyanate dextran, and altered sodium ion selectivity at apical tight junctions (21). Furthermore, overexpression of STK39 impairs the intestinal barrier and enhances the permeability of the intestinal epithelium (22). Therefore, it is highly likely that STK39 is involved in the progression of MASH through the intestinal barrier. 5-chloro-N-(5-chloro-4-((4-chlorophenyl)(cyano)methyl)-2-methylphenyl)-2-hydroxybenzamide (ZT-1a) is a potent, non-ATP-competitive, and selective STK39 inhibitor (23). ZT-1a has previously been shown to be neuroprotective in murine ischemic stroke models (24). However, whether ZT-1a could be used to protect the intestinal barrier and thereby mitigate MASH remains unknown.

In this study, we systematically investigated the impact of STK39 inhibitors on the pathogenesis of MASH. STK39 was overexpressed in colon tissues

from MASH patients and mice. In the HFMCD-induced MASH mouse model, ZT-1a exhibited attenuated liver inflammation and liver cirrhosis, without changes in liver lipid accumulation. This may be partly due to reduced intestinal permeability and decreased LPS production. Furthermore, inhibiting STK39 reduced dextran sulfate sodium (DSS)-induced intestinal barrier damage and prevented LPS-induced hepatic inflammation or fibrosis. Here, our data support the idea that targeting STK39 may be a potent strategy to improve MASH.

2. Materials and Methods

2.1. Mice

STK39^{-/-} mice were purchased from VIEWSSOLID Ltd. All mice were housed at up to 5 mice per cage in specific-pathogen-free conditions under a 12 h light/dark cycle at constant temperature (22°C). The animals had free access to water and standard laboratory chow. Animal care and experimental procedures were conducted in accordance with national and international laws and policies and were approved by the Animal Care and Use Committee of Sichuan University (No. 2020455A). The animal study protocol was approved by the Ethics Committee of West China Hospital of 20230530005 and date of 2023.05.31.

2.2. Informed consent Statement

Informed consent was obtained from all subjects involved in the study. Written informed consent has been obtained from the patient(s) to publish this paper.

2.3. MASH diet

To establish MASH model, mice were subjected to HFMCD diet or HFD diet with 1% sulfate sodium (DSS). For HFMCD model, 6-8 weeks-old male WT mice and STK39^{-/-} mice were fed a high fat (60 Kcal%), methionine (1%) without choline (HFMCD, A06071302, ReadyDietech) for 8 weeks. The normal diet was standard mouse chow containing 16% protein, 61% carbohydrate, and 7.2% fat. For HFD + 1% DSS model, mice were fed a high fat, high cholesterol (HFD), and 1% DSS for 4 weeks. The diet consisted of 0.2% cholesterol, 20% protein, 43% CHO2I, and 23% fat (6.6% trans-fat) (D09100310, ReadyDietech). Additionally, 1% DSS was provided in the drinking water. A normal diet was mentioned as above.

2.4. ZT-1a treatment

ZT-1a (HY-136532, MedChemExpress), a non-ATP-competitive, selective SPAK inhibitor that inhibits SPAK activity (23), was concomitantly administered weekly *via* intraperitoneal injection (100 mg/kg) to

mice during induction of MASH.

2.5. Lentivirus transduction

HepG2 and SW480 cell lines were seeded in a 6-well plate and cultured for 12-24 h to 20-30% confluence in complete medium before transfection. The culture medium was replaced with serum-free medium containing lentivirus (Weizhen; Shandong, China) and 5 µg/ml polybrene (Weizhen). As a negative control, cells were transduced with an empty vector. After incubating for 8-12 h, the serum-free medium was changed to complete medium. Transfection efficiency was observed under a fluorescence microscope at 48-72 h after infection. Then, cells were treated with 5 µg/ml puromycin (MCE) for 2 days to select stably transfected cells.

2.6. Histology

Excised liver tissues were fixed in 10% neutral buffer formalin and embedded in paraffin. Formalin-fixed liver tissue sections were stained with H&E or Sirius Red. A blinded pathologist performed histologic grading of the liver tissue sections using the MASH-CRN scoring system. Colons were embedded in Tissue-Tek OCT compound (Sakura Finetek USA, Inc, Torrance, CA) and flash-frozen in liquid nitrogen. Colonic cryosections were stained with H&E. Histology images were obtained using a Zeiss Light Microscope (Leica, Jena, Germany).

2.7. Immunohistochemistry and Immunofluorescence

Liver cryosections were fixed with 4% paraformaldehyde in phosphate-buffered saline, and blocked with 3% bovine serum albumin in phosphate-buffered saline. Colonic cryosections were fixed with acetone for 5 minutes at -20°C and blocked with 5% bovine serum albumin in phosphate-buffered saline. The following primary antibodies (dilutions 1:100) were used: F4/80 (70076, Cell Signaling Technology), CD68 (ER1901-32, Huabio), and STK39 (ab128894, Abcam) Both liver and colonic cryosections were incubated with primary antibodies overnight at 4°C. Slides were washed twice with PBS-T and incubated with Rabbit EnVision+ System-HRP (Dako) or Mouse EnVision+ System-HRP (Dako) at RT for 30 min. Sections were counterstained with Mayer's hematoxylin and dehydration was performed by incubation in 70% and 100% ethanol followed by xylene, before slides were mounted using Pertex (Histolab).

For immunofluorescence analysis, tissue samples were dissected, washed with ice-cold PBS, and then fixed with 4% PFA in PBS for 12 h at 4°C. The tissues were incubated in 30% sucrose (Sigma-Aldrich) overnight, embedded in optimal cutting temperature

compound (Sakura Finetek, America), frozen on dry ice, and sectioned at -20°C. The frozen tissues were sectioned at a thickness of 4 µm on a cryostat (Leica). When applicable, sections were incubated in blocking buffer (5% milk powder in PBS-T) for 30 min at 25°C, and stained with primary antibodies directed against the following proteins: Occludin (1:200; R1510-33 Huabio) and ZO1 (1:200; ER41204, HuaBio), in blocking buffer overnight at 4°C. After washing in PBS-T, the slides were incubated for 2 h with the following secondary antibodies: goat anti-rabbit IgG (H+L) secondary antibody, and DAPI (Sigma-Aldrich) for 30 min at 25°C and washed in PBS-T. Tissues were mounted in VECTASHIELD HardSet Antifade Mounting Medium (Vector Labs) prior to sample acquisition on a Leica Dive confocal/multiphoton microscope or a Nikon A1R HD25 confocal microscope. Images were processed with ImageJ (National Institutes of Health; Bethesda, MD, USA).

2.8. Quantitative Reverse Transcription PCR

Total RNA was isolated from liver tissue using the RNeasy Mini Kit (Qiagen, Valencia, CA) according to the manufacturer's instructions. RNA (1 mg) was reverse-transcribed to complementary DNA using the Bio-Rad iScript complementary DNA synthesis kit (Bio-Rad, Hercules, CA). Quantitative reverse-transcription PCR was performed using gene-specific primer sets (Supplementary Table S1, <http://www.biosciencetrends.com/action/getSupplementalData.php?ID=205>) and IQ SYBR Green Supermix (Bio-Rad) on a Mastercycler ep realplex PCR instrument (Eppendorf, Hamburg, Germany). The reaction conditions were 95°C for 15 seconds, followed by 40 cycles of 95°C for 3 seconds, 55°C for 15 seconds, and 72°C for 20 seconds. Relative expression was calculated using the DDCT method with GAPDH serving as the reference housekeeping gene. Expression of the respective genes was normalized to that of GAPDH rRNA, and the normalized data are presented as the fold change in gene expression compared with that of control mice fed a normal diet.

2.9. Western blot

Cellular proteins were extracted from c-Kit⁺ cells after various treatments, and a BCA Protein Assay Kit (Beyotime Technology; Shanghai, China) was used to quantify total protein. Homogenates containing 50 µg of protein per sample were mixed with 5× loading buffer and denatured at 95°C for 5 min. Proteins were separated via SDS-PAGE (Baihe; Chengdu, China) and transferred onto 0.45 µm PVDF membranes (Millipore). The membranes were blocked with 5% non-fat dried milk, which was diluted in TBST, at room temperature for 2 h and incubated overnight at 4°C with primary antibodies

diluted in the same blocking buffer. The following primary antibodies (dilutions 1:1000) were used: TGF β 1 (ER31210, Huabio), α -SMA (ET1607-53, Huabio), IL-6(ab233706, Abcam), IL-17(RT1326, Huabio), NF- κ B (ET1603-12, Huabio) and GAPDH (ET1601-4, Huabio). After washing 3 times with TBST, membranes were incubated with HRP-conjugated secondary antibody for 1 h at RT. The membranes were visualized using the Gel Doc™ XR System (Bio-Rad).

2.10. Serum chemistry

ALT and AST levels in the serum were measured using aspartate aminotransferase and alanine transaminase activity assay kits (Sigma-Aldrich). Total serum cholesterol and triglyceride levels were measured on the CX7 chemistry autoanalyzer (Beckman Coulter Diagnostics, Miami, FL).

2.11. Cytokine analysis

The concentration of key inflammatory cytokines in the serum were quantified using the Milliplex Map Kit (EMD Millipore Corporation, Billerica, MA) on a Bio-Plex 200 System (Bio-Rad). For liver cytokine analysis, frozen liver tissue samples were homogenized in cell extraction buffer supplemented with 1 mmol/L phenylmethylsulfonyl fluoride and protease inhibitor cocktail (Life Technologies), and the supernatants were analyzed by multiplex enzyme-linked immunosorbent assay.

2.12. *In vivo* permeability assay

Intestinal permeability was assessed by *in vivo* FITC-dextran (FD4; Sigma-Aldrich) permeability assay as described previously¹⁷. Mice fasted for 4 h were gavaged with 0.6 mg/g body weight FITC-dextran (4 kDa) solution and blood was collected by submandibular bleeding after 3 h. Fluorescence intensity in the serum was measured using Fluorescence Spectrophotometer. FITC-dextran concentrations were determined from a standard curve generated by serial dilutions of FITC dextran.

2.13. Statistical analysis

Statistical differences were analyzed by unpaired Student's *t*-test analysis for multiple group comparison. A *p* value < 0.05 was considered statistically significant. Except for the human data, all animal experiments were repeated at least two times on two separate occasions.

3. Results

3.1. MASLD patients and MASH mice have enhanced STK39 expression in the colonic mucosa.

We initially explored the role of STK39 in colon tissues from MASLD. Biopsies taken from the proximal colon of six patients with MASLD and five subjects without MASLD (controls), who underwent surveillance colonoscopy, were examined for STK39 protein expression using immunochemistry. Individuals with elevated serum aspartate aminotransferase (AST) and alanine aminotransferase (ALT) levels, increased serum cholesterol and triglycerides, and hepatic steatosis confirmed by a right upper quadrant ultrasound (RUQ US) were diagnosed with MASLD (Figure 1A-C). Due to the absence of liver biopsy specimens, we were unable to specifically identify patients with MASH. Therefore, we collectively referred to the study cohort as having MASLD. Subjects with a body mass index of less than 25 kg/m², normal serum AST levels (\leq 40 U/L), and a negative liver ultrasonography were defined as controls (Figure 1D). The intestinal mucosa tissue of MASLD patients exhibited noticeably increased STK39 protein levels, as shown in Figure 1E. Remarkably, higher intestinal mucosal STK39 expression was associated with more severe mucosal inflammation in MASLD patients, as evidenced by a greater infiltration of immune cells in the mucosa (Figure 1F). Interestingly, we discovered the Occludin was also suppressed in colon tissues from MASLD patients (Figure 1G). Additionally, we examined STK39 expression in colon tissues from MASH model mice. Consistent with human observations, STK39 was upregulated in colon tissues from MASH mice (Figure 1H). We examined the hepatic stellate cell (HSCs) and Kupper cells infiltration in liver from mouse MASH model and control. we found the protein expression of α -SMA, a key marker of hepatic stellate cell (HSC) activation, was significantly upregulated in MASH mice (Figure 1I). And CD68 staining revealed increased infiltration of hepatic macrophages in MASH mice (Figure 1J). These results indicated more α -SMA⁺ HSCs infiltration and CD68⁺ Kupffer cells in mouse MASH model.

3.2. STK39 deletion attenuates HFMCD induced liver injury.

To investigate the role of STK39 in MASH, systemic STK39-deficient (STK39^{-/-}) mice were established (Figure 2A). These mice were born and developed normally, exhibiting no apparent functional defects (Figure 2B and Figure S1, <http://www.biosciencetrends.com/action/getSupplementalData.php?ID=205>). Subsequently, STK39^{-/-} mice and their control littermates were administered HFMCD diet for 8 weeks. STK39^{-/-} and control mice fed a normal diet served as controls. When fed either a normal diet (ND) or an HFMCD diet, there was a negligible difference in liver morphology and liver-to-body weight ratio between STK39^{-/-} and control mice (Figure 2C and D). Intriguingly, histological examination revealed

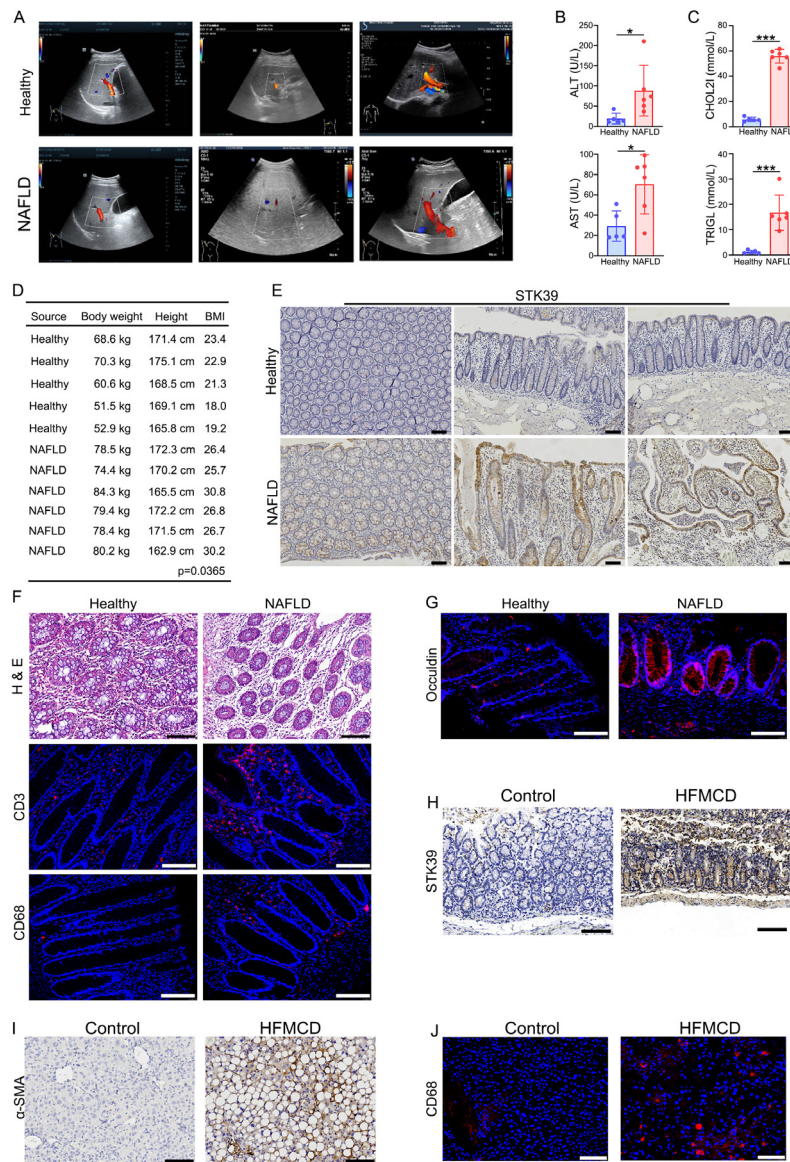


Figure 1. Colonic STK39 expression increased in MASLD patients. (A) Ultrasound imaging of healthy and MASLD patients. (B) Serum ALT and AST levels in healthy and MASLD patients. (C) Serum CHO2L and TRIGL levels in healthy and MASLD patients. (D) The weight, height, and BMI of healthy and MASLD. (E) Immunohistochemistry analyses of STK39 in colon tissue sections from healthy and MASLD patients. (F) Photomicrographs of H&E-, CD3 and CD68 stained colon tissue sections from healthy and MASLD patients. (G) Immunofluorescence analyses of Occulidin in colon tissue sections from healthy and MASLD patients. (H) Immunohistochemistry analyses of STK39 in colon tissue sections of ND and 8-week-HFMCD-induced mice. (I) Immunofluorescence analyses of α -SMA in liver tissues of ND and 8-week-HFMCD-induced mice. (J) Immunohistochemistry analyses of CD68 in liver tissue sections of ND and 8-week-HFMCD-induced mice. Scale bars: 100 μ m in (E), (F), (G), (H), (I) and (J). *indicates $p < 0.05$; **indicates $p < 0.01$; ***indicates $p < 0.001$.

that STK39^{-/-} mice developed less severe phenotypes of MASH, as indicated by reduced inflammatory cell infiltration, and decreased incidence of periportal and sinusoidal fibrosis (Figure 2E). Additionally, liver fibrosis marker genes and proteins were also evaluated. As shown in Figure 2F, the expression of α -SMA and TGF- β 1 (another profibrogenic protein), was markedly lower in STK39^{-/-} mouse livers. Similarly, the transcript levels of key molecules associated with hepatic fibrogenesis, including tissue inhibitor of metalloproteinase 1 (TIMP-1), and collagen 1 (α 1 and α 2), were also significantly decreased (Figure 2G). The MASH-CRN scores exhibited a significant decrease

of 1.53-fold in STK39^{-/-} mice fed an HFMCD diet compared to control mice fed the same diet (Figure 2H). Furthermore, the serum concentrations of AST and ALT were significantly lower in STK39^{-/-} mice fed an HFMCD diet compared to control mice, with reductions of 2.73-fold and 5.07-fold, respectively (Figure 2I and J).

To unravel the underlying molecular mechanism involved in HFMCD-induced MASH in STK39^{-/-} mice, we employed immunohistochemistry (IHC) to evaluate additional markers of hepatic inflammation. F4/80 and CD68 staining revealed decreased infiltration of hepatic macrophages or Kupffer cells in HFMCD-fed STK39^{-/-} mice (Figure 2K). The results of this study demonstrated

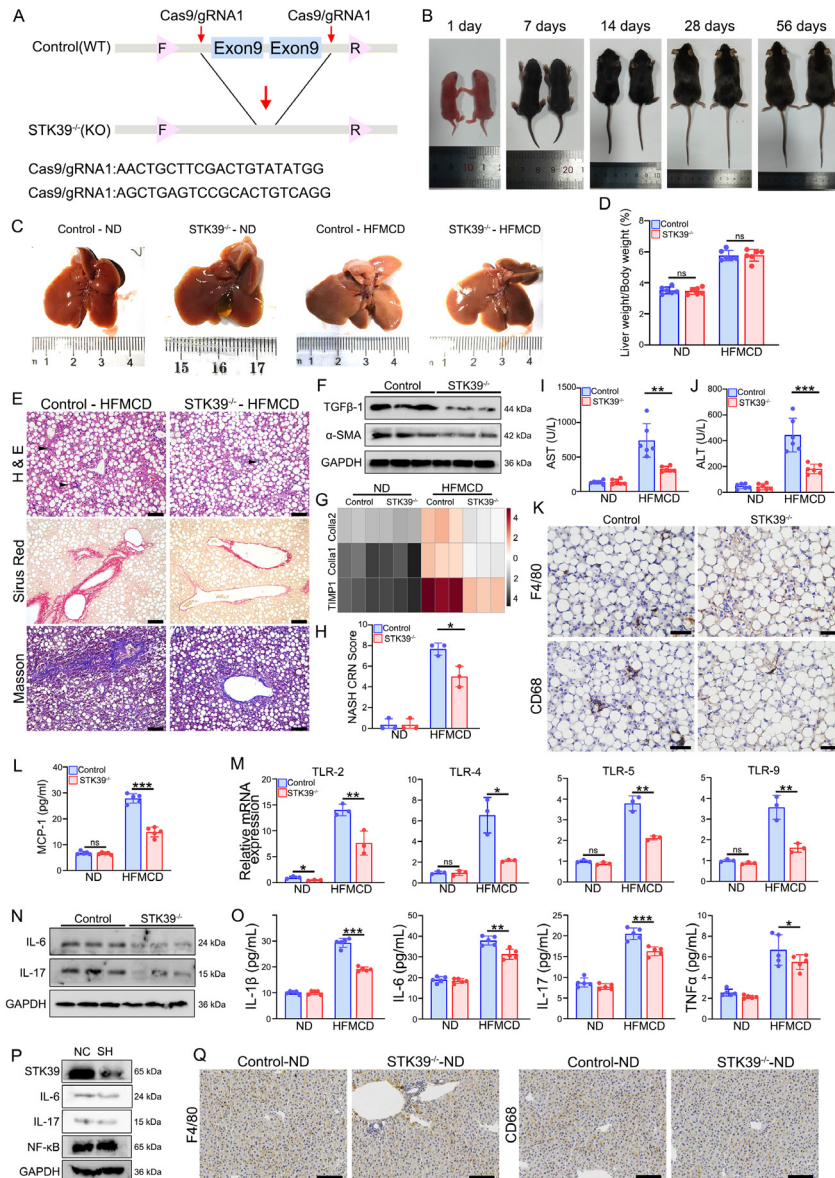


Figure 2. *STK39*^{-/-} mice fed a HFMCD developed modest histologic features of MASH. (A) Schematic of *STK39*-knockout in exons 9 and 10 using CRISPR/Cas9. (B) Representative images of control (wild-type [WT]) and *STK39*^{-/-} mice for 1, 7, 14, 30, and 56 days. (C) Representative gross images of livers from WT and *STK39*^{-/-} mice fed a ND or HFMCD for 8 weeks. (D) Liver weight/ Body weight analysis of WT and *STK39*^{-/-} mice fed a ND or HFMCD for 8 weeks. (E) Photomicro-graphs of H&E, Sirius Red, and Masson-stained liver tissue sections of WT and *STK39*^{-/-} mice fed a HFMCD for 8 weeks (*n* = 3). (F) Western blots demonstrating levels of TGF- β and α -SMA in liver tissues of WT and *STK39*^{-/-} mice fed a HFMCD for 8 weeks (*n* = 3). (G) Heatmap showing TIMP1, Colla1, and Colla2 mRNA expression in liver tissues of WT and *STK39*^{-/-} mice fed a ND or HFMCD for 8 weeks (*n* = 3). (H) MASH-CRN score in WT and *STK39*^{-/-} mice fed a ND or HFMCD for 8 weeks (*n* = 3). (I) Serum AST levels in WT and *STK39*^{-/-} mice fed a ND or HFMCD for 8 weeks (*n* = 6). (J) Serum ALT levels in the control (wild-type [WT]) and *STK39*^{-/-} mice fed a ND or HFMCD for 8 weeks (*n* = 6). (K) Immunohistochemical analyses of F4/80 and CD68 in liver tissue sections of WT and *STK39*^{-/-} mice fed a HFMCD for 8 weeks. (L) Quantification of the hepatic monocyte chemoattractant protein 1 (MCP-1) expression in WT and *STK39*^{-/-} mice fed a normal diet (ND) or a HFMCD for 8 weeks (*n* = 5). (M) QT-PCR showing TLR2, TLR4, TLR5, and TLR9 mRNA expression in liver tissues of WT and *STK39*^{-/-} mice fed a ND or HFMCD for 8 weeks (*n* = 3). (N) Western blots demonstrating levels of IL-6 and IL-17 in liver tissues of WT and *STK39*^{-/-} mice fed a HFMCD for 8 weeks (*n* = 3). (O) Serum IL-1 β , IL-6, IL-17, and TNF α levels (*n* = 5). (P) Western blots demonstrating the levels of IL-6, IL-17 and NF- κ B in PA treated HepG2 cell lines with or without *STK39* knockdown. (Q) Immunohistochemical analyses of F4/80 and CD68 in liver tissue sections of WT and *STK39*^{-/-} mice fed a ND. Scale bars: 50 μ m in (K) and 100 μ m in (E) and (Q). *indicates *p* < 0.05; **indicates *p* < 0.01; ***indicates *p* < 0.001.

a strong association between decreased levels of monocyte chemoattractant protein 1 (MCP-1, 1.87-fold) in the livers of *STK39*^{-/-} mice fed an HFMCD diet (Figure 2L). Further investigation revealed that the livers of HFMCD-fed *STK39*^{-/-} mice exhibited significantly reduced expression levels of Toll-like receptors (TLRs)-

2 (1.84-fold), TLR-4 (3.02-fold), TLR-5 (1.79-fold), and TLR-9 (2.21-fold), which are the primary TLRs involved in the recognition of bacterial pathogen-associated molecular patterns (Figure 2M). Consistent with these findings, the hepatic protein levels of key proinflammatory cytokines associated with MASH, IL-

6, and IL-17, exhibited a notable decrease in HFMCD-fed STK39^{-/-} mice compared to control mice (Figure 2N). Furthermore, HFMCD-fed STK39^{-/-} mice had significantly lower circulating levels of IL-1β (1.53-fold), IL-6 (1.21-fold), IL-17 (1.26-fold), and tumor necrosis factor-α (TNFα, 1.21-fold) (Figure 2O).

Conversely, in palmitic acid (PA)-treated HepG2 cells, there was no discernible difference in the levels of proinflammatory cytokines (IL-6 and IL-17) and transcription factor (NF-κB) between cells with or without STK39 expression (Figure 2P). Taken together, these findings suggest that TLR-mediated activation and recruitment of innate immune system cells are the causes of decreased hepatic inflammation in HFMCD-fed STK39^{-/-} mice. However, no differences in hepatic inflammatory parameters or immune cell infiltration were observed between control and STK39^{-/-} mice fed a normal diet (Figure 2Q).

Interestingly, for both the ND and HFMCD diet-fed mice, no difference was found in lipid droplet accumulation in the liver of both genotypes of mice (Figure 3A). Liver histopathology (Figure 3B), serum biochemical parameters of MASH, and molecular markers of fibrosis did not significantly differ between normal diet-fed control and STK39^{-/-} mice (Figure 2G-J). No significant differences were observed with respect to metabolic parameters, including cholesterol (CHO2I) or triglyceride (TRIGL) levels (Figure 3C and D). In

addition, the expression of genes involved in de novo lipogenesis (Fas and Pparα), lipid transport (Cpt1a), and β-oxidation (Acox1) were also not significantly lower in STK39^{-/-} mice than in HFMCD-fed controls (Figure 3E). Furthermore, we evaluated the impact of STK39 knockdown on lipid metabolism *in vitro*. In a palmitic acid (PA)-induced MASH model, STK39 knockdown *via* short-hairpin RNA (shRNA) had little impact on lipid accumulation in HepG2 cells (Figure 3F).

In summary, STK39 Knockout mice reduced HFMCD-induced liver inflammation but had minimal effects on hepatic lipid metabolism.

3.3. STK39 ablation improves intestinal epithelial permeability in HFMCD mouse model.

HFMCD consumption causes damage to the intestinal epithelial barrier, leading to increased translocation of gut-associated microbial products and consequent excessive hepatic inflammation. The attenuated hepatic inflammation in STK39^{-/-} mice prompted us to determine whether STK39 impairs the intestinal epithelial barrier. We measured intestinal epithelial permeability using an *in vivo* FITC-dextran permeability assay, and the serum lipopolysaccharide (LPS) concentration was used as an indicator of increased microbial product translocation. Compared with that in normal diet-fed WT mice, the dextran flux in HFMCD-

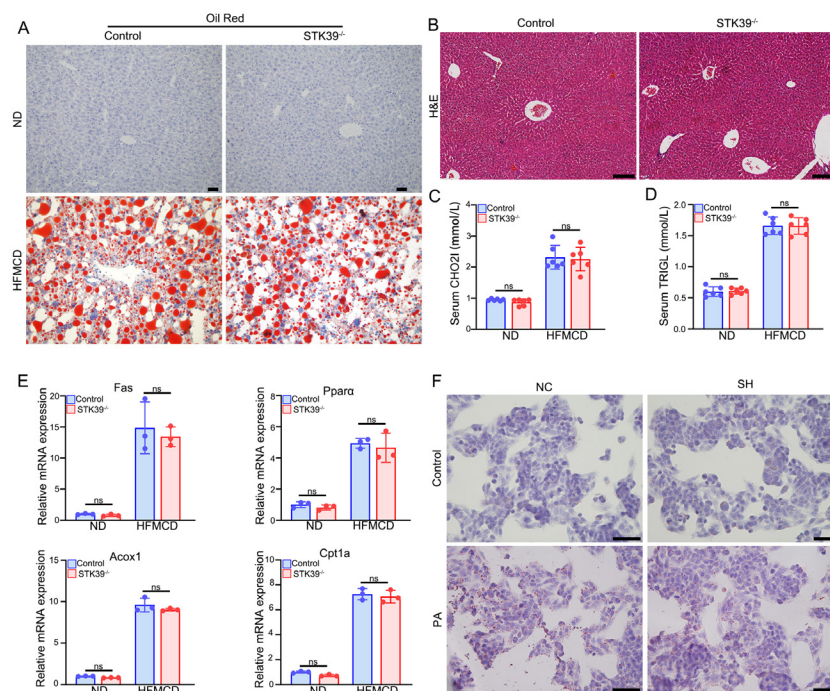


Figure 3. STK39^{-/-} mice exhibited no significant differences in lipid metabolism. (A) Photomicrographs of Oil Red-stained liver tissue sections of WT and STK39^{-/-} mice fed a ND or HFMCD for 8 weeks. (B) Photomicrographs of H&E-stained liver tissue sections of WT and STK39^{-/-} mice fed a ND. (C) Serum CHO2I levels of WT and STK39^{-/-} mice fed a ND or HFMCD for 8 weeks. (D) Serum TRIGL levels of WT and STK39^{-/-} mice fed a ND or HFMCD for 8 weeks. (E) Quantification of the Fas, Pparα, Acox1, and Cpt1a expression in WT and STK39^{-/-} mice fed a normal diet (ND) or a HFMCD for 8 weeks. (F) Photomicrographs of Oil Red-stained HepG2 cell lines of PA treated with or without STK39 knockdown. Scale bars: 50 μm in (F) and 100 μm in (A) and (B). *indicates *p* < 0.05; **indicates *p* < 0.01; ***indicates *p* < 0.001.

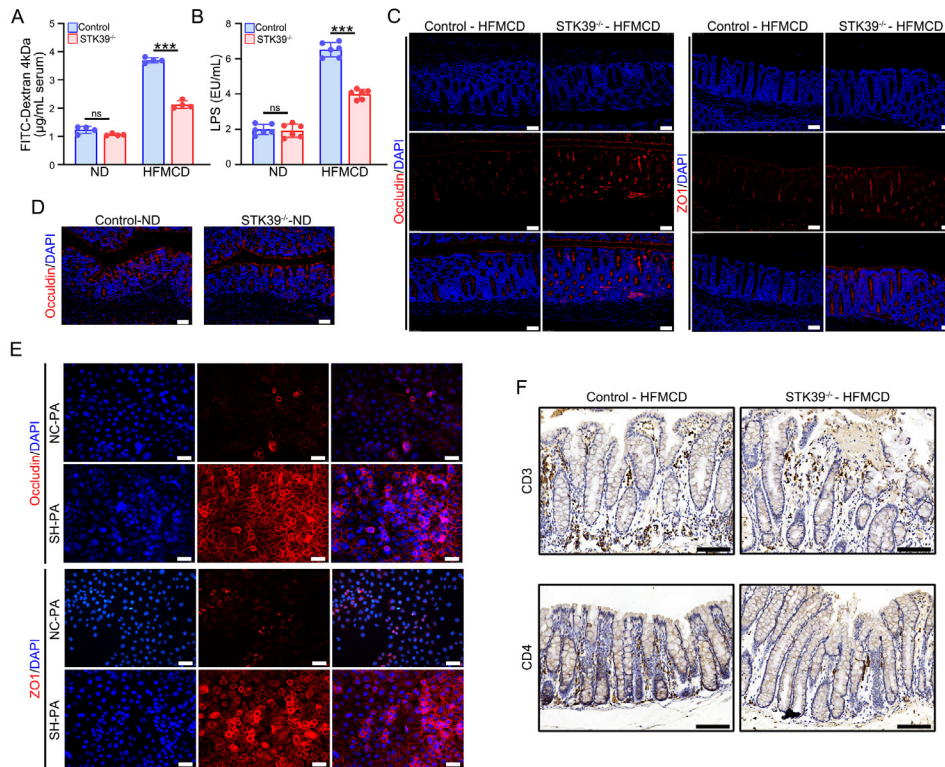


Figure 4. STK39-ablation attenuated HFMCD-induced intestinal epithelial permeability and bacterial translocation. (A) Intestinal permeability to FITC-dextran in WT and STK39^{-/-} mice fed a normal diet (ND) or a HFMCD for 8 weeks ($n = 4$). (B) Serum LPS levels after 8 weeks of ND and HFMCD feeding ($n = 6$). (C) Immunofluorescence analyses of Occludin and ZO1 in colon tissue sections of WT and STK39^{-/-} mice fed a HFMCD for 8 weeks. (D) Immunofluorescence analyses of Occludin in colon tissue sections of WT and STK39^{-/-} mice fed a ND for 8 weeks. (E) Immunofluorescence analyses of Occludin and ZO1 in SW480 cell lines of control and STK39 knockdown treated with PA. (F) Immunohistochemistry analyses of CD3 and CD4 in colon tissue sections of WT and STK39^{-/-} mice fed a HFMCD for 8 weeks. Scale bars: 50 µm in (C), (D), (E), and (F). *indicates $p < 0.05$; **indicates $p < 0.01$; ***indicates $p < 0.001$.

fed WT mice was 3-fold greater, but the dextran flux in HFMCD-fed STK39^{-/-} mice was much lower (1-fold) (Figure 4A). This indicated that consumption of HFMCD led to impairment of intestinal epithelial barrier function, and knockout of STK39 alleviated this injury, thereby delaying MASH development in STK39^{-/-} mice. Similarly, we also observed a 1.63-fold reduction in the serum LPS concentration in HFMCD-fed STK39^{-/-} mice compared to that in HFMCD-fed control mice (Figure 4B).

Additionally, the expression and distribution of the tight junction proteins (Occludin and ZO-1) were determined *via* immunofluorescence. As shown in Figure 4C, Occludin and ZO-1 expression was more intact in HFMCD-fed STK39^{-/-} mice, compared with HFMCD-fed control mice. However, no significant difference in Occludin expression was observed between the two genotypic mouse strains fed a normal diet (Figure 4D). To further explore the role of STK39 in regulating tight junctions (TJs), STK39 was silenced in SW480 cells, a colorectal cancer cell line. Consistent with the findings *in vivo*, STK39 knockdown led to maintained Occludin and ZO-1 expression in PA-treated model (Figure 4E). In addition to protecting TJs, knockout of STK39 in mice also suppressed HFMCD-induced intestinal

inflammation (Figure 4F).

Taken together, these findings suggest that STK39 plays a negative role in intestinal barrier integrity.

3.4. STK39 knockout delays MASH formation in the HFD+DSS-induced model.

As shown above, HFMCD can impair the intestinal barrier, which promotes MASH development. Colitis is primarily characterized by damage to the intestinal barrier and is caused by the administration of dextran sulfate sodium (DSS) in mice (23). A high-fat diet (HFD) is commonly used to induce MASLD without liver fibrosis and less inflammatory cell infiltration compared with HFMCD. To further investigate the association between intestinal barrier integrity and MASH, STK39^{-/-} and control mice were fed a HFD or HFD + DSS (1%) for 4 weeks (Figure 5A). Compared with those in the HFD group, the mice in the HFD + DSS group developed more severe histological features of MASH, including liver fibrosis and inflammatory cell infiltration, suggesting that the combination of HFD and DSS could trigger MASH (Figure 5B-D). Notably, ablation of STK39 significantly reduced MASH incidence, as indicated by fibrosis and inflammatory cell infiltration (Figure 5E and F), even

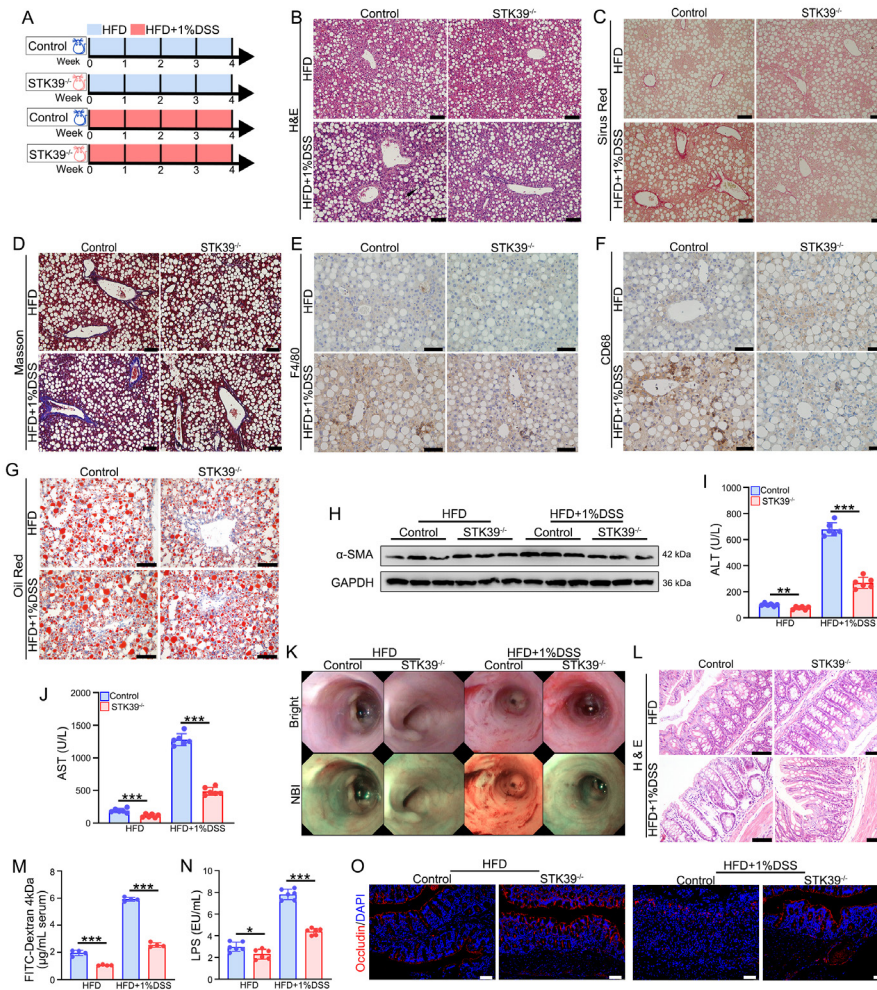


Figure 5. STK39 knockout delayed MASH in the HFD+DSS-induced model. (A) Schematic of the WT and STK39^{-/-} mice and experiment protocol; DSS: 1%. (B) Photomicrographs of H&E-stained liver tissue sections of WT and STK39^{-/-} mice fed a HFD and HFD+DSS for 4 weeks (n = 6). (C) Photomicrographs of Sirius Red-stained liver tissue sections of WT and STK39^{-/-} mice fed a HFD and HFD+DSS for 4 weeks. (D) Photomicrographs of Masson-stained liver tissue sections of WT and STK39^{-/-} mice fed a HFD and HFD+DSS for 4 weeks. (E) Immunohistochemistry analyses of F4/80 in liver tissue sections of WT and STK39^{-/-} mice fed a HFD and HFD+DSS for 4 weeks. (F) Immunohistochemistry analyses of CD68 in liver tissue sections of WT and STK39^{-/-} mice fed a HFD and HFD+DSS for 4 weeks. (G) Photomicrographs of Oil Red-stained liver tissue sections of WT and STK39^{-/-} mice fed a HFD or HFD+DSS for 4 weeks. (H) Western blots demonstrating lev-els of α -SMA in liver tissues of WT and STK39^{-/-} mice fed a HFD and HFD+DSS for 4 weeks. (I, J) Serum ALT AND AST levels in the WT and STK39^{-/-} mice fed a HFD and HFD+DSS for 4 weeks (n = 6). (K) Representative morphology images of colonoscopy from WT and STK39^{-/-} mice fed a HFD or HFD+DSS for 4 weeks. (L) Photomicrographs of H&E-stained colon tissue sections of WT and STK39^{-/-} mice fed a HFD or HFD+DSS for 4 weeks. (M) Intestinal permeability to FITC-dextran in WT and STK39^{-/-} mice fed a HFD or HFD+DSS for 4 weeks. (N) Serum LPS levels in WT and STK39^{-/-} mice fed a HFD or HFD+DSS for 4 weeks. (O) Immunofluorescence analyses of Occludin in WT and STK39^{-/-} mice fed a HFD or HFD+DSS for 4 weeks. Scale bars: 50 μ m in (E), (F), (G), (L), and (O); 100 μ m in (B), (C), and (D). *indicates $p < 0.05$; **indicates $p < 0.01$; ***indi-cates $p < 0.001$.

though the accumulation of lipids was unaffected (Figure 5G). Consistent with the findings in HFMCD-induced MASH, the α -SMA protein expression showed that ablation of STK39 significantly reduced fibrosis (Figure 5H). Furthermore, the serum AST and ALT concentrations were also significantly lower in STK39^{-/-} mice than in WT mice (Figure 5I and J).

Moreover, colonoscopy and histological analysis revealed milder colonic damage in STK39^{-/-} mice (Figure 5K and L). The dextran flux and serum LPS levels were lower in STK39^{-/-} mice than in control mice, regardless of DSS administration (Figure 5M and N). Additionally, the expression of Occludin was much greater in STK39^{-/-}

mice in both the HFD and HFD + DSS (1%) groups (Figure 5O). Taken together, these data provide evidence that STK39 ablation can alleviate MASH induced by HFD and DSS by reducing intestinal barrier disruption caused by DSS.

3.5. ZT-1a attenuates HFMCD induced liver injury by improving intestinal epithelia permeability.

The above results prompted us to investigate whether inhibiting STK39 activity prevents the progression of MASH. Mice were treated with 100 mg/kg ZT-1a, a specific STK39 inhibitor, through intraperitoneal

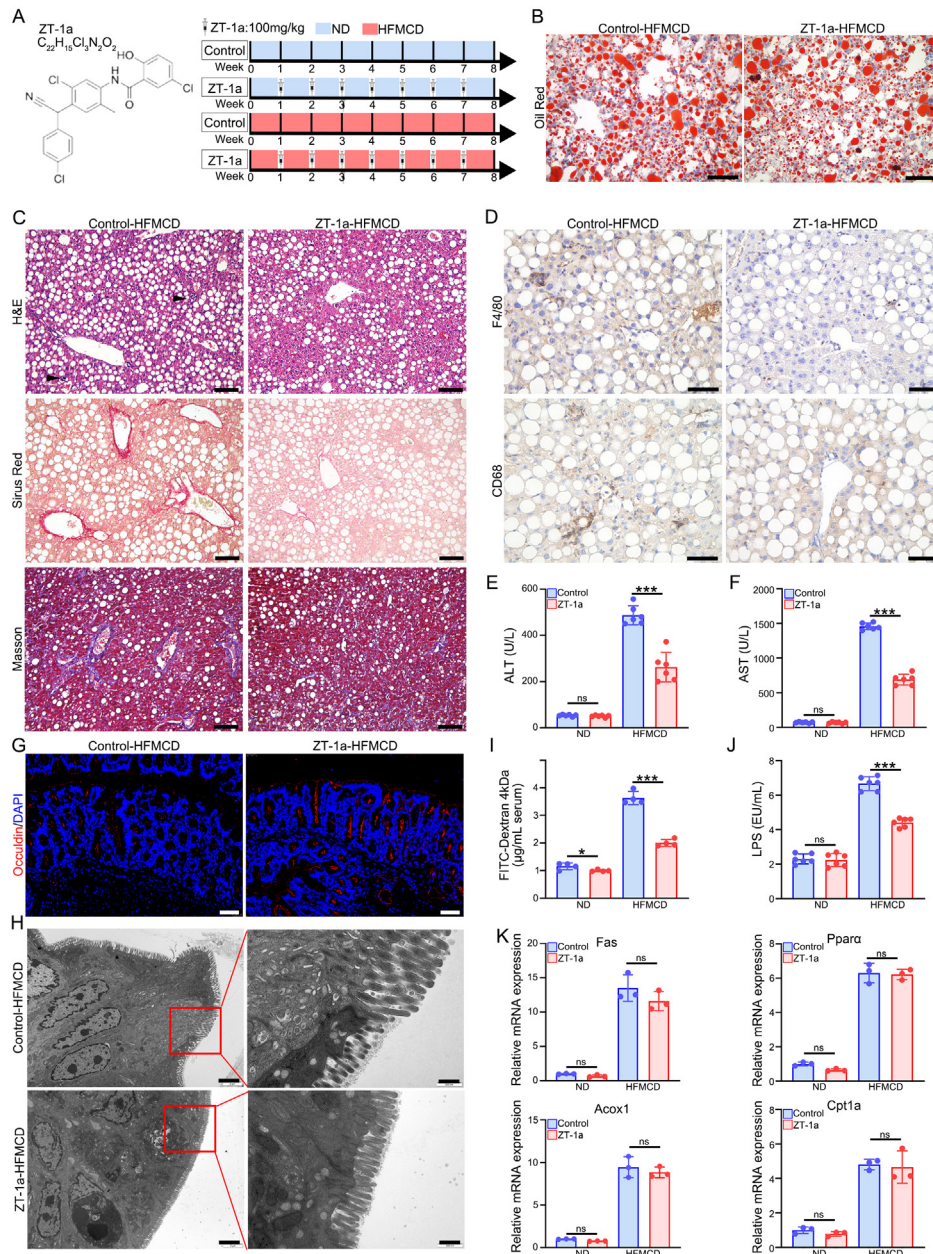


Figure 6. STK39 inhibition by ZT-1a attenuated HFMCD-induced MASH. (A) Structural formula of ZT-1a and schematic of the experiment protocol. (B) Oil Red O staining of steatosis in liver tissues of control and ZT-1a treated mice fed a HFMCD for 8 weeks. (C) Photomicrographs of H&E, Sirius Red O and Masson-stained liver tissue sections of control and ZT-1a treated mice fed a HFMCD for 8 weeks. ($n = 6$). (D) Immunohistochemistry analyses of F4/80 and CD68 in liver tissue sections of control and ZT-1a treated mice fed a HFMCD for 8 weeks. (E, F) Serum ALT and AST levels in the control and ZT-1a treated mice fed a HFMCD for 8 weeks ($n = 6$). Scheme of the Control and STK39^{-/-} mice and experiment protocol; DSS:1%. (G) Immunofluorescence analyses of Occludin in liver tissue sections of control and ZT-1a treated mice fed a HFMCD for 8 weeks. (H) Transmission electron microscopy analyses of TJs in colon tissue sections of control and ZT-1a treated mice fed a HFMCD for 8 weeks. (I) Intestinal permeability to FITC-dextran in the control and ZT-1a treated mice fed a HFMCD for 8 weeks ($n = 4$). (J) Serum LPS levels in the control and ZT-1a treated mice fed a HFMCD for 8 weeks ($n = 6$). (K) Quantification of the Fas, Ppara, Acox1, and Cpt1a expression in Control and ZT-1a treated mice fed a HFMCD for 8 weeks. Scale bars: 50 μm in (B), (D) and (G); 100 μm in (C); 2 μm (left) and 500 nm (right) in (H). Statistics: Unpaired two-tailed Student's t test in (E), (F), (H), and (I). *indicates $p < 0.05$; **indicates $p < 0.01$; ***indicates $p < 0.001$.

injection after 1 week of HFMCD treatment (24) (Figure 6A). Although no significant differences were observed in steatosis between the control group and the ZT-1a treatment group (Figure 6B), liver fibrosis and inflammation were significantly reduced after ZT-1a treatment, as assessed by H&E, Masson, Sirius Red, F4/80, and CD68 staining (Figure 6C and D).

Consistent with these results, the serum ALT and AST levels were also lower in ZT-1a-treated mice than in control mice (Figure 6E and F). As expected, ZT-1a protected TJs against HFMCD-induced impairment, as measured by Occludin immunofluorescence staining (Figure 6G). We further examined the TJs by transmission electron microscopy. Consistently, we

found ZT-1a protected the TJs (Figure 6H). Similarly, the serum dextran flux and LPS concentration in the ZT-1A-treated mice were 1.74-fold and 1.51-fold lower, respectively, than those in the control group (Figure 6I and J). Interestingly, ZT-1a also had minimal impact in the lipid metabolism pathway (Figure 6K).

4. Discussion

In the present study, we present experimental evidence indicating that intestinal epithelial barrier function plays a pivotal role in the progression of MASLD. STK39 was overexpressed in colon tissues from MASH patients and mice. Knockout of STK39 and inhibition of STK39 activity using ZT-1a significantly alleviated HFMCD-induced MASH in mice by reducing hepatic inflammation and fibrosis. Mechanistically, the knockout of STK39 ameliorated MASH through the attenuation of gut inflammation, enhancement of intestinal barrier functions and decreased intestinal bacterial translocation (Figure 7).

The incidence of MASH, which increases the risk of diabetes, cardiovascular diseases, and cancer, is rising worldwide (25). Consequently, it is imperative to explore therapeutic targets aimed at preventing adverse outcomes. STK39 is a serine/threonine kinase believed to function within the cellular stress response pathway. The kinase becomes activated in response to hypotonic stress, triggering the phosphorylation of several cation-chloride-coupled cotransporters. The catalytically active form of STK39 specifically activates the p38 MAP kinase pathway, and its interaction with p38 diminishes during cellular stress, indicating that this kinase may serve as a mediator in the cellular stress response (26,27). In our research, when STK39 was systemically knocked out, the progression of hepatic fibrosis and inflammation caused by the HFMCD

diet was markedly inhibited. This inhibition was similar to the phenotype observed following intestinal knockout of STK39. MASH is generally considered to be the outcome of excessive accumulation of hepatic lipids, leading to hepatocyte rupture and death, as well as the recruitment of inflammatory factors that exacerbate the development of hepatic inflammation and fibrosis (28). However, we discovered that hepatic genes pertaining to lipid metabolism, encompassing those involved in de novo lipogenesis, transport, and β -oxidation, were not significantly altered when STK39 was knocked out either *in vivo* or *in vitro*. This suggested that STK39 does not affect lipid metabolism in the liver. We subsequently delved deeper into the changes in the expression of STK39 in the liver during the development of MASH. Our findings revealed that STK39 expression was not significantly upregulated when hepatic inflammation was not evident. Nevertheless, the protein level of STK39 was significantly elevated in the presence of increased macrophage infiltration (Figure S2, <http://www.biosciencetrends.com/action/getSupplementalData.php?ID=205>). This may be attributed to the fact that when hepatic inflammation becomes apparent, proinflammatory factors such as NF- κ B upregulate the expression of STK39, which subsequently exacerbates the progression of hepatic inflammation and fibrosis, which aligns with previous reports by Tsai-Jung Lin (29). Collectively, our findings confirm that STK39 is not involved in the progression of MASH through its influence on lipid metabolism. Consequently, these findings prompted us to explore novel mechanisms underlying how STK39 contributes to the progression of MASH.

Bidirectional crosstalk along the gut-liver axis controls gastrointestinal health and disease, exploiting environmental and host mediators (7). Nutrients,

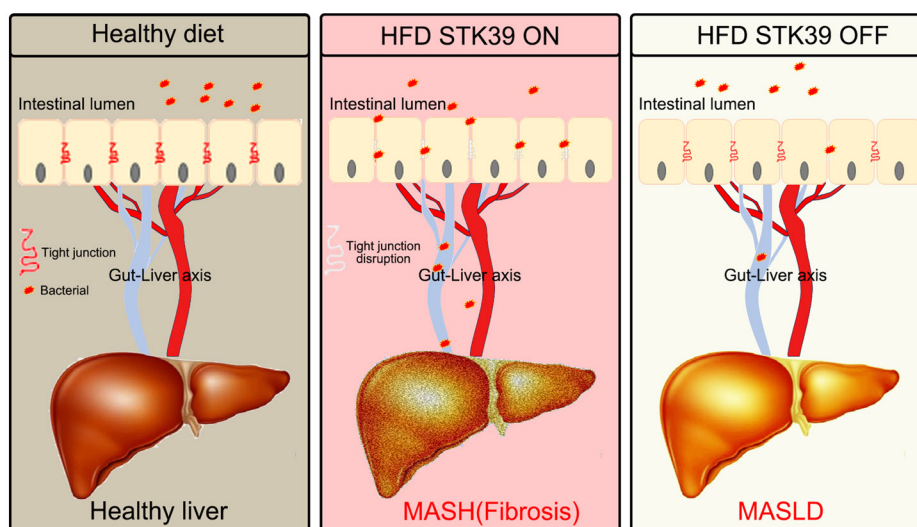


Figure 7. Modulation of intestinal epithelial permeability by STK39 promotes MAFLD /MASH progression.

microbial antigens, metabolites, and bile acids modulate metabolism and immune responses in both the gut and liver, which in turn mutually influence the structure and function of the microbial community. Perturbation in these host-microbe interactions are observed in various experimental liver diseases and are exacerbated by an impaired intestinal barrier, which fuels hepatic inflammation and disease progression (30). Clinical evidence demonstrates perturbation of the gut-liver crosstalk in MASLD, alcoholic liver disease, and primary sclerosing cholangitis (31). In liver cirrhosis, a common sequela of these diseases, the intestinal microbiota and microbial pathogen-associated molecular patterns contribute to liver inflammation and clinical complications (32). Recent studies have shown that STK39 expression is enhanced in colon tissues from patients with Crohn's disease (CD) and ulcerative colitis (UC) (21). Notably, the intestinal barrier is significantly impaired in CD and UC patients. Numerous studies have reported that intestinal barrier damage is linked to liver disease, including MASLD/MASH, liver cirrhosis, and hepatocellular carcinoma (33-35). We discovered that suppressing STK39 protected the intestinal barrier and reduced inflammatory cell infiltration in colonic tissues. These findings suggest that STK39 may be involved in the development of MASH through intestinal barrier damage. Moreover, STK39 knockout protected tight junction proteins (Occludin and ZO1) from HFD-induced damage. These findings indicate that STK39 may negatively regulate the intestinal barrier integrity. The HFD+DSS model further supports our hypothesis. A HFD reduces tight junction proteins in the gut, but only causes mild inflammation and fibrosis in the liver. We found that the combination of HFD+DSS led to significant MASH symptoms, including severe inflammation and fibrosis. Moreover, the clearance of STK39 significantly inhibited the damage to intestinal tight junction proteins caused by HFD+DSS. The serum LPS concentration was reduced, and intestinal bacterial translocation was also significantly reduced. Eventually, the degree of liver fibrosis and inflammation are significantly attenuated, strongly delaying the progression of MASH. Although we have demonstrated that STK39 is associated with tight junction proteins, the exact mechanism by which STK39 regulates the expression of these proteins needs to be further explored. Given the crucial role of STK39 in the gut-liver axis, it may represent a novel target for the treatment of MASH.

There is also growing evidence that drugs developed to target the intestinal barrier, such as those for MASLD/MASH, can be effective in treating liver disease (36). Here, we chose the pharmacological inhibitor, ZT-1a, a potent non-ATP-competitive and selective SPAK inhibitor that inhibits STK39 activity, which has been shown to effectively and efficiently improve neurological function after ischemic stroke

(24). In the present study, we found that after ZT-1a treatment, the level of tight junction proteins in the intestinal epithelium was maintained, and the intestinal barrier was protected, thereby reducing hepatic fibrosis and inflammatory cell infiltration and effectively slowing the progression of MASH. These findings not only strongly demonstrate the important role of STK39 in MASH, but also provide a new therapeutic strategy for treating MASH.

Taken together, our work demonstrates a crucial role for intestinal epithelial permeability in MASH progression and underscores the intricate role of diet in regulating gut homeostasis, inflammation, and liver health. Given our data showing increased STK39 expression in colonic biopsy specimens from MASLD patients, it suggests that genetic or epigenetic vulnerabilities of proteins regulating intestinal epithelial barrier integrity may predispose human to MASLD progression. In conclusion, our data have revealed that defective intestinal epithelial barrier, dysbiosis, and associated activation of the innate immune system caused by increased translocation of gut microbial products are risk factors associated with MASLD progression. Mice fed HFMC diet exhibited a superimposed hit, driving a proinflammatory gut microbial composition that exacerbated gut permeability. In turn, enhanced gut leakiness results in microbial product translocation, which induces hepatic inflammation and injury, ultimately leading to the progression of MASLD to MASH. STK39 inhibition prevented this process. The present findings strongly justify the consideration of therapies targeting the intestinal epithelial barrier, dysbiosis, innate immune function, or a combination of these factors to significantly slow or halt MASH progression.

Funding: This work was supported by a grant from the Science Foundation of Sichuan, China (NO.2023NSFSC1613) and the Postdoctoral Foundation of West China Hospital, Sichuan University (NO. 2023HXBH020).

Conflict of Interest: The authors have no conflicts of interest to disclose.

References

1. Ray K. NAFLD-the next global epidemic. *Nat Rev Gastroenterol Hepatol.* 2013; 10:621.
2. Younossi Z, Tacke F, Arrese M, Chander Sharma B, Mostafa I, Bugianesi E, Wai-Sun Wong V, Yilmaz Y, George J, Fan J, Vos MB. Global Perspectives on Nonalcoholic Fatty Liver Disease and Nonalcoholic Steatohepatitis. *Hepatology.* 2019; 69:2672-2682.
3. Anstee QM, Reeves HL, Kotsiliti E, Govaere O, Heikenwalder M. From NASH to HCC: current concepts and future challenges. *Nat Rev Gastroenterol Hepatol.* 2019; 16:411-428.

4. De Munck TJI, Xu P, Verwijs HJA, Masclee AAM, Jonkers D, Verbeek J, Koek GH. Intestinal permeability in human nonalcoholic fatty liver disease: A systematic review and meta-analysis. *Liver Int.* 2020; 40:2906-2916.
5. Rahman K, Desai C, Iyer SS, Thorn NE, Kumar P, Liu Y, Smith T, Neish AS, Li H, Tan S, Wu P, Liu X, Yu Y, Farris AB, Nusrat A, Parkos CA, Anania FA. Loss of Junctional Adhesion Molecule A Promotes Severe Steatohepatitis in Mice on a Diet High in Saturated Fat, Fructose, and Cholesterol. *Gastroenterology.* 2016; 151:733-746.e12.
6. He S, Cui S, Song W, Jiang Y, Chen H, Liao D, Lu X, Li J, Chen X, Peng L. Interleukin-17 Weakens the NAFLD/NASH Process by Facilitating Intestinal Barrier Restoration Depending on the Gut Microbiota. *mBio.* 2022; 13:e0368821.
7. Albillos A, de Gottardi A, Rescigno M. The gut-liver axis in liver disease: Pathophysiological basis for therapy. *J Hepatol.* 2020; 72:558-577.
8. Leshem A, Liwinski T, Elinav E. Immune-Microbiota Interplay and Colonization Resistance in Infection. *Mol Cell.* 2020; 78:597-613.
9. Moreira AP, Texeira TF, Ferreira AB, Peluzio Mdo C, Alfenas Rde C. Influence of a high-fat diet on gut microbiota, intestinal permeability and metabolic endotoxaemia. *Br J Nutr.* 2012; 108:801-809.
10. Pandyala S, Walker JM, Holt PR. A high-fat diet is associated with endotoxemia that originates from the gut. *Gastroenterology.* 2012; 142:1100-1101.e2.
11. Otani T, Furuse M. Tight Junction Structure and Function Revisited. *Trends Cell Biol.* 2020; 30:805-817.
12. Buckley A, Turner JR. Cell Biology of Tight Junction Barrier Regulation and Mucosal Disease. *Cold Spring Harb Perspect Biol.* 2018; 10:a029314.
13. Kaushal K, Agarwal S, Sharma S, Goswami P, Singh N, Sachdev V, Poudel S, Das P, Yadav R, Kumar D, Pandey G, Gunjan D, Saraya A. Demonstration of Gut-Barrier Dysfunction in Early Stages of Non-alcoholic Fatty Liver Disease: A Proof-Of-Concept Study. *J Clin Exp Hepatol.* 2022; 12:1102-1113.
14. Luther J, Garber JJ, Khalili H, Dave M, Bale SS, Jindal R, Motola DL, Luther S, Bohr S, Jeoung SW, Deshpande V, Singh G, Turner JR, Yarmush ML, Chung RT, Patel SJ. Hepatic Injury in Nonalcoholic Steatohepatitis Contributes to Altered Intestinal Permeability. *Cell Mol Gastroenterol Hepatol.* 2015; 1:222-232.
15. Csak T, Ganz M, Pespisa J, Kodys K, Dolganiuc A, Szabo G. Fatty acid and endotoxin activate inflammasomes in mouse hepatocytes that release danger signals to stimulate immune cells. *Hepatology.* 2011; 54:133-144.
16. Henaoui-Mejia J, Elinav E, Jin C, Hao L, Mehal WZ, Strowig T, Thaiss CA, Kau AL, Eisenbarth SC, Jurczak MJ, Camporez JP, Shulman GI, Gordon JI, Hoffman HM, Flavell RA. Inflammasome-mediated dysbiosis regulates progression of NAFLD and obesity. *Nature.* 2012; 482:179-185.
17. Tsukita S, Furuse M, Itoh M. Multifunctional strands in tight junctions. *Nat Rev Mol Cell Biol.* 2001; 2:285-293.
18. Pitman RS, Blumberg RS. First line of defense: the role of the intestinal epithelium as an active component of the mucosal immune system. *J Gastroenterol.* 2000; 35:805-814.
19. Wang W, Zhao J, Gui W, Sun D, Dai H, Xiao L, Chu H, Du F, Zhu Q, Schnabl B, Huang K, Yang L, Hou X. Tauroursodeoxycholic acid inhibits intestinal inflammation and barrier disruption in mice with non-alcoholic fatty liver disease. *Br J Pharmacol.* 2018; 175:469-484.
20. Johnston AM, Naselli G, Gonez LJ, Martin RM, Harrison LC, DeAizpurua HJ. SPAK, a STE20/SPS1-related kinase that activates the p38 pathway. *Oncogene.* 2000; 19:4290-4297.
21. Zhang Y, Viennois E, Xiao B, Baker MT, Yang S, Okoro I, Yan Y. Knockout of Ste20-like proline/alanine-rich kinase (SPAK) attenuates intestinal inflammation in mice. *Am J Pathol.* 2013; 182:1617-1628.
22. Yan Y, Laroui H, Ingersoll SA, Ayyadurai S, Charania M, Yang S, Dalmasso G, Obertone TS, Nguyen H, Sitaraman SV, Merlin D. Overexpression of Ste20-related proline/alanine-rich kinase exacerbates experimental colitis in mice. *J Immunol.* 2011; 187:14961-505.
23. Zhang J, Bhuiyan MIH, Zhang T *et al.* Modulation of brain cation-Cl⁻ cotransport *via* the SPAK kinase inhibitor ZT-1a. *Nature Communications.* 2020; 11:78.
24. Bhuiyan MIH, Fischer S, Patel SM, Oft H, Zhang T, Foley LM, Zhang J, Hitchens TK, Molyneaux BJ, Deng X, Sun D. Efficacy of novel SPAK inhibitor ZT-1a derivatives (1c, 1d, 1g & 1h) on improving post-stroke neurological outcome and brain lesion in mice. *Neurochem Int.* 2023; 162:105441.
25. Harrison SA, Allen AM, Dubourg J, Noureddin M, Alkhoury N. Challenges and opportunities in NASH drug development. *Nat Med.* 2023; 29:562-573.
26. Rinehart J, Maksimova YD, Tanis JE, Stone KL, Hodson CA, Zhang J, Risinger M, Pan W, Wu D, Colangelo CM, Forbush B, Joiner CH, Gulcicek EE, Gallagher PG, Lifton RP. Sites of regulated phosphorylation that control K⁺-Cl⁻ cotransporter activity. *Cell.* 2009; 138:525-536.
27. Richardson C, Rafiqi FH, Karlsson HK, Moleleki N, Vandewalle A, Campbell DG, Morrice NA, Alessi DR. Activation of the thiazide-sensitive Na⁺-Cl⁻ cotransporter by the WNK-regulated kinases SPAK and OSR1. *J Cell Sci.* 2008; 121(Pt 5):675-684.
28. Xu X, Poulsen KL, Wu L, Liu S, Miyata T, Song Q, Wei Q, Zhao C, Lin C, Yang J. Targeted therapeutics and novel signaling pathways in non-alcohol-associated fatty liver/steatohepatitis (NAFL/NASH). *Signal Transduct Target Ther.* 2022; 7:287.
29. Lin TJ, Yang SS, Hua KF, Tsai YL, Lin SH, Ka SM. SPAK plays a pathogenic role in IgA nephropathy through the activation of NF- κ B/MAPKs signaling pathway. *Free Radic Biol Med.* 2016; 99:214-224.
30. de Vos WM, Tilg H, Van Hul M, Cani PD. Gut microbiome and health: mechanistic insights. *Gut.* 2022; 71:1020-1032.
31. Tilg H, Adolph TE, Trauner M. Gut-liver axis: Pathophysiological concepts and clinical implications. *Cell Metab.* 2022; 34:1700-1718.
32. Tilg H, Zmora N, Adolph TE, Elinav E. The intestinal microbiota fuelling metabolic inflammation. *Nat Rev Immunol.* 2020; 20:40-54.
33. Tilg H, Adolph TE, Dudek M, Knolle P. Non-alcoholic fatty liver disease: the interplay between metabolism, microbes and immunity. *Nat Metab.* 2021; 3:1596-1607.
34. Muñoz L, Borrero MJ, Úbeda M, Conde E, Del Campo R, Rodríguez-Serrano M, Lario M, Sánchez-Díaz AM, Pastor O, Díaz D, García-Bermejo L, Monserrat J, Álvarez-Mon M, Albillos A. Intestinal Immune Dysregulation Driven by Dysbiosis Promotes Barrier Disruption and Bacterial Translocation in Rats With

- Cirrhosis. *Hepatology*. 2019; 70:925-938.
35. Schneider KM, Mohs A, Gui W *et al.* Imbalanced gut microbiota fuels hepatocellular carcinoma development by shaping the hepatic inflammatory microenvironment. *Nature Communications* 2022; 13:3964.
36. Schuster S, Cabrera D, Arrese M, Feldstein AE. Triggering and resolution of inflammation in NASH. *Nat Rev Gastroenterol Hepatol*. 2018; 15:349-364.

Received April 18, 2024; Revised June 16, 2024; Accepted June 22, 2024.

§These authors contributed equally to this work.

*Address correspondence to:

Yujun Shi and Yongjie Zhou, Institute of Clinical Pathology & Department of Pathology, Key Laboratory of Transplant Engineering and Immunology, NHC, West China Hospital, Sichuan University, Chengdu 610041, China.

E-mail: shiyujun@scu.edu.cn (YS); yongjiezhou@scu.edu.cn (YZ)

Released online in J-STAGE as advance publication June 26, 2024.



Guide for Authors

1. Scope of Articles

BioScience Trends (Print ISSN 1881-7815, Online ISSN 1881-7823) is an international peer-reviewed journal. *BioScience Trends* devotes to publishing the latest and most exciting advances in scientific research. Articles cover fields of life science such as biochemistry, molecular biology, clinical research, public health, medical care system, and social science in order to encourage cooperation and exchange among scientists and clinical researchers.

2. Submission Types

Original Articles should be well-documented, novel, and significant to the field as a whole. An Original Article should be arranged into the following sections: Title page, Abstract, Introduction, Materials and Methods, Results, Discussion, Acknowledgments, and References. Original articles should not exceed 5,000 words in length (excluding references) and should be limited to a maximum of 50 references. Articles may contain a maximum of 10 figures and/or tables. Supplementary Data are permitted but should be limited to information that is not essential to the general understanding of the research presented in the main text, such as unaltered blots and source data as well as other file types.

Brief Reports definitively documenting either experimental results or informative clinical observations will be considered for publication in this category. Brief Reports are not intended for publication of incomplete or preliminary findings. Brief Reports should not exceed 3,000 words in length (excluding references) and should be limited to a maximum of 4 figures and/or tables and 30 references. A Brief Report contains the same sections as an Original Article, but the Results and Discussion sections should be combined.

Reviews should present a full and up-to-date account of recent developments within an area of research. Normally, reviews should not exceed 8,000 words in length (excluding references) and should be limited to a maximum of 10 figures and/or tables and 100 references. Mini reviews are also accepted, which should not exceed 4,000 words in length (excluding references) and should be limited to a maximum of 5 figures and/or tables and 50 references.

Policy Forum articles discuss research and policy issues in areas related to life science such as public health, the medical care system, and social science and may address governmental issues at district, national, and international levels of discourse. Policy Forum articles should not exceed 3,000 words in length (excluding references) and should be limited to a maximum of 5 figures and/or tables and 30 references.

Communications are short, timely pieces that spotlight new research findings or policy issues of interest to the field of global health and medical practice that are of immediate importance. Depending on their content, Communications will be published as "Comments" or "Correspondence". Communications should not exceed 1,500 words in length (excluding references) and should be limited to a maximum of 2 figures and/or tables and 20 references.

Editorials are short, invited opinion pieces that discuss an issue of immediate importance to the fields of global health, medical practice, and basic science oriented for clinical application. Editorials should not exceed 1,000 words in length (excluding references) and should be limited to a maximum of 10 references. Editorials may contain one figure or table.

News articles should report the latest events in health sciences and medical research from around the world. News should not exceed 500 words in length.

Letters should present considered opinions in response to articles published in *BioScience Trends* in the last 6 months or issues of general interest. Letters should not exceed 800 words in length and may contain a maximum of 10 references. Letters may contain one figure or table.

3. Editorial Policies

For publishing and ethical standards, *BioScience Trends* follows the Recommendations for the Conduct, Reporting, Editing, and Publication of Scholarly Work in Medical Journals issued by the International Committee of Medical Journal Editors (ICMJE, <https://icmje.org/recommendations>), and the Principles of Transparency and Best Practice in Scholarly Publishing jointly issued by the Committee on Publication Ethics (COPE, <https://publicationethics.org/resources/guidelines-new/principles-transparency-and-best-practice-scholarly-publishing>), the Directory of Open Access Journals (DOAJ, <https://doaj.org/apply/transparency>), the Open Access Scholarly Publishers Association (OASPA, <https://oaspa.org/principles-of-transparency-and-best-practice-in-scholarly-publishing-4>), and the World Association of Medical Editors (WAME, <https://wame.org/principles-of-transparency-and-best-practice-in-scholarly-publishing>).

BioScience Trends will perform an especially prompt review to encourage innovative work. All original research will be subjected to a rigorous standard of peer review and will be edited by experienced copy editors to the highest standards.

Ethical Approval of Studies and Informed Consent: For all manuscripts reporting data from studies involving human participants or animals, formal review and approval, or formal review and waiver, by an appropriate institutional review board or ethics committee is required and should be described in the Methods section. When your manuscript contains any case details, personal information and/or images of patients or other individuals, authors must obtain appropriate written consent, permission and release in order to comply with all applicable laws and regulations concerning privacy and/or security of personal information. The consent form needs to comply with the relevant legal requirements of your particular jurisdiction, and please do not send signed consent form to *BioScience Trends* to respect your patient's and any other individual's privacy. Please instead describe the information clearly in the Methods (patient consent) section of your manuscript while retaining copies of the signed forms in the event they should be needed. Authors should also state that the study conformed to the provisions of the Declaration of Helsinki (as revised in 2013, <https://wma.net/what-we-do/medical-ethics/declaration-of-helsinki>). When reporting experiments on animals, authors should indicate whether the institutional and national guide for the care and use of laboratory animals was followed.

Reporting Clinical Trials: The ICMJE (<https://icmje.org/recommendations/browse/publishing-and-editorial-issues/clinical-trial-registration.html>) defines a clinical trial as any research project that prospectively assigns people or a group of people to an intervention, with or without concurrent comparison or control groups, to study the relationship between a health-related intervention and a health outcome. Registration of clinical trials in a public trial registry at or before the time of first patient enrollment is a condition of consideration for publication in *BioScience Trends*, and the trial registration number will be published at the end of the Abstract. The registry must be independent of for-profit interest and publicly accessible. Reports of trials must conform to CONSORT 2010 guidelines (<https://consort-statement.org/consort-2010>). Articles reporting the results of randomized trials must include the CONSORT flow diagram showing the progress of patients throughout the trial.

Conflict of Interest: All authors are required to disclose any actual or potential conflict of interest including financial interests or relationships with other people or organizations that might raise questions of bias

in the work reported. If no conflict of interest exists for each author, please state "There is no conflict of interest to disclose".

Submission Declaration: When a manuscript is considered for submission to *BioScience Trends*, the authors should confirm that 1) no part of this manuscript is currently under consideration for publication elsewhere; 2) this manuscript does not contain the same information in whole or in part as manuscripts that have been published, accepted, or are under review elsewhere, except in the form of an abstract, a letter to the editor, or part of a published lecture or academic thesis; 3) authorization for publication has been obtained from the authors' employer or institution; and 4) all contributing authors have agreed to submit this manuscript.

Initial Editorial Check: Immediately after submission, the journal's managing editor will perform an initial check of the manuscript. A suitable academic editor will be notified of the submission and invited to check the manuscript and recommend reviewers. Academic editors will check for plagiarism and duplicate publication at this stage. The journal has a formal recusal process in place to help manage potential conflicts of interest of editors. In the event that an editor has a conflict of interest with a submitted manuscript or with the authors, the manuscript, review, and editorial decisions are managed by another designated editor without a conflict of interest related to the manuscript.

Peer Review: *BioScience Trends* operates a single-anonymized review process, which means that reviewers know the names of the authors, but the authors do not know who reviewed their manuscript. All articles are evaluated objectively based on academic content. External peer review of research articles is performed by at least two reviewers, and sometimes the opinions of more reviewers are sought. Peer reviewers are selected based on their expertise and ability to provide quality, constructive, and fair reviews. For research manuscripts, the editors may, in addition, seek the opinion of a statistical reviewer. Every reviewer is expected to evaluate the manuscript in a timely, transparent, and ethical manner, following the COPE guidelines (https://publicationethics.org/files/cope-ethical-guidelines-peer-reviewers-v2_0.pdf). We ask authors for sufficient revisions (with a second round of peer review, when necessary) before a final decision is made. Consideration for publication is based on the article's originality, novelty, and scientific soundness, and the appropriateness of its analysis.

Suggested Reviewers: A list of up to 3 reviewers who are qualified to assess the scientific merit of the study is welcomed. Reviewer information including names, affiliations, addresses, and e-mail should be provided at the same time the manuscript is submitted online. Please do not suggest reviewers with known conflicts of interest, including participants or anyone with a stake in the proposed research; anyone from the same institution; former students, advisors, or research collaborators (within the last three years); or close personal contacts. Please note that the Editor-in-Chief may accept one or more of the proposed reviewers or may request a review by other qualified persons.

Language Editing: Manuscripts prepared by authors whose native language is not English should have their work proofread by a native English speaker before submission. If not, this might delay the publication of your manuscript in *BioScience Trends*.

The Editing Support Organization can provide English proofreading, Japanese-English translation, and Chinese-English translation services to authors who want to publish in *BioScience Trends* and need assistance before submitting a manuscript. Authors can visit this organization directly at <https://www.iacmhr.com/iac-eso/support.php?lang=en>. IAC-ESO was established to facilitate manuscript preparation by researchers whose native language is not English and to help edit works intended for international academic journals.

Copyright and Reuse: Before a manuscript is accepted for publication in *BioScience Trends*, authors will be asked to sign a transfer of copyright agreement, which recognizes the common

interest that both the journal and author(s) have in the protection of copyright. We accept that some authors (*e.g.*, government employees in some countries) are unable to transfer copyright. A JOURNAL PUBLISHING AGREEMENT (JPA) form will be e-mailed to the authors by the Editorial Office and must be returned by the authors by mail, fax, or as a scan. Only forms with a hand-written signature from the corresponding author are accepted. This copyright will ensure the widest possible dissemination of information. Please note that the manuscript will not proceed to the next step in publication until the JPA Form is received. In addition, if excerpts from other copyrighted works are included, the author(s) must obtain written permission from the copyright owners and credit the source(s) in the article.

4. Cover Letter

The manuscript must be accompanied by a cover letter prepared by the corresponding author on behalf of all authors. The letter should indicate the basic findings of the work and their significance. The letter should also include a statement affirming that all authors concur with the submission and that the material submitted for publication has not been published previously or is not under consideration for publication elsewhere. The cover letter should be submitted in PDF format. For an example of Cover Letter, please visit: <https://www.biosciencetrends.com/downcentre> (Download Centre).

5. Submission Checklist

The Submission Checklist should be submitted when submitting a manuscript through the Online Submission System. Please visit Download Centre (<https://www.biosciencetrends.com/downcentre>) and download the Submission Checklist file. We recommend that authors use this checklist when preparing your manuscript to check that all the necessary information is included in your article (if applicable), especially with regard to Ethics Statements.

6. Manuscript Preparation

Manuscripts are suggested to be prepared in accordance with the "Recommendations for the Conduct, Reporting, Editing, and Publication of Scholarly Work in Medical Journals", as presented at <https://www.ICMJE.org>.

Manuscripts should be written in clear, grammatically correct English and submitted as a Microsoft Word file in a single-column format. Manuscripts must be paginated and typed in 12-point Times New Roman font with 24-point line spacing. Please do not embed figures in the text. Abbreviations should be used as little as possible and should be explained at first mention unless the term is a well-known abbreviation (*e.g.* DNA). Single words should not be abbreviated.

Title page: The title page must include 1) the title of the paper (Please note the title should be short, informative, and contain the major key words); 2) full name(s) and affiliation(s) of the author(s), 3) abbreviated names of the author(s), 4) full name, mailing address, telephone/fax numbers, and e-mail address of the corresponding author; 5) author contribution statements to specify the individual contributions of all authors to this manuscript, and 6) conflicts of interest (if you have an actual or potential conflict of interest to disclose, it must be included as a footnote on the title page of the manuscript; if no conflict of interest exists for each author, please state "There is no conflict of interest to disclose").

Abstract: The abstract should briefly state the purpose of the study, methods, main findings, and conclusions. For articles that are Original Articles, Brief Reports, Reviews, or Policy Forum articles, a one-paragraph abstract consisting of no more than 250 words must be included in the manuscript. For Communications, Editorials, News, or Letters, a brief summary of main content in 150 words or fewer should be included in the manuscript. For articles reporting clinical trials, the trial registration number should be stated at the end of the Abstract. Abbreviations must be kept to a minimum and non-standard

abbreviations explained in brackets at first mention. References should be avoided in the abstract. Three to six key words or phrases that do not occur in the title should be included in the Abstract page.

Introduction: The introduction should provide sufficient background information to make the article intelligible to readers in other disciplines and sufficient context clarifying the significance of the experimental findings

Materials/Patients and Methods: The description should be brief but with sufficient detail to enable others to reproduce the experiments. Procedures that have been published previously should not be described in detail but appropriate references should simply be cited. Only new and significant modifications of previously published procedures require complete description. Names of products and manufacturers with their locations (city and state/country) should be given and sources of animals and cell lines should always be indicated. All clinical investigations must have been conducted in accordance Materials/Patients and Methods.

Results: The description of the experimental results should be succinct but in sufficient detail to allow the experiments to be analyzed and interpreted by an independent reader. If necessary, subheadings may be used for an orderly presentation. All Figures and Tables should be referred to in the text in order, including those in the Supplementary Data.

Discussion: The data should be interpreted concisely without repeating material already presented in the Results section. Speculation is permissible, but it must be well-founded, and discussion of the wider implications of the findings is encouraged. Conclusions derived from the study should be included in this section.

Acknowledgments: All funding sources (including grant identification) should be credited in the Acknowledgments section. Authors should also describe the role of the study sponsor(s), if any, in study design; in the collection, analysis, and interpretation of data; in the writing of the report; and in the decision to submit the paper for publication. If the funding source had no such involvement, the authors should so state.

In addition, people who contributed to the work but who do not meet the criteria for authors should be listed along with their contributions.

References: References should be numbered in the order in which they appear in the text. Citing of unpublished results, personal communications, conference abstracts, and theses in the reference list is not recommended but these sources may be mentioned in the text. In the reference list, cite the names of all authors when there are fifteen or fewer authors; if there are sixteen or more authors, list the first three followed by *et al.* Names of journals should be abbreviated in the style used in PubMed. Authors are responsible for the accuracy of the references. The EndNote Style of *BioScience Trends* could be downloaded at **EndNote** (https://ircabssagroup.com/examples/BioScience_Trends.ens).

Examples are given below:

Example 1 (Sample journal reference):

Inagaki Y, Tang W, Zhang L, Du GH, Xu WF, Kokudo N. Novel aminopeptidase N (APN/CD13) inhibitor 24F can suppress invasion of hepatocellular carcinoma cells as well as angiogenesis. *Biosci Trends*. 2010; 4:56-60.

Example 2 (Sample journal reference with more than 15 authors):

Darby S, Hill D, Auvinen A, *et al.* Radon in homes and risk of lung cancer: Collaborative analysis of individual data from 13 European case-control studies. *BMJ*. 2005; 330:223.

Example 3 (Sample book reference):

Shalev AY. Post-traumatic stress disorder: Diagnosis, history and life course. In: *Post-traumatic Stress Disorder, Diagnosis, Management and Treatment* (Nutt DJ, Davidson JR, Zohar J, eds.). Martin Dunitz, London, UK, 2000; pp. 1-15.

Example 4 (Sample web page reference):

World Health Organization. The World Health Report 2008 – primary health care: Now more than ever. http://www.who.int/whr/2008/whr08_en.pdf (accessed September 23, 2022).

Tables: All tables should be prepared in Microsoft Word or Excel and should be arranged at the end of the manuscript after the References section. Please note that tables should not in image format. All tables should have a concise title and should be numbered consecutively with Arabic numerals. If necessary, additional information should be given below the table.

Figure Legend: The figure legend should be typed on a separate page of the main manuscript and should include a short title and explanation. The legend should be concise but comprehensive and should be understood without referring to the text. Symbols used in figures must be explained. Any individually labeled figure parts or panels (A, B, *etc.*) should be specifically described by part name within the legend.

Figure Preparation: All figures should be clear and cited in numerical order in the text. Figures must fit a one- or two-column format on the journal page: 8.3 cm (3.3 in.) wide for a single column, 17.3 cm (6.8 in.) wide for a double column; maximum height: 24.0 cm (9.5 in.). Please make sure that the symbols and numbers appeared in the figures should be clear. Please make sure that artwork files are in an acceptable format (TIFF or JPEG) at minimum resolution (600 dpi for illustrations, graphs, and annotated artwork, and 300 dpi for micrographs and photographs). Please provide all figures as separate files. Please note that low-resolution images are one of the leading causes of article resubmission and schedule delays.

Units and Symbols: Units and symbols conforming to the International System of Units (SI) should be used for physicochemical quantities. Solidus notation (*e.g.* mg/kg, mg/mL, mol/mm²/min) should be used. Please refer to the SI Guide www.bipm.org/en/si/ for standard units.

Supplemental data: Supplemental data might be useful for supporting and enhancing your scientific research and *BioScience Trends* accepts the submission of these materials which will be only published online alongside the electronic version of your article. Supplemental files (figures, tables, and other text materials) should be prepared according to the above guidelines, numbered in Arabic numerals (*e.g.*, Figure S1, Figure S2, and Table S1, Table S2) and referred to in the text. All figures and tables should have titles and legends. All figure legends, tables and supplemental text materials should be placed at the end of the paper. Please note all of these supplemental data should be provided at the time of initial submission and note that the editors reserve the right to limit the size and length of Supplemental Data.

5. Submission Checklist

The Submission Checklist will be useful during the final checking of a manuscript prior to sending it to *BioScience Trends* for review. Please visit Download Centre and download the Submission Checklist file.

6. Online Submission

Manuscripts should be submitted to *BioScience Trends* online at <https://www.biosciencetrends.com/login>. Receipt of your manuscripts submitted online will be acknowledged by an e-mail from Editorial Office containing a reference number, which should be used in all future communications. If for any reason you are unable to submit a file online, please contact the Editorial Office by e-mail at office@biosciencetrends.com

8. Accepted Manuscripts

Page Charge: Page charges will be levied on all manuscripts accepted for publication in *BioScience Trends* (Original Articles / Brief Reports / Reviews / Policy Forum / Communications: \$140 per page for black white pages, \$340 per page for color pages; News / Letters: a total cost of \$600). Under exceptional circumstances, the author(s) may apply to the editorial office for a waiver of the publication charges by stating the reason in the Cover Letter when the manuscript online.

Misconduct: *BioScience Trends* takes seriously all allegations of potential misconduct and adhere to the ICMJE Guideline (<https://icmje.org/recommendations>) and COPE Guideline (https://publicationethics.org/files/Code_of_conduct_for_journal_editors.pdf). In cases of

suspected research or publication misconduct, it may be necessary for the Editor or Publisher to contact and share submission details with third parties including authors' institutions and ethics committees. The corrections, retractions, or editorial expressions of concern will be performed in line with above guidelines.

(As of December 2022)

BioScience Trends
Editorial and Head Office
Pearl City Koishikawa 603,
2-4-5 Kasuga, Bunkyo-ku,
Tokyo 112-0003, Japan.

E-mail: office@biosciencetrends.com

